

Simulation and Analysis of Closed System Methane Combustion

by

Eric Haake

Submitted in Partial Fulfillment of the Requirements

for the Degree of

Master of Science in Engineering

in the

Mechanical Engineering

Program

YOUNGSTOWN STATE UNIVERSITY

December 2020

Simulation and Analysis of Closed System Methane Combustion

Eric Haake

I hereby release this thesis to the public. I understand that this thesis will be made available from the OhioLINK ETD Center and the Maag Library Circulation Desk for public access. I also authorize the University or other individuals to make copies of this thesis as needed for scholarly research.

Signature:

Eric Haake, Student Date

Approvals:

Stefan Moldovan, Thesis Advisor Date

Kyosung Choo, Committee Member Date

Kevin Disotell, Committee Member Date

Dr. Salvatore A. Sanders, Dean of Graduate Studies Date

ABSTRACT

This project was funded by a company where some work is proprietary and is not recorded in this paper. The purpose of this project was to simulate, analyze and improve an enclosed methane combustion. The final goal was to reduce the overall pressure in the system along with determining if the system could be analyzed without the need of simulations. Simulation and Analysis of the combustion model requires a fundamental understanding of all the basic processes used. An understanding of the simulation software fluent along with the ability to manipulate the settings to what is required for the specific simulation being performed. An understanding of the chemical kinetics is required for proper setup of the simulation model. Prior to simulating the full model, multiple small simulations were performed to determine the settings needed for Ansys Fluent. Once these settings were determined then full model simulations with varying properties were performed. Based on both the simulations and literature it was found that when the combustion is performed at the stoichiometric ratio, the combustion is at its hottest adiabatic flame temperature and results in the highest pressures in the chamber. With changes to both the initial pressure and concentration of nitrogen the resulting pressures were determined to be lower than the base line model as expected. While these lower values were expected, there is a large percent change in the pressure across the model. The major findings from this project have been the interactions of the shock waves in the chamber. Depending on what is in the chamber, these shock waves can cause irreversible damage to the part. With the introduction of complex geometry in the chamber the approximation of the shock waves become much more complex and analysis of the part though simulation would be the best course of action in the determination of these shock waves. An attempt to lower the shock waves pressure peaks were made with results in drastically lower pressures due to forcing the detonation combustion to turn turbulent. With the flame front no longer driving the pressure shock the maximum pressure observed in the chamber is lower.

Table of Contents

1	Introduction	1
1.1	Combustion	1
1.1.1	Combustion Stoichiometry	2
1.1.2	Shock Waves	3
1.1.3	Ansys Fluent	4
1.1.4	Experimental Apparatus	5
2	Experimental Testing	6
2.1	Thermocouple Test	6
2.2	Experimental Testing	9
2.2.1	Experimental Instrumentation	9
2.2.2	Experimental Shim Holder	11
3	Modeling	19
3.1	Pre-Mixing Block Pipe Flow	19
3.1.1	Mesh	19
3.1.2	Boundary Conditions	19
3.1.3	Variable Properties	21
3.1.4	Pre-Mixing Block Pipe Flow Results	21
3.2	Axisymmetric Flow Model	22
3.2.1	Axisymmetric Flow Model Mesh	22
3.2.2	Axisymmetric Flow Boundary Conditions	24
3.2.3	Axisymmetric Flow Results	25
3.3	Combustion Model Test 1	31
3.3.1	Combustion Testing Boundary Conditions	31
3.3.2	Combustion Testing Mesh	31
3.3.3	Combustion Testing Results	33
3.4	Combustion Model Test 2	36
3.4.1	Combustion Model Testing 2 Boundary Conditions	36
3.4.2	Combustion Model Testing 2 Meshes	36
3.4.3	Combustion Model Test 2 Results	39
3.5	Combustion Model 1 (Normal Model)	40
3.5.1	Combustion Model 1 Boundary Conditions	40
3.5.2	Combustion Model 1 Mesh	40
3.6	Combustion Model 2	41

3.6.1	Combustion Model 2 Boundary Conditions	41
3.6.2	Combustion Model 2 Mesh	41
3.7	Combustion Model 3	43
3.7.1	Combustion Model 3 Boundary Conditions	43
3.7.2	Combustion Model 3 Mesh	43
3.8	Combustion Model 4 (Low Pressure Model)	44
3.8.1	Combustion Model 4 Boundary Conditions	44
3.8.2	Combustion Model 4 Mesh	44
3.9	Combustion Model 5 (Nitrogen Model)	44
3.9.1	Combustion Model 5 Boundary Conditions	44
3.9.2	Combustion Model 5 Mesh	44
3.9.3	Combustion Model 6 Boundary Conditions	45
3.9.4	Combustion Model 6 Mesh	45
3.10	Combustion Model 7	45
3.10.1	Combustion Model 7 Boundary Conditions	46
3.10.2	Combustion Model 7 Mesh	47
4	Results	48
4.1	Combustion Model 1 (Normal Model)	48
4.1.1	Combustion Model 1 Contour Plots	48
4.1.2	Combustion Model 1 Full Wall Values	51
4.1.3	Combustion Model 1 Single Position Wall Values	52
4.2	Combustion Model 2	61
4.2.1	Combustion Model 2 Contour Plots	61
4.3	Combustion Model 3	62
4.3.1	Combustion Model 3 Results	62
4.4	Combustion Model 4 (Low Pressure Model)	65
4.4.1	Combustion Model 4 Contour Plots	65
4.4.2	Combustion Model 4 Full Wall Values	67
4.4.3	Combustion Model 4 Single Wall Values	68
4.5	Combustion Model 5 (Nitrogen Model)	77
4.6	Combustion Model 6 (Stoichiometric Model)	77
4.7	Combustion Model 7	77
4.7.1	Combustion Model 7 Contour Plots	78
4.8	Full Model Comparison	79

4.9	Wall Data Comparison	80
5	Conclusion and Future Work	86
5.1	Conclusions	86
5.2	Future Work	86
	References	87
	Appendix A	1
	Combustion Model 5 (Nitrogen Model)	1
	Combustion Model 5 Results	1
	Combustion Model 5 Full Wall Values	3
	Combustion Model 5 Single Wall Values	4
	Combustion Model 6 (Stoichiometric Model)	11
	Combustion Model 6 Contour Plots	11
	Combustion Model 6 Full Wall Values	12
	Combustion Model 6 Single Wall Values	14
	Variable Properties	21
	Appendix B	44
	Code	44
	Low Pressure Model Code	44
	Nitrogen Model Code	45
	Combination Plot Code	46

List of Figures

Figure 1. Adiabatic Flame Temperature based on Equivalence Ratio [8]	3
Figure 2. Axisymmetric Model [9]	4
Figure 3. Plot of Thermocouple Flame Test	7
Figure 4. Plots of Best Thermocouple Flame Test	8
Figure 5. Sensor Locations	9
Figure 6. Experimental Testing Apparatus External View	10
Figure 7. Experimental Testing Apparatus Internal View	11
Figure 8. Experimental Shim Holder	12
Figure 9. Experimental Shim Holder with Shim	12
Figure 10. Rectangular Shim Test 1 Results	13
Figure 11. Rectangular Shim Test 2 Results	13
Figure 12. Shim Test 1 Results	14
Figure 13. Shim Test 2 Results	14
Figure 14. Shim Test 3 Results	15
Figure 15. Shim Test 4 Results	15
Figure 16. Shim Test 5 Results	16
Figure 17. Shim Test Result	17
Figure 18. Shim After an Experimental Run	17
Figure 19. Stoichiometric Test 1 Results	18
Figure 20. Stoichiometric Test 2 Results	18
Figure 21. Pipe Mesh	19
Figure 22. Pipe Model Boundary Conditions (Not to Scale)	20
Figure 23. Oxygen Temperature Across the Pipe	21
Figure 24. Methane Temperature Across the Pipe	21
Figure 25. Axisymmetric Model	22
Figure 26. Axisymmetric Model Large Fillet	23
Figure 27. Axisymmetric Model Small Fillet	23
Figure 28. Axisymmetric Model Boundary Conditions	24
Figure 29. Static Pressure Contour	25
Figure 30. Velocity Contour	25
Figure 31. Velocity Contour of Chamber	26
Figure 32. Mach Disk [11]	26
Figure 33. Mach Disk	27
Figure 34. Pressure Build Up	28
Figure 35. Velocity Vectors	29
Figure 36. Normalized Velocity Vectors	29
Figure 37. Normalized Velocity Vectors Critical Region	30
Figure 38. Normalized Velocity Vectors Recurlation Region	30
Figure 39. Combustion Model Test 1 Boundary Conditions	31
Figure 40. Combustion Model Test 1 Mesh	31
Figure 41. Combustion Model Test 1 Mesh Closeup	32
Figure 42. Simple Combustion Results Pressure (a), Velocity (b), Mach Number (c)	33
Figure 43. Combustion Pressure Contour	34
Figure 44. Combustion Velocity Vectors	34
Figure 45. Combustion Model Temperature	35

Figure 46. Velocity Vector Exiting Pipe	35
Figure 47. Combustion Model Test 2 Boundary Conditions	36
Figure 48. Combustion Model Test 2 Mesh	36
Figure 49. Combustion Model Test 2 Mesh Wall Contact	37
Figure 50. Combustion Model Test 2 Mesh Curved Surface	38
Figure 51. Combustion Model Test 2 Pipe Mesh	38
Figure 52. Results from Combustion Test 2 for Both Pipe and No Pipe Models at timestep 8000 (a), 12500 (b)	39
Figure 53. Combustion Model 1 Boundary Condition	40
Figure 54. Combustion Model 2 Boundary Conditions	41
Figure 55. Combustion Model 2 Full Mesh	42
Figure 56. Combustion Model 2 New Solid Domain Mesh	42
Figure 57. Combustion Model 3 Full Mesh	43
Figure 58. Combustion Model 7 Geometry	46
Figure 59. Combustion Model 7 Geometry Closeup	46
Figure 60. Combustion Model 7 Full Mesh	47
Figure 61. Combustion Model 7 Mesh Closeup	47
Figure 62. Combustion Model 1 Pressure Results at timestep 7500 (a), 12500 (b), 14500 (c)	49
Figure 63. Combustion Model 1 Temperature Results at timestep 7500 (a), 15900 (b), 19000(c)	50
Figure 64. Normal Model Full Wall Pressure at Time One	51
Figure 65. Normal Model Full Wall Pressure at Time Two	51
Figure 66. Normal Model Pressure Values 1	52
Figure 67. Normal Model Pressure Values 2	53
Figure 68. Normal Model Pressure Values 3	53
Figure 69. Normal Model Temperature Values 1	54
Figure 70. Normal Model Temperature Values 2	55
Figure 71. Normal Model Temperature Values 3	55
Figure 72. Normal Model Temperature Values 4	56
Figure 73. Normal Model Temperature Values 5	56
Figure 74. Normal Model Pressure and Temperature at Position 1	57
Figure 75. Normal Model Pressure and Temperature at Position 2	58
Figure 76. Normal Model Pressure and Temperature at Position 3	58
Figure 77. Normal Model Pressures at Position 1	59
Figure 78. Normal Model Pressures at Position 2	59
Figure 79. Normal Model Pressures at Position 3	60
Figure 80. Combustion Model 2 Pressure Shocks at timestep 6000 (a), 14000 (b)	61
Figure 81. Combustion Model 3 Pressure Results at timestep 5000 (a), 10000(b)	62
Figure 82. Combustion Model 3 Temperature Results at timestep 5000 (a), 10000 (b)	63
Figure 83. Combustion Model 3 Overlaid Pressure and Temperature at timestep 5000 (a), 10000 (b), 12000 (c)	64
Figure 84. Combustion Model 4 Pressure at timestep 8000 (a), 12500 (b)	65
Figure 85. Combustion Model 4 Temperature at timestep 7500 (a), 12500 (b), 14500 (c)	66
Figure 86. Low Pressure Model Mid Wall Values	67

Figure 87. Low Pressure Model Wall Shock Combination	67
Figure 88. Low Pressure Model Pressure Values 1	68
Figure 89. Low Pressure Model Pressure Values 2	69
Figure 90. Low Pressure Model Pressure Values 3	69
Figure 91. Low Pressure Model Temperature Values 1	70
Figure 92. Low Pressure Model Temperature Values 2	71
Figure 93. Low Pressure Model Temperature Values 3	71
Figure 94. Low Pressure Model Temperature Values 4	72
Figure 95. Low Pressure Model Temperature Values 5	72
Figure 96. Low Pressure Model Pressure and Temperature at Position 1	73
Figure 97. Low Pressure Model Pressure and Temperature at Position 2	74
Figure 98. Low Pressure Model Pressure and Temperature at Position 3	74
Figure 99. Low Pressure Model Pressures at Position 1	75
Figure 100. Low Pressure Model Pressures at Position 2	76
Figure 101. Low Pressure Model Pressures at Position 3	76
Figure 102. Combustion Model 7 Overlaid Contours at timestep 3000 (a), 7000 (b), 13000 (c)	78
Figure 103. Position 1 Static Pressure Comparison	80
Figure 104. Position 1 Static Pressure Comparison	81
Figure 105. Position 2 Static Pressure Comparison	81
Figure 106. Position 2 Static Pressure Comparison	82
Figure 107. Position 3 Static Pressure Comparison	82
Figure 108. Position 3 Static Pressure Comparison	83

List of Tables

Table 1. 28 Reaction Model [2]	2
Table 2. Tabulated Thermocouple Data	6
Table 3. Mass Fraction Conversion	20
Table 4. Mass Transfer	20
Table 5. Velocity Calculations	20
Table 6. Pipe Boundary Conditions	20
Table 7. Tabulated Temperature Calculation	22
Table 8. Tabulated Velocity Calculation	22
Table 9. Axisymmetric Boundary Conditions	24
Table 10. Combustion Model 1 Initialization Values	40
Table 11. Combustion Model 2 Initialization Values	41
Table 12. Combustion Model 3 Initial Settings	43
Table 13. Low Pressure Model	44
Table 14. Combustion Model 5 Initial Conditions	44
Table 15. Stoichiometric Model Initial Conditions	45
Table 16. Combustion Model 7 Initial Conditions	45
Table 17. 10000 Time Step Pressures	79
Table 18. 20000 Time Step Pressures	79
Table 19. Tabulated Pressure Peaks	84
Table 20. Peak Velocities	85

List of Appendix Figures

Figure A1. Combustion Model 5 Pressure at timestep 8000 (a), 12500 (b)	1
Figure A2. Combustion Model 5 Temperature at timestep 7500 (a), 12500 (b), 14500 (c)	2
Figure A3. Nitrogen Model Mid Wall Values	3
Figure A4. Nitrogen Model Wall Shock Combination	3
Figure A5. Nitrogen Model Pressure Values 1	4
Figure A6. Nitrogen Model Pressure Values 2	4
Figure A7. Nitrogen Model Pressure Values 3	5
Figure A8. Nitrogen Model Temperature Values 1	5
Figure A9. Nitrogen Model Temperature Values 2	6
Figure A10. Nitrogen Model Temperature Values 3	6
Figure A11. Nitrogen Model Temperature Values 4	7
Figure A12. Nitrogen Model Temperature Values 5	7
Figure A13. Nitrogen Model Pressure and Temperature at Position 1	8
Figure A14. Nitrogen Model Pressure and Temperature at Position 2	8
Figure A15. Nitrogen Model Pressure and Temperature at Position 3	9
Figure A16. Nitrogen Model Pressures at Position 1	9
Figure A17. Nitrogen Model Pressures at Position 2	10
Figure A18. Nitrogen Model Pressures at Position 3	10
Figure A19. Combustion Model 6 Pressure at timestep 5000 (a), 12500 (b),	11
Figure A20. Combustion Model 6 Temperature at timestep 3000 (a), 12500 (b), 14500 (c)	12
Figure A21. Stoichiometric Model Mid Wall Values	13
Figure A22. Stoichiometric Model Wall Shock Combination	13
Figure A23. Stoichiometric Model Pressure Values 1	14
Figure A24. Stoichiometric Model Pressure Values 2	14
Figure A25. Stoichiometric Model Pressure Values 3	15
Figure A26. Stoichiometric Model Temperature Values 1	15
Figure A27. Stoichiometric Model Temperature Values 2	16
Figure A28. Stoichiometric Model Temperature Values 3	16
Figure A29. Stoichiometric Model Temperature Values 4	17
Figure A30. Stoichiometric Model Temperature Values 5	17
Figure A31. Stoichiometric Model Pressure and Temperature at Position 1	18
Figure A32. Stoichiometric Model Pressure and Temperature at Position 2	18
Figure A33. Stoichiometric Model Pressure and Temperature at Position 3	19
Figure A34. Stoichiometric Model Pressures at Position 1	19
Figure A35. Stoichiometric Model Pressures at Position 2	20
Figure A36. Stoichiometric Model Pressures at Position 3	20
Figure A37. Variable Density of O ₂	24
Figure A38. Variable Viscosity of O ₂	25
Figure A39. Variable Thermal Conductivity of O ₂	26
Figure A40. Variable Specific Heat of O ₂	27
Figure A41. Variable Density of CH ₄	28

Figure A42. Variable Viscosity of CH ₄	29
Figure A43. Variable Thermal Conductivity of CH ₄	30
Figure A44. Variable Specific Heat of CH ₄	31
Figure A45. Variable Density of CO ₂	32
Figure A46. Variable Viscosity of CO ₂	33
Figure A47. Variable Thermal Conductivity of CO ₂	34
Figure A48. Variable Specific Heat of CO ₂	35
Figure A49. Variable Density of N ₂	36
Figure A50. Variable Viscosity of N ₂	37
Figure A51. Variable Thermal Conductivity of N ₂	38
Figure A52. Variable Specific Heat of N ₂	39
Figure A53. Variable Density of H ₂ O	40
Figure A54. Variable Viscosity of H ₂ O	41
Figure A55. Variable Thermal Conductivity of H ₂ O	42
Figure A56. Variable Specific Heat of H ₂ O	43

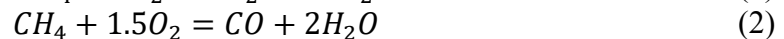
1 Introduction

This project was funded by a company in the precision manufacturing field with goals set by them for the simulations. Due to the work being proprietary, the information talked about in the thesis is generalized when needed and some information is left out.

1.1 Combustion

Combustion is an interdisciplinary subject that requires the use of fluid dynamics, chemical kinetics, thermodynamics, statistical physics, and kinetic theory [1]. This creates a complex system when it comes to simulation of combustion. Due to the complexity of the simulation there is expected error to occur in the simulations. In these experiments and simulations, the combustion of methane and oxygen is done in a way that causes the methane to detonate. A detonation is a type of combustion that contains a supersonic front that generates a shock front. The combustion that happened within the combustion chamber is a detonation combustion due to the nature of the system.

Methane combustion is generally modeled in either 1-step or 2-step processes. A study found that when using 28 elementary reactions as kinetic mechanisms with 13 different species five of the reactions were found to be negligible [2]. In order to reduce the simulation time, the 1-step process is used in this study. The 1-step equation can be seen in Equation 1. When going with the 2-step process the model must track additional species along with perform an additional calculation for the second equation. The 2-step equations can be found in Equations 2 and 3.



The list of the 28 reactions from the study into the reaction mechanism from “Prediction of Propagating Methane-Air Flames” can be seen in Table 1 [2]. These values have been converted into a chem-kin file, discussed in section 1.1.3, and applied to the numerical simulations. The effect on computational time of these models produced, was an increase by a factor of 4 in computational time. This increase resulted in the computation of the models taking upwards of four months. It was decided that this complex reaction mechanism would not be used in the combustion models as time was extremely valuable. In future work, the larger chemical kinematics can be introduced to provide more accurate results when they are needed.

Table 1. 28 Reaction Model [2]

Reaction	Source
$CH_4 + OH = CH_3 + H_2O$	[3] [4]
$CH_4 + H = CH_3 + H_2$	[5]
$CH_4 + O = CH_3 + OH$	[5]
$CH_3 + O = CH_2O + H$	[6]
$CH_3 + O_2 = CH_2O + OH$	[6]
$CH_2O + N = CO + H_2 + N$	[7]
$CH_2O + OH = CHO + H_2O$	[7]
$CH_2O + OH = CHO + OH$	[5]
$CH_2O + H = CHO + H_2$	[5]
$CHO + O_2 = CO + HO_2$	[7]
$CHO + OH = CO + H_2O$	[4]
$CHO + O = CO + OH$	[5]
$CHO + N = CO + H + N$	[4]
$CO + OH = CO_2 + H$	[3]
$CO + O + N = CO_2 + N$	[5]
$HO_2 + O = O_2 + OH$	[6]
$HO_2 + OH = O_2 + H_2O$	[6]
$HO_2 + H = 2OH$	[3]
$HO_2 + H = H_2 + O_2$	[3]
$H + O_2 + N = HO_2 + N$	[3]
$H + O_2 = OH + O$	[3] [6]
$O + H_2 = OH + H$	[3]
$OH + H = H_2O + O$	[3]
$OH + OH = H_2O + O$	[3]
$H + OH + N = H_2O + N$	[3]
$O + H + N = OH + N$	[3]
$H + H + N = H_2 + N$	[3]
$O + O + N = O_2 + N$	[3]

1.1.1 Combustion Stoichiometry

The combustion intensity between the fuel and oxidizer depend on their relative concentrations [8]. For the combustion used in the project the stoichiometric ratio can be seen in Equation 1. When a combustion occurs with a stoichiometric ratio, the intensity of the combustion is near the highest [8]. To measure how far a combustion is from stoichiometric, Equation 4 is used, where F/O defines the ratio of the fuel and oxidizer mass and the subscript st represents the ratio of the fuel and oxidizer at stoichiometric values.

$$\phi = \frac{F/O}{(F/O)_{st}} \quad (4)$$

When $\phi < 1$ the combustion is fuel-lean, at $\phi = 1$ the combustion is stoichiometric and $\phi > 1$ the combustion is fuel-rich. These values are normalized in Equation 5. In the normalized state $0 < \Phi < 0.5$ is fuel-lean, $\Phi = 0.5$ is stoichiometric and $0.5 < \Phi < 1$ is fuel-rich.

$$\Phi = \frac{\phi}{1 + \phi} \quad (5)$$

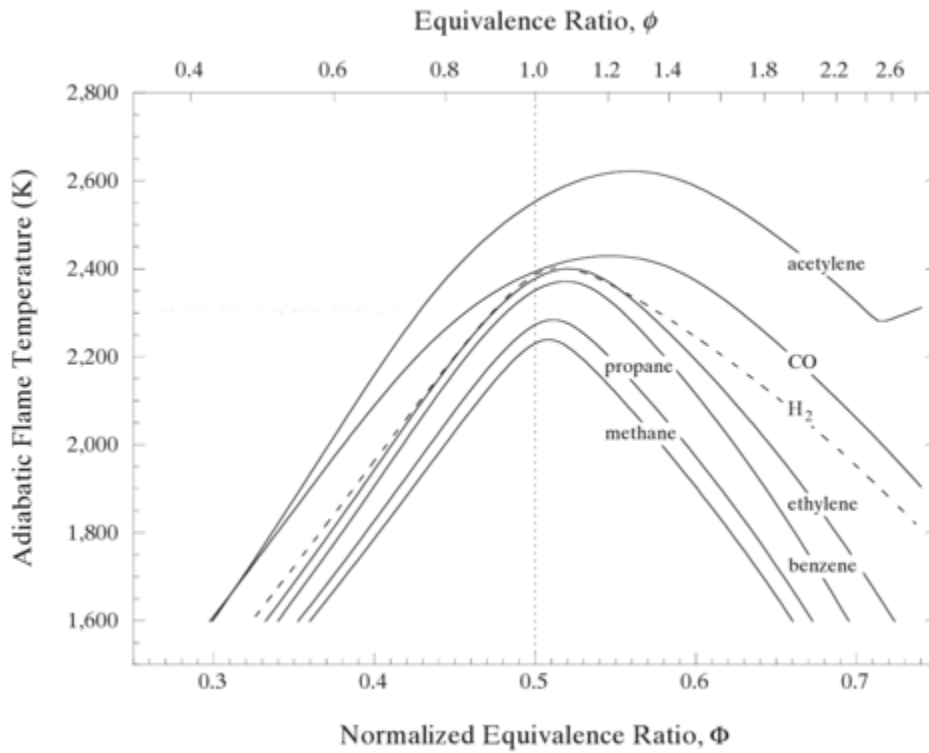


Figure 1. Adiabatic Flame Temperature based on Equivalence Ratio [8]

It can be observed in Figure 1 for methane that the highest adiabatic flame temperature is slightly over 2200 kelvin. This high adiabatic temperature occurs at a normalized value slightly over 0.5. For all experiments and simulations performed the normalized equivalence ratio was 0.5 or lower.

1.1.2 Shock Waves

When a fluid travels across a shock wave there is an increase in pressure, temperature, and density while the velocity of the fluid decreases. During a detonation combustion the flame front is behind a shock wave that is driving the combustion process. This shock wave creates extreme pressures and temperatures for a short time as the shock passes over an area.

1.1.3 Ansys Fluent

According to Ansys Fluent manual, a combustion that is considered a detonation must be modeled as a Species-Transport model with Finite-Rate Chemistry. This model can handle the sonic flamelets caused by the detonation. Running the model requires a chemistry kinetics (chem-kin) file to be imported into fluent so the program knows the reactions stichometry and energy. A default chem-kin file is available in fluent for the methane and air combustion. The chem-kin file gives the kinetics of the chemical reaction in a form that Ansys Fluent can use in calculations for heat generated/required for the reaction. The default chem-kin file does not take in account of all the possible reactions that can occur during the combustion process which is explained in section 1.1.

To keep the computation times at a minimum during the early phases of combustion modeling, the geometry was simplified into a 2-dimensional model. This drastically reduces the number of elements in the model and helps reduce the time needed for computation. Due to the design of the chamber, a 2-dimensional model that is axisymmetric is an accurate representation of the geometry. In Figure 2 the shaded plane is the modeled region. This region is then rotated about the y axis to generate the 3-dimensional model.

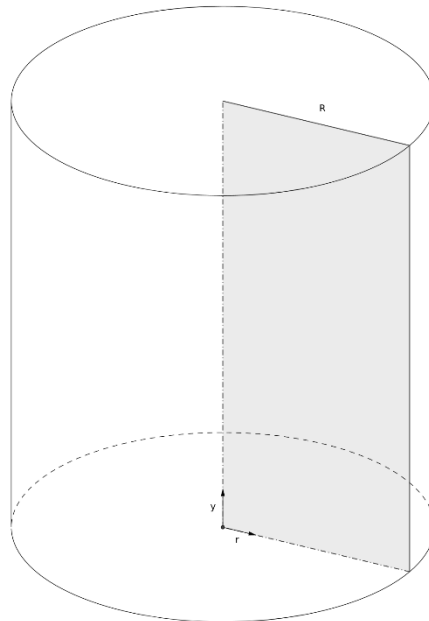


Figure 2. Axisymmetric Model [9]

1.1.4 Experimental Apparatus

For experimental data, the use of both pressure transducers and thermocouples were used. The choice of not using of hot wire anemometers was due to the high temperatures. The explosion temperature would fuse the wires together causing the need to replace them for every experiment. [10] The thermocouples were expected to experience the same issue as the hot wire anemometers, but with the ability to possibly last a few runs before needing replaced. An in depth look at the thermocouple choices are in section 2.1. When collecting the pressure data, the fastest possible response rate was desired. Kistler was contacted to give us the best option for the pressure sensors due to the extreme pressure and temperatures expected in the system. The pressure sensors chosen are Kistler 601CAA Piezoelectric Pressure Sensors. These sensors record the dynamic pressure at a rate that is over 100 kHz. The calibrated pressure range of the sensors is from 0 Bar to 250 Bar and output a signal from -10V to 10V. If pressures exceed these values, they are only recorded at the maximum calibrated value. Based on the cards, chase, thermocouples, pressure transducers, and computational limitations a sampling rate of 140 kHz per channel was chosen. The data acquisition tools used are talked about in section 2.2.1.

2 Experimental Testing

2.1 Thermocouple Test

To capture the flame propagation through the combustion chamber, a fast response time is required. Multiple thermo couples were tested to determine the best thermocouple to use to gather experimental data. The different thermocouples were tested using a 100Hz data acquisition card. Each thermo couple had a flame from a lighter placed under to find the time it would take each thermocouple to respond to the flame. Once the thermocouple reached its peak temperature the flame was removed so the thermocouple could cool before being reheated. This was done a total of 3 times for each of the thermocouples. The results of these test can be seen in Figure 3.

Analyzing the data from each of the thermocouple heat-ups it can be observed that there are inconsistencies in the shape of the temperature rise. This is due to the flame of the lighter moving away from the desired location. Due to the slight movement in the flame causing large data disturbances each thermocouple was heated up 3 times. A calculation of the temperature increase of the thermocouple per second was done. A temperature range from 100K to 600K was chosen as the calculation range. Using this range and time to cover this range, a change in temperature per second can be calculated for each of the thermocouples. Figure 4 show the plot of temperature vs. time for each of the thermocouples in their most consistent heat up. The time that each thermocouple took to increase from 100K to 200K was recorded along with the temperature change within that time. The change in temperature over time was calculated for each of the thermocouples. Table 2 shows the values of each thermocouple tabulated.

Table 2. Tabulated Thermocouple Data

	Δ Time	Δ Temp	Δ Temp/s	Max Temp (K)
0.062 Exposed	2	503.3587	251.6793	769.2469
0.02 Grounded	0.82	493.9194	602.3407	1026.519
0.02 Exposed	0.58	497.3363	857.4764	984.9415

The 0.02 exposed tip thermocouple has the highest temperature increase per second. This would be the optimal choice for the experiments. But due to the nature of the combustion both the 0.02 exposed and grounded were chosen to be used. While the grounded has a slower temperature increase per second, it is expected that the grounded thermocouples can last for more experimental test than the exposed tip thermocouples.

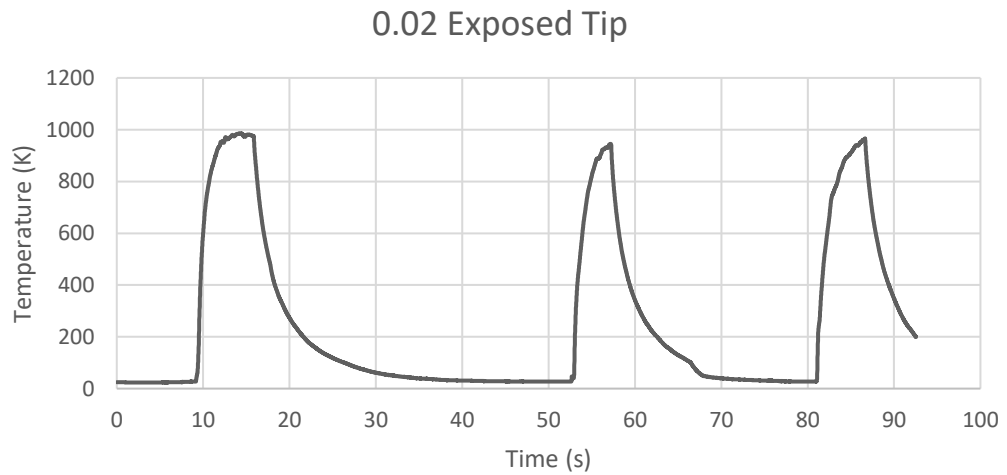
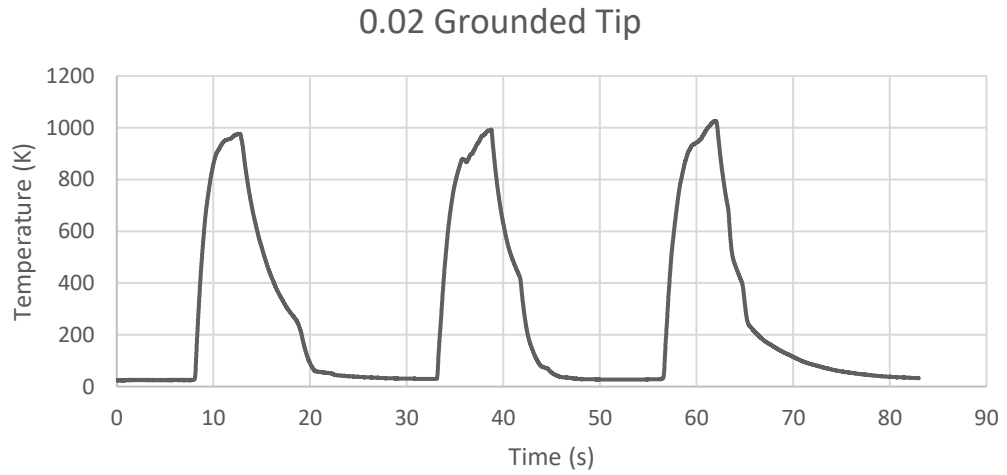
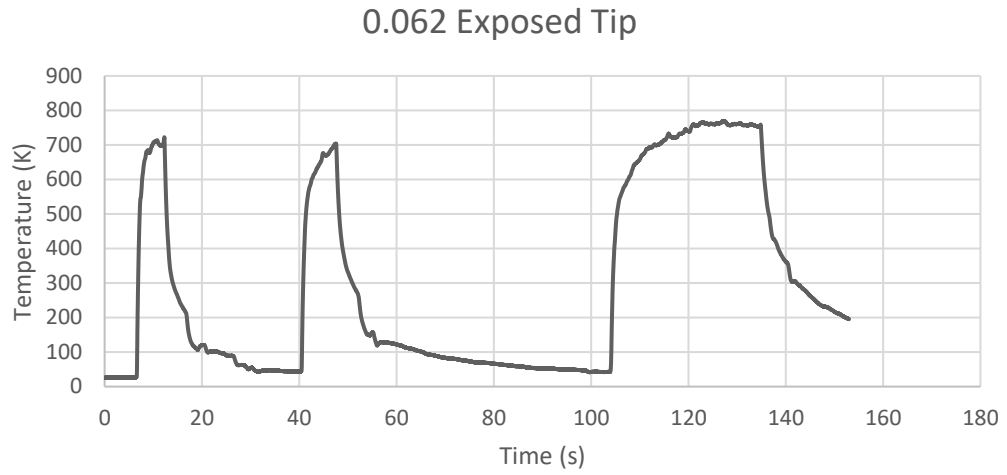


Figure 3. Plot of Thermocouple Flame Test

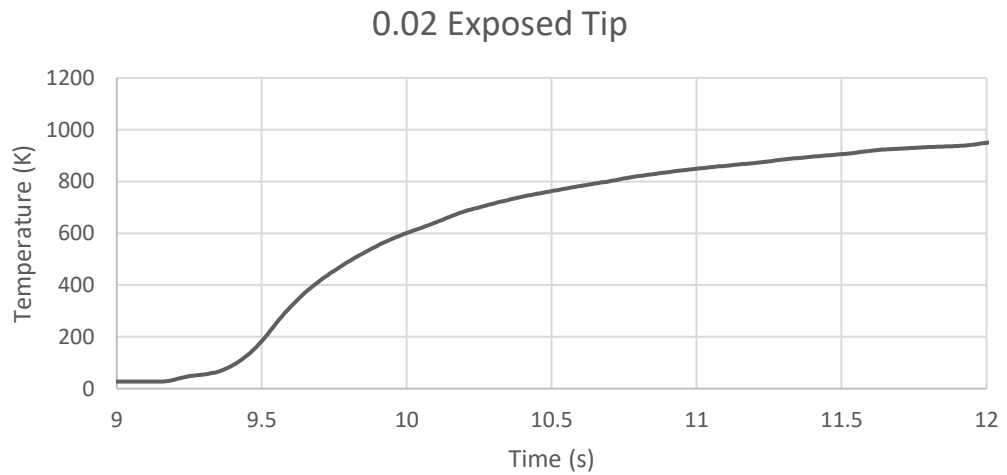
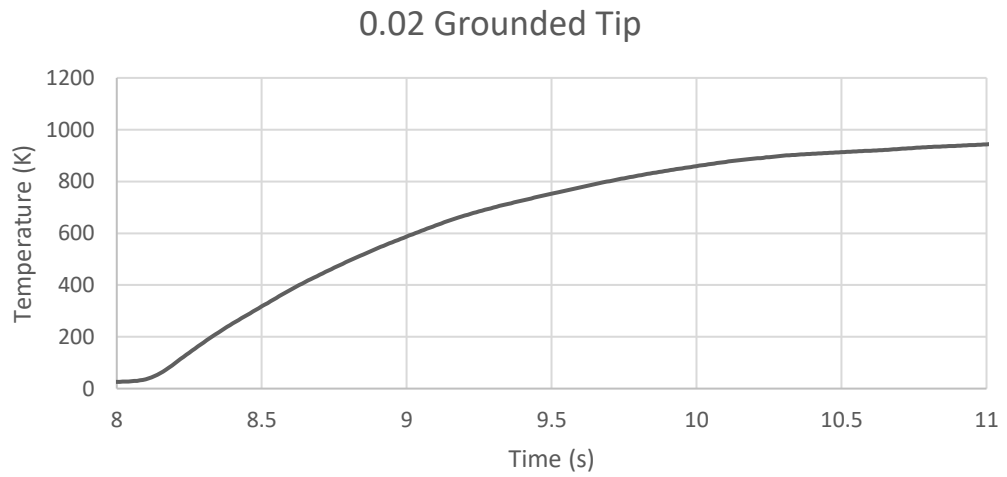
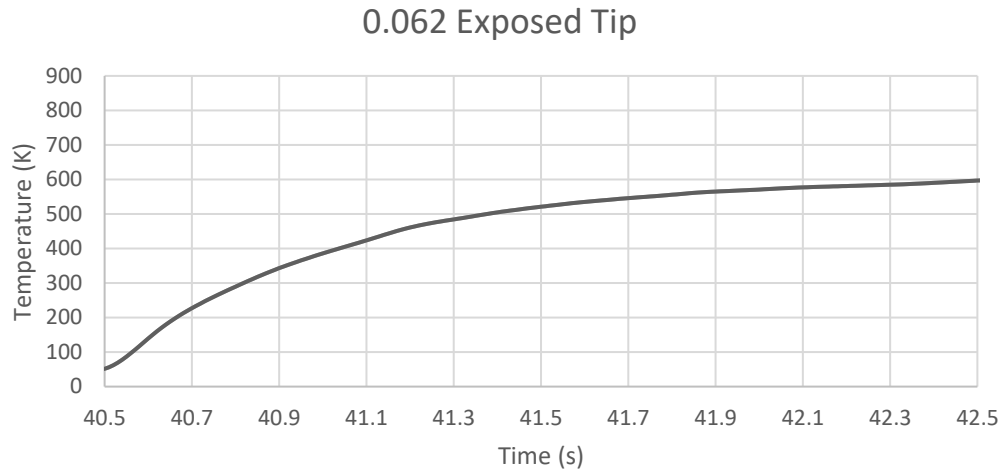


Figure 4. Plots of Best Thermocouple Flame Test

2.2 Experimental Testing

2.2.1 Experimental Instrumentation

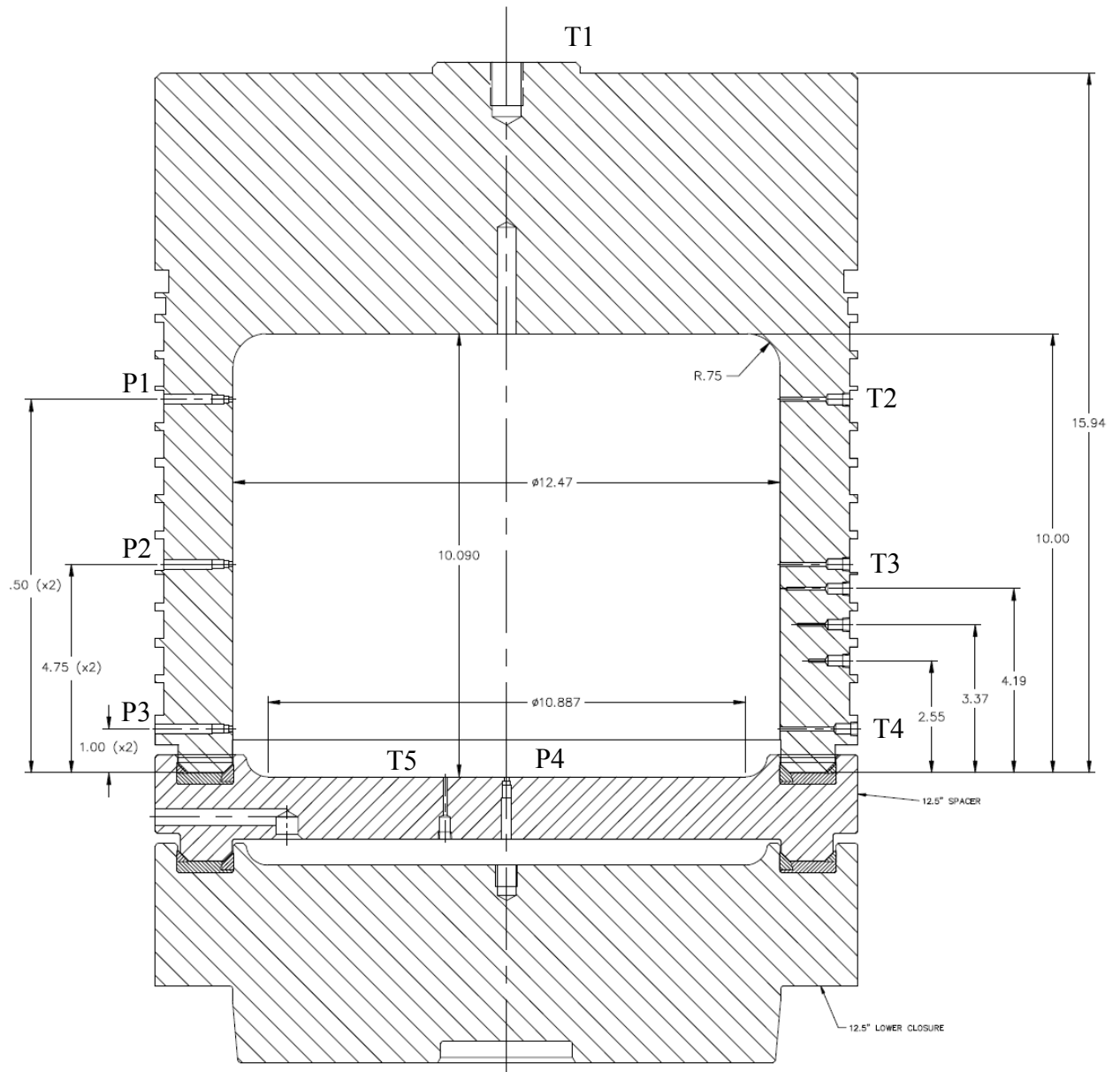


Figure 5. Sensor Locations

The instrumentation used for the experimental data were all from national instruments and data acquisition was recorded using LabVIEW. NI 9212 was used for the temperature readings. The card has a sampling of 75S/s/ch. NI 9223 was used for the pressure readings. Both cards were placed into a Ni cDAQ 9178. During the initial testing one temperature and all 4 pressures were being recorded. These initial tests were performed to get an insight on how the equipment would perform.



Figure 6. Experimental Testing Apparatus External View



Figure 7. Experimental Testing Apparatus Internal View

From the experimental testing it was found that data could only be recorded for a limited amount of time at the 140 kHz chosen. Due to this the data acquisition does not start until a few moments before the ignition is started. The data is then collected for as long as possible prior to the combustion to gather steady state values. After a given time the data acquisition is changed from 140 kHz to only 100 Hz. This is to allow for data collection during a long period of time after the combustion. Due to there being no more pressure shocks in the chamber, only the temperatures are recorded during this time.

2.2.2 Experimental Shim Holder

A shim holder was created so that testing on machined shims could be performed consecutively with as much accuracy as possible between tests.

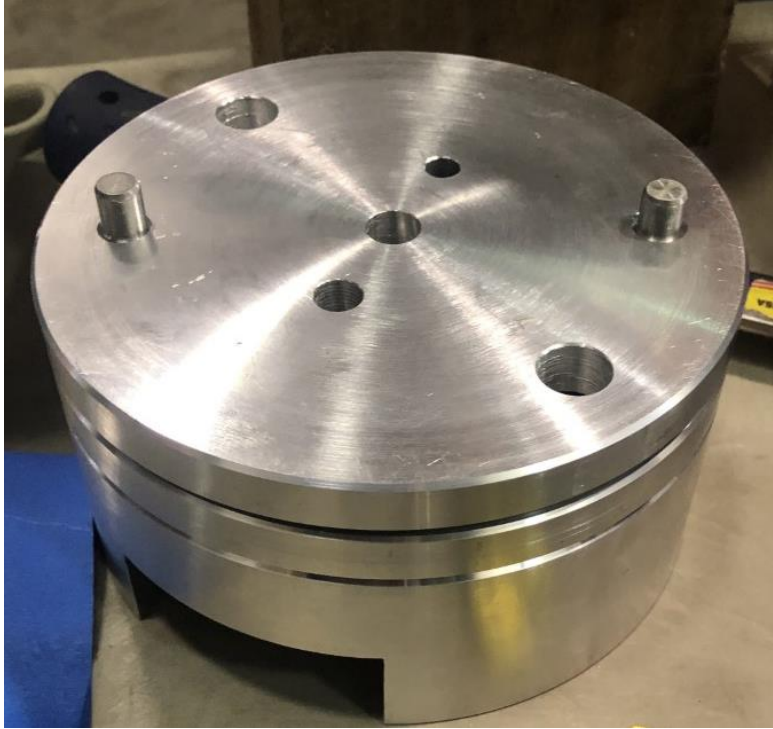


Figure 8. Experimental Shim Holder

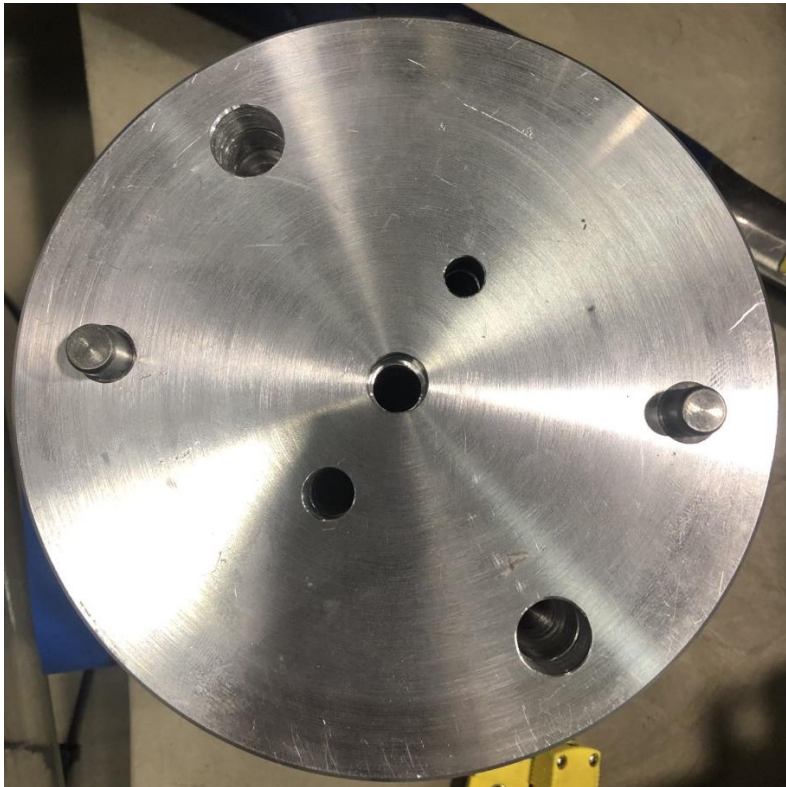


Figure 9. Experimental Shim Holder with Shim

Results from the experimental data can be seen in Figure 10 through Figure 20. The rectangular shim test was performed with the chamber empty and a sheet of aluminum placed into it. The Shim test were run with the shim holder inside of the chamber and the stoichiometric test were run with nothing in the chamber.

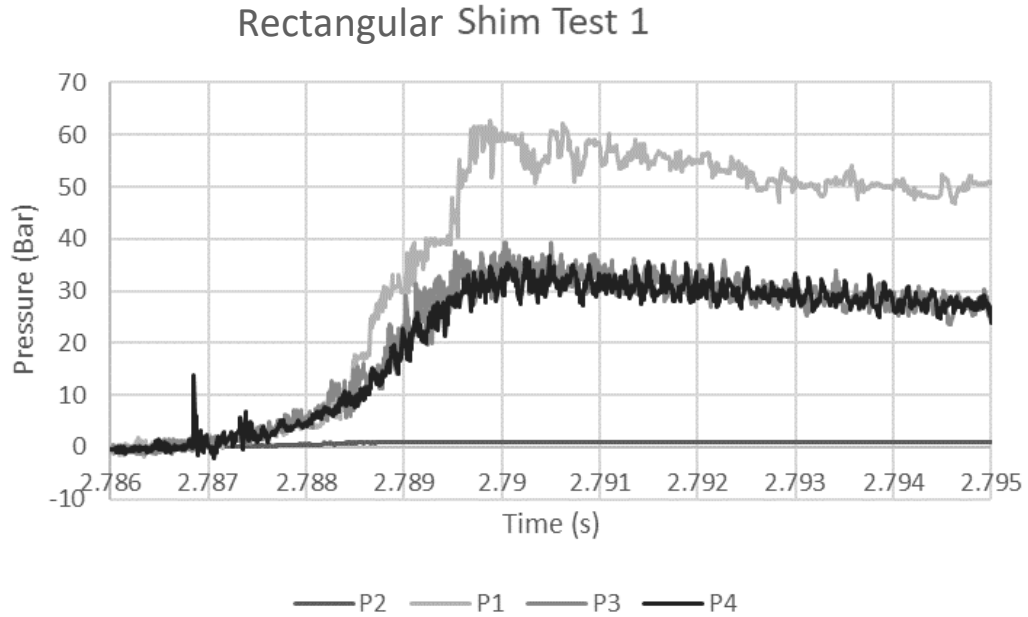


Figure 10. Rectangular Shim Test 1 Results

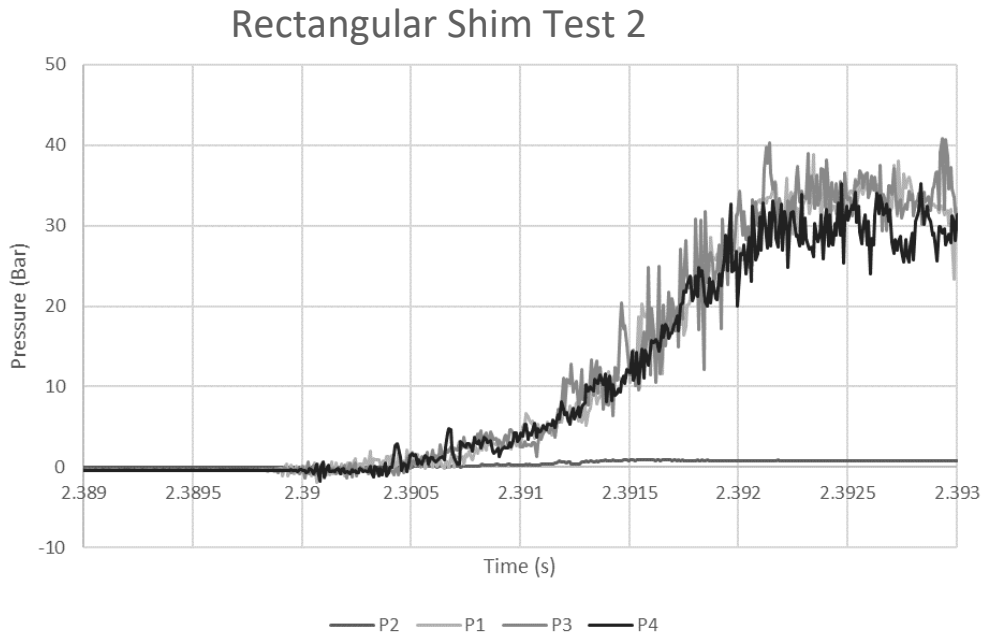


Figure 11. Rectangular Shim Test 2 Results

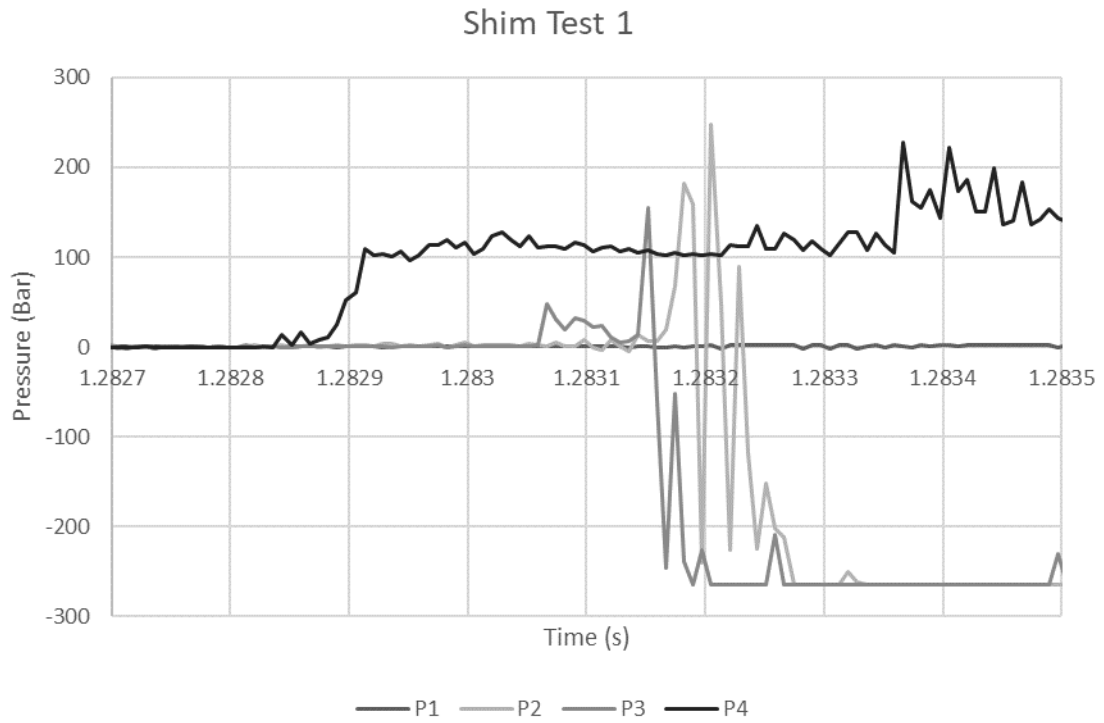


Figure 12. Shim Test 1 Results

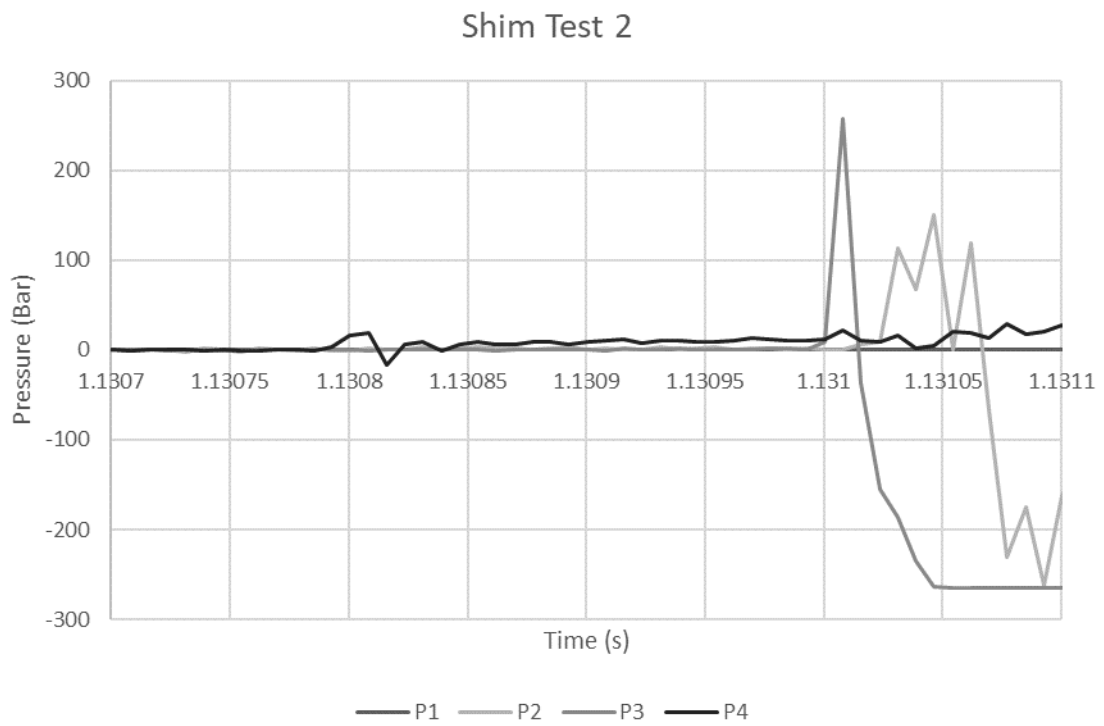


Figure 13. Shim Test 2 Results

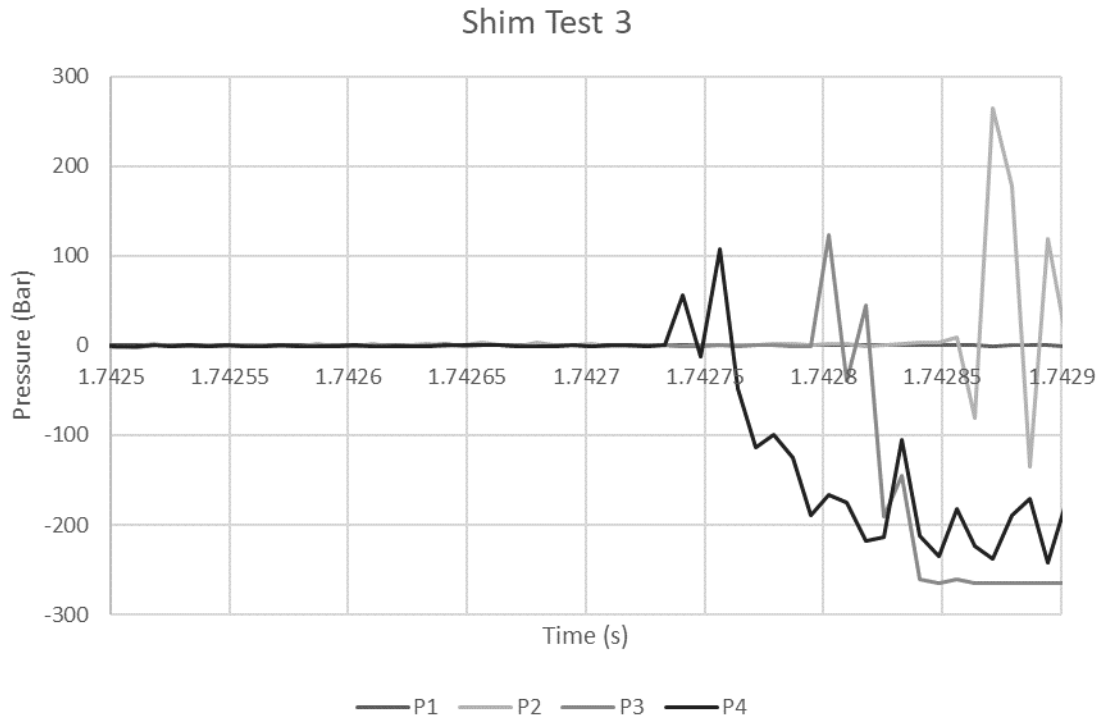


Figure 14. Shim Test 3 Results

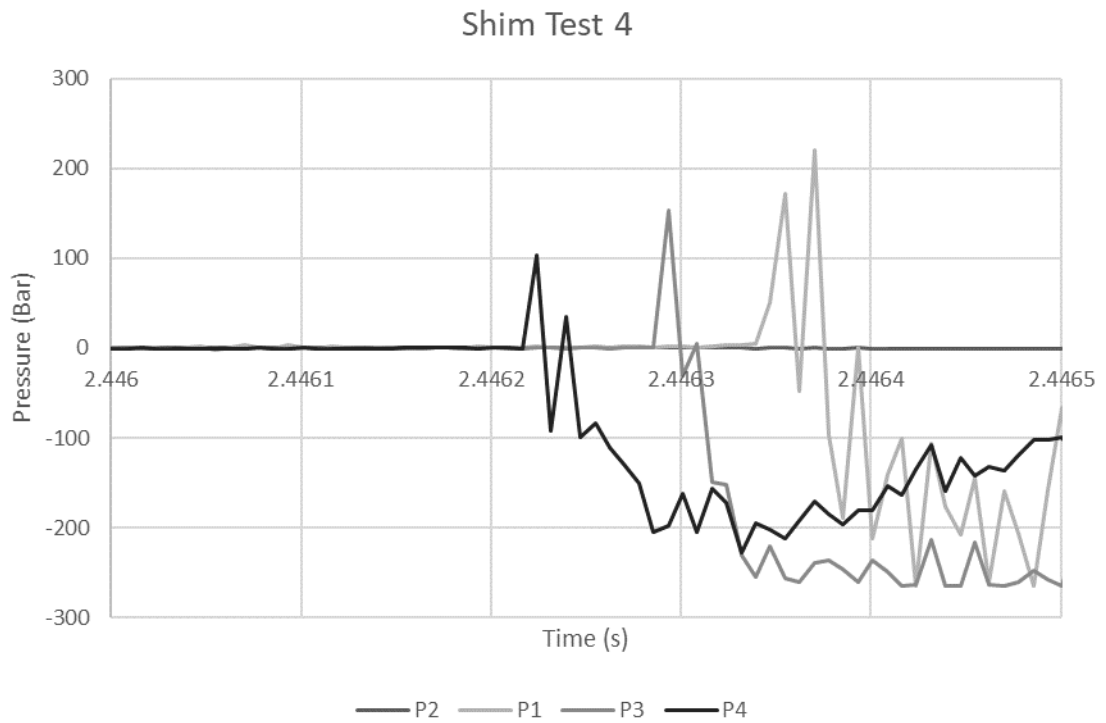


Figure 15. Shim Test 4 Results

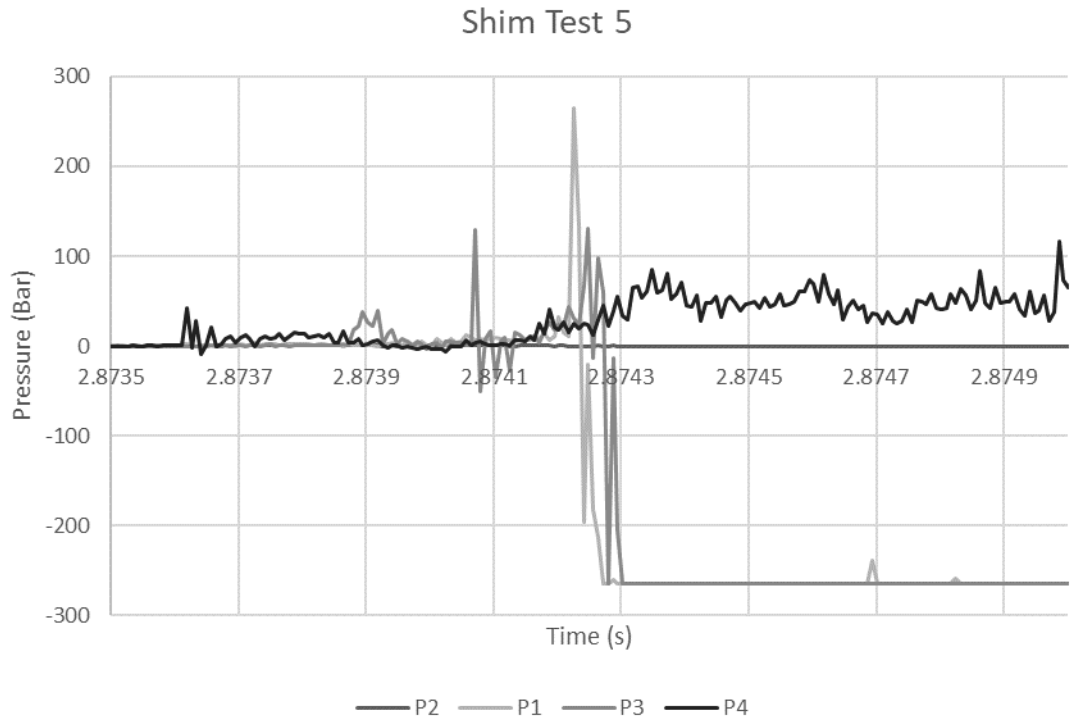


Figure 16. Shim Test 5 Results

All the shim tests ran with the same settings during the experiments. The ratio 3.12:1 Oxygen:Methane was used for these experiments to match general application and the modeling. The pressure of the test was kept at 5Bar but due to an increase of ambient temperature in the chamber from prior test the pressure slightly increased with each subsequent tests. During the testing there were simulations where the shim holder had moved or flipped over as seen in Figure 17. The shims were observed after the test were ran and then replaces with new shims. Figure 18 shows a shim after it had gone through one of the experimental runs. In most of the shim test results, the pressure spikes occur in 1 sample. This means that the sample rate is not high enough to capture the full effect of the pressure. The pressure spikes difference across the pressure transducers vary from 0.0001 to 0.00003 seconds. In the rectangular shim results, the pressure is much lower and has a more gradual pressure increase. This can be due to a different combustion occurring due to the lack of a geometry in the chamber compared to the shim test. In Figure 12 through Figure 16, then the pressure spikes at positive or negative 250 bar, this is the limit of the pressure transducer and the pressure in the chamber is greater than the recorded value.



Figure 17. Shim Test Result



Figure 18. Shim After an Experimental Run

One thing that is noticed from the shim testing is that there is also a force that is also acting on the shim that causes it to not only be partially deburred but also to be bent around the edge of the inner cutout in the shim holder. This force is assumed to be a pressure shock that is driving through the center hole and bending the metal from the high-pressure differential it creates.

Both stoichiometry test were ran with a ratio 2:1 of Oxygen:Methane. There were no parts inside of the chamber during testing. These tests were done to see how greatly the fuel to oxygen ratio effects the pressure readings. When comparing Figure 20 and Figure 10, the stoichiometric model reached a higher pressure. This is expected as the adiabatic flame temperature of the stoichiometric model is higher, as seen in Figure 1.

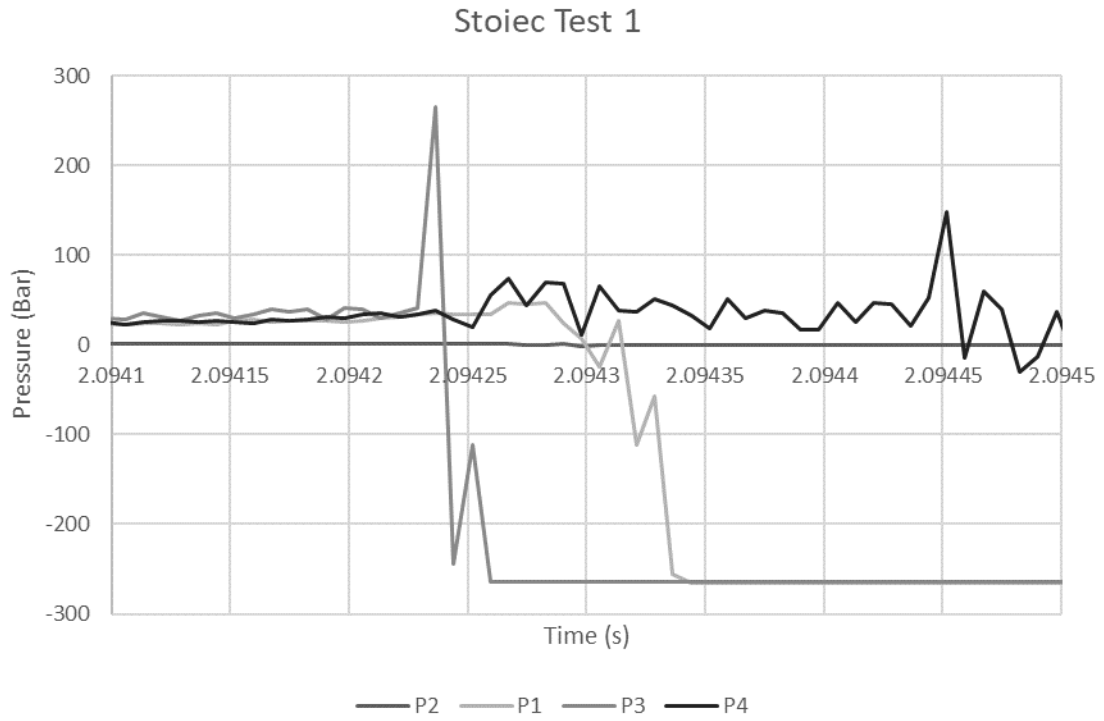


Figure 19. Stoichiometric Test 1 Results

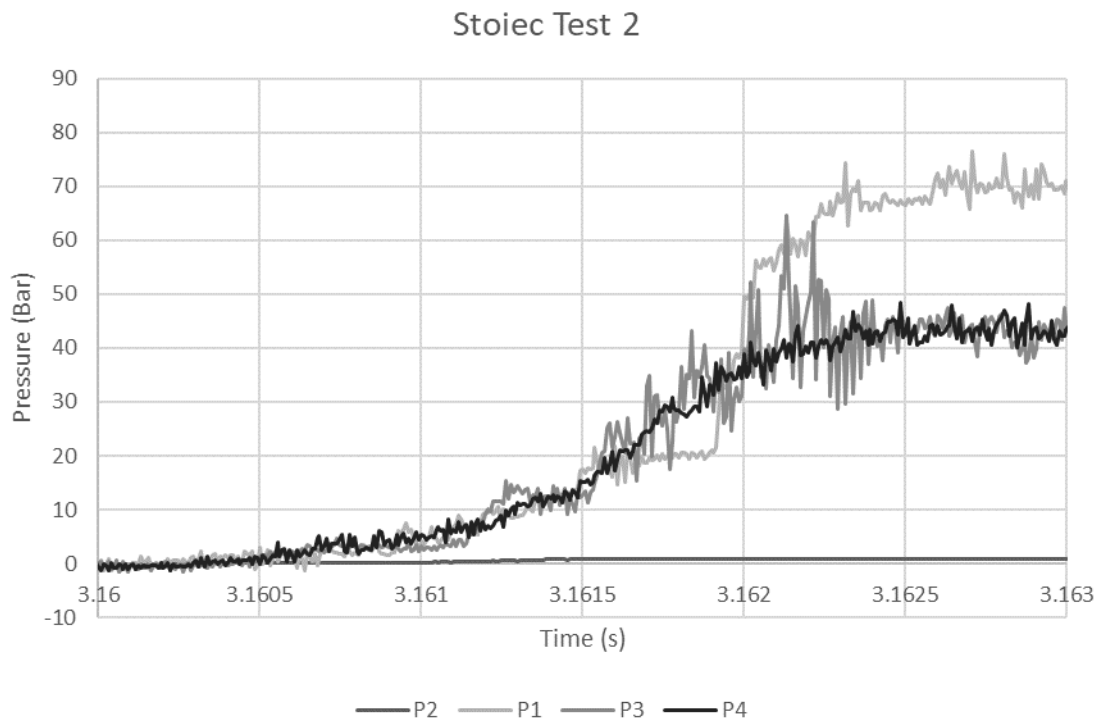


Figure 20. Stoichiometric Test 2 Results

3 Modeling

In this section, all the Ansys Fluent models that were ran are presented in the order that they were ran. All fluent models are 2D axisymmetric to help reduce computation times while still providing accurate results. When making Fluent axisymmetric models the axis of rotation must be on the x-axis. This causes all the models to be rotated 90 degrees compared to the actual chamber.

3.1 Pre-Mixing Block Pipe Flow

For a more accurate simulation of the piping leading to the mixing block the two separate pipes from both methane and oxygen leading into the mixing block were simulated. The pipes diameters are 0.343in and 0.375in for methane and oxygen, respectively. The pipes were modeled to be 10 feet in length to accurately represent the piping of the system. To increase the speed of the calculations 2D axisymmetric models were used.

3.1.1 Mesh

To accurately simulate the highspeed flow, a dense mesh was generated. Near the edge of the walls a small element size was chosen to help capture the effects of the boundary layer. This boundary layer mesh can be seen in Figure 21. The mesh is orthogonal to generate the most accurate results.

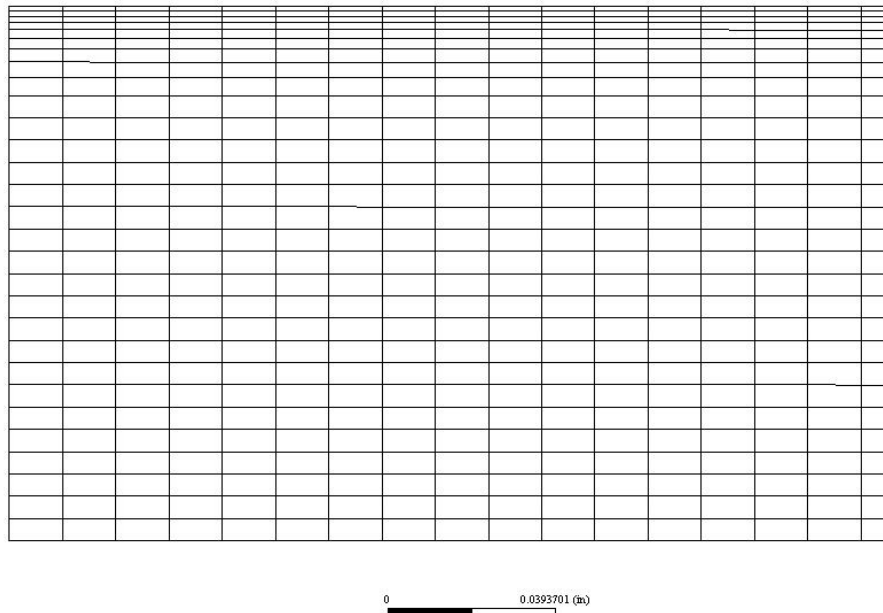


Figure 21. Pipe Mesh

3.1.2 Boundary Conditions

Based on the flow rate of 900L/min, given by the company, along with the known pipe diameters and the volumetric ratio of 3.12:1 $O_2:CH_4$, the velocity inlet speed was calculated. The volumetric ratio of the fluids was converted to mass fractions. This is due to Fluent requiring inlet conditions being in terms of mass fraction. The mass fraction conversion can be seen in Table 3. The velocity of both fluids was found by

taking the mass fractions of the mixture and applying it to the mixtures mass flow rate. These values can be seen in Table 4 and Table 5.

Table 3. Mass Fraction Conversion

	% Vol	g/mol	g/mol air	mass %
O2	3.12	32	99.84	0.861559
CH4	1	16.043	16.043	0.138441

Table 4. Mass Transfer

\dot{m}	\dot{m}_{O_2}	\dot{m}_{CH_4}	
0.084894	0.073141	0.011752861	kg/s
\dot{V}	\dot{V}_{O_2}	\dot{V}_{CH_4}	
0.014992	0.011368	0.003623847	m ³ /s

Table 5. Velocity Calculations

	Flow Rate m ³ /s	Radius in	Radius m	Area m ²	Velocity m/s
Oxygen	0.011368	0.1875	0.004763	7.12557E-05	159.5346
Methane	0.003624	0.171875	0.004366	5.98746E-05	60.52393

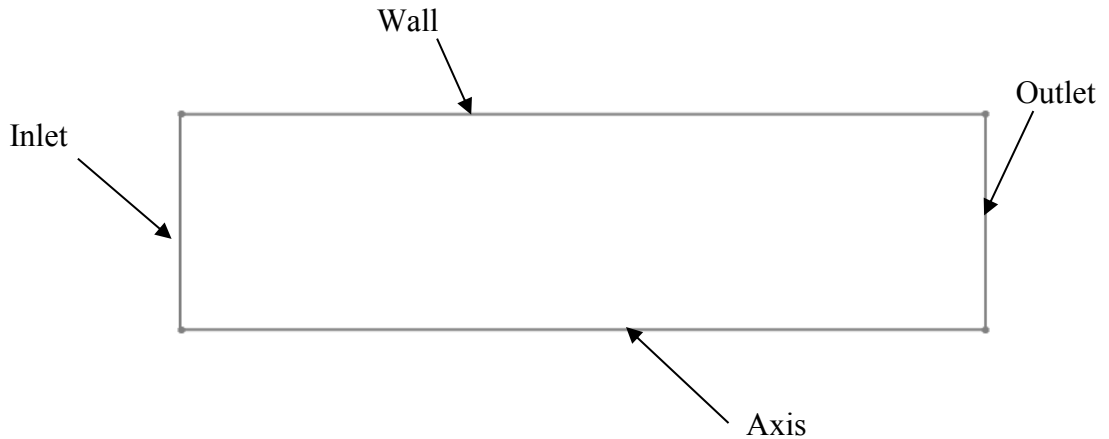


Figure 22. Pipe Model Boundary Conditions (Not to Scale)

Table 6. Pipe Boundary Conditions

Boundary	Value
Velocity Inlet	Fluid Speed
Pressure Outlet	0 Gauge Pressure
Wall	No Slip
Axis	Axis

3.1.3 Variable Properties

In both the pipe model and flow model, variable fluid properties were used. These values are critical in generating more accurate results in the simulations. The List of equations can be seen in Appendix A.

3.1.4 Pre-Mixing Block Pipe Flow Results

The model was used to calculate the temperature of the feed gases in the entry tube before the mixing block, with the center line temperatures as shown below.

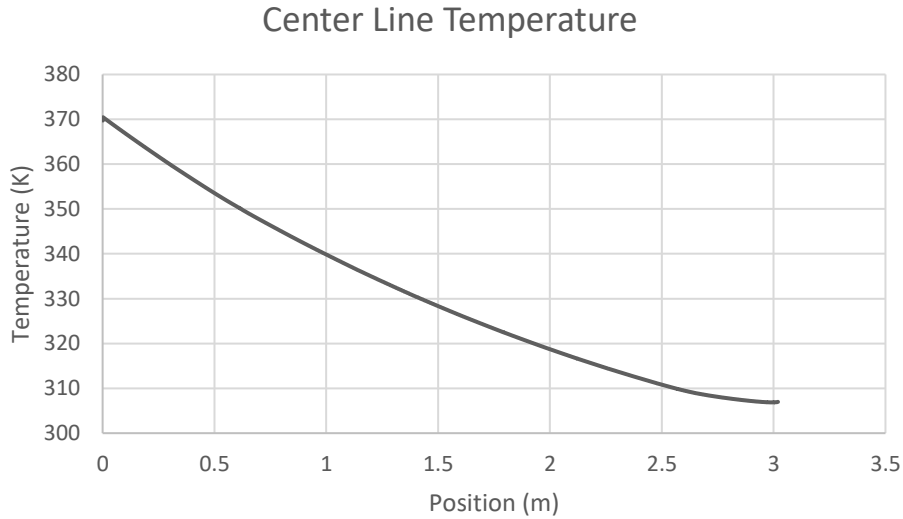


Figure 23. Oxygen Temperature Across the Pipe

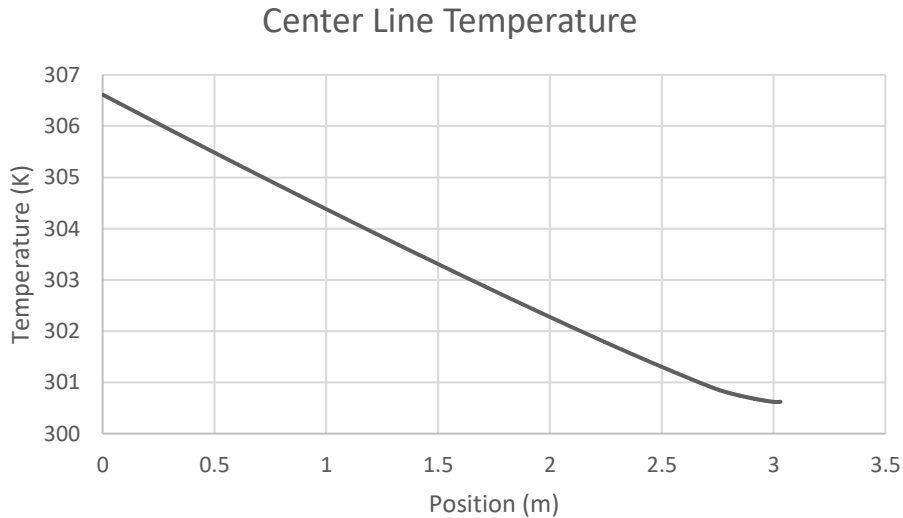


Figure 24. Methane Temperature Across the Pipe

Due to the higher speed of the oxygen, the temperature of the oxygen increased by almost 70 K while the methane only increased by approximately 7 K. To get the temperature of the mixture after the mixing block, an energy balance was performed using Equation 6.

The results can be seen in Table 7. The velocity after the mixing block can be seen in Table 8.

$$\sum \dot{m}c_pT = [\dot{m}c_pT]_{combined} \quad 6$$

Table 7. Tabulated Temperature Calculation

	\dot{m} (kg/s)	c_p (kJ/g K)	T (K)
o2	0.073141	942.6747	376.31745
ch4	0.011753	2268.439	306.896
combined	0.084894	1264.462	317.9319843

Table 8. Tabulated Velocity Calculation

Flow Rate	Radius		Area	Velocity
m^3/min	in	m	m^2	m/s
0.9	0.125	0.003175	3.16692E-05	473.6461

3.2 Axisymmetric Flow Model

Prior to running the combustion model, the flow model was ran to simulate the filling and stagnation of the fluid in the chamber. With a known time of 2 seconds prior to detonation, the flow within the chamber can be modeled to determine if there is any fluid motion at the time of detonation. If there is still motion, then the model will be used as the initial condition to the combustion model to get a more accurate effect. To allow the simulation to be performed in a 2D axisymmetric model, the entry pipe was placed vertically rather than having a 90 degrees bend. This is due to the fact an angled pipe will create a disk rather than a pipe when rotated around the symmetry axis.

3.2.1 Axisymmetric Flow Model Mesh

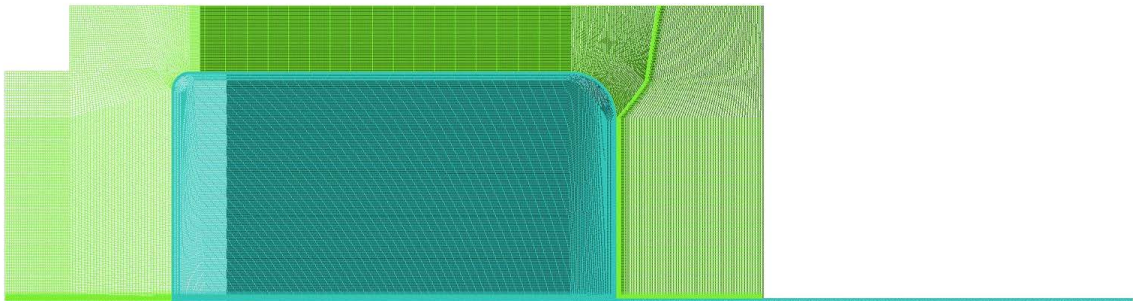


Figure 25. Axisymmetric Model

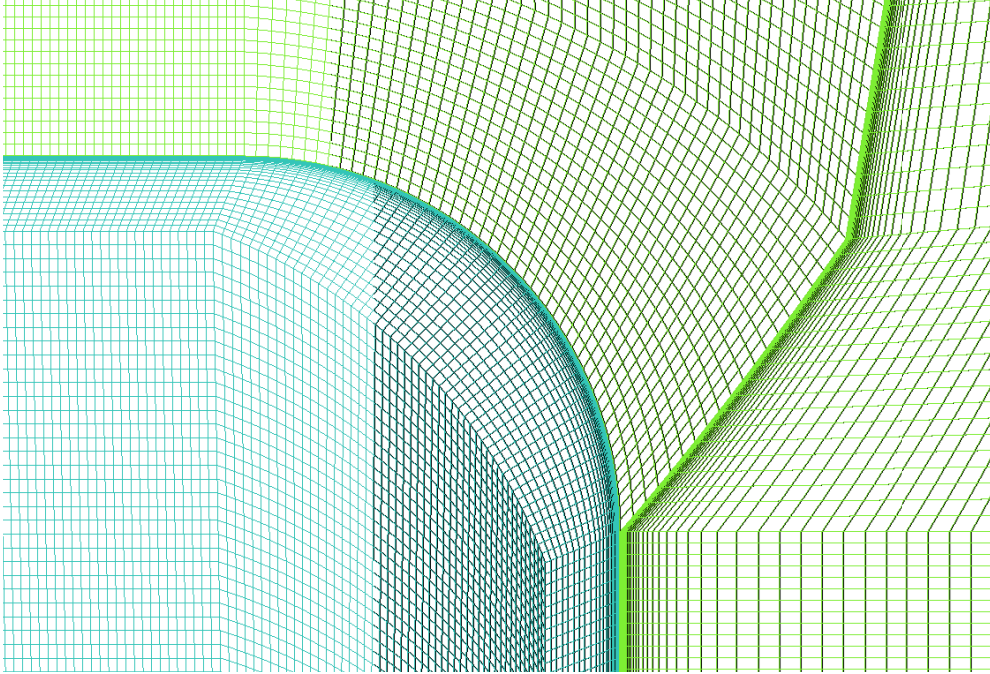


Figure 26. Axisymmetric Model Large Fillet

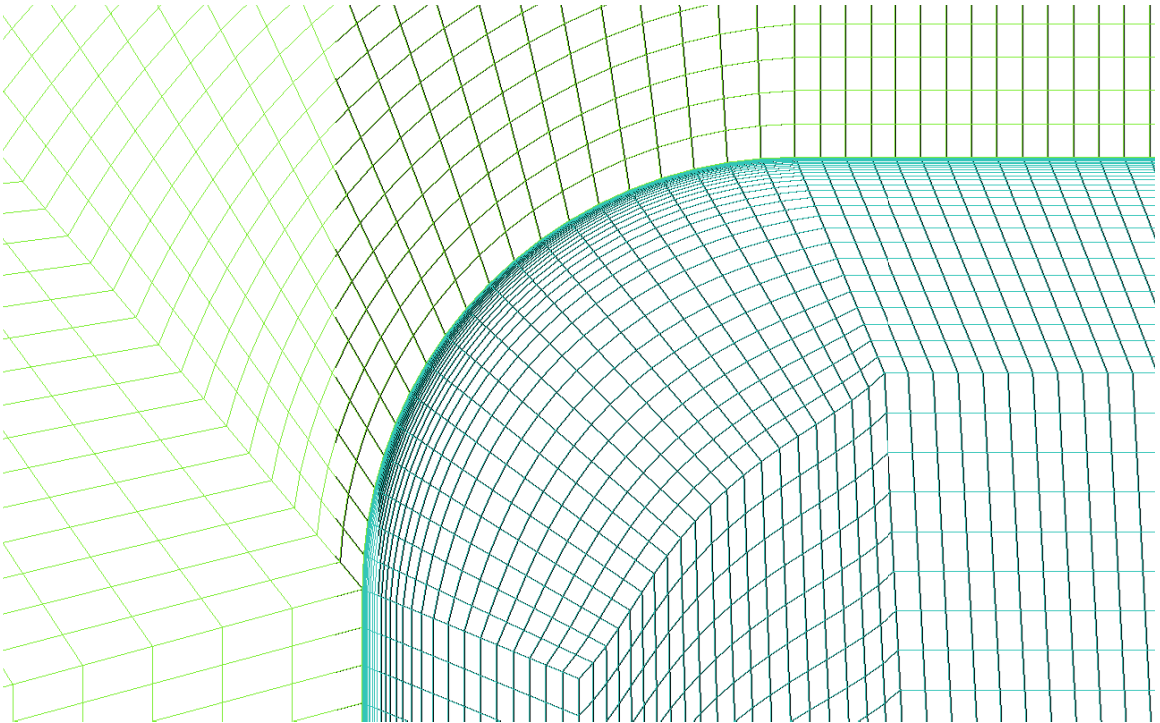


Figure 27. Axisymmetric Model Small Fillet

3.2.2 Axisymmetric Flow Boundary Conditions

Using these boundary layer profiles is critical because the flow is developed at the inlet, providing more accurate results. An outlet is not used in this model due to it being a pressure vessel. The boundary conditions can be seen in Figure 28 along with their values in Table 9.

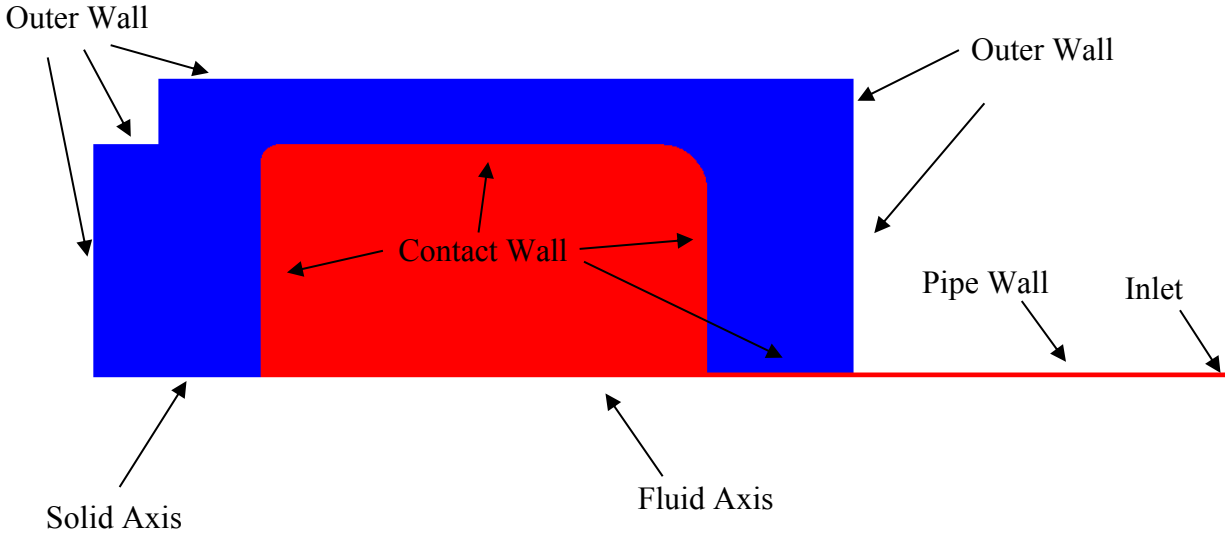


Figure 28. Axisymmetric Model Boundary Conditions

Table 9. Axisymmetric Boundary Conditions

Boundary	Value
Outer Wall	Wall
Pipe Wall	No Slip
Contact Wall	No Slip, Coupled
Solid Axis	Axis
Fluid Axis	Axis
Inlet	Velocity, Temperature, Mass Fraction Profile

To correctly run the model the variable density of the mixture had to be changed from a mixing law to an ideal gas. With the ideal gas density, fluent can add moles of the mixture into the system and increase the pressure. If the density is based only on temperature as a polynomial function, the moles coming into the system are ignored. All other fluid properties were set to be variable with temperature and the mixtures properties were calculated based on volume percentage. The ideal gas model for density corrected many issues that were arising in the fluid flow such as the pressurization not being dependent on the time step. This meant that no matter how large the time step was, the pressure would always increase the same amount.

3.2.3 Axisymmetric Flow Results

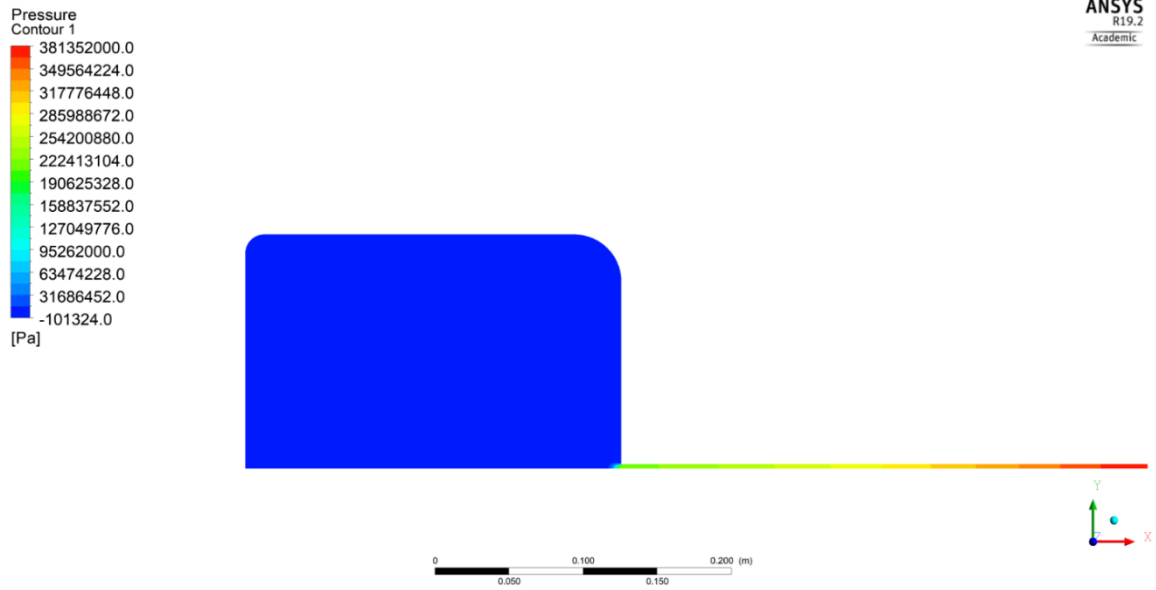


Figure 29. Static Pressure Contour

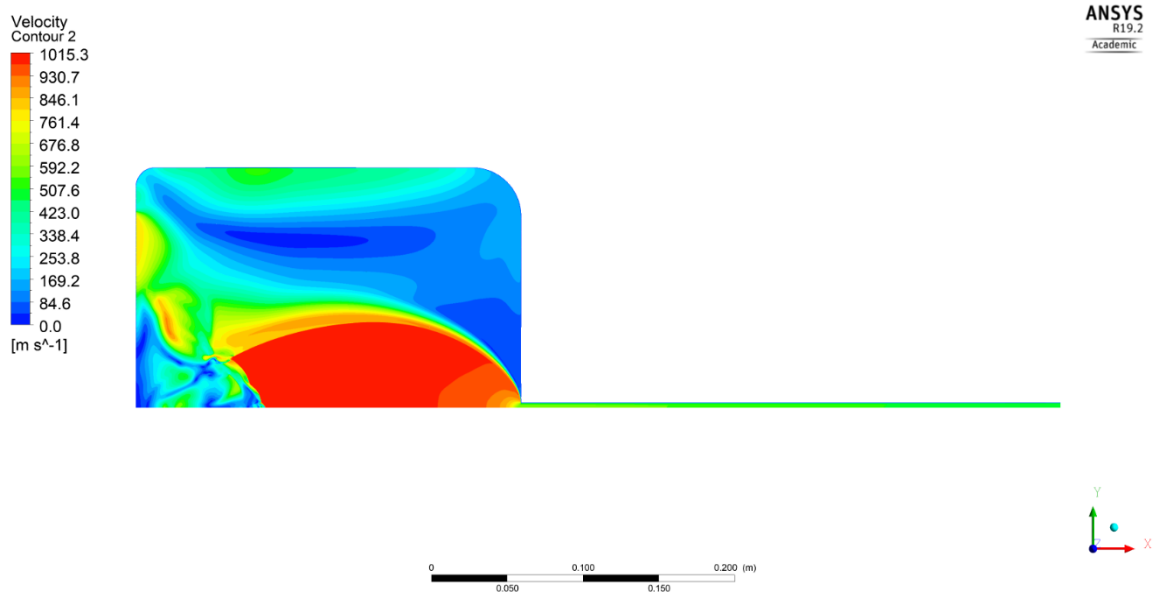


Figure 30. Velocity Contour

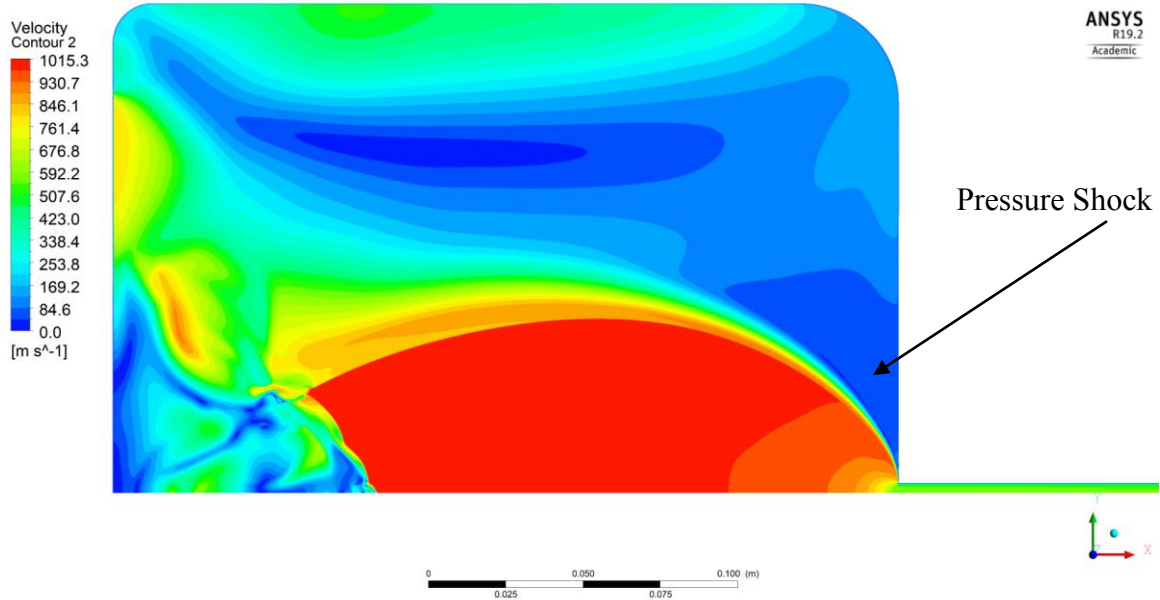


Figure 31. Velocity Contour of Chamber

A pressure shock can be seen occurring as the flow enters the chamber. This is expected from the supersonic flow and it creates a Mach Disk which is also observed when jets exhaust into atmosphere, seen in Figure 31. The pressure shock near the end is not what would be expected in a Mach Disk. This is due to pressure build up occurring at the bottom wall of the chamber.

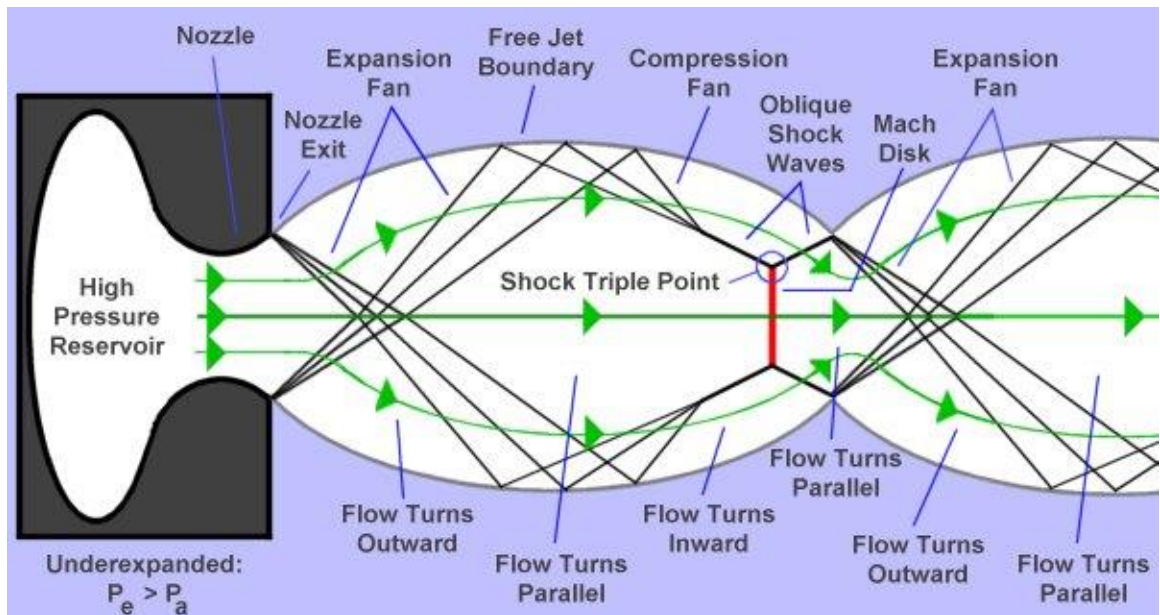


Figure 32. Mach Disk [11]

Figure 32 shows a simplified jet engine exhaust. The flow observed in the chamber is similar to this flow with the major difference being at the end of the Mach disk. In the case of the jet engine exhaust, the flow is going into an open atmosphere so there is no

pressure build up. In Figure 33, the Mach disk can be seen but with deformations occurring due to the effects of the chamber bottom wall.

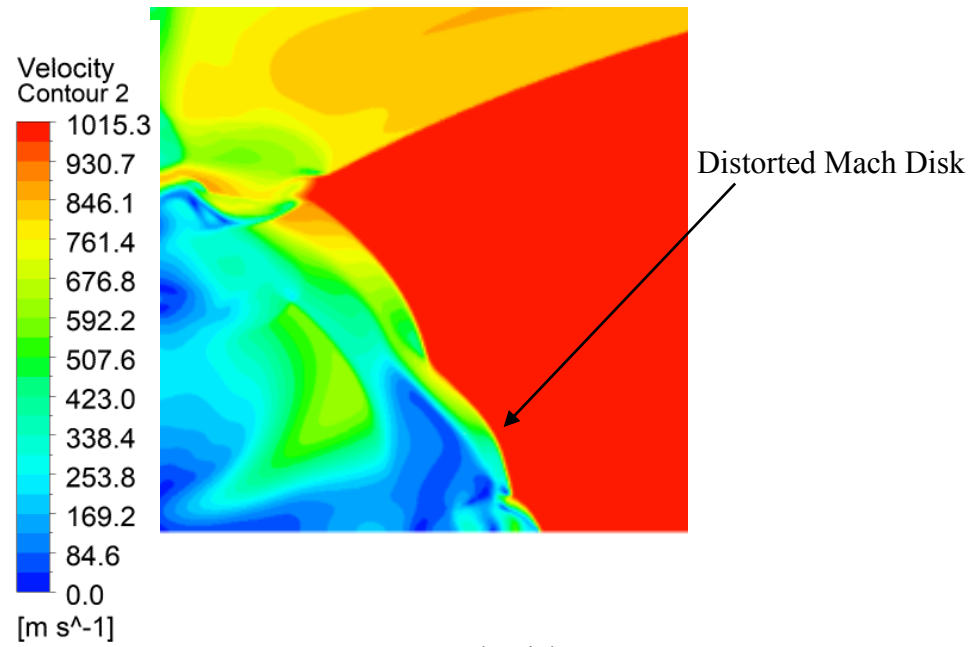


Figure 33. Mach Disk

Pressure
Contour 1

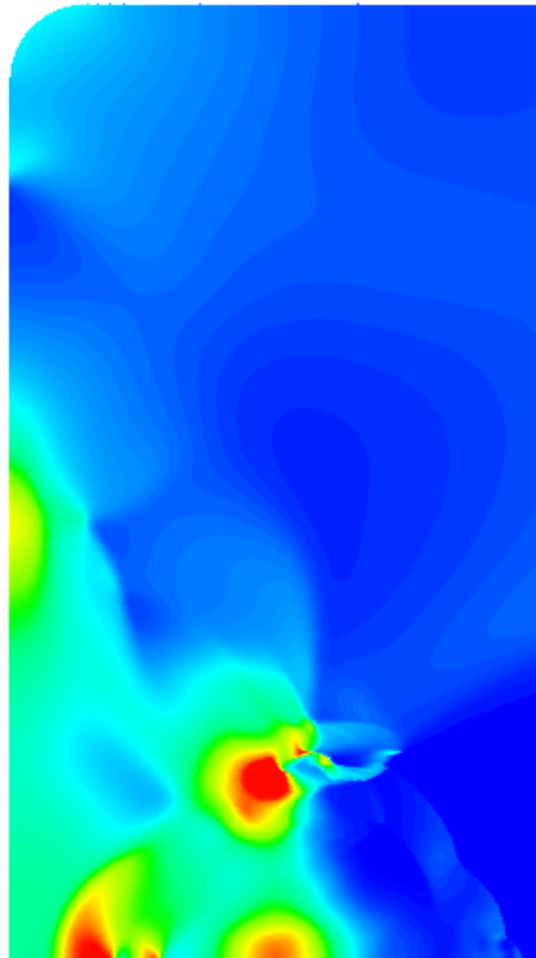
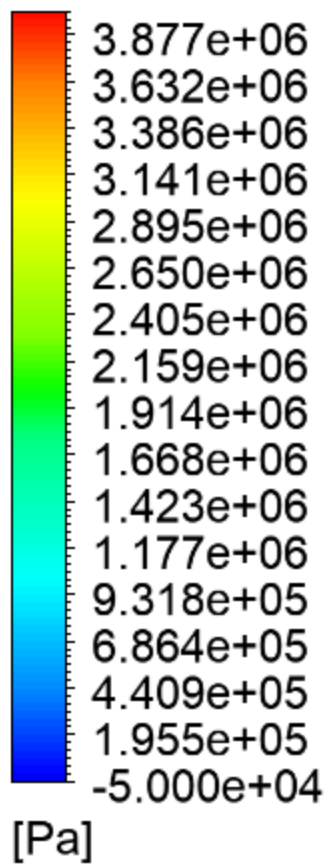


Figure 34. Pressure Build Up

The Mach Disk not forming properly in Figure 33, is due to the pressure buildup that is forming along the center bottom wall. Figure 34, shows the pressure buildup forming at the bottom center wall. As you move further away from the center location you can see the pressure is dropping drastically. The high pressure in the center is due to the moving fluid impacting the wall, while when moving further away from the center location the fluid is no longer directly impacting the wall which results in much lower pressures.

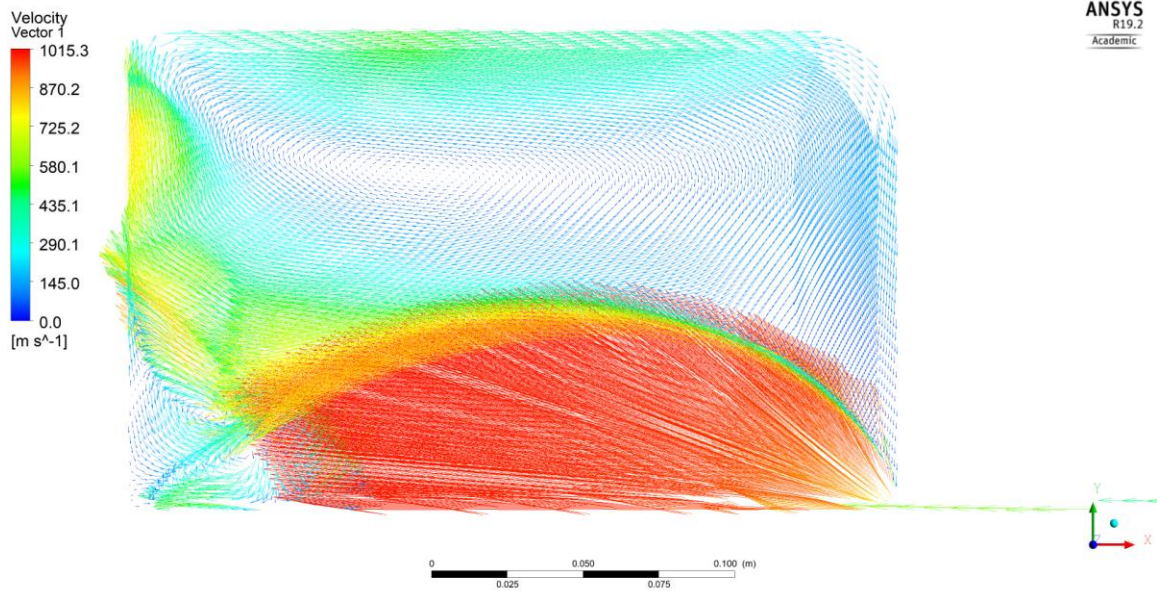


Figure 35. Velocity Vectors

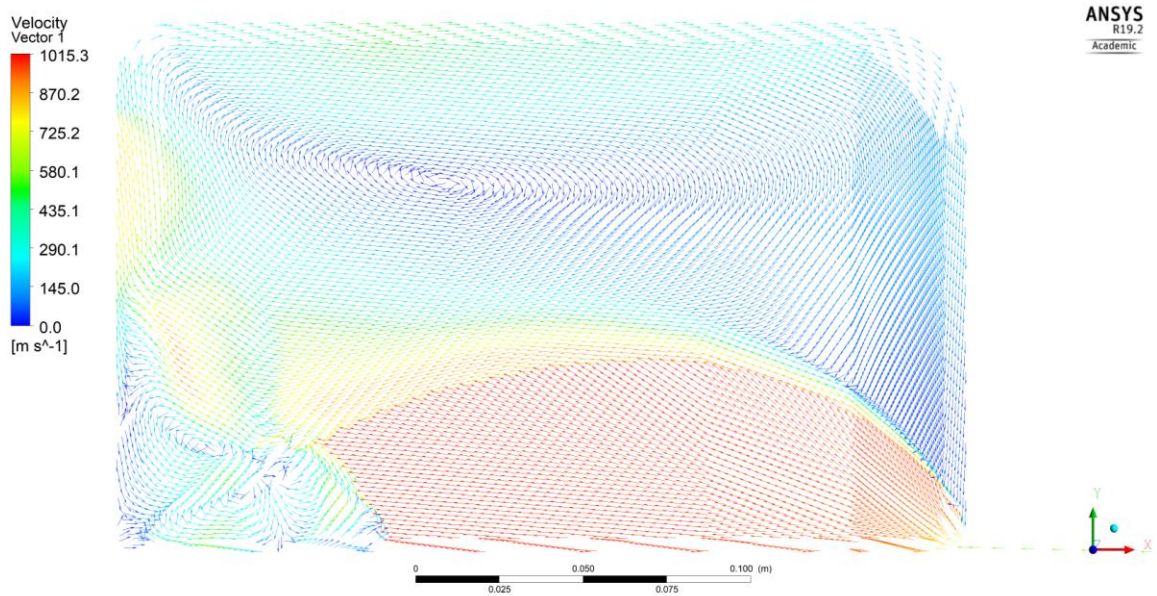


Figure 36. Normalized Velocity Vectors

When looking at velocity vectors, the recirculation in the chamber can be observed. The flow is acting as an impinging jet flow causing the air flow to spread out from the center and wrap around the walls until it reaches the inlet flow. This type of circulation is expected due to the high speeds of the mixture.

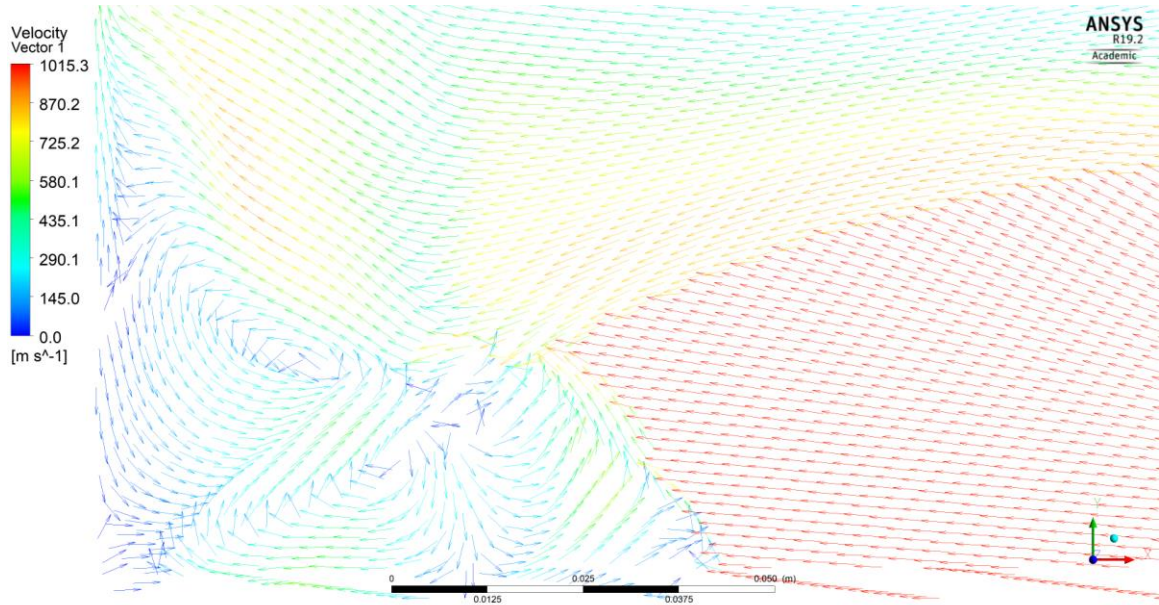


Figure 37. Normalized Velocity Vectors Critical Region

In the region between the shock and the wall the flow has high circulation. This is due to the pressure building up at the wall causing the flow to shock. Once the flow shocks there is high circulation that occurs naturally.

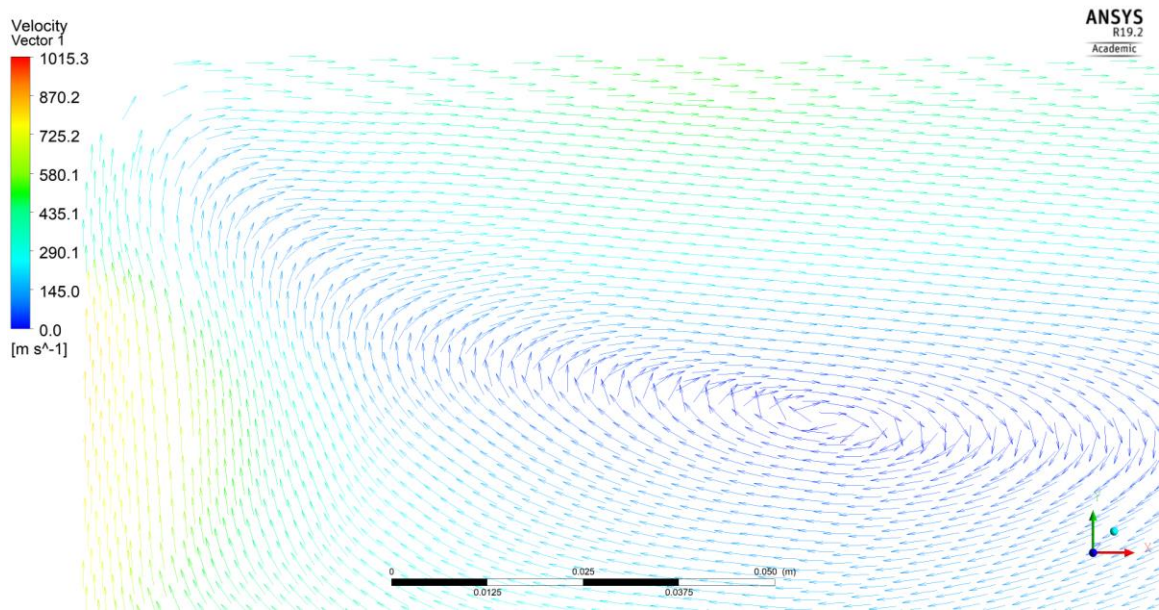


Figure 38. Normalized Velocity Vectors Recurlation Region

The flow as it gets further away from the shock is not as chaotic. The circulation is not centered but rather closer to the bottom of the chamber. This is due to the much higher speeds that are occurring at the bottom of the chamber versus the slower speeds that are at the top of the chamber. It was determined that the flow model was not needed for the combustion as the final velocity in the chamber was magnitudes lower than that of the

pressure shock. To introduce the flow into the chamber prior to combustion also increases computation time. This can be done in future work to determine the best resting time for the flow.

3.3 Combustion Model Test 1

A simplified combustion model was created to test the settings for the software. The combustion model is using a more complex turbulence model to properly calculate the flame propagation. While the flow model did not need this model, to properly run a combustion based off the flow results, the model needs the terms from the more complex turbulence model. The combustion model Test 1 was much smaller than the actual combustion chamber being just 2in by 4in.

3.3.1 Combustion Testing Boundary Conditions

The model was made as just the fluid domain. All the boundary conditions except the axis of rotation are set as walls.

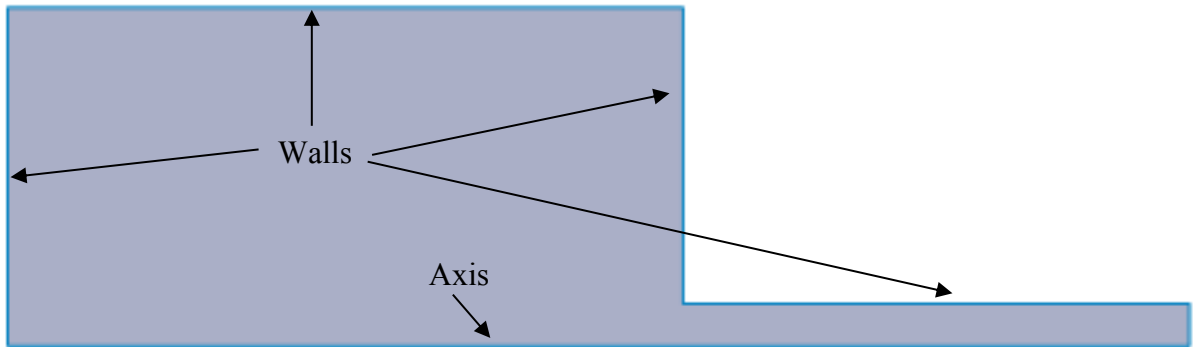


Figure 39. Combustion Model Test 1 Boundary Conditions

3.3.2 Combustion Testing Mesh

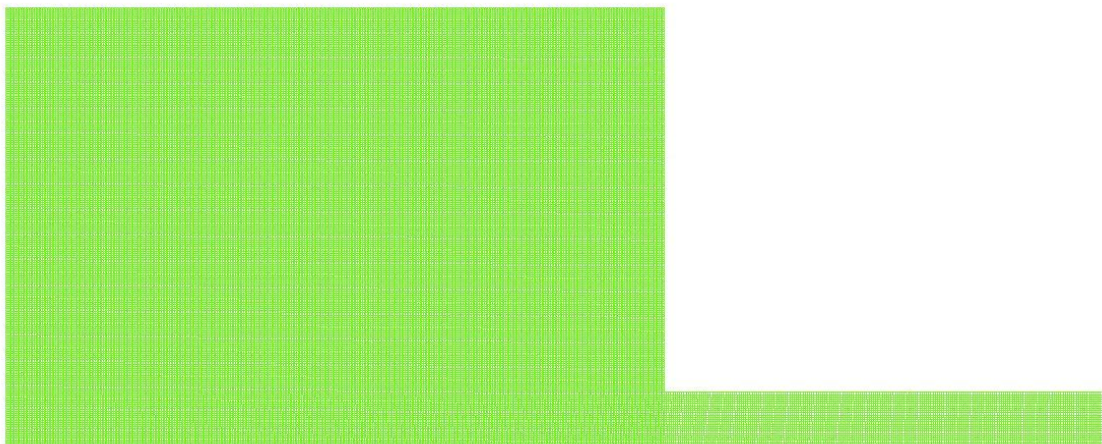


Figure 40. Combustion Model Test 1 Mesh

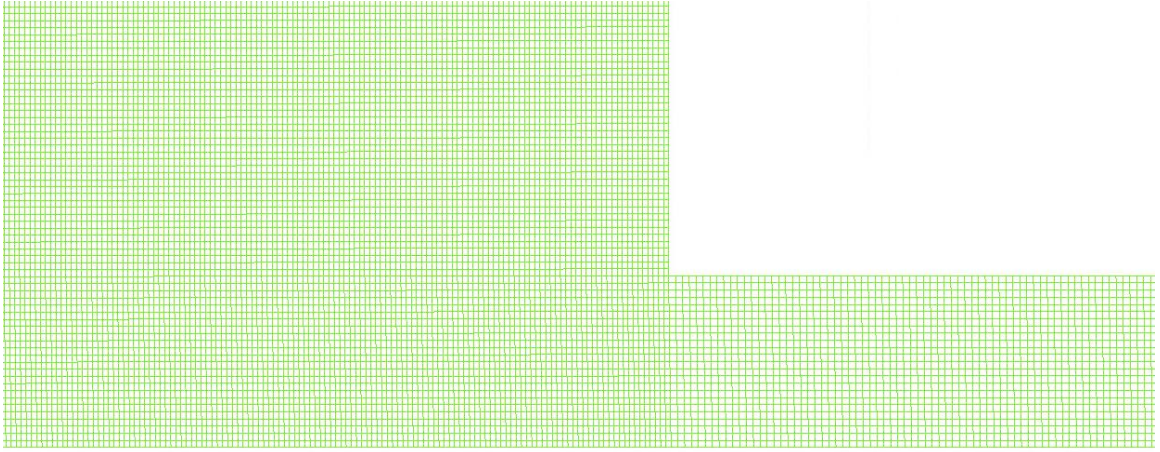
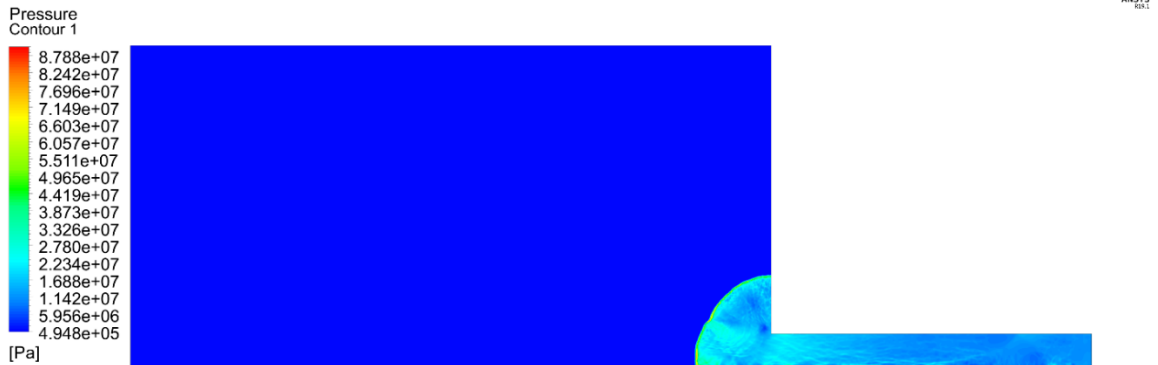


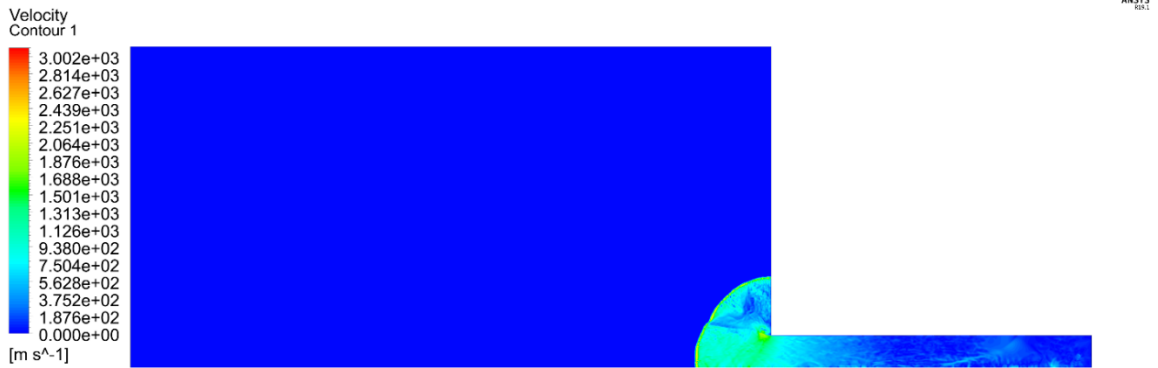
Figure 41. Combustion Model Test 1 Mesh Closeup

3.3.3 Combustion Testing Results

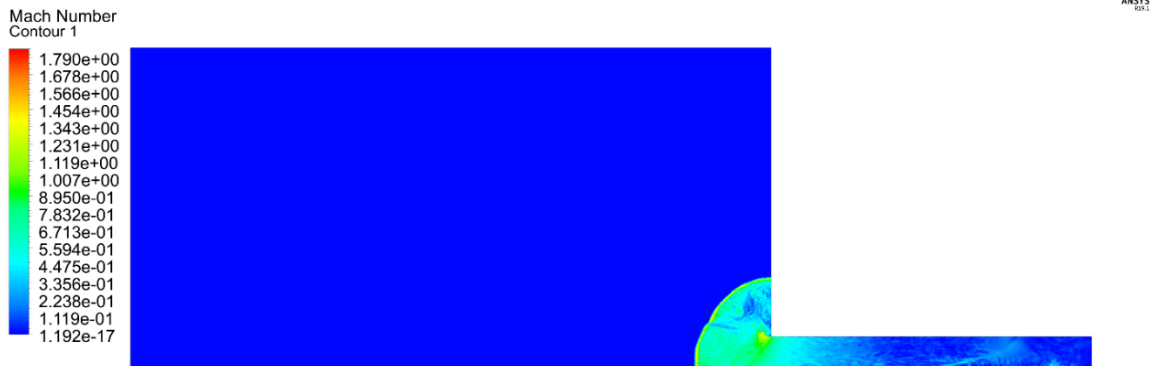
The flow when exiting the pipe has a high speed compared to the area beside it. This is due to the combustion flame forcing the fluid out of the pipe as it has nowhere else to go. As the combustion spreads/ in the chamber, the flame front starts to get separated. This can be seen in Figure 44. This separation is due to the flame moving faster than normal from the high-speed exiting flow.



(a)



(b)



(c)

Figure 42. Simple Combustion Results Pressure (a), Velocity (b), Mach Number (c)

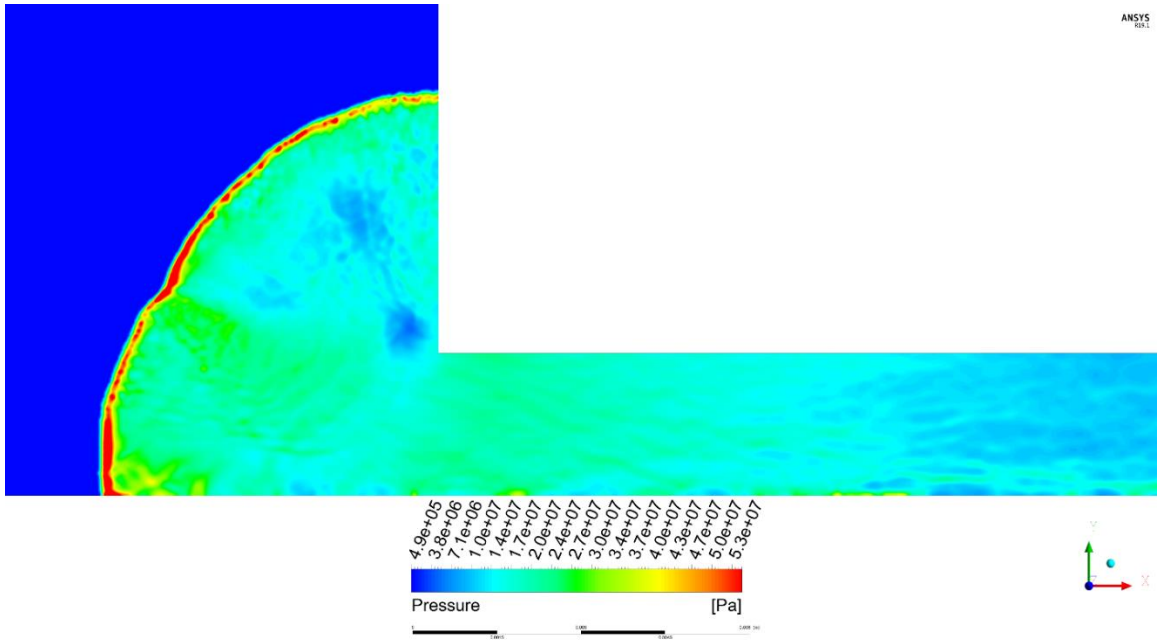


Figure 43. Combustion Pressure Contour

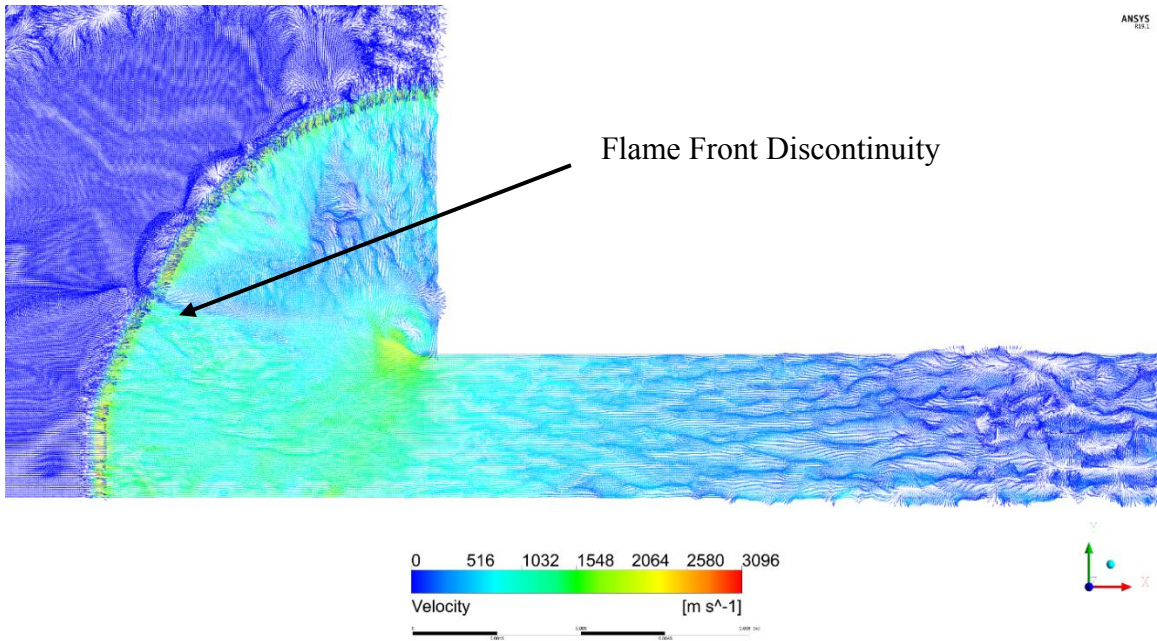


Figure 44. Combustion Velocity Vectors

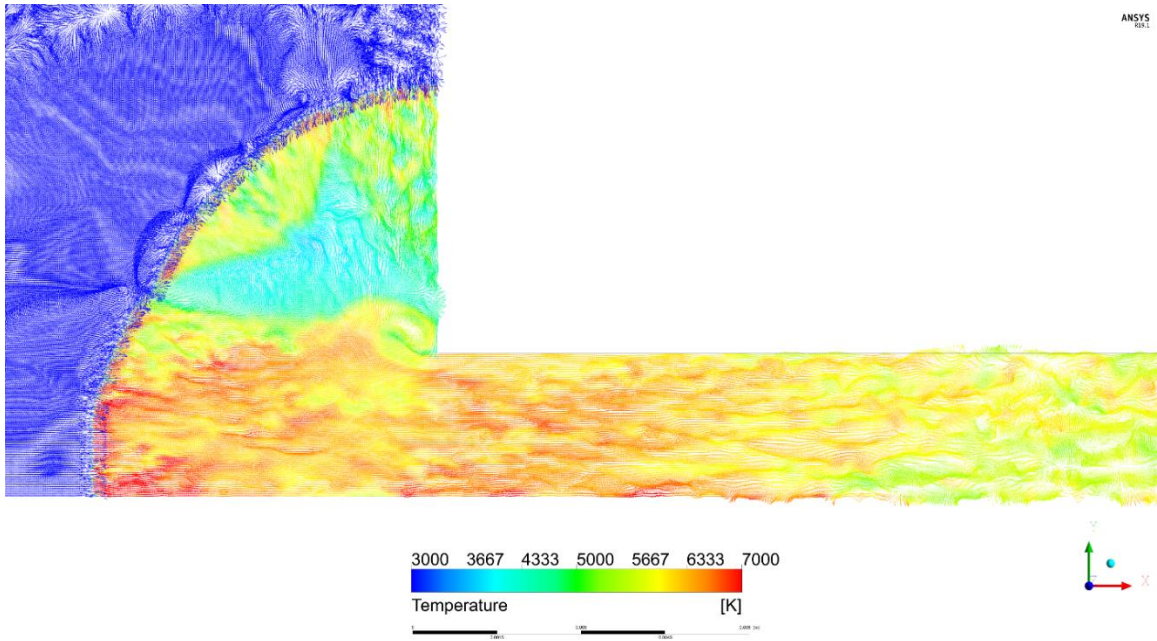


Figure 45. Combustion Model Temperature

The temperature in the model, Figure 45, is higher than expected. This is due to the model being small but ran with a high initial pressure. The cold spot is occurring due to a pressure shock that forms from the opening. Most of the heat is in the center position. This is due to the buildup of heat as the combustion went through the pipe. Due to there being nowhere for the heat to go, it was propagated down the pipe and into the chamber.

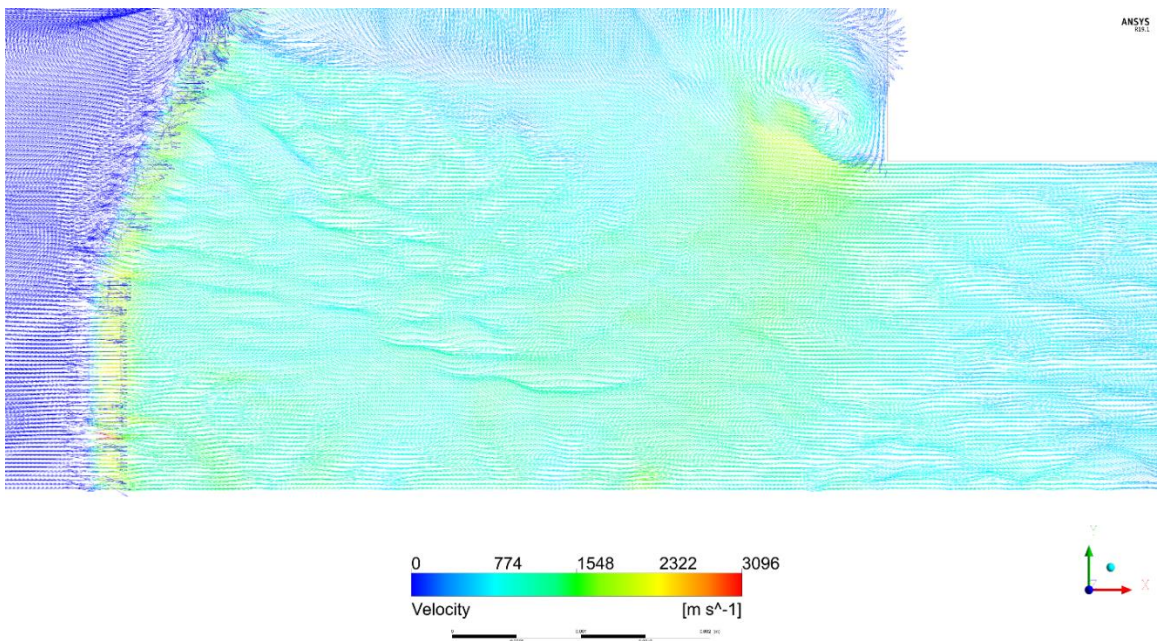


Figure 46. Velocity Vector Exiting Pipe

An expected recirculation occurs at the exit of the pipe due to there being a sharp corner. The recirculation can be another cause for the shock and colder temperatures that are observed in Figure 45.

3.4 Combustion Model Test 2

More tests were performed to further improve the settings of the combustion model, the geometry of the chamber. In these tests the effects of the pipe entering the chamber were observed. Two separate geometries were made, one with the inlet pipe and one without the inlet pipe. Both were run with identical settings so the results can be compared.

3.4.1 Combustion Model Testing 2 Boundary Conditions

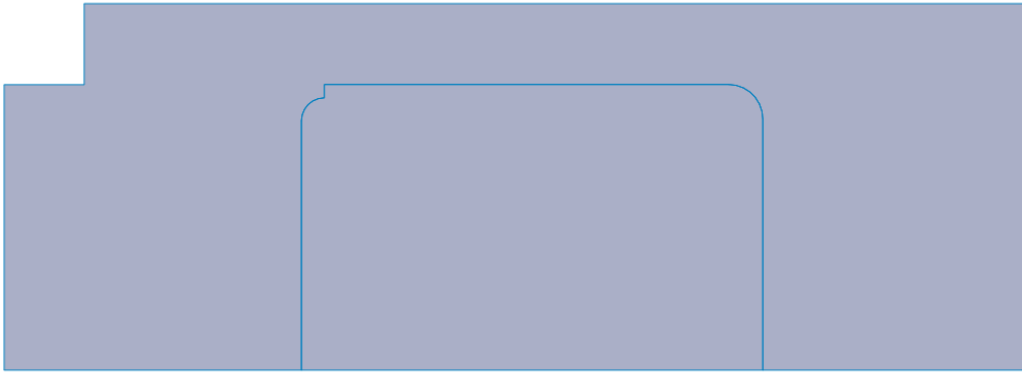


Figure 47. Combustion Model Test 2 Boundary Conditions

3.4.2 Combustion Model Testing 2 Meshes

The fluid domain of the model was meshed with a high density to account for the high speeds of the pressure shock. The mesh density of the solid is much lower as only heat transfer will be happening through the solid. The orthogonality of the mesh was kept as close to 1.0 as possible but due to geometry some locations have lower mesh quality.



Figure 48. Combustion Model Test 2 Mesh

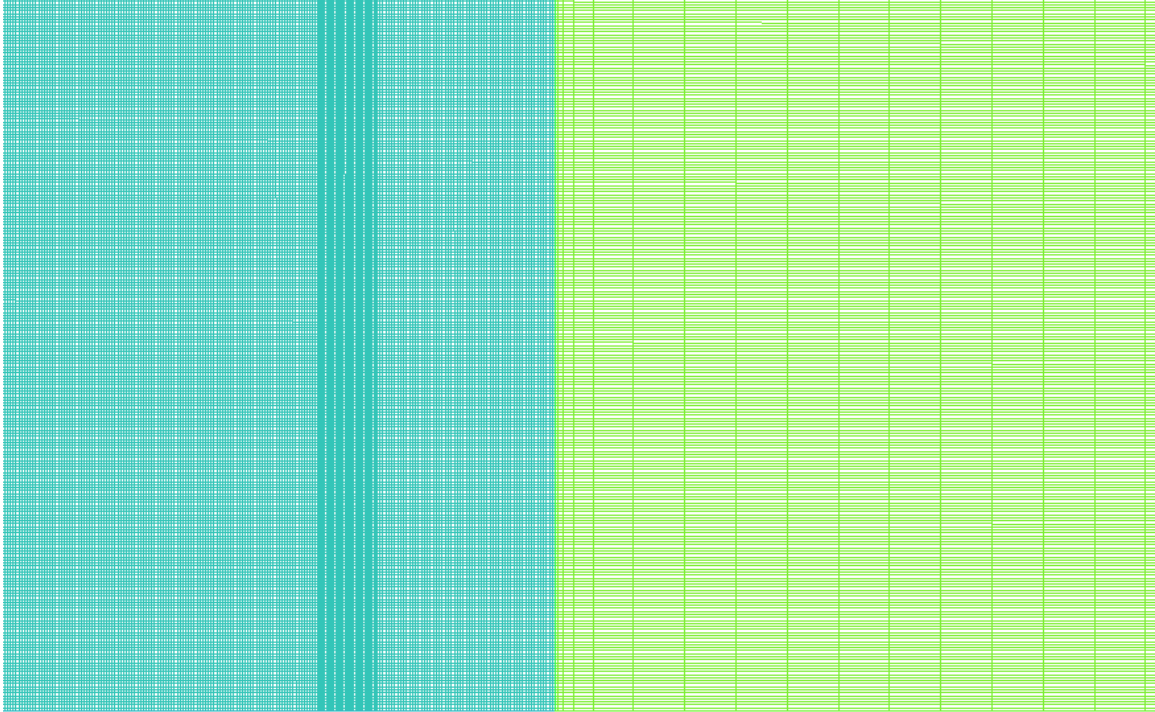


Figure 49. Combustion Model Test 2 Mesh Wall Contact

This location is one of the walls where the fluid and solid domain meet. The mesh sizing across domains was matched but as the solid domain moves further from the fluid domain the sizing of the elements increases. This is done as heat transfer is not affected as greatly from element size as fluid flow is. All mesh elements in these regions along with most of the domains have high orthogonality values. Figure 50 has one of the regions with a lower orthogonality.

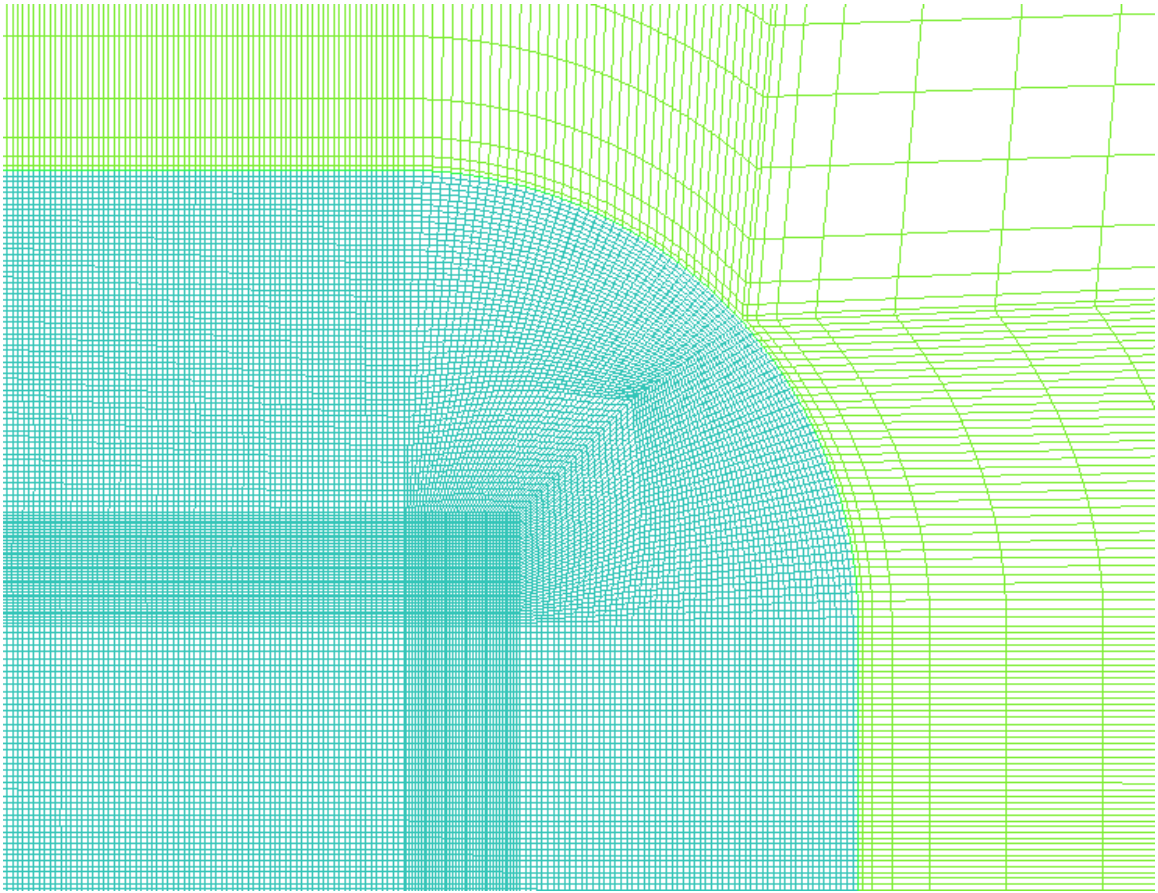


Figure 50. Combustion Model Test 2 Mesh Curved Surface

The location of the lowest quality of elements occurs at the curved surfaces. Due to the higher density mesh in the fluid domain the quality is higher than that of the solid domain. Though this region of mesh is lower quality, it still exceeds a quality value of 0.6.



Figure 51. Combustion Model Test 2 Pipe Mesh

The meshing parameters between the two models were kept identical in all possible locations. Due to the addition of the inlet pipe which requires a higher mesh density, a portion of the solid had a mesh density increase.

3.4.3 Combustion Model Test 2 Results

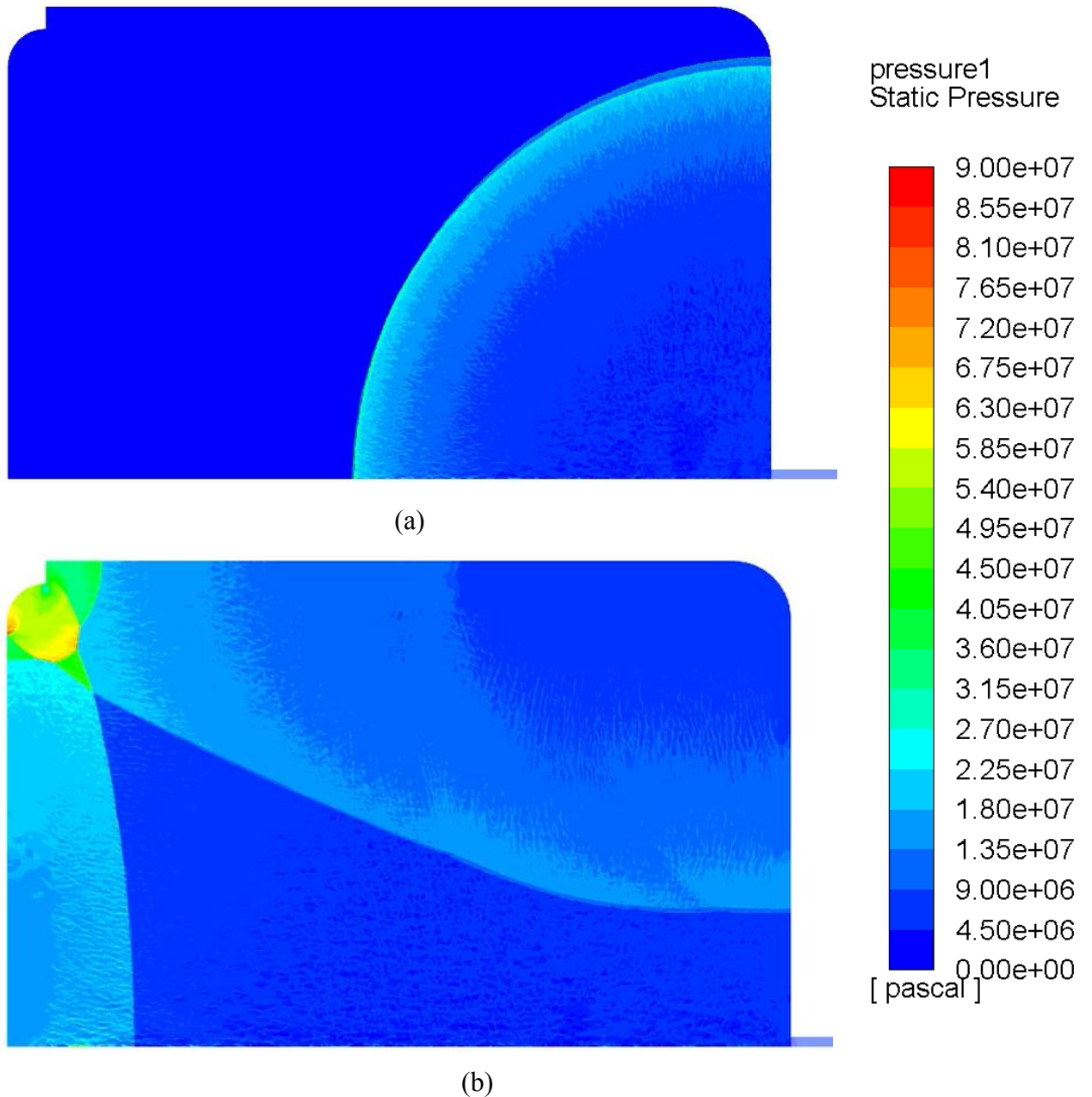


Figure 52. Results from Combustion Test 2 for Both Pipe and No Pipe Models at timestep 8000 (a), 12500 (b)

At both instances captured, the pressure shocks from both the pipe and no pipe model can be seen at near identical locations. The slight variation in the shock is due to placement of the spark in the no pipe model. The sparks location is slightly lower than the top of the model and is on the x-axis. From these models it is concluded that the pipe is not needed in the geometry as it has little to no effect on the resulting pressure shock formation but doubles the computation time needed to run the model. For all future models, the pipe will not be included into the geometry for the decrease in total computation time.

3.5 Combustion Model 1 (Normal Model)

This initial model of the combustion was performed using the settings found in the combustion testing model 1 along with the geometry findings of the combustion model testing 2. This model was run with initialization settings to simulate the experimental testing. This was done to generate data that is comparable to the experimental results. The initialization setting can be seen in Table 10.

Table 10. Combustion Model 1 Initialization Values

NORMAL MODEL	
PRESSURE (PA)	500,000
TEMPERATURE (K)	300
O2 (% MASS)	0.737651
CH4 (% MASS)	0.111056

3.5.1 Combustion Model 1 Boundary Conditions

The model is composed of two different surfaces to represent the fluid and solid domain. All contacts lines between the domains are walls along with the outer region of lines for the solid domain. Both the solid and fluid domain have their own axis lines that are used for rotation in fluent.

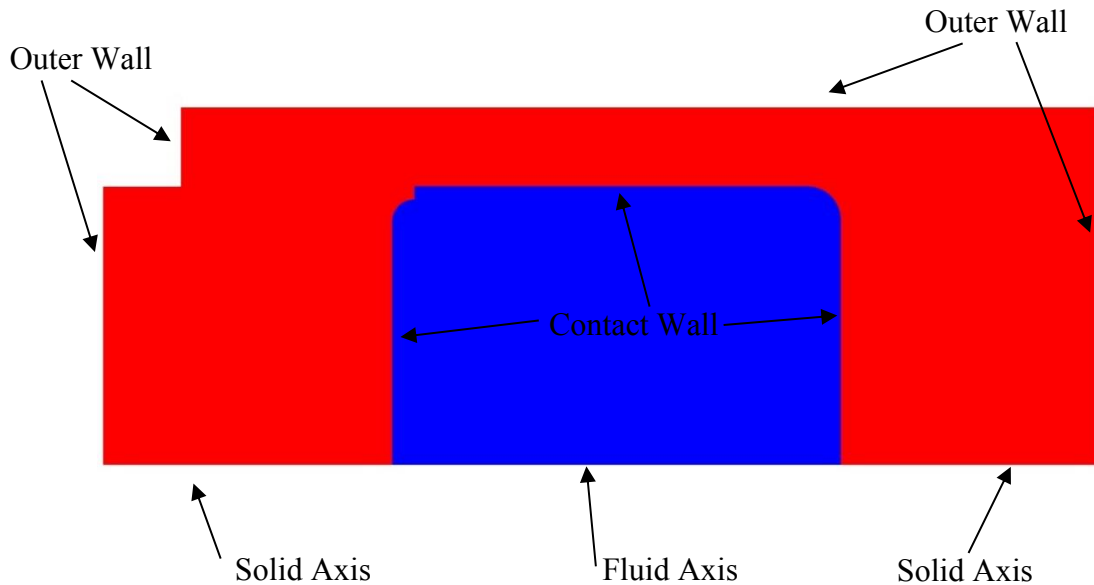


Figure 53. Combustion Model 1 Boundary Condition

3.5.2 Combustion Model 1 Mesh

The mesh used in this model is the same mesh that was used for Combustion Model Test 2, Figure 48, Figure 49, and Figure 50.

3.6 Combustion Model 2

In experimental testing a block was placed into the combustion chamber for testing. This block was designed to be axisymmetric so it can be modeled in 2D. This model was run with the initialization values seen in Table 11.

Table 11. Combustion Model 2 Initialization Values

COMBUSTION MODEL 2	
PRESSURE (PA)	500,000
TEMPERATURE (K)	300
O2 (% MASS)	0.737651
CH4 (% MASS)	0.111056

3.6.1 Combustion Model 2 Boundary Conditions

In this model the boundary conditions are identical to the prior model with the addition of the solid block that is placed in the middle of the domain. This part adds 4 wall boundary conditions into the model.

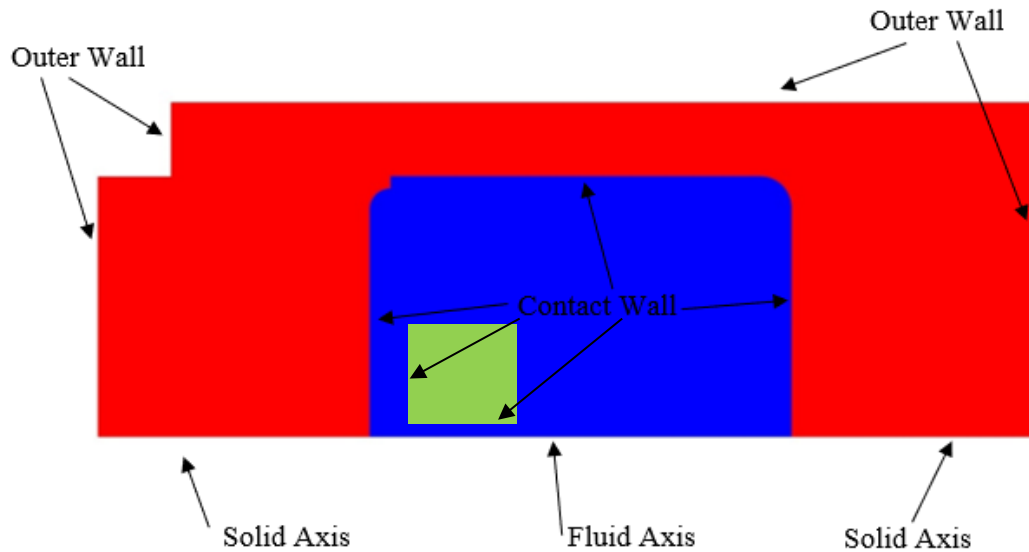


Figure 54. Combustion Model 2 Boundary Conditions

3.6.2 Combustion Model 2 Mesh

The mesh used in this combustion model is identical to the mesh of the combustion model 1. To simulate the solid block inside the chamber, a rectangular region was identified in the fluid domain and was assigned to the new solid domain.



Figure 55. Combustion Model 2 Full Mesh

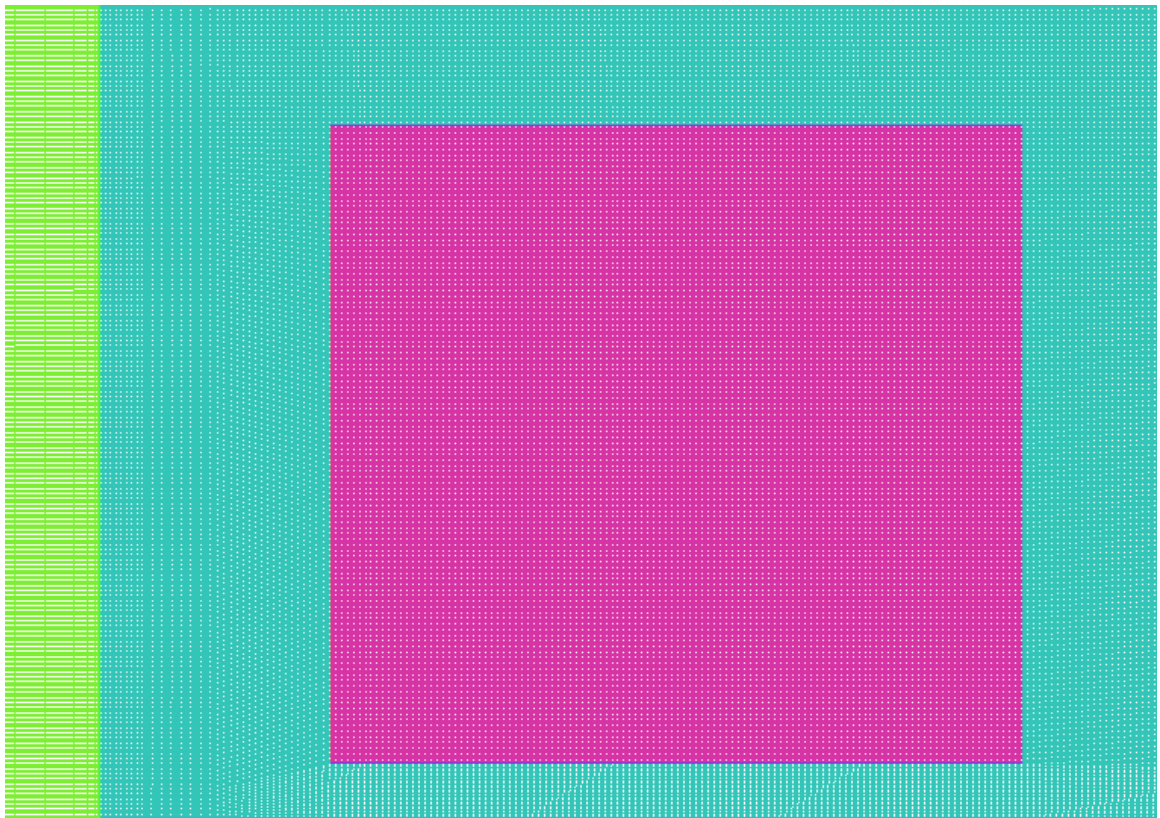


Figure 56. Combustion Model 2 New Solid Domain Mesh

3.7 Combustion Model 3

A perforated plate was used to force a laminar combustion to become turbulent in the hopes of reducing the overall pressure shock force that is generated. The plate has a thickness of 1 inch with 0.5-inch holes spaced every inch.

Table 12. Combustion Model 3 Initial Settings

COMBUSTION MODEL 3	
PRESSURE (PA)	500,000
TEMPERATURE (K)	300
O2 (% MASS)	0.737651
CH4 (% MASS)	0.111056

3.7.1 Combustion Model 3 Boundary Conditions

The boundary conditions for combustion model 3 were like that of combustion model 2. Rather than having one large block being treated as a solid inside the domain, there were multiple smaller blocks.

3.7.2 Combustion Model 3 Mesh

The mesh of this model is the same as the mesh of the combustion model 1. Just like with combustion model 2, a section of the fluid domain was selected and transferred to a new solid domain.

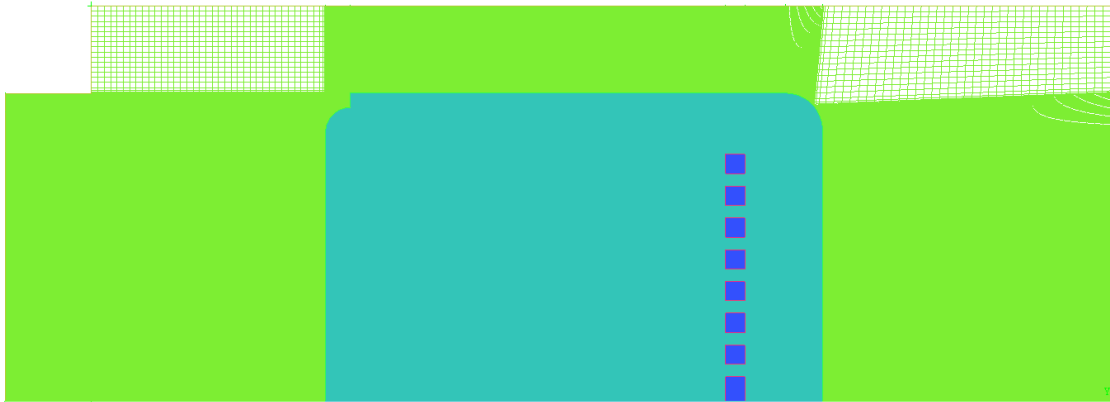


Figure 57. Combustion Model 3 Full Mesh

3.8 Combustion Model 4 (Low Pressure Model)

In this model the effects of having a lowing initial pressure were investigated. The primary reason for the lower pressure start was to see how the peak and stagnant pressures differ from the pressures in combustion model 1. The initialization values used for combustion model 4 can be seen in Table 13.

Table 13. Low Pressure Model

LOW PRESSURE	
PRESSURE (PA)	400,000
TEMPERATURE (K)	300
O2 (% MASS)	0.737651
CH4 (% MASS)	0.111056

3.8.1 Combustion Model 4 Boundary Conditions

The Combustion Model 4 is using the same geometry and boundary conditions as Combustion Model 1 seen in Figure 53.

3.8.2 Combustion Model 4 Mesh

The mesh is the same as Combustion Model Test 2, Figure 48, Figure 49, and Figure 50.

3.9 Combustion Model 5 (Nitrogen Model)

This model has an increase in the initial nitrogen in the model. This was done to observe the effects of having a large excess of a gas that is not a part of the combustion. The initial values used in the model can be seen in Table 14.

Table 14. Combustion Model 5 Initial Conditions

NITROGEN MODEL	
PRESSURE (PA)	500,000
TEMPERATURE (K)	300
O2 (% MASS)	0.697088
CH4 (% MASS)	0.104949

3.9.1 Combustion Model 5 Boundary Conditions

The Combustion Model 5 is using the same geometry and boundary conditions as Combustion Model 1 seen in Figure 53.

3.9.2 Combustion Model 5 Mesh

The mesh is the same as Combustion Model Test 2, Figure 48, Figure 49, and Figure 50.

Combustion Model 6 (Stoichiometric Model)

This combustion model was ran with the stoichiometric ratio of the combustion reaction to see what the effects of excess gas.

Table 15. Stoichiometric Model Initial Conditions

STOIC MODEL	
PRESSURE (PA)	500,000
TEMPERATURE (K)	300
O2 (% MASS)	0.651086
CH4 (% MASS)	0.1477

3.9.3 Combustion Model 6 Boundary Conditions

The Combustion Model 5 is using the same geometry and boundary conditions as Combustion Model 1 seen in Figure 53.

3.9.4 Combustion Model 6 Mesh

The mesh is the same as Combustion Model Test 2, Figure 48, Figure 49, and Figure 50.

3.10 Combustion Model 7

Combustion model 6 was created with holes that are 0.3cm wide at their largest diameter and 0.1cm at their smallest. The goal for these holes is to slow down the pressure shock as it passes through the holes. The model was run with settings that match the first combustion model, these initial values can be seen in Table 16.

Table 16. Combustion Model 7 Initial Conditions

COMBUSTION MODEL 7	
PRESSURE (PA)	500,000
TEMPERATURE (K)	300
O2 (% MASS)	0.737651
CH4 (% MASS)	0.111056

3.10.1 Combustion Model 7 Boundary Conditions

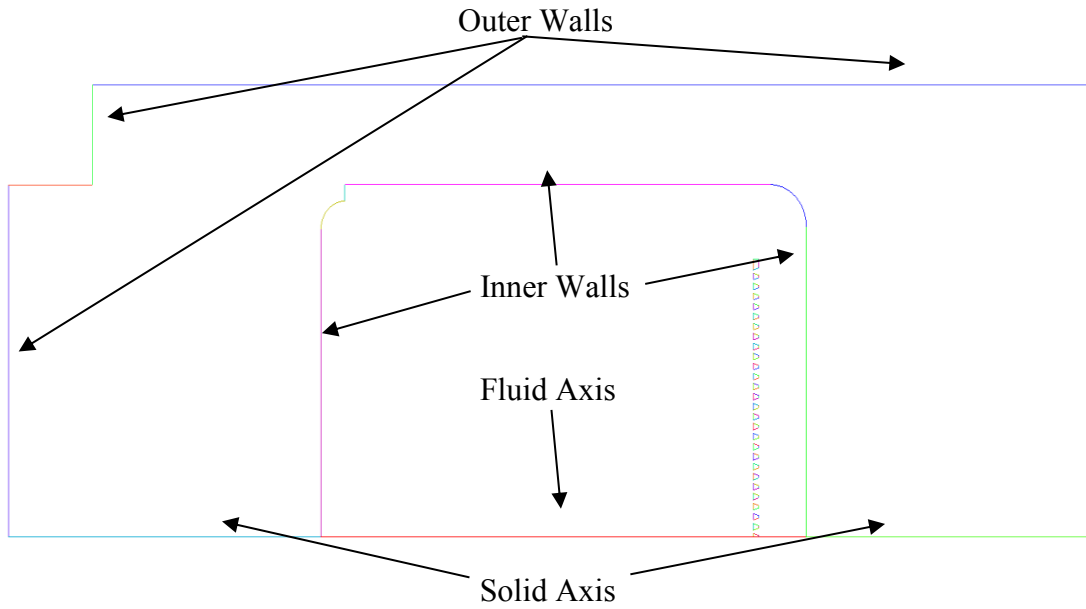


Figure 58. Combustion Model 7 Geometry

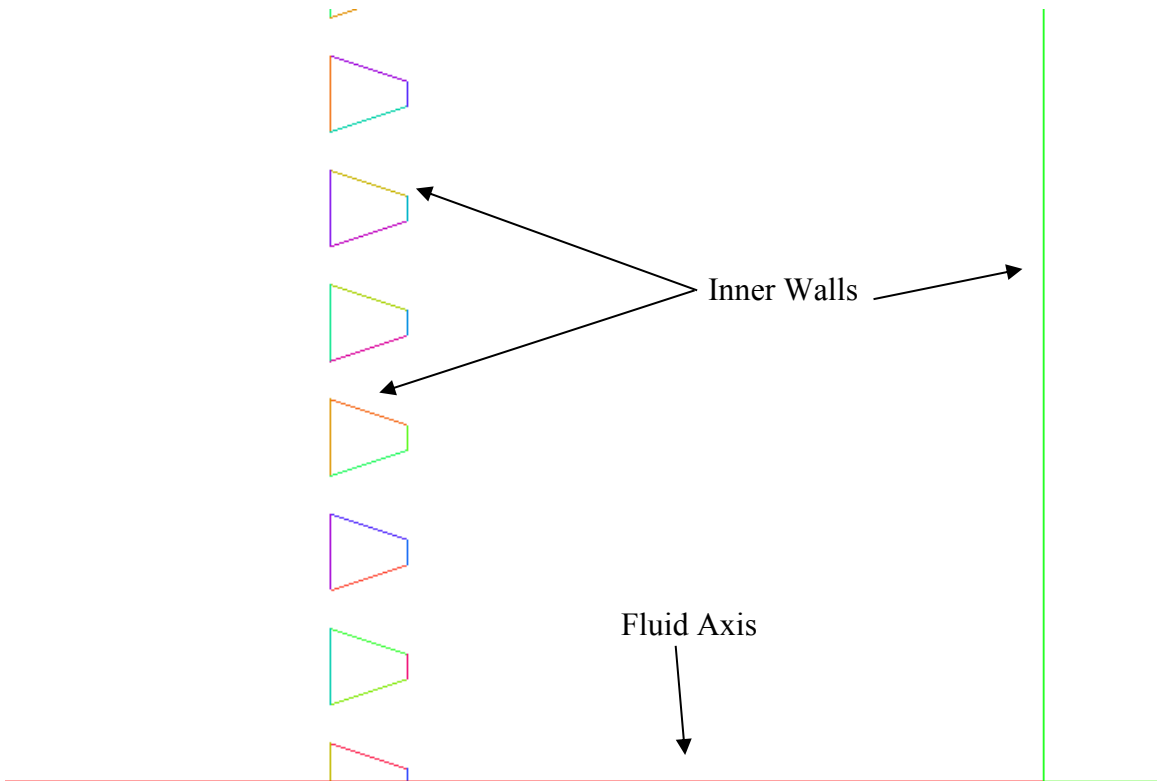


Figure 59. Combustion Model 7 Geometry Closeup

3.10.2 Combustion Model 7 Mesh



Figure 60. Combustion Model 7 Full Mesh

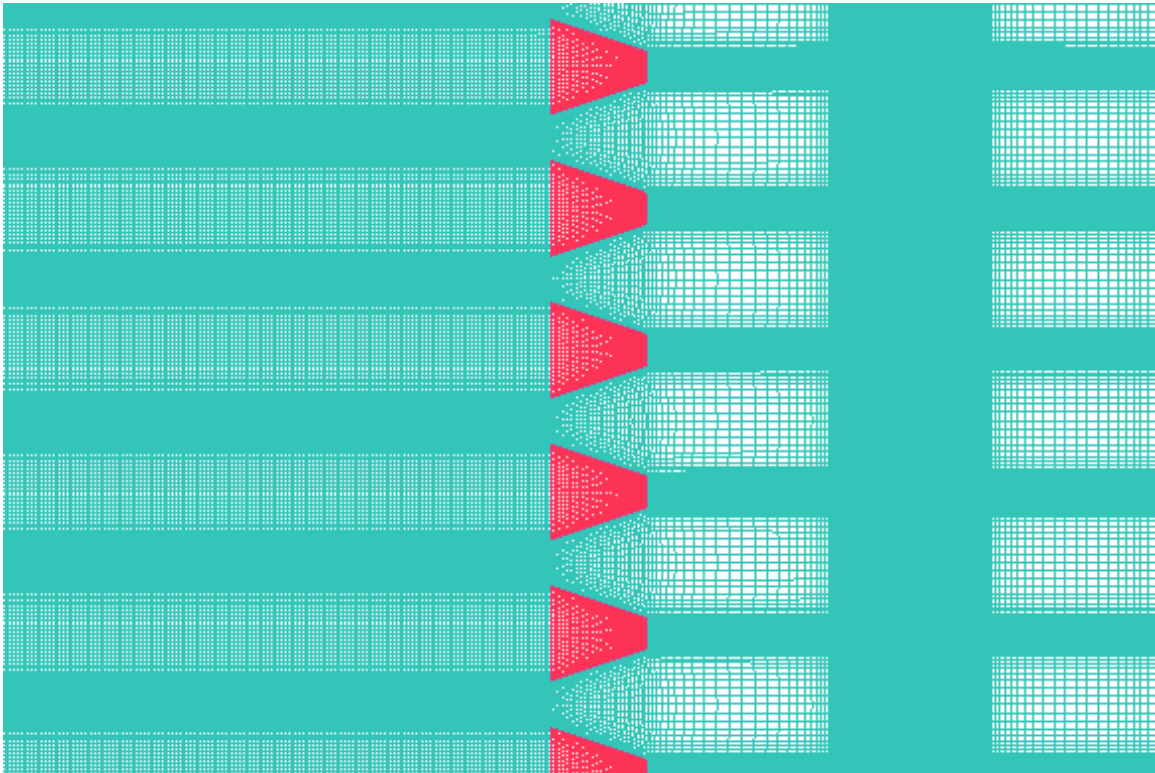


Figure 61. Combustion Model 7 Mesh Closeup

Due to the variable hole sizing, element sizing from one side of the hole to the other changed. To combat this and create a good mesh a higher density was used along with variable mesh sizing through the zone to create smooth transitions.

4 Results

Wall data was collected at two vertical locations, position one was at a y height of 6.235 inches which is in the fluid domain and the second position occurs at 3.236 inches which is in the solid domain. All plots of wall data show multiple locations and their respective Pressures or Temperatures vs Time. Combustion Models 1, 4, 5 and 6 are the models that had these wall position values saved. These models were chosen as they were all the same geometry with varying parameters. This was chosen to see the effects of changing the parameters of the combustion.

4.1 Combustion Model 1 (Normal Model)

The normal model was initialized with the values designated for the baseline settings. All results for this model are based on the wall values recorded during the combustion simulation.

4.1.1 Combustion Model 1 Contour Plots

When looking at the pressures in Figure 62 (a) the shock wave is bouncing off the side walls and reflecting back towards the center of the geometry. As the shock progresses towards (b) a high pressure increase at the bottom of the fluid domain can be observed. This is from the combination of the side wall reflection and the bottom wall reflection. At the final time location (c) the original pressure shock reflection from the side wall is combined with other reflections from the axisymmetric geometry to create a very large pressure spike that propagates from the top of the fluid domain to the bottom of the domain.

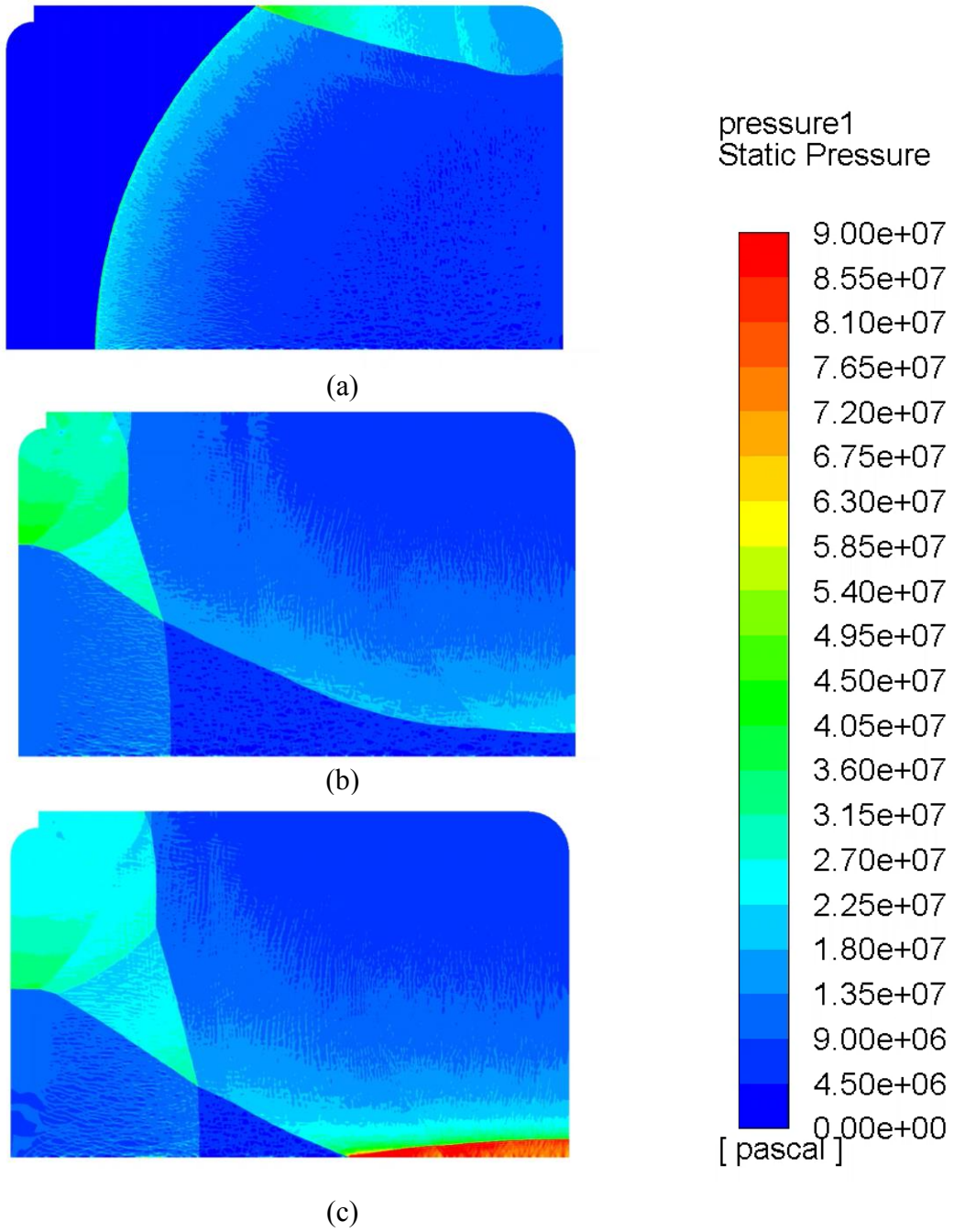


Figure 62. Combustion Model 1 Pressure Results at timestep 7500 (a), 12500 (b), 14500 (c)

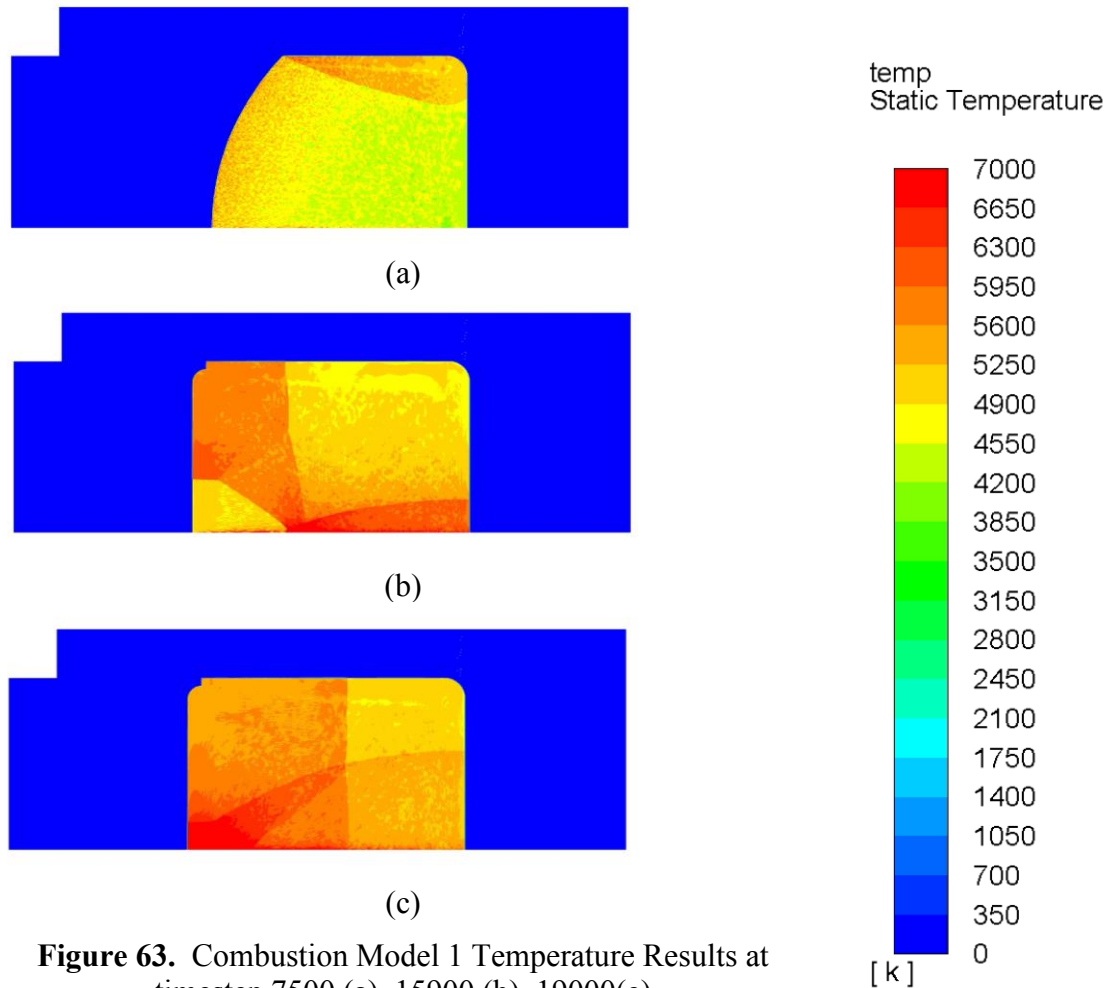


Figure 63. Combustion Model 1 Temperature Results at timestep 7500 (a), 15900 (b), 19000(c)

When the pressure shocks combine and there is a spike in pressure within the region, the temperature for the region also increases. Results from the Fluent simulation provided results such as pressure shocks with the flame front, pressure shock reflections and temperature variation due to the combustion. The temperature values are high, and this is due to Fluent not having all the steps in the combustion to properly dissipate some of the energy into more reactions that should be occurring. With this information the next step was to simulate the second part of the experiments that had the shim holder in the chamber.

4.1.2 Combustion Model 1 Full Wall Values

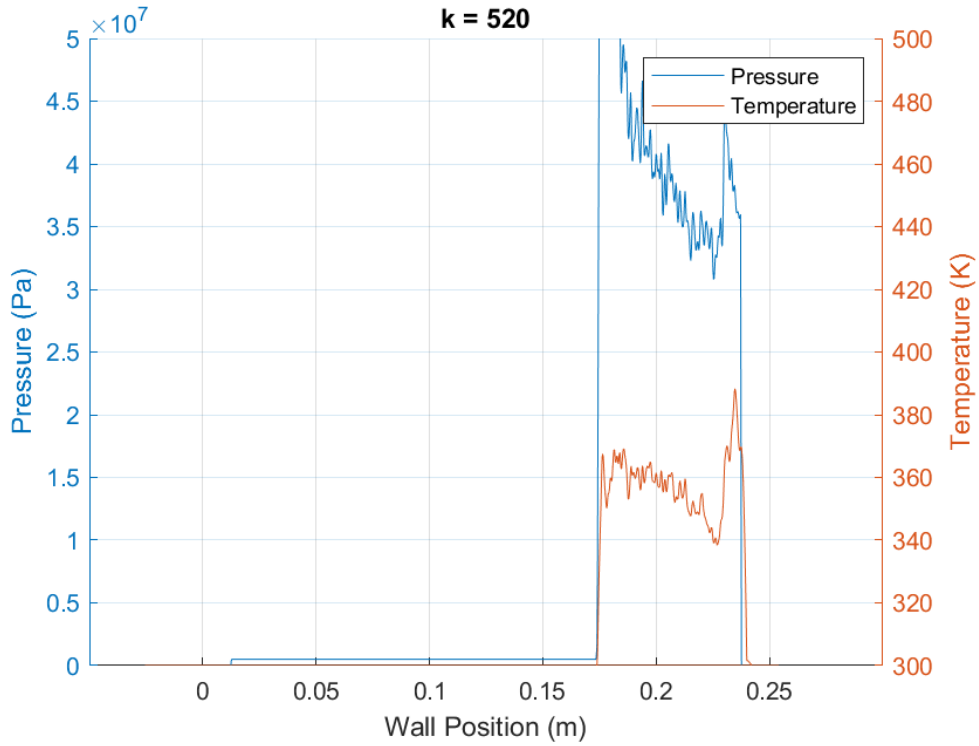


Figure 64. Normal Model Full Wall Pressure at Time One

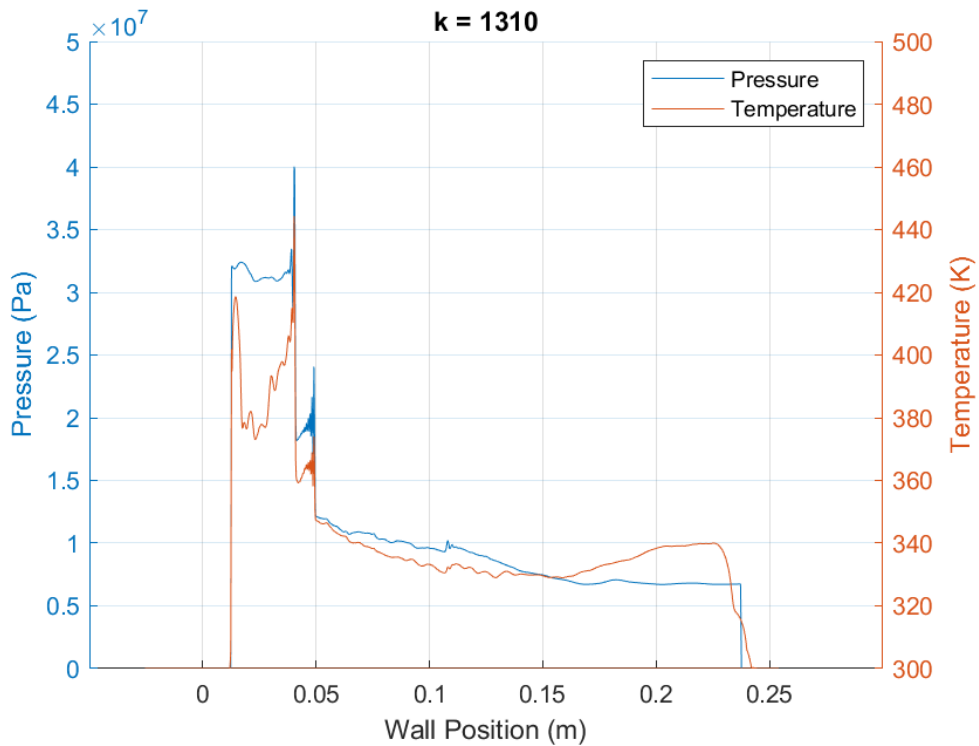


Figure 65. Normal Model Full Wall Pressure at Time Two

Figure 64 shows the side walls static pressure and temperature at a time near the beginning of the combustion. It can be observed that the temperature follows the pressure values. The temperature is caused by both the combustion of methane and the pressure shock being formed by the combustion. Figure 65 is later step and the pressure shock has already bounced off the bottom wall and began to travel back up the wall. At this point in time there is no more methane in the chamber and all the temperature increases are due to pressure shocks.

4.1.3 Combustion Model 1 Single Position Wall Values

In the upcoming Figures, there are multiple lines being plotted. Each line represents a location along the wall. Figure 66 through Figure 68 are the pressure values vs time at different locations on the wall. The locations remain the same for all graphs and the plots are of different ranges for ease of reading. Figure 68 displays every tenth location of the prior figures to give ease of reading with less locations.

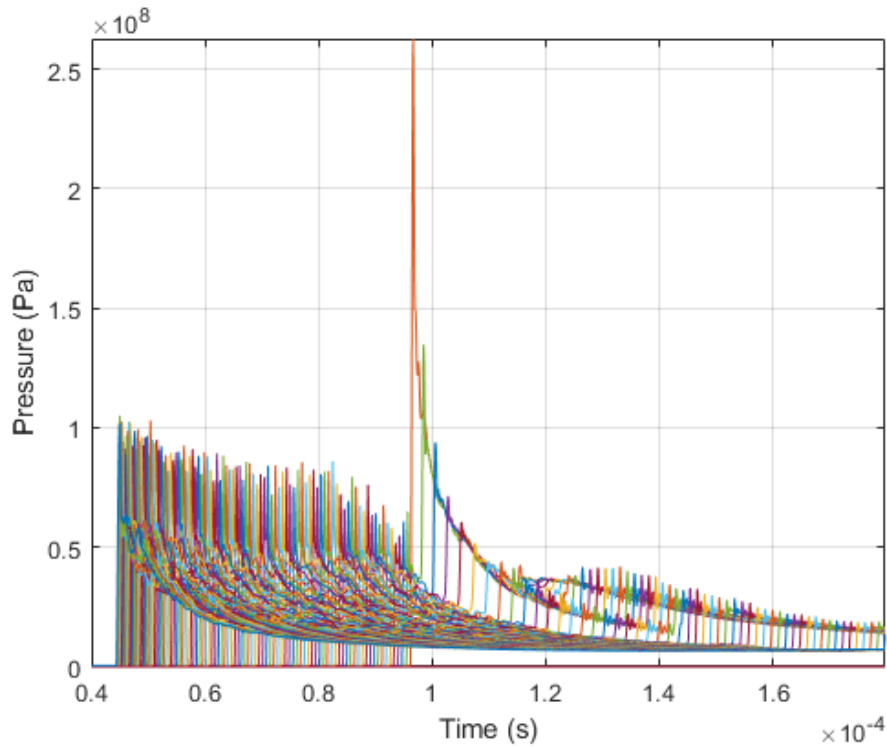


Figure 66. Normal Model Pressure Values 1

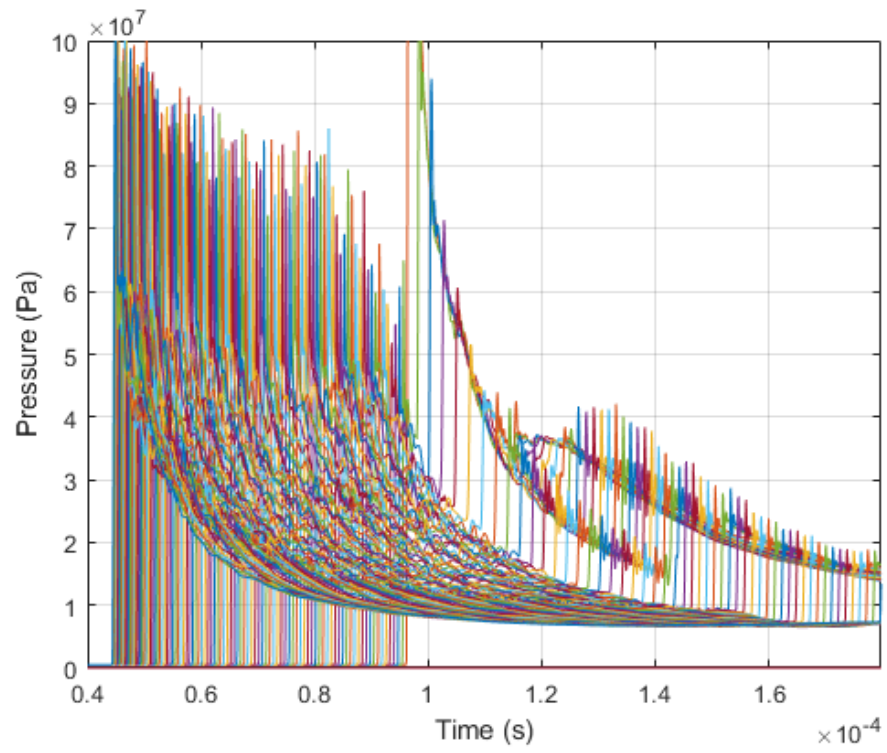


Figure 67. Normal Model Pressure Values 2

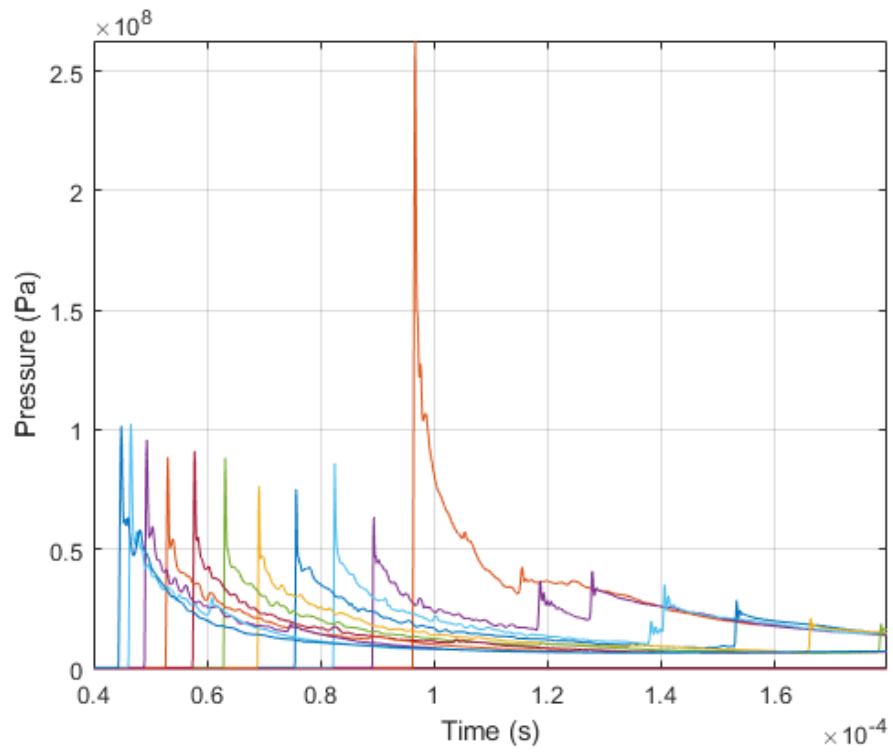


Figure 68. Normal Model Pressure Values 3

Looking at the values of Figure 68, it can be observed that the pressure shock has two waves that interact with the wall but eventually combine over time along with die down in the intensity. It also can be observed that after the pressure shock, the pressure reduces to new stagnate pressure. Figure 69 through Figure 73 are the same as the prior figures but display the temperature values instead of the pressure values.

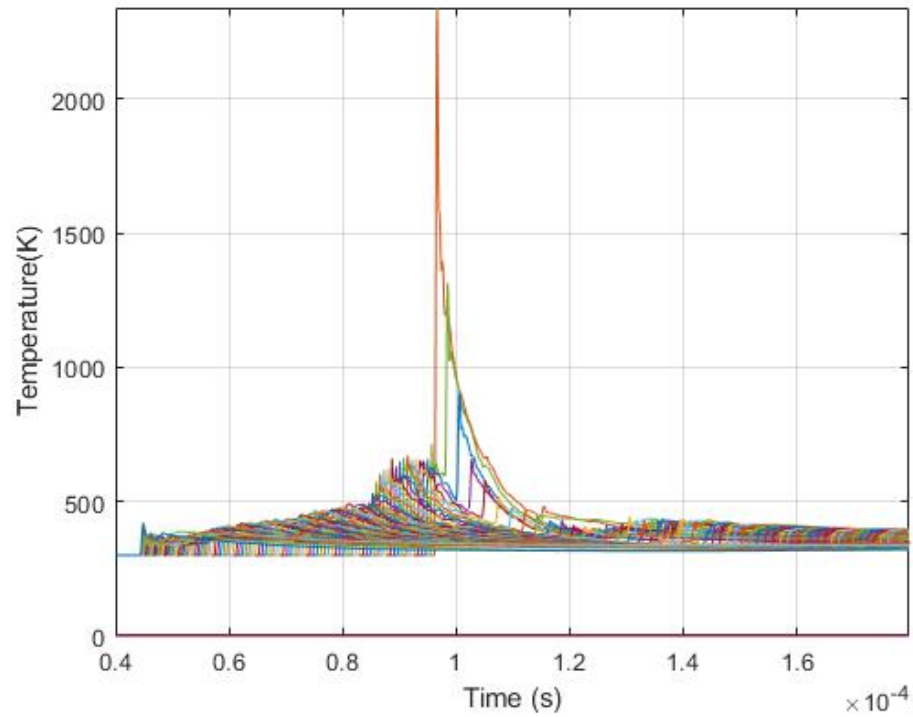


Figure 69. Normal Model Temperature Values 1

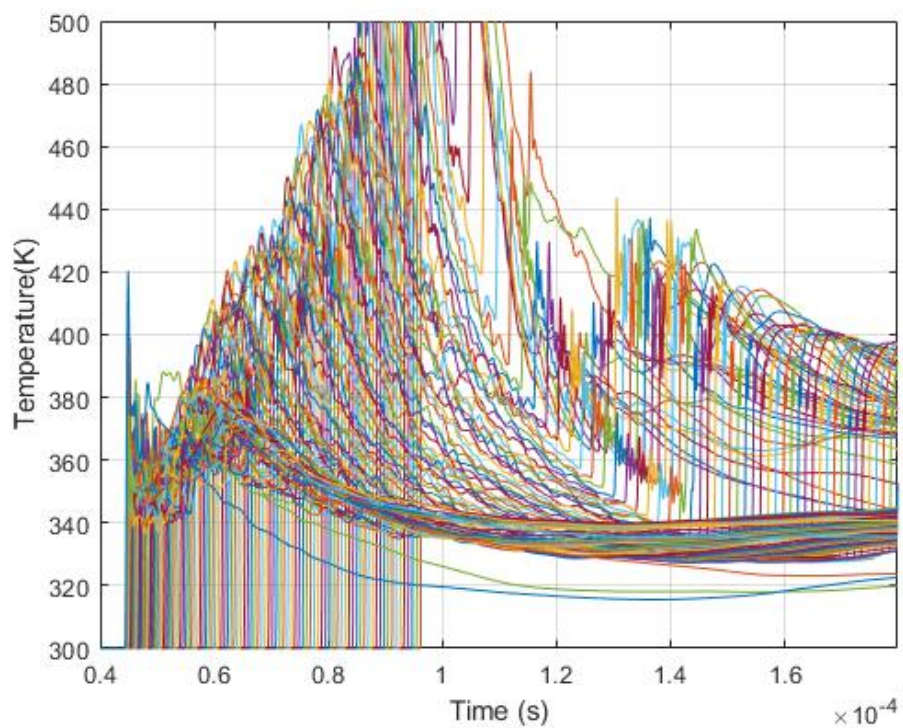


Figure 70. Normal Model Temperature Values 2

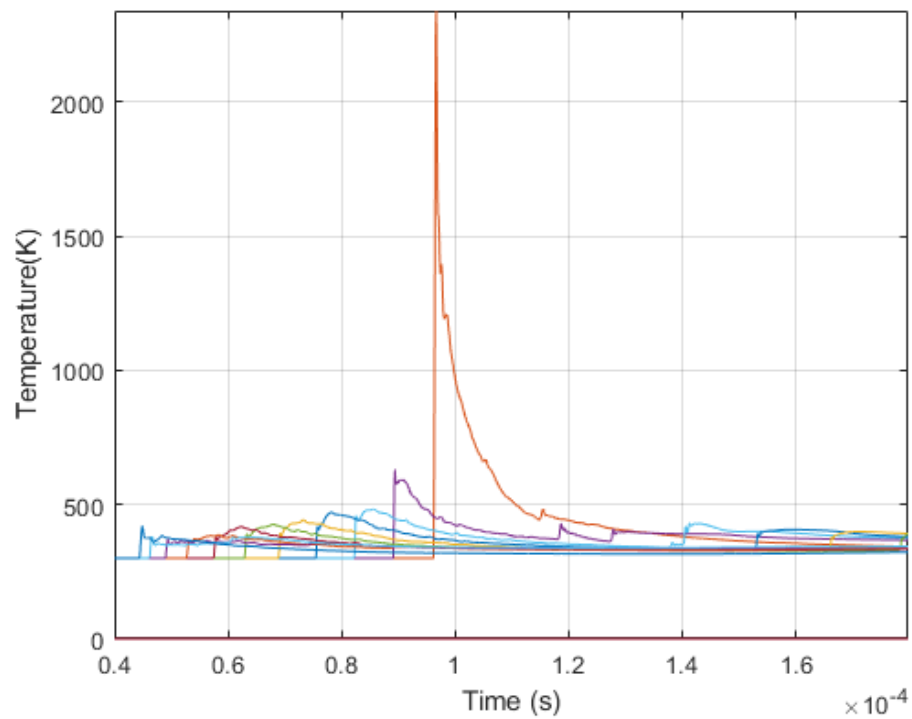


Figure 71. Normal Model Temperature Values 3

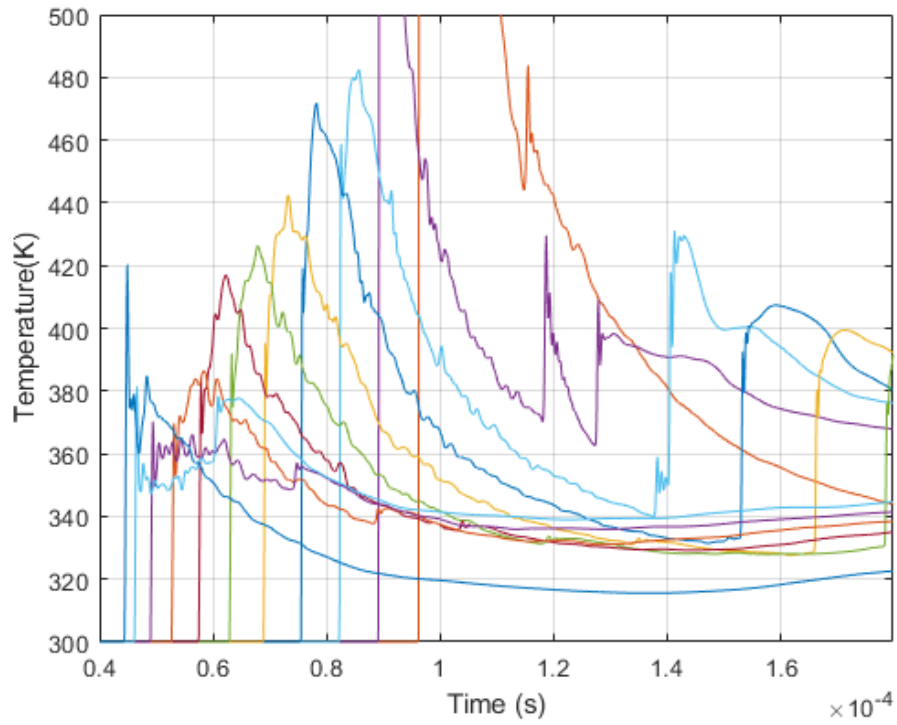


Figure 72. Normal Model Temperature Values 4

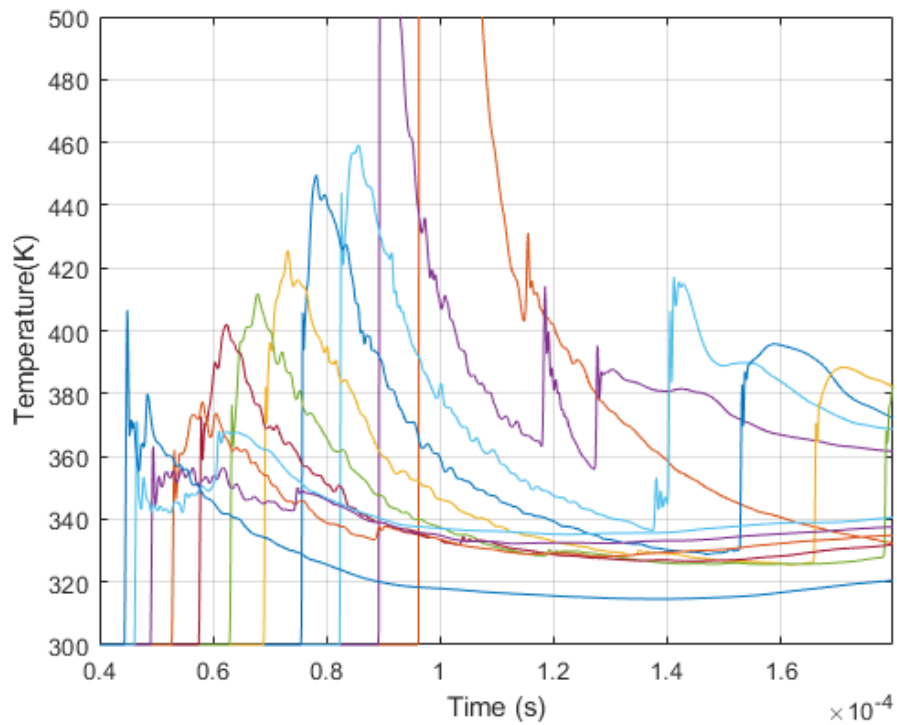


Figure 73. Normal Model Temperature Values 5

Figure 72 and Figure 73 shows the same positions along the wall, but vary due to the solid line is being taken from inside the solid wall. This causes there to be lower temperatures as there is conduction that is happening. Figure 74 through Figure 76 display the pressure and temperatures with respect to time at a multiple position along the wall. The first position is near the top of the wall, the second position is at the middle of the wall and the final position is near the bottom of the wall. There are two major spikes in the temperature that correspond with a pressure shock, a smaller third pressure spike occurs but does not produce the same temperature as the prior two. As the pressure slowly diminishes past the shock waves, the temperature fluctuates. This is due to convection happening in the chamber.

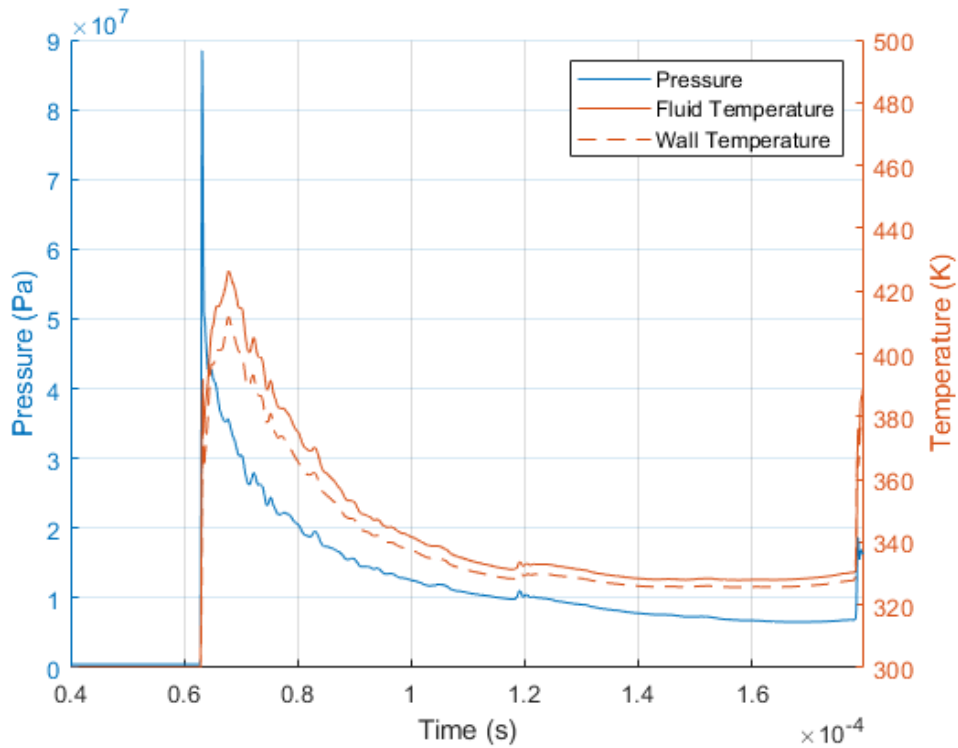


Figure 74. Normal Model Pressure and Temperature at Position 1

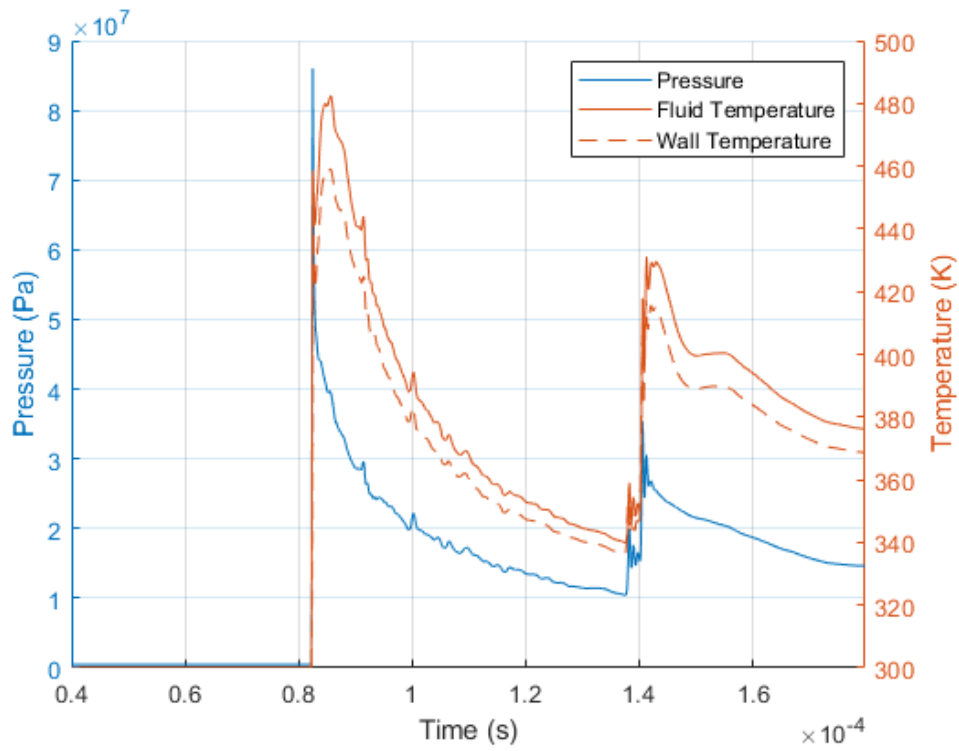


Figure 75. Normal Model Pressure and Temperature at Position 2

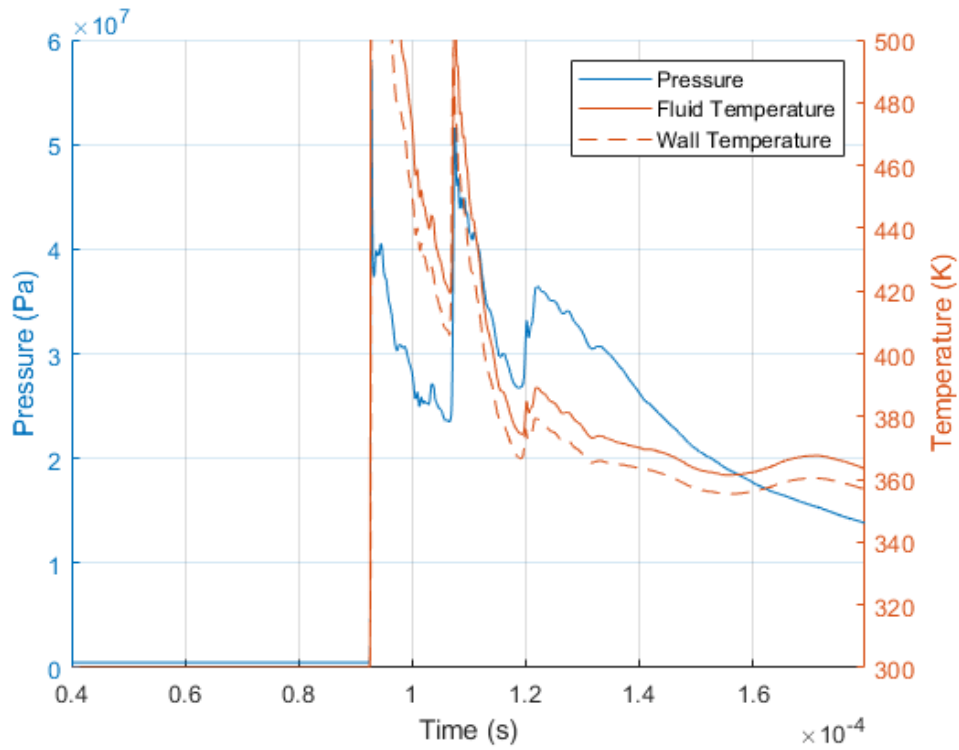


Figure 76. Normal Model Pressure and Temperature at Position 3

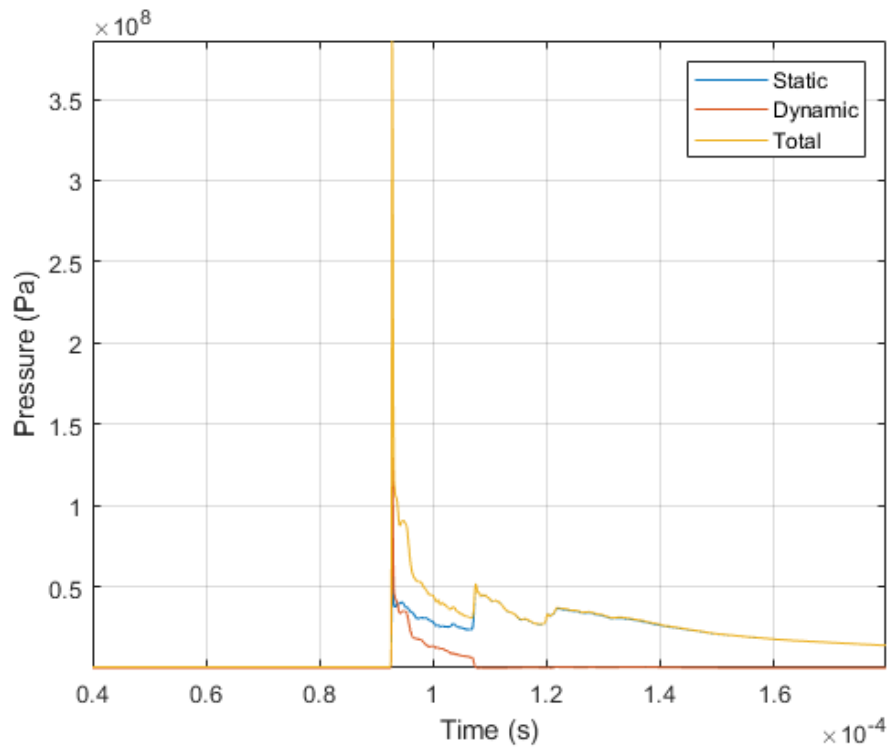


Figure 77. Normal Model Pressures at Position 1

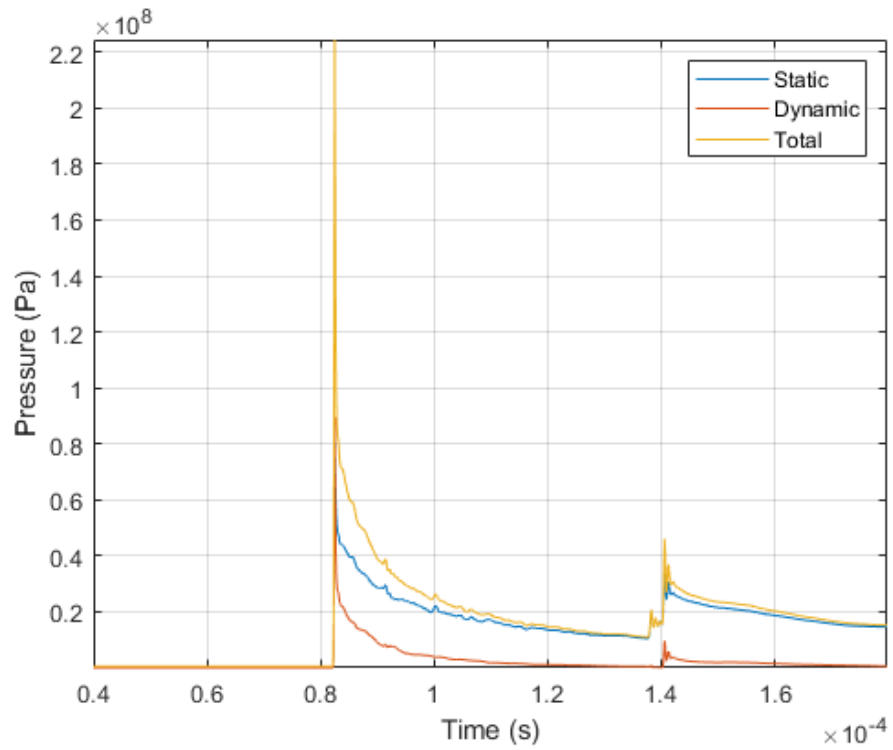


Figure 78. Normal Model Pressures at Position 2

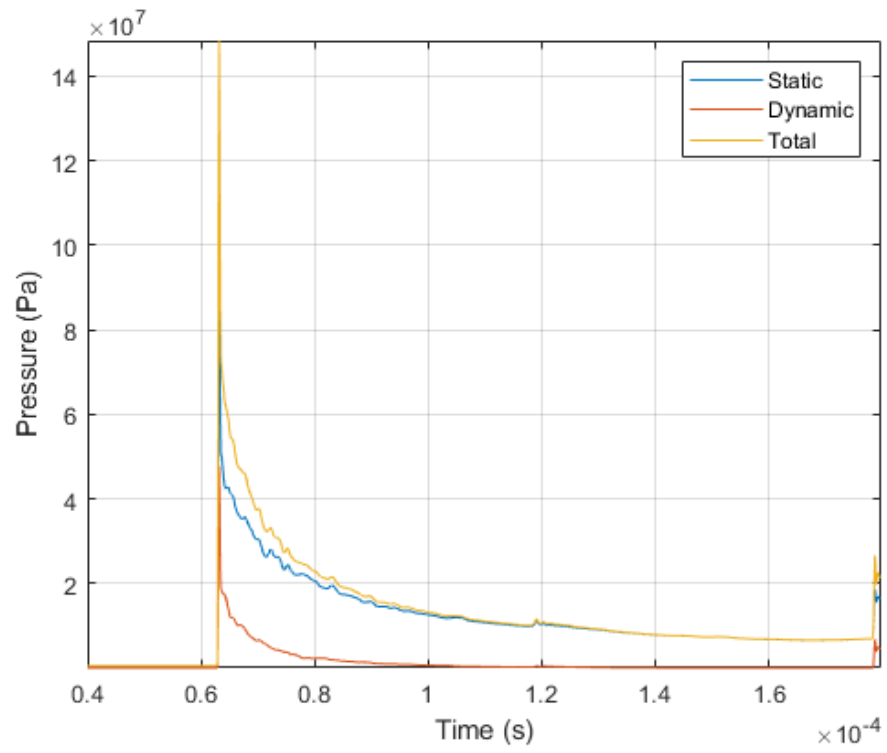


Figure 79. Normal Model Pressures at Position 3

4.2 Combustion Model 2

This model ran with the same settings as the normal model. All results for this model are based on the wall values recorded during the combustion simulation.

4.2.1 Combustion Model 2 Contour Plots

With the addition of a solid part into the chamber there are drastic changes to the pressure shocks. With more reflections happening there are more locations that can have pressure concentrations.

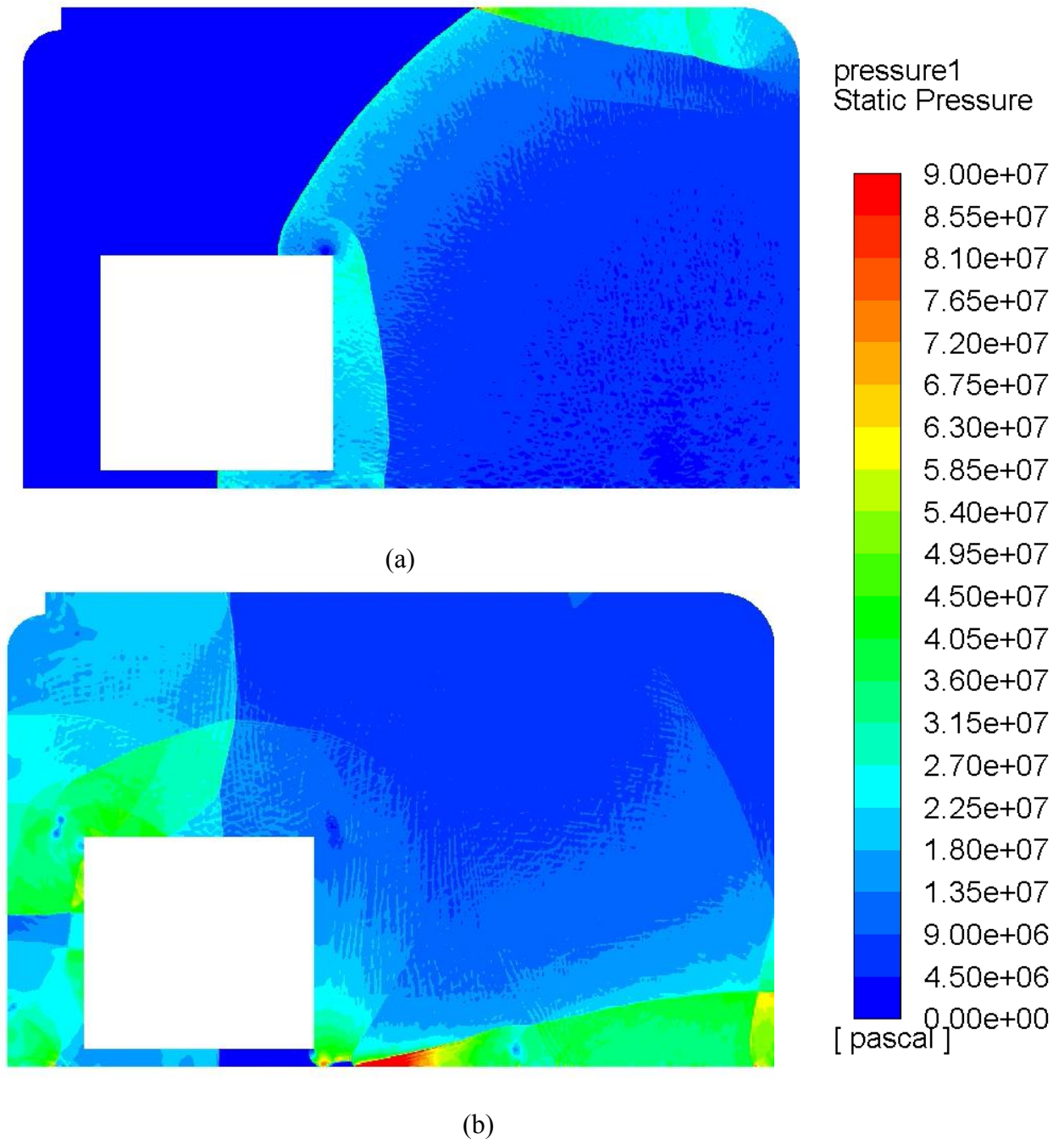


Figure 80. Combustion Model 2 Pressure Shocks at timestep 6000 (a), 14000 (b)

4.3 Combustion Model 3

This model ran with the same settings as the normal model. All results for this model are based on the wall values recorded during the combustion simulation.

4.3.1 Combustion Model 3 Results

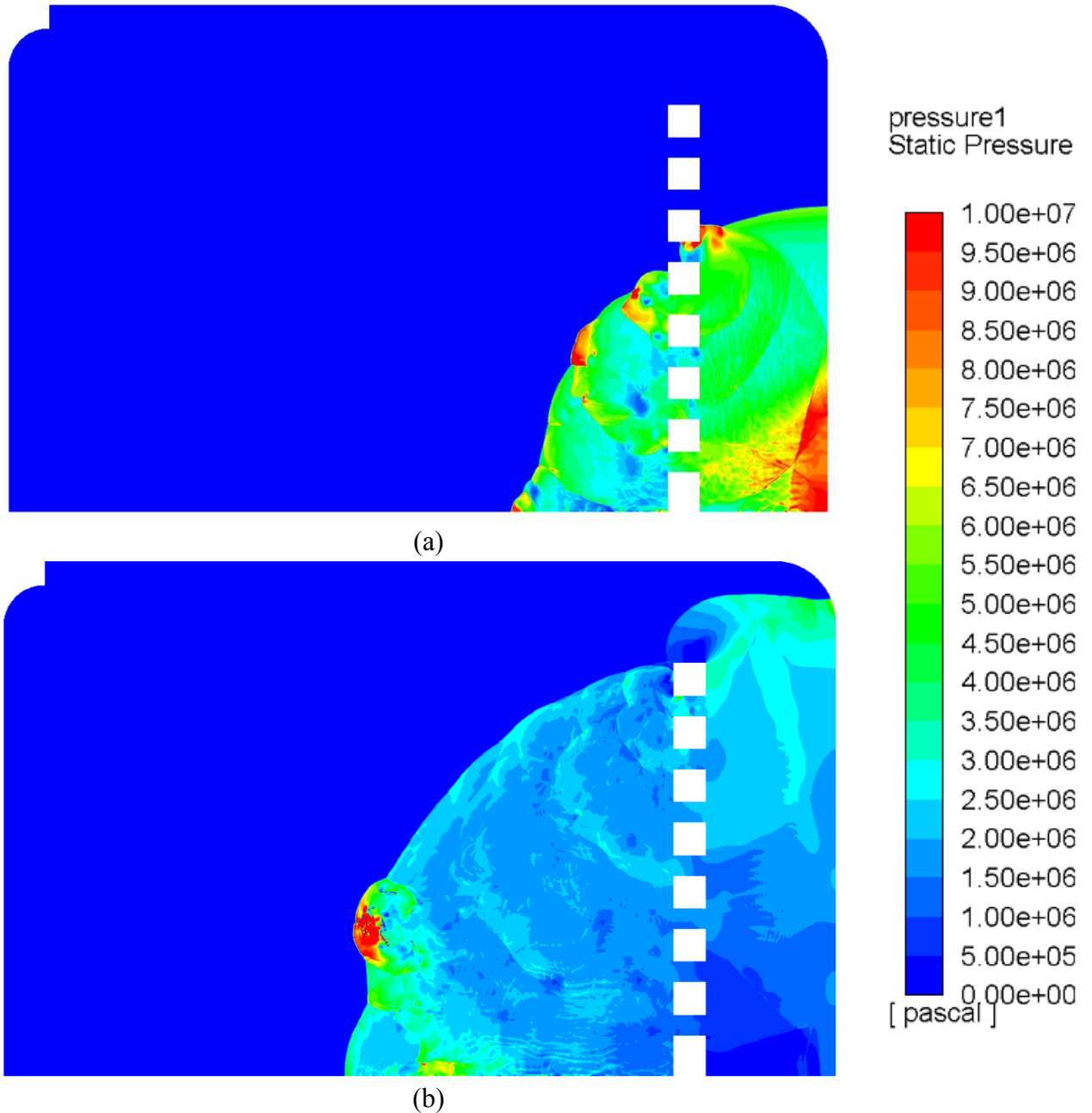


Figure 81. Combustion Model 3 Pressure Results at timestep 5000 (a), 10000(b)

Comparing the static pressure across the front of the pressure shock wave with prior models that did not include the perforated plate, the pressure peaks are much lower across the shock. There are more locations of pressure spikes in the model with the perforated

plate due to the shock waves combining when exiting the holes in the plate. These pressure concentrations have a maximum pressure value that is lower than the prior models.

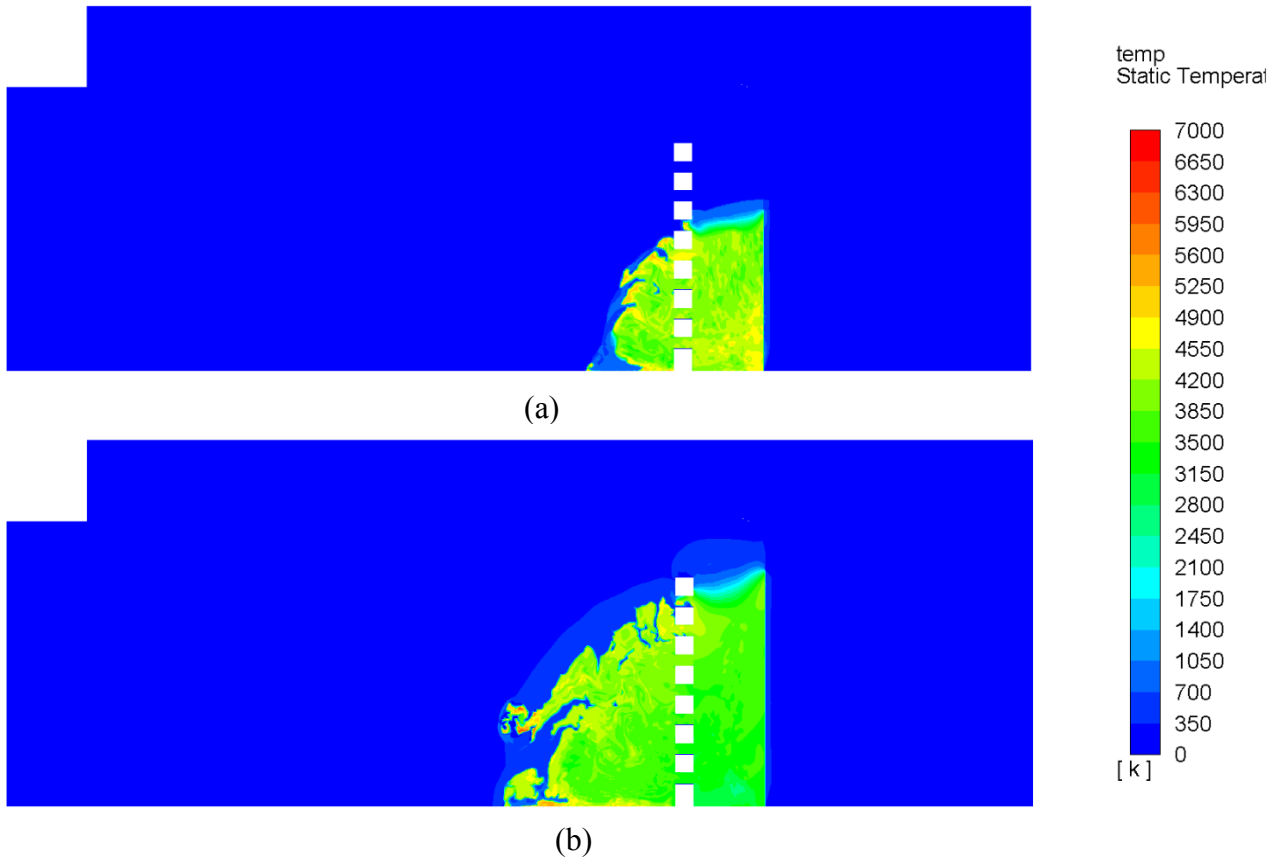
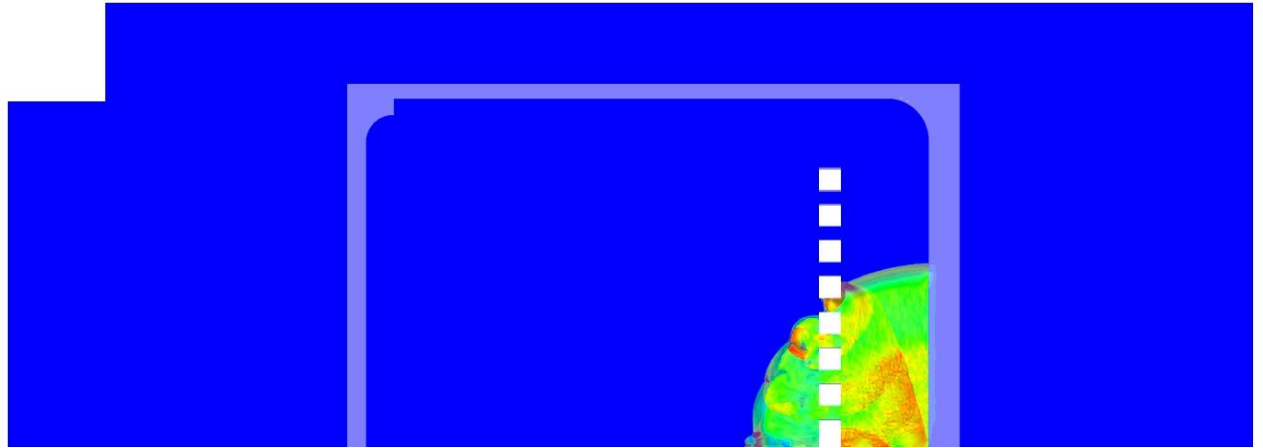


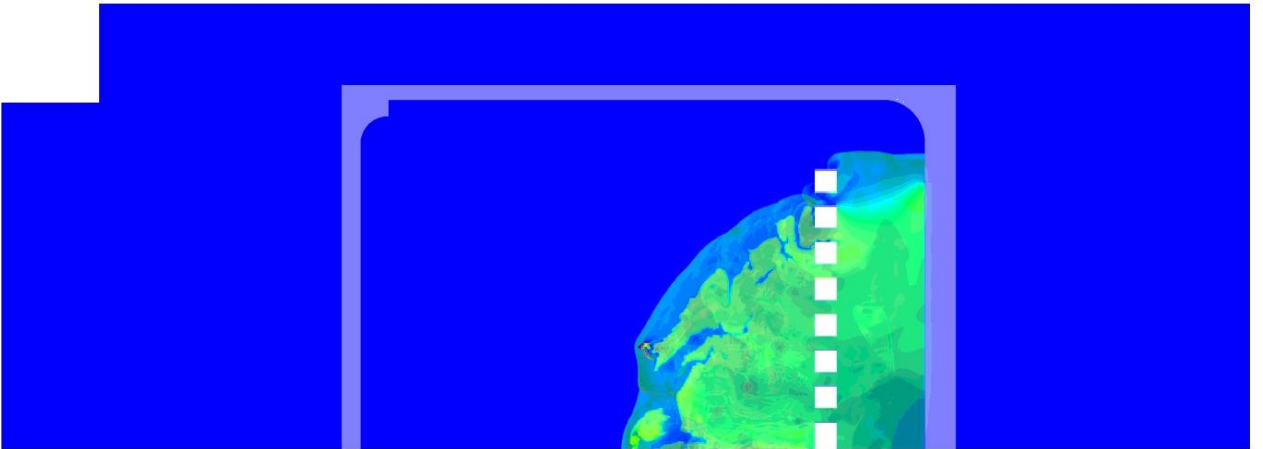
Figure 82. Combustion Model 3 Temperature Results at timestep 5000 (a), 10000 (b)

The flame front of the combustion no longer follows directly behind the pressure shock. This is due to the perforated plates forcing a turbulent combustion to occur. As the combustion progresses the flame front becomes more chaotic in nature. Overlaid pressure and temperature contours can be seen in Figure 83. A combination of the flame falling behind the pressure front and pressure shocks combining can cause a sudden reignition of the methane during the combustion process.

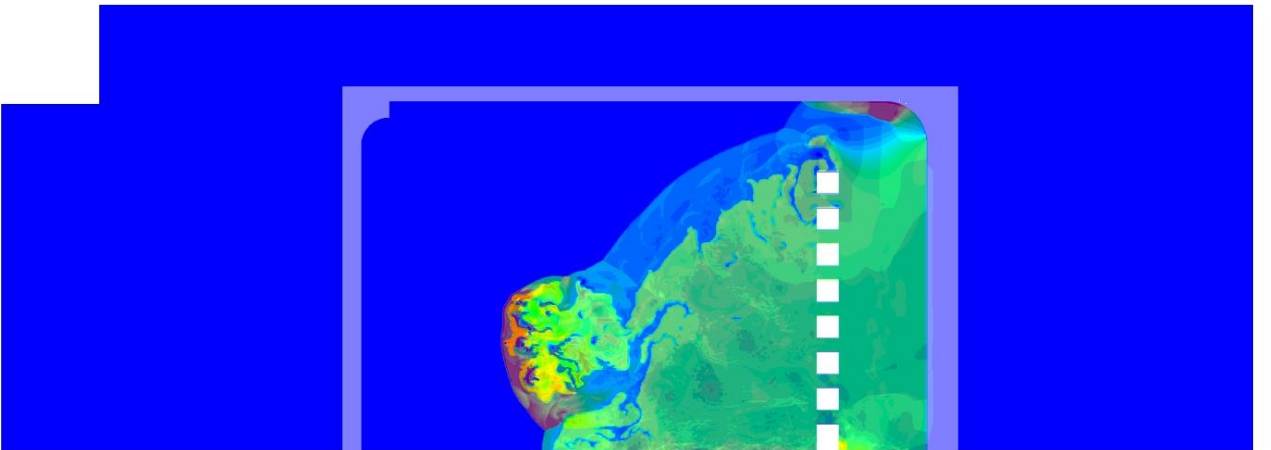
At the beginning of the combustion the flame front is moving along with the pressure shock. As the flame propagates further, separation occurs between the flame front and pressure shock. Due to the high-pressure shock ahead of the flame, autoignition occurs and the flame speeds up to the pressure shock which can be seen in Figure 83 (c). This combustion that occurs is laminar with the flame front moving directly behind the pressure shock while other portions of the combustion remain turbulent. This autoignition causes for very high-pressure shocks.



(a)



(b)



(c)

Figure 83. Combustion Model 3 Overlaid Pressure and Temperature at timestep 5000 (a), 10000 (b), 12000 (c)

4.4 Combustion Model 4 (Low Pressure Model)

The low-pressure model was initialized with a pressure of 4Bar, 20% lower than the normal model. All results for this model are based on the wall values recorded during the combustion simulation.

4.4.1 Combustion Model 4 Contour Plots

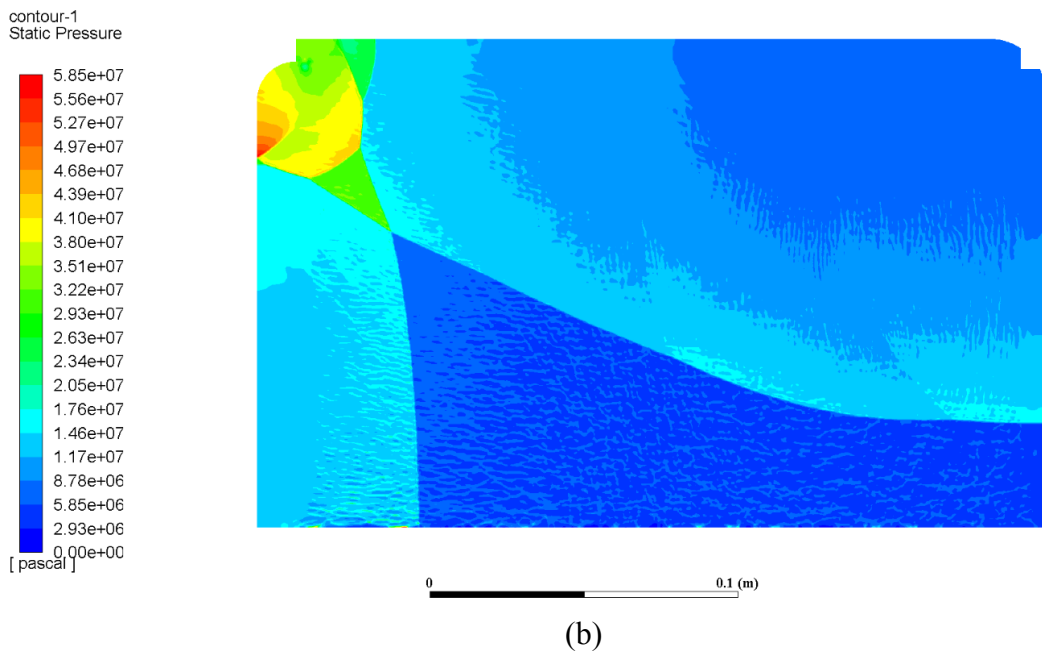
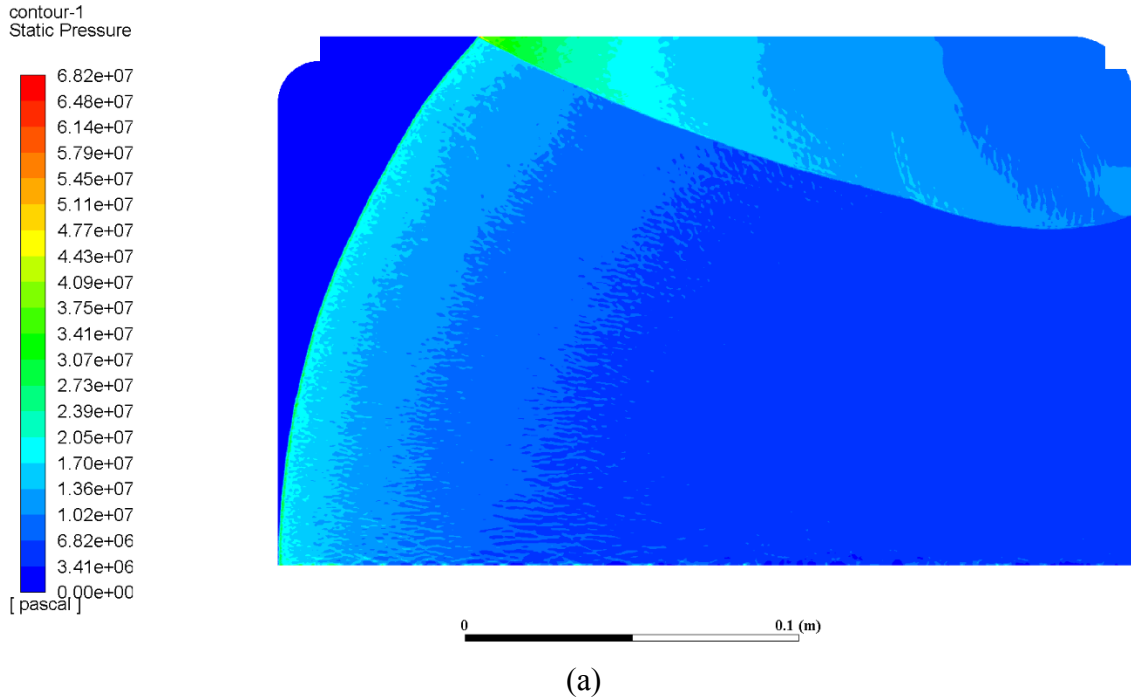


Figure 84. Combustion Model 4 Pressure at timestep 8000 (a), 12500 (b)

The pressure shocks observed in Model 4 are very similar to those observed in Model 1. The only major difference between the two is the magnitude of the pressure. The shock reflections match those of the first model.

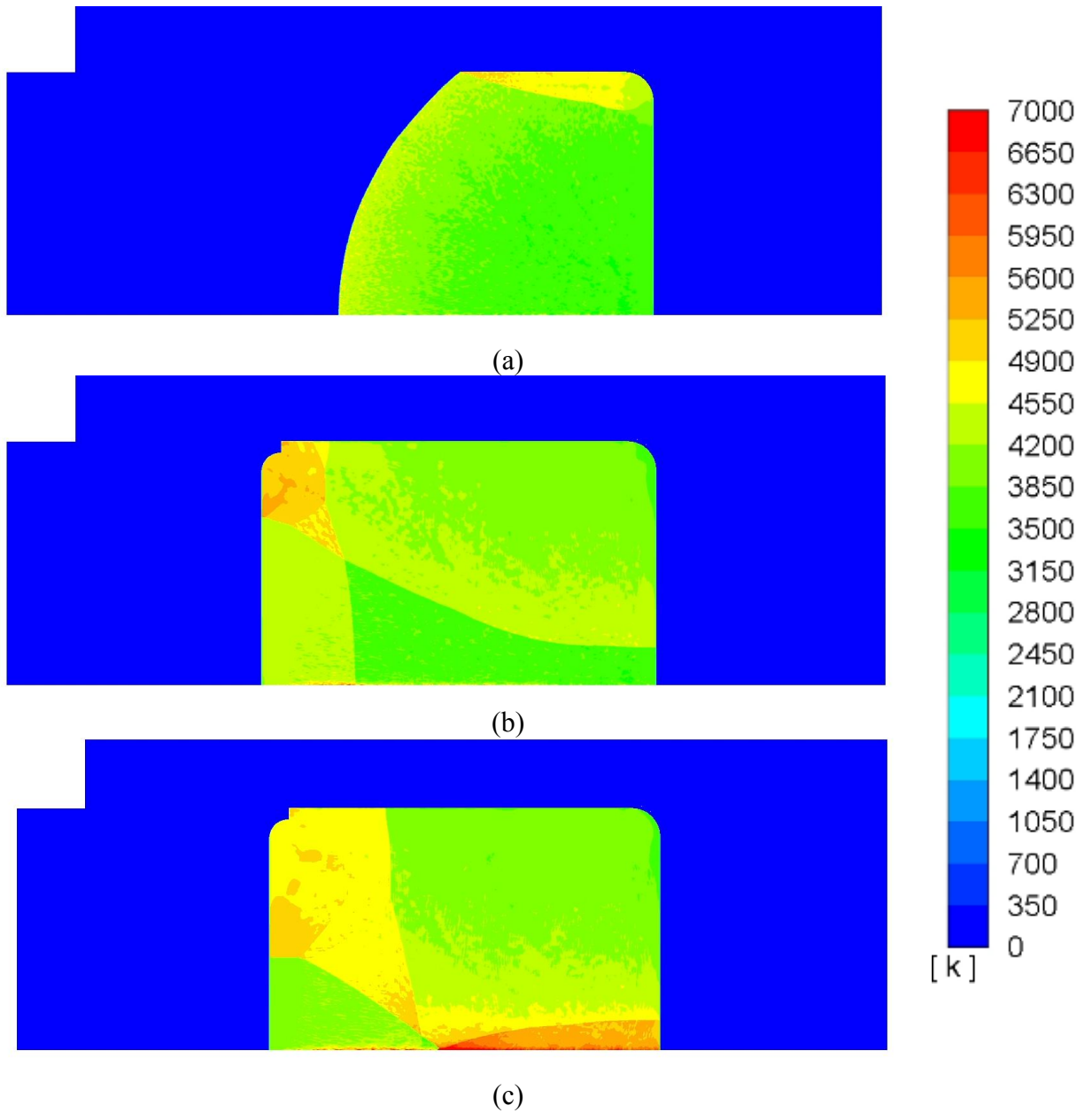


Figure 85. Combustion Model 4 Temperature at timestep 7500 (a), 12500 (b), 14500 (c)

The temperature is also lower in the low-pressure model when compared to the first model.

4.4.2 Combustion Model 4 Full Wall Values

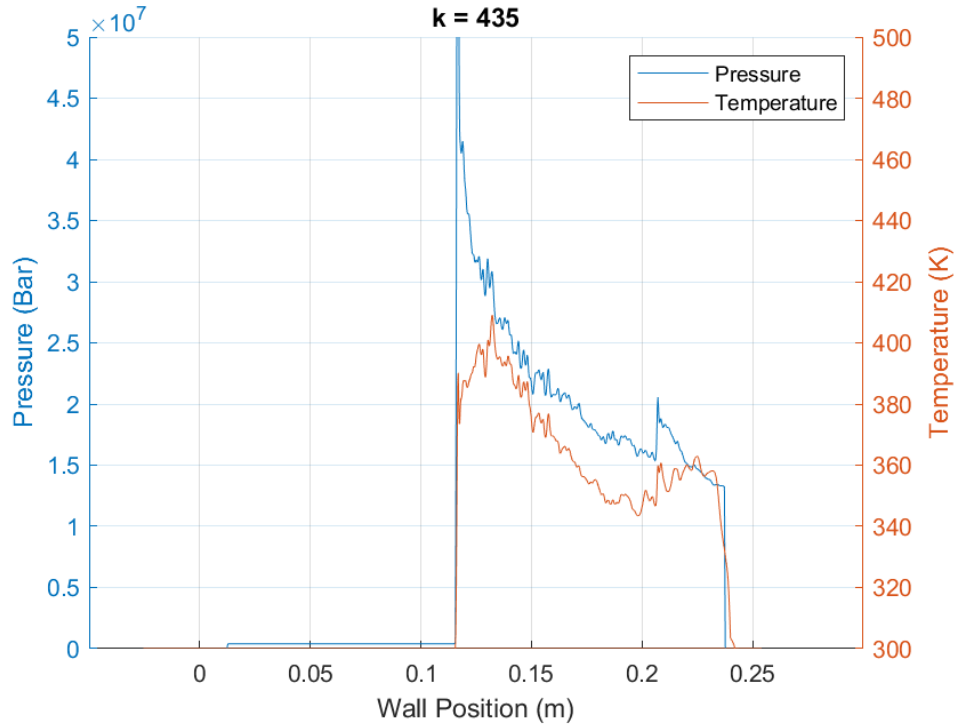


Figure 86. Low Pressure Model Mid Wall Values

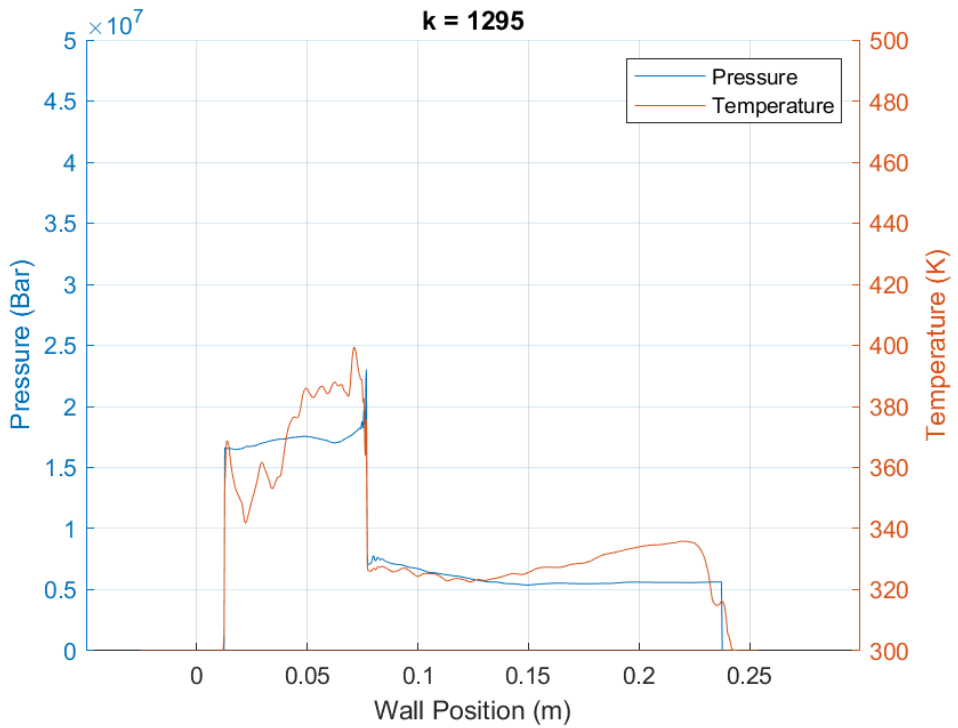


Figure 87. Low Pressure Model Wall Shock Combination

It can be observed between Figure 86 and Figure 87 that there are multiple shock reflections that travel back up the wall and eventually combine into one wave. It also can be observed between the two, around position 0.15 to 0.2 that the temperature increases even though no new shock has traveled over that portion. This is due to convection heating from the surrounding gas.

4.4.3 Combustion Model 4 Single Wall Values

In the upcoming Figures, there are multiple lines being plotted. Each line represents a location along the wall. Figure 88 through Figure 90 are the pressure values vs time at different locations on the wall. The locations remain the same for every plot and the plots are of different ranges for ease of reading. Figure 90 displays every tenth location of the prior figures to give ease of reading with less locations.

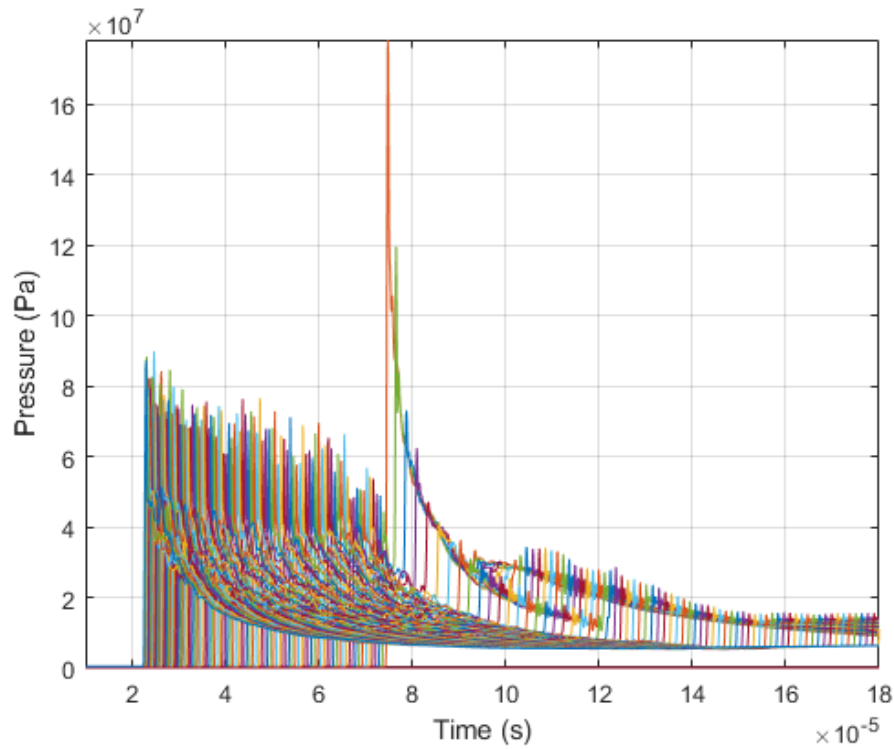


Figure 88. Low Pressure Model Pressure Values 1

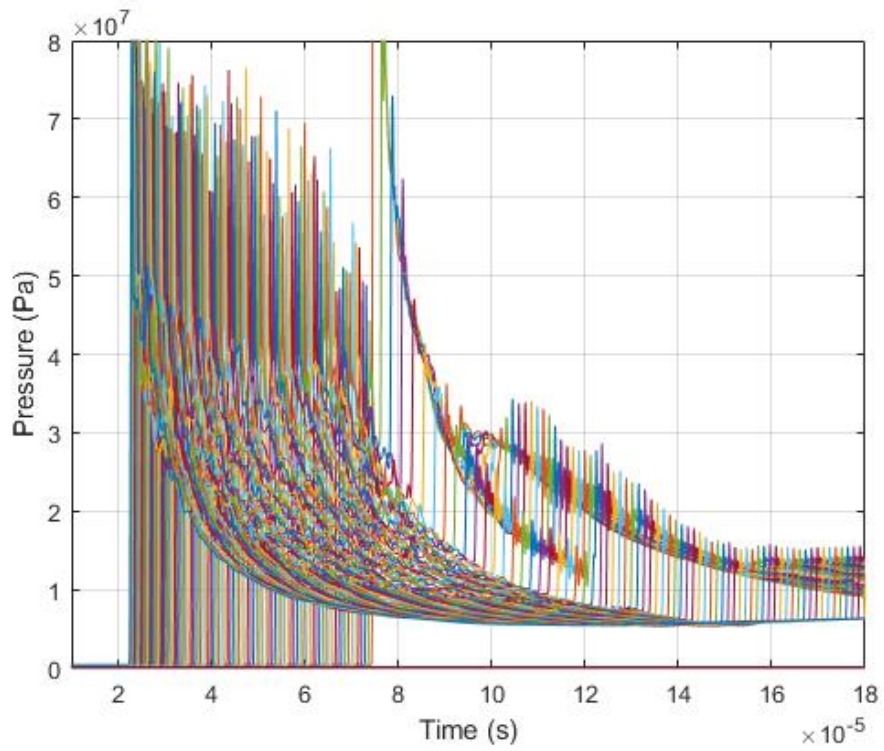


Figure 89. Low Pressure Model Pressure Values 2

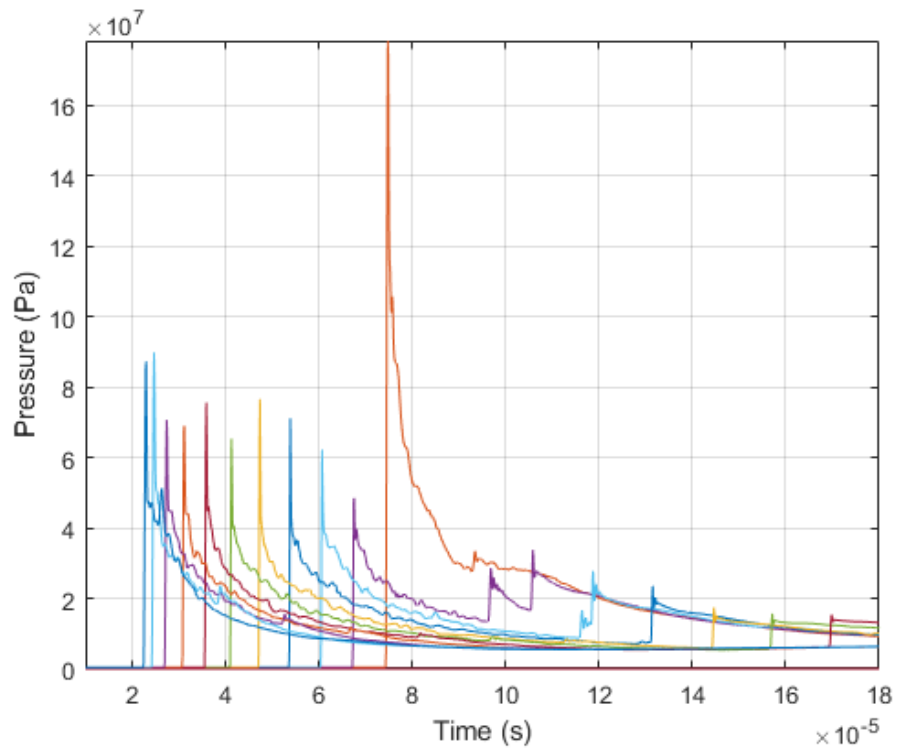


Figure 90. Low Pressure Model Pressure Values 3

Looking at the values of Figure 90, it can be observed that the pressure shock has two waves that interact with the wall but eventually combine over time along with die down in the intensity. It also can be observed in Figure 90 that after the pressure shock, the pressure reduces to new stagnate pressure. Figure 91 through Figure 95 are the same as the prior figures but display the temperature values instead of the pressure values.

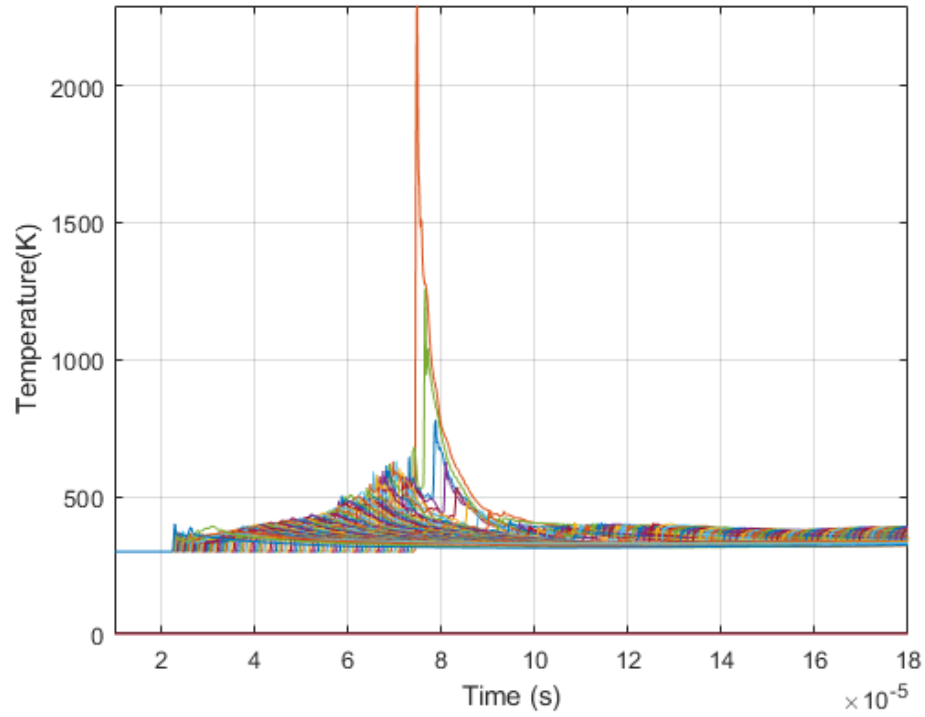


Figure 91. Low Pressure Model Temperature Values 1

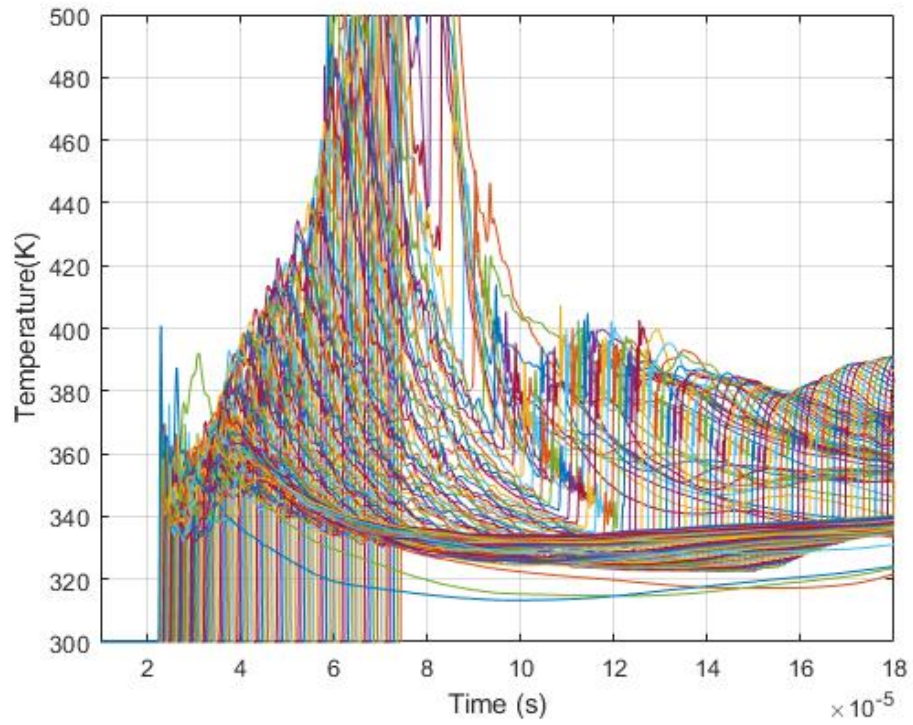


Figure 92. Low Pressure Model Temperature Values 2

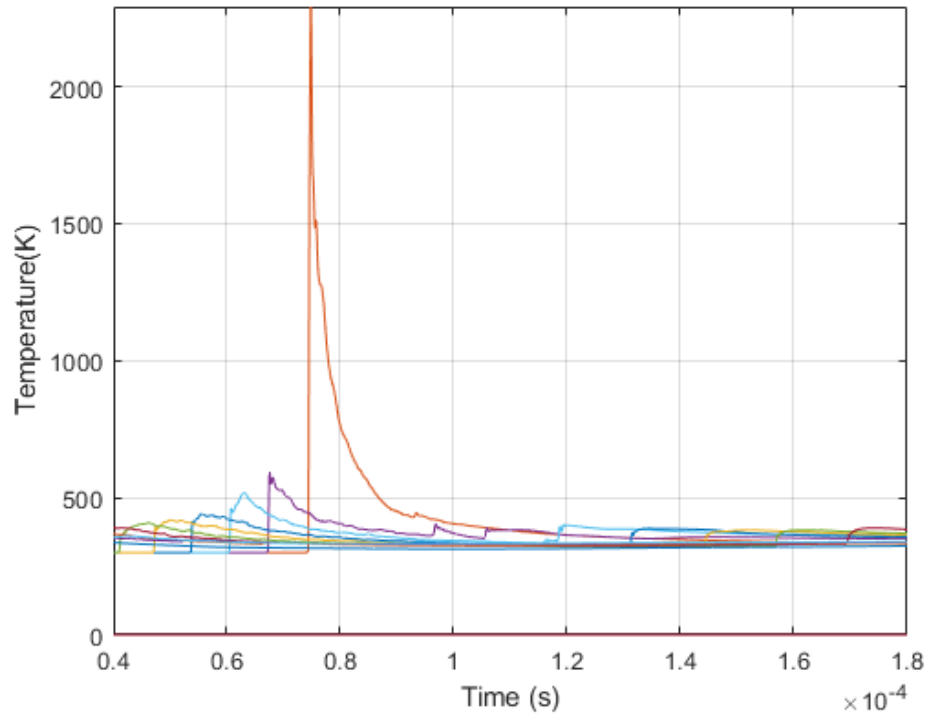


Figure 93. Low Pressure Model Temperature Values 3

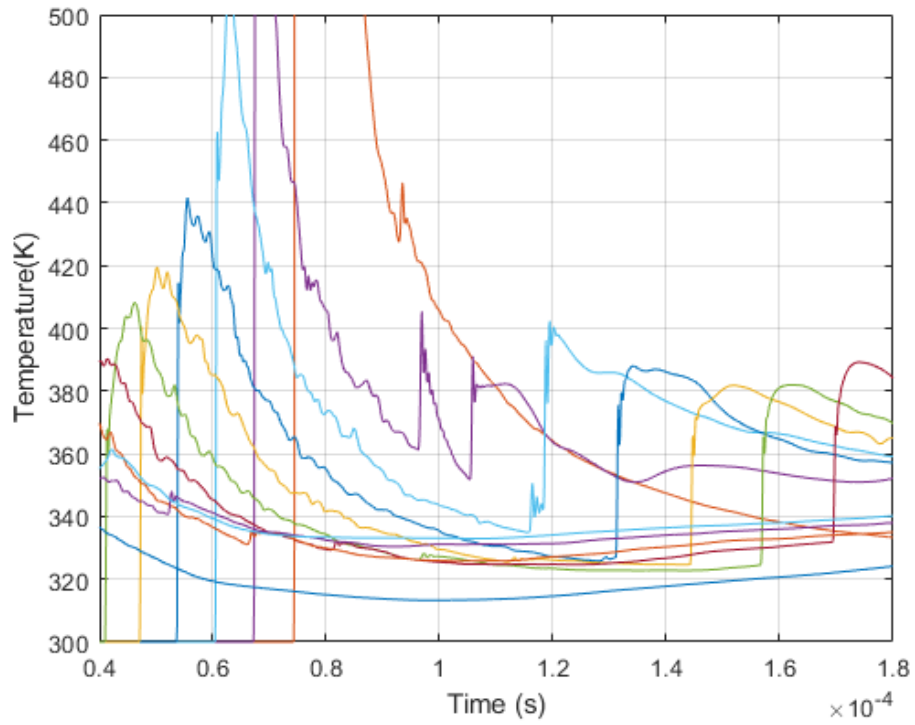


Figure 94. Low Pressure Model Temperature Values 4

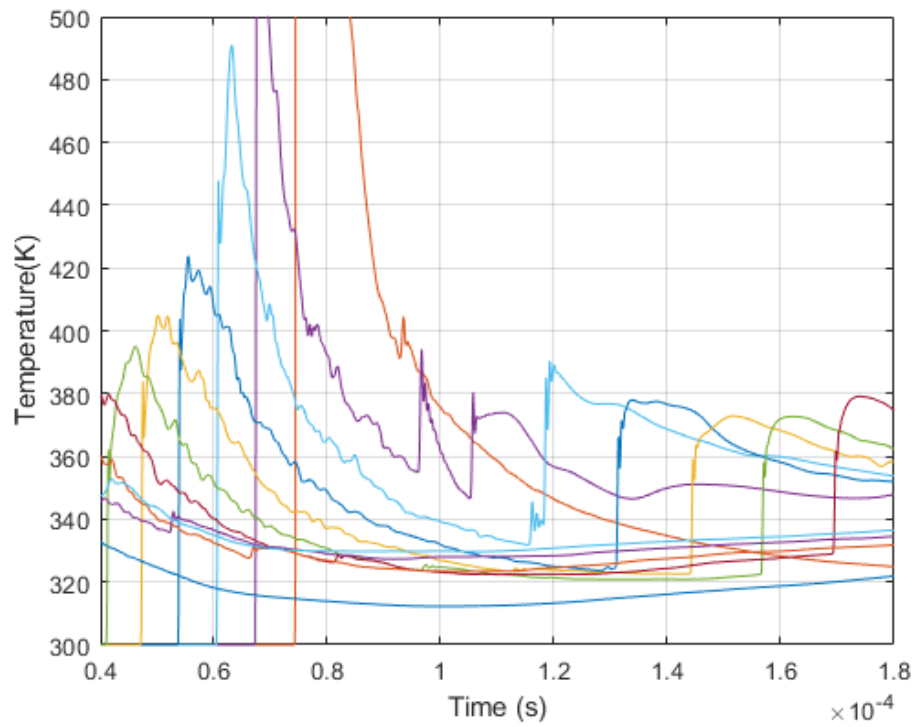


Figure 95. Low Pressure Model Temperature Values 5

Figure 94 and Figure 95 shows the same positions along the wall, but vary due to the solid line is being taken from inside the solid wall. This causes there to be lower temperatures as there is conduction that is happening. Figure 96 through Figure 98 display the pressure and temperatures with respect to time at different positions.

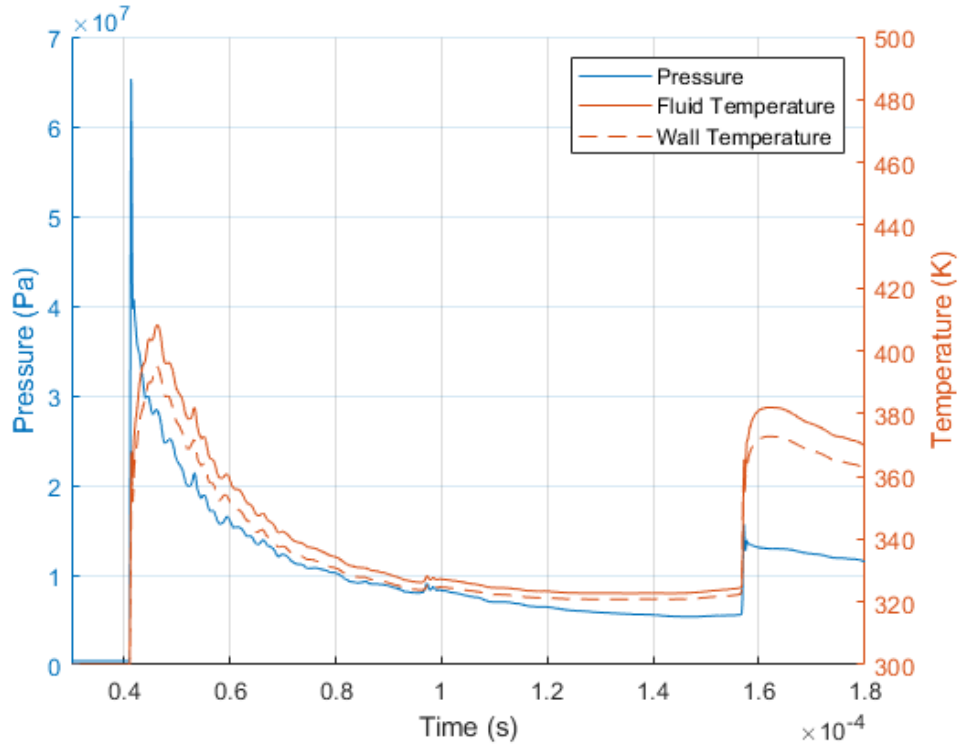


Figure 96. Low Pressure Model Pressure and Temperature at Position 1

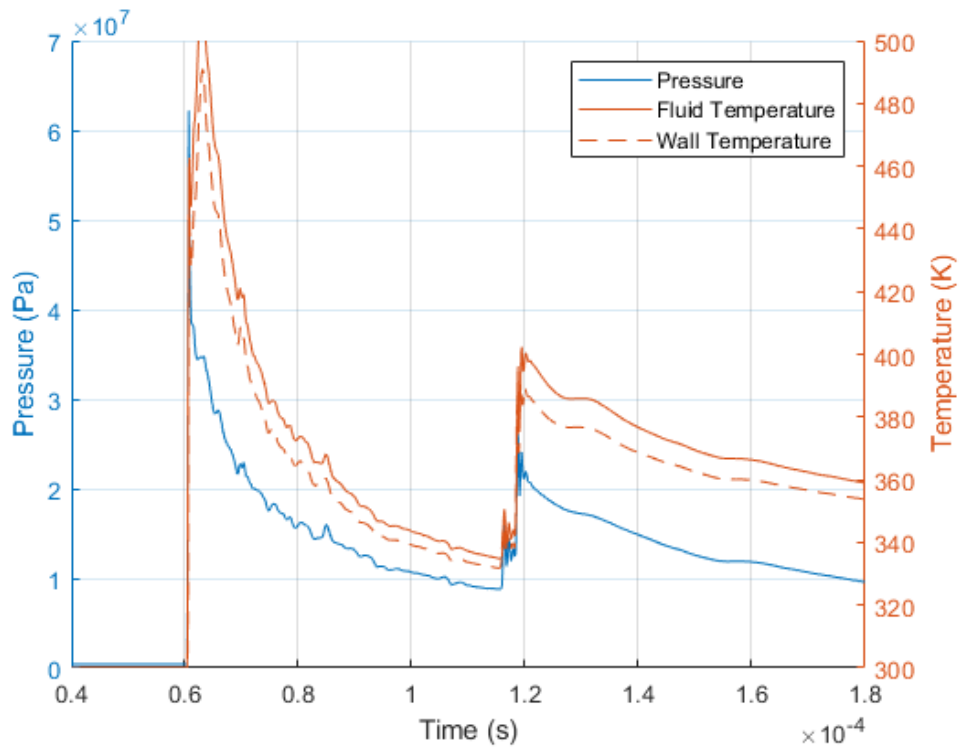


Figure 97. Low Pressure Model Pressure and Temperature at Position 2

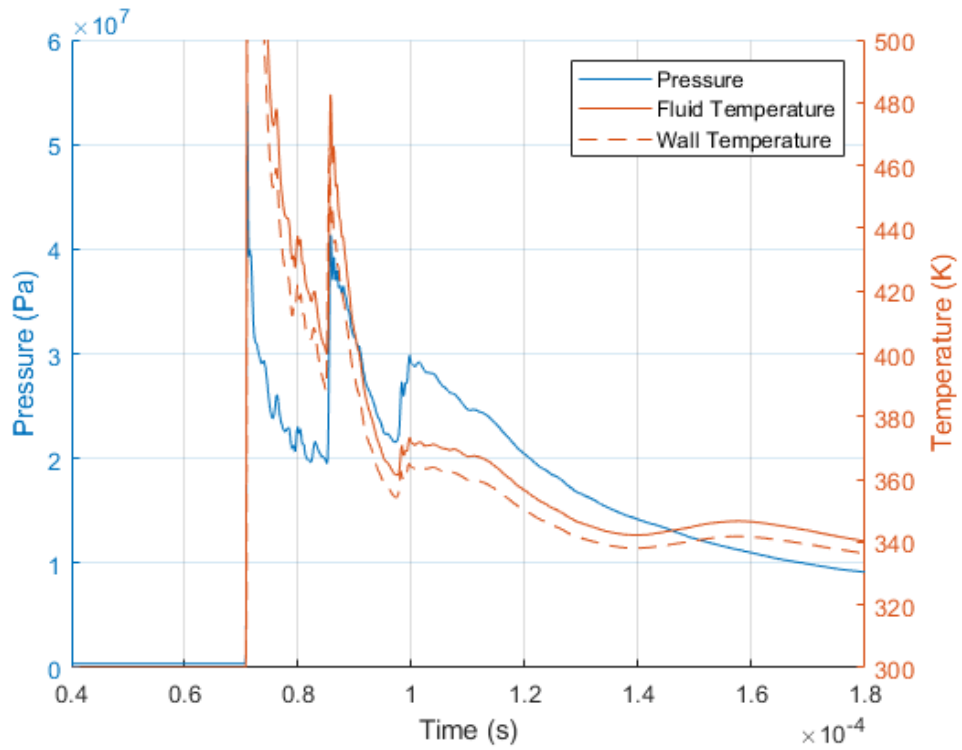


Figure 98. Low Pressure Model Pressure and Temperature at Position 3

Figure 96 is a position near the top of the wall, Position One. There are two major spikes in the temperature that correspond with a pressure shock, a smaller third pressure spike occurs but does not produce the same temperature as the prior two. As the pressure slowly diminishes past the shock waves, the temperature fluctuates. This is due to convection happening in the chamber. In Figure 97 the same pressure spike can be observed at a later time with the secondary pressure spike occurring earlier. Figure 98 has the shortest time between the two pressure shocks, this is due to its position being near the bottom of the chamber.

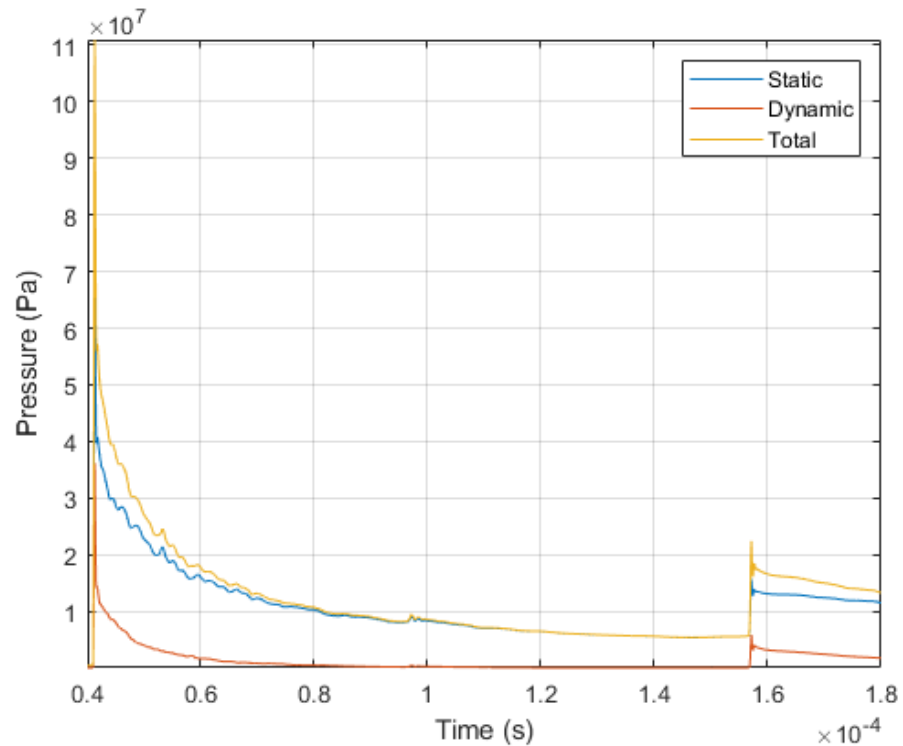


Figure 99. Low Pressure Model Pressures at Position 1

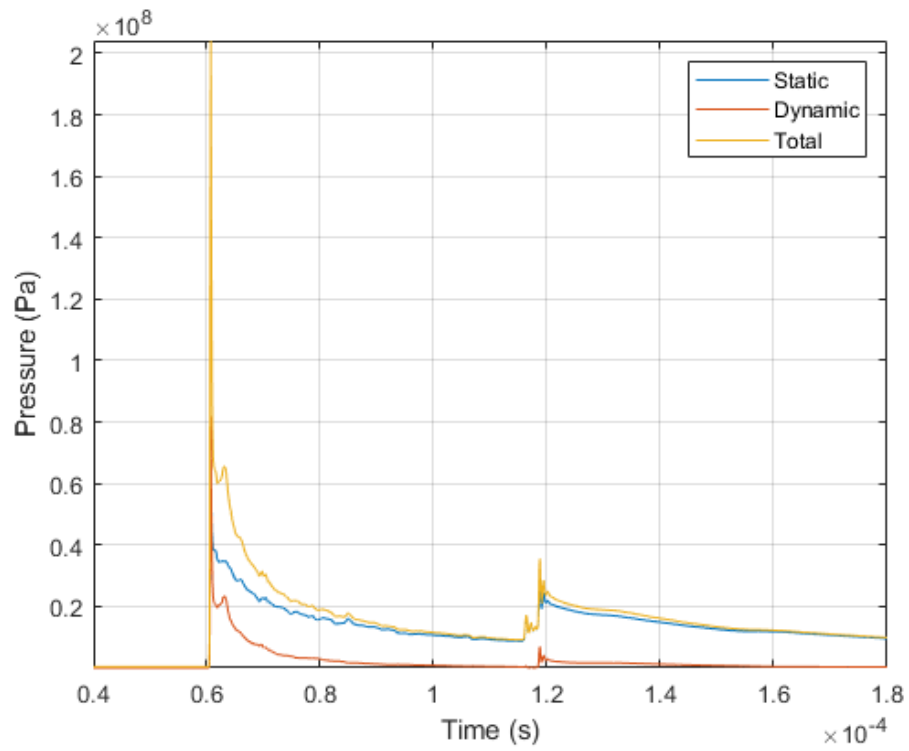


Figure 100. Low Pressure Model Pressures at Position 2

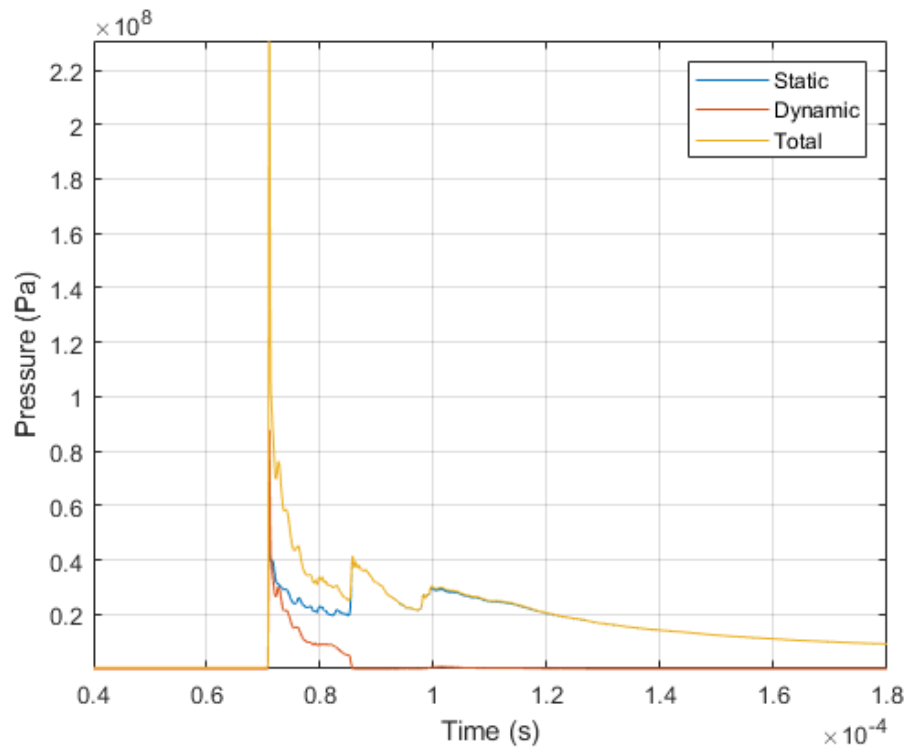


Figure 101. Low Pressure Model Pressures at Position 3

4.5 Combustion Model 5 (Nitrogen Model)

Due to similarities in the plots with prior models, the results of combustion model 5 are in Appendix A Figure A1 to Figure A18.

The pressure and temperature in this model is slightly higher than the normal and low pressure model. Like the prior models, when the pressure shocks combine in the chamber there is an increase in temperature. These values can be seen in Figure A1 and Figure A2. The temperature values of the nitrogen model follow closely to those of the normal model and the low pressure model. The major difference in the nitrogen model is the higher peak temperature. The slight varying in the timing of these shocks is due to the shocks traveling at slightly different speeds. The peak speeds of the models are recorded in Table 20. The differences in temperature across the models results in varying velocities for the pressure shock. The temperature plots can be seen in Figure A8 through Figure A12.

4.6 Combustion Model 6 (Stoichiometric Model)

Due to similarities in the plots with prior models, the results of combustion model 5 are in Appendix A Figure A19 to Figure A36.

The overall temperatures in the stoichiometric model were higher than the first model. This is expected as the adiabatic flame temperature of a stoichiometric combustion is higher than that of a fuel rich combustion as seen in Figure 1. The pressure and temperature of the model can be seen in Figure A19 and Figure A20. The pressure shocks in the stoichiometric model are traveling at a faster velocity than the prior models, these velocities can be seen in Table 20. There is also a greater temperature experienced in the stoichiometric model. This is due to the stoichiometric combustion having a higher adiabatic flame temperature. The plots of the pressure at varying positions can be seen in Figure A34 through Figure A36.

4.7 Combustion Model 7

This model ran with the same settings as the normal model. All results for this model are based on the wall values recorded during the combustion simulation.

4.7.1 Combustion Model 7 Contour Plots

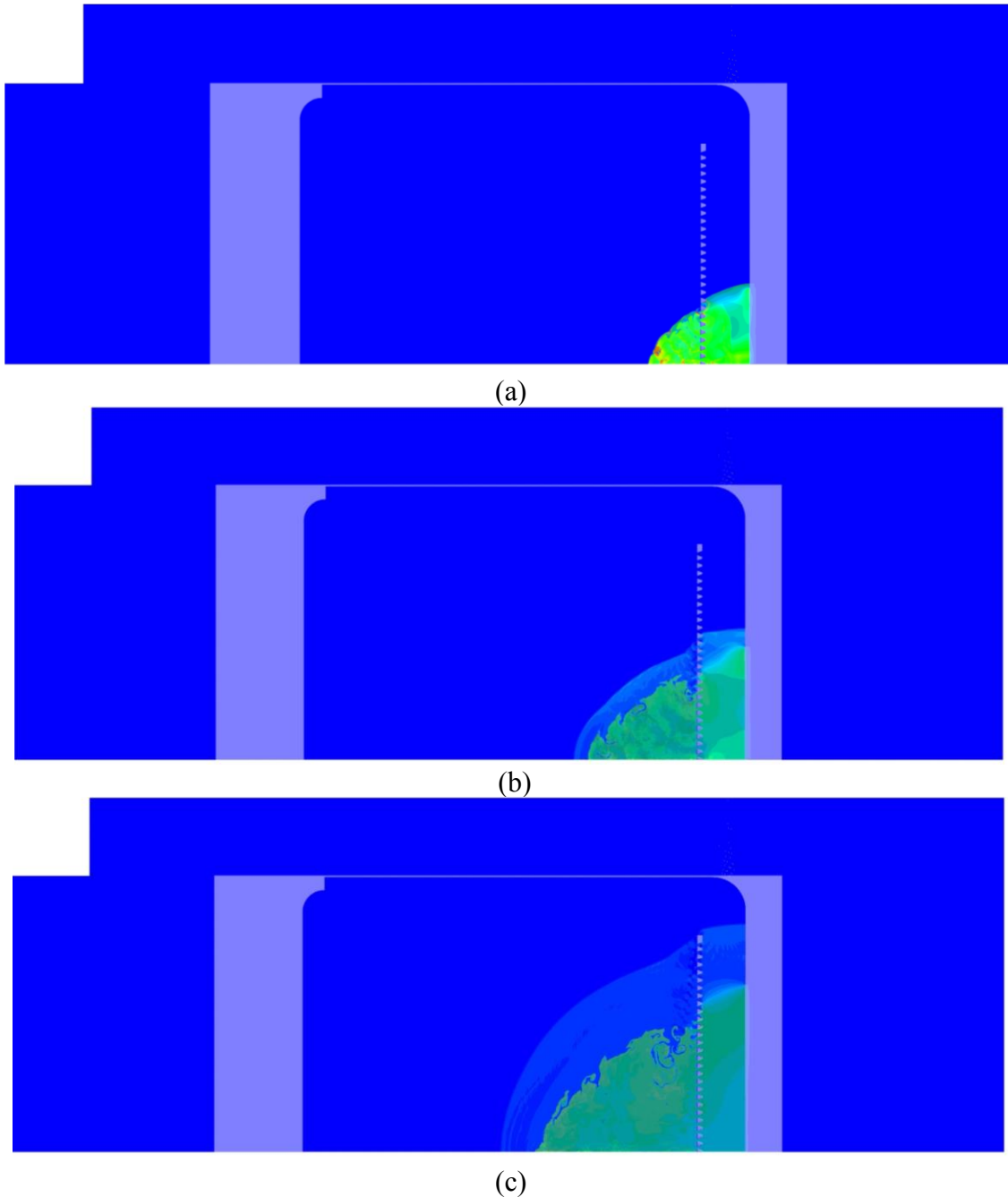


Figure 102. Combustion Model 7 Overlaid Contours at timestep 3000 (a), 7000 (b), 13000 (c)

The combustion flame travels at a slower speed due to the combustion being a turbulent combustion and not a detonation. With the smaller holes in the model, there is a lower pressure in the chamber. These results show that adding a perforated plate can help in the reduction of the pressure in the chamber.

4.8 Full Model Comparison

The average pressures across the models at different time steps were taken and recorded in Table 17 and Table 18.

Table 17. 10000 Time Step Pressures

	Normal Model			Nitrogen Model		
	Static	Dynamic	Total	Static	Dynamic	Total
Pressure (Pa)	9499595.3	1323896	10993040	8731079	1189761	10070870
Percent of Total	0.864%	0.120%		0.867%	0.118%	
	Low Pressure Model			Stoichiometric Model		
	Static	Dynamic	Total	Static	Dynamic	Total
Pressure (Pa)	7787199	1070880	8993912	12557290	1106130	13757670
Percent of Total	0.866%	0.119%		0.913%	0.080%	

Table 18. 20000 Time Step Pressures

	Normal Model			Nitrogen Model		
	Static	Dynamic	Total	Static	Dynamic	Total
Pressure (Pa)	17188550	1468622	19003130	15043740	1754478	18251920
Percent of Total	0.905%	0.077%		0.824%	0.096%	
	Low Pressure Model			Stoichiometric Model		
	Static	Dynamic	Total	Static	Dynamic	Total
Pressure (Pa)	14009390	1181391	15424060	15532490	1036616	16623240
Percent of Total	0.908%	0.077%		0.934%	0.062%	

At the 10,000th time step the normal, low pressure, and nitrogen model all have varying total static, dynamic, and total pressures. The percentages of the static and dynamic pressure of those models are all within a range of 2% of each other as the stoichiometric model is at a much larger difference. This is due to the large difference in the composition of the fluid. At the 20,000th time step there is a larger variance across the models. This variance is due to the varying fluid compositions. The normal model and low pressure model have identical fluid composition and their percentages of pressures are very similar while the nitrogen and stoichiometric have large differences in fluid composition and have large differences in their percentage of pressures.

4.9 Wall Data Comparison

Figure 103 through Figure 108 show the static pressure at a given location across the four models with respect to time. The peak pressure values from these graphs are in Table 19.

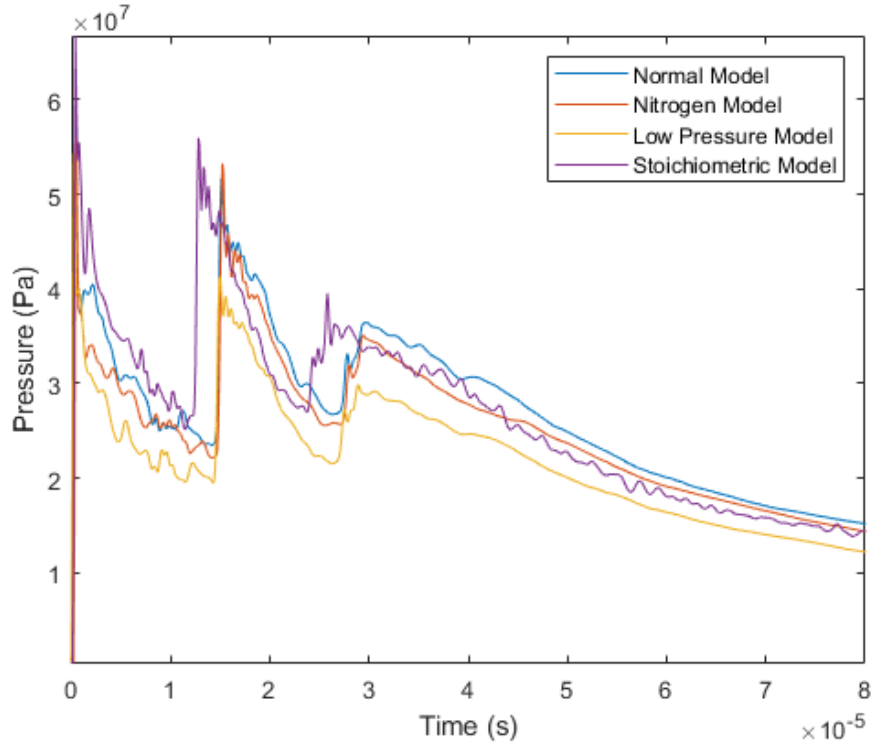


Figure 103. Position 1 Static Pressure Comparison

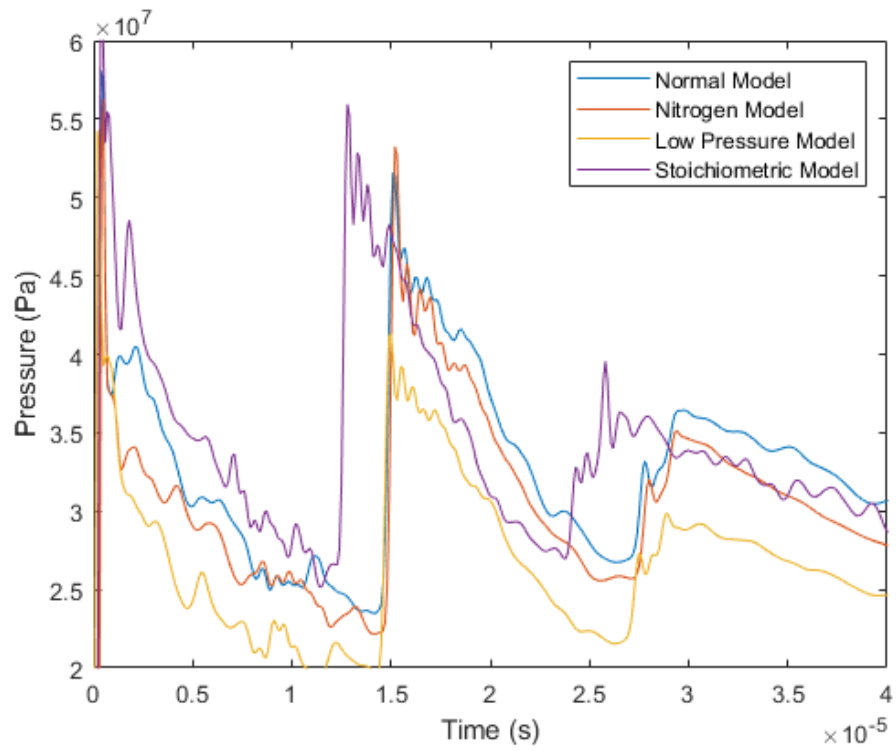


Figure 104. Position 1 Static Pressure Comparison

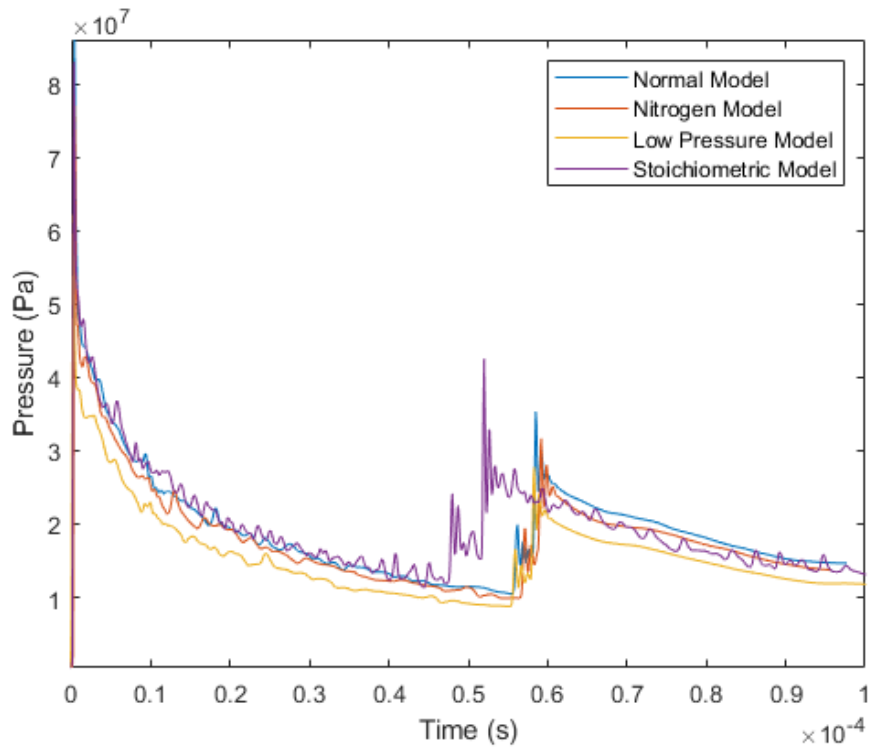


Figure 105. Position 2 Static Pressure Comparison

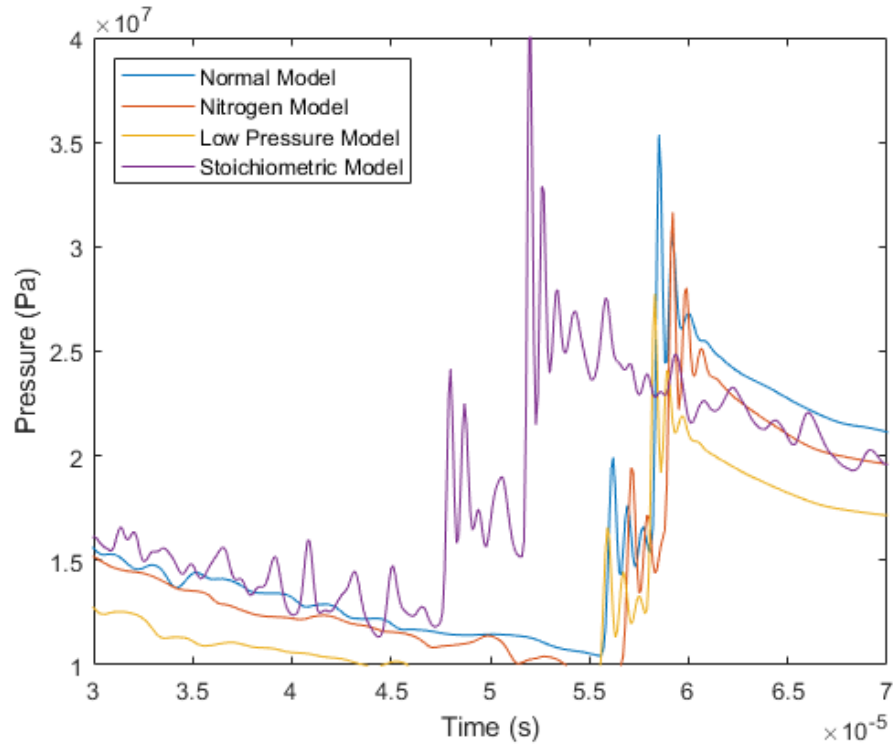


Figure 106. Position 2 Static Pressure Comparison

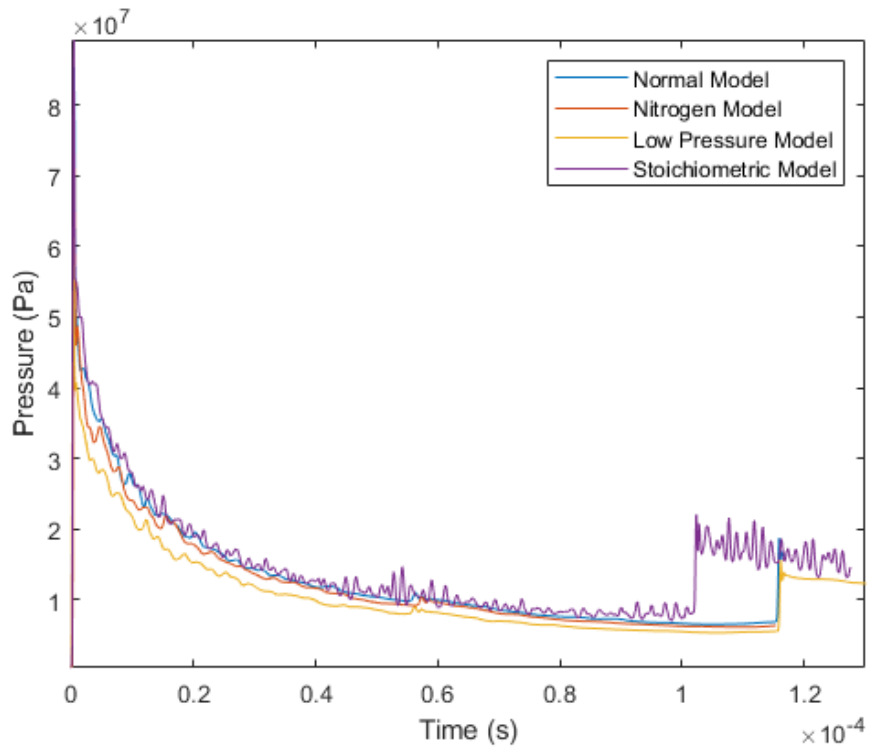


Figure 107. Position 3 Static Pressure Comparison

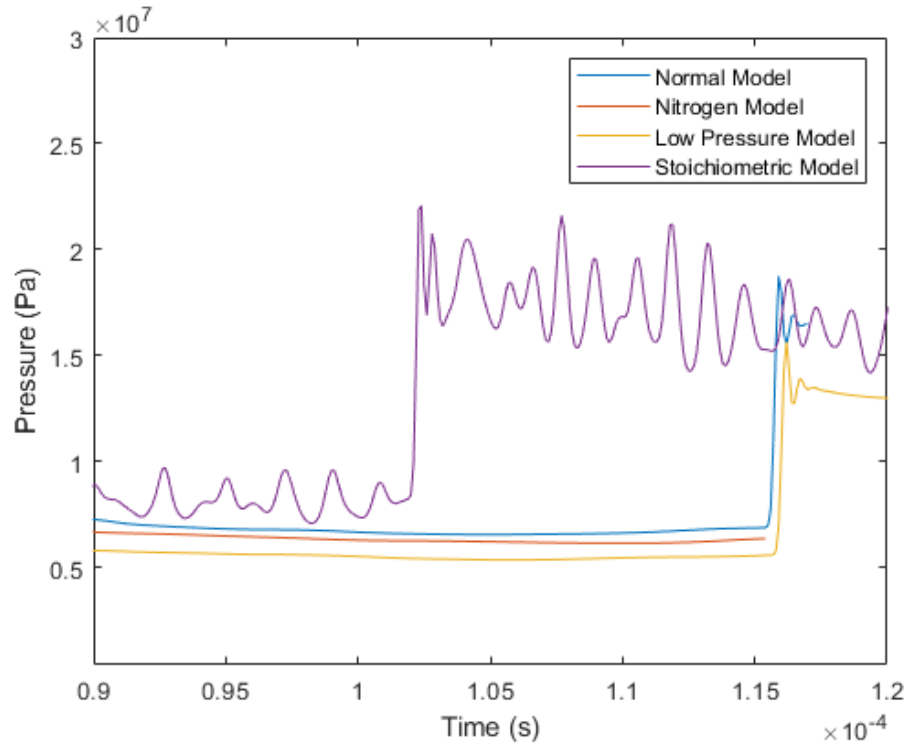


Figure 108. Position 3 Static Pressure Comparison

The pressure in the models have similar peaks pressure peaks. The variation in the pressure across the models is a result of the fluid composition and initial pressure of the system. The most notable difference between the models is the stoichiometric models pressure shocks spiking ahead of the other three models. This means that the pressure shock is traveling slightly faster than the other models. Between the first three models the pressure spikes are within a close range of each other. The stoichiometric model has higher-pressure spikes. Table 20 shows the velocity of the pressure shocks, in these tables it is observed that the stoichiometric model has the highest peak velocities. These pressure shocks in the system are the primary source of the pressure that occurs and are the most important when it comes to reducing the pressure and temperatures in the system. The peak pressures of the normal, low pressure, and nitrogen models are all with in a similar range of each other. The stoichiometric model has much higher peak pressures due to the higher temperatures in the system. As the pressure shock moves across the models, all models experience a drop in pressures. This is due to the pressure shock slowly losing its energy as it is converted to temperature.

Table 19. Tabulated Pressure Peaks

Normal Model											
Position 1						Position 2			Position 3		
Peak 1			Peak 2			Peak 1			Peak 1		
Static	Dynamic	Total	Static	Dynamic	Total	Static	Dynamic	Total	Static	Dynamic	Total
34,530,000	21,700,000	62,790,000	51,600,000	14,140	51,610,000	35,350,000	9,600,000	46,110,000	18,730,000	6,745,000	26,580,000

Low Pressure Model											
Position 1						Position 2			Position 3		
Peak 1			Peak 2			Peak 1			Peak 1		
Static	Dynamic	Total	Static	Dynamic	Total	Static	Dynamic	Total	Static	Dynamic	Total
28,020,000	20,310,000	55,550,000	41,320,000	3,125	41,390,000	27,740,000	6,989,000	35,510,000	15,640,000	5,800,000	22,410,000

Nitrogen Model											
Position 1						Position 2			Position 3		
Peak 1			Peak 2			Peak 1			Peak 1		
Static	Dynamic	Total	Static	Dynamic	Total	Static	Dynamic	Total	Static	Dynamic	Total
30,820,000	18,580,000	54,710,000	53,240,000	7,919	53,550,000	31,650,000	6,919,000	39,230,000			

Stoichiometric Model											
Position 1						Position 2			Position 3		
Peak 1			Peak 2			Peak 1			Peak 1		
Static	Dynamic	Total	Static	Dynamic	Total	Static	Dynamic	Total	Static	Dynamic	Total
66,730,000	109,700,000	291,100,000	55,940,000	34,740	56,280,000	82,980,000	81,560,000	2.08E+08	89,220,000	48,290,000	147,700,000

Table 20. Peak Velocities

TIME STEP	4000		10000		20000	
	Velocity (m/s)	Mach	Velocity (m/s)	Mach	Velocity (m/s)	Mach
NORMAL	1813	1.35	1857	1.39	4578	2.5
LOW PRESSURE	1751	1.33	2196	1.53	4349	2.26
NITROGEN	1803	1.35	1876	1.46	5777	4.05
STOICHIOMETRIC	1983	1.25	2726	1.75	3474	1.92

The peak velocity for both the 4,000th and 10,000th time step is maximum in the stoichiometric model; this is due to the increased adiabatic flame temperature. While the velocity of the pressure shock is faster, the Mach number is lower due to the air properties being different than the other models. In the 20,000th time step the stoichiometric models' velocity is lower than the other models. This can be due to the pressure shock being further ahead than the other models resulting in more energy being lost and a slower shock speed. The overall increase in velocity for all models at the 20,000th time step is caused from the combination of the reflected shock waves. The large variance in Mach number across the 20,000th time step is due to the different fluid composition and chamber pressure.

5 Conclusion and Future Work

5.1 Conclusions

The primary findings of the simulations presented in this work are the pressure shocks in the chamber. It was previously unknown that these shocks were forming in the chamber or that the pressure shocks were peaking at such high values. Varying initial properties in the chamber such as the pressure, adding inert gas and changing the mixture ratio provides a change in the chamber's pressures and temperatures. The introduction of perforated plating caused a change in the combustion that resulted in lower pressures and temperatures in the chamber. These perforated plates also caused the combustion to happen at a slower rate. When the need for a lower pressure in the chamber it is best to have a lower initial pressure when pressurizing the chamber. If a higher chamber is needed, then moving to a more fuel-lean ratio to lower the adiabatic flame temperature can be done. Another option to lower the pressure in the chamber without adjusting the initial pressure would be to introduce more inert gas in the chamber. With these discoveries there is now future work that can be done in this process.

5.2 Future Work

Future experimentation with higher sampling rates for experimental data with pressure transducers that allow for higher pressure readings. These values will provide more accurate data that can be used for comparison with simulation data. A new approach for recording temperature values inside the chamber can be done. A part can be manufactured with varying hole diameters, shapes, and porosity to determine the full effects that are produced in the chamber along with the ability to have experimental data to compare to simulation data of these geometries. Future simulation work is to run the 28-model combustion for a more accurate representation of the combustion along with moving into 3D models. Both simulations will drastically increase the computation time of the simulations. Additional models can be run that include the flow into the chamber to determine the effects of this flow based on the time allowed for the flow to settle prior to ignition. This will cause there to be slight variances in the fluid's mixture prior to combustion.

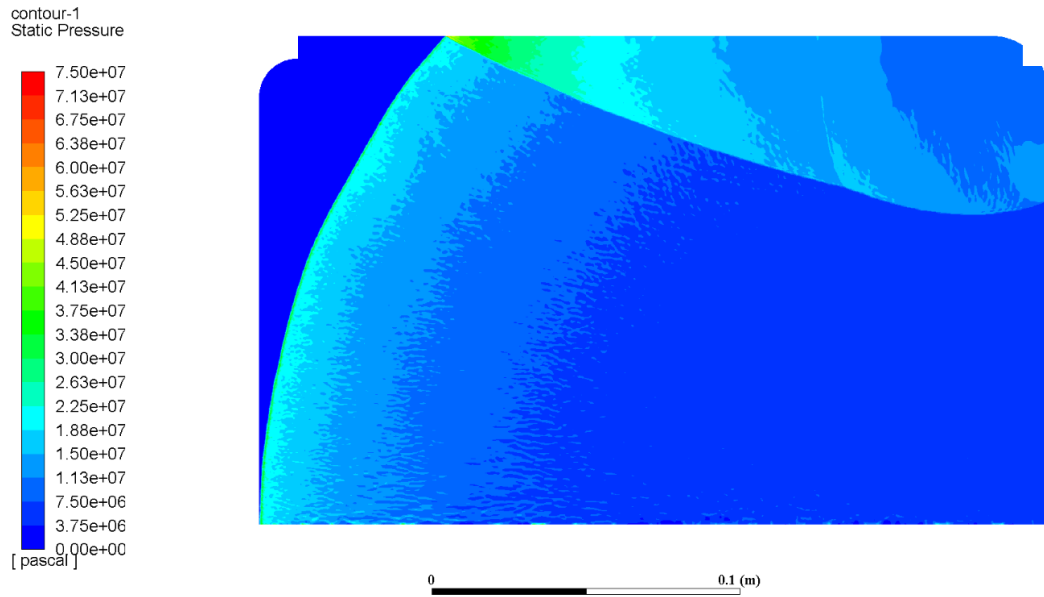
References

- [1] M. A. Liberman, Introduction to Physics and Chemistry of Combustion, Springer, 2010.
- [2] D. L. Smoot, W. C. Hecker and G. A. Williams, "Prediction of Propagating Methane-Air Flames," *Combustion and Flame*, no. 26, pp. 323-342, 1976.
- [3] D. E. Jensen and G. A. Jones, "Gas-phase reaction rate coefficients for rocketry applications," Rocket Propulsion Establishment, Westcott Buckinghamshire, England, 1971.
- [4] C. T. Bowman and D. J. Seery, Investigation of NO formation kinetics in combustion processes: the methane-oxygen-nitrogen reaction, Boston: Springer, 1972, pp. 123-139.
- [5] R. Edelman, J. Boccio and G. Weilerstein, "The roles of mixing and kinetics in combustion generated NOx," Federal Applied Science Laboratories, Inc, Westbury, 1973.
- [6] A. A. Cordeiro, P. M. Becker and R. J. Heinsohn, "Computer Simulations of Two Lean Premixed Methane Oxygen Flames," Pennsylvania State University, 1974.
- [7] J. Peeters and G. Mahnen, "Reaction mechanisms and rate constants of elementary steps in methane-oxygen flames," *Symposium (International) on Combustion*, vol. 14, no. 1, pp. 133-146, 1973.
- [8] C. K. Law, Combustion Physics, Cambridge University Press, 2010.
- [9] "https://doc.notus-cfd.org/axisymmetric_coordinate_system.png".
- [10] G. E. Andrews and D. Bradley, "The Burning Velocity of Methane-Air Mixtures," *Combustion and Flame*, no. 19, pp. 275-288, 1972.
- [11] "<http://www.aerospaceweb.org/question/propulsion/q0224.shtml>".
- [12] P. Zitzewitz and N. Robert, Physics, New York: Glencoe/McGraw-Hil, 1995.
- [13] A. J. Aspden, M. S. Day and J. B. Bell, "Three-dimensional direct numerical simulation of turbulent lean premixed methane combustion with detailed kinetics," *Combustion and Flame*, no. 166, pp. 266-283, 2016.
- [14] B. D. L. Ferreira, J. M. Paulo, J. P. Braga and R. C. O. Sebastiao, "METHANE COMBUSTION KINETIC RATE CONSTANTS DETERMINATION: AN ILL-POSED INVERSE PROBLEM ANALYSIS," *Quim. Nova*, vol. 36, no. 2, pp. 262-266, 2013.
- [15] T. Schmitt, Y. Mery, M. Boileau and S. Candel, "Large-Eddy Simulation of oxygen/methane flames under transcritical conditions," *Proceedings of the Combustion Institute*, no. 33, pp. 1383-1390, 2011.

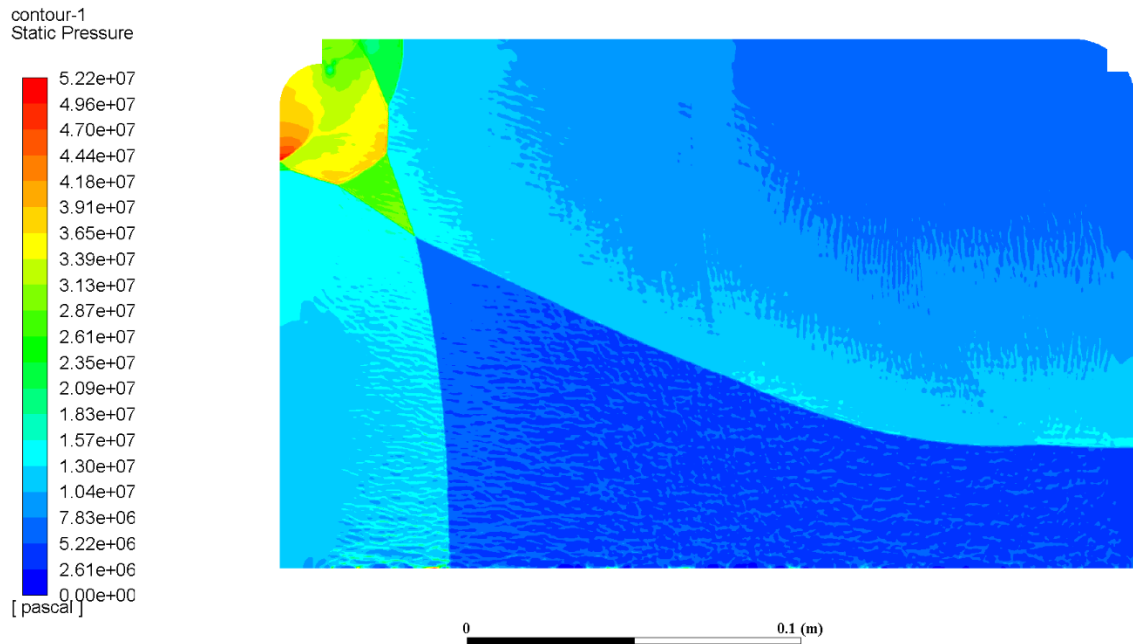
Appendix A

Combustion Model 5 (Nitrogen Model)

Combustion Model 5 Results



(a)



(b)

Figure A1. Combustion Model 5 Pressure at timestep 8000 (a), 12500 (b)

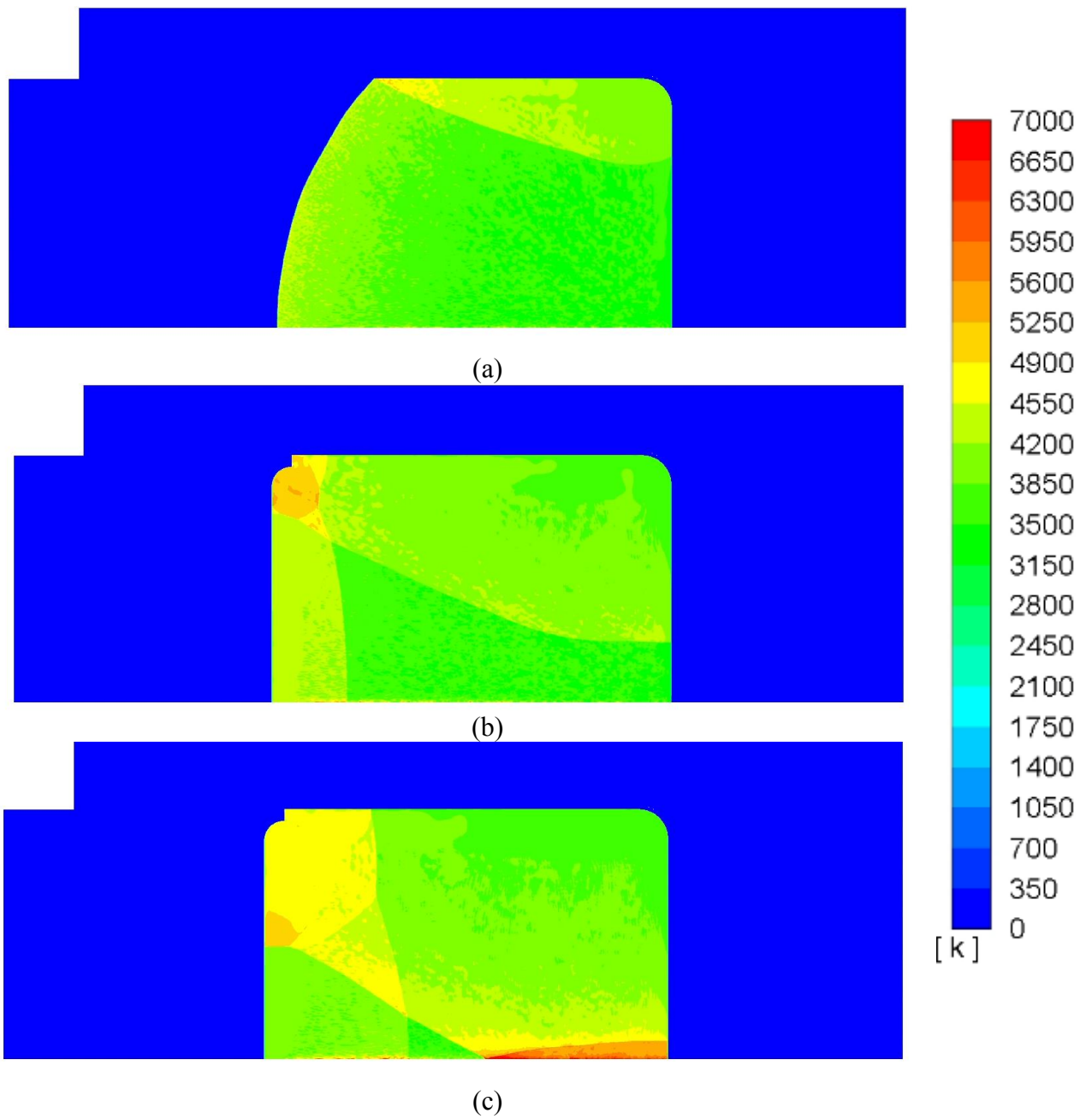


Figure A2. Combustion Model 5 Temperature at timestep 7500 (a), 12500 (b), 14500 (c)

Combustion Model 5 Full Wall Values

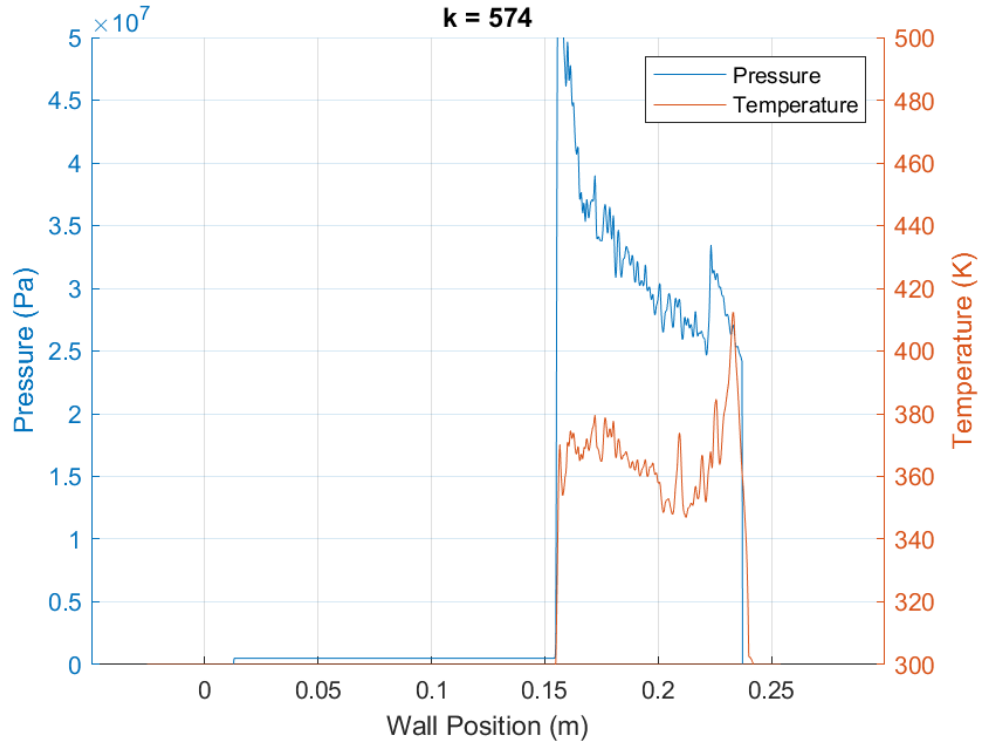


Figure A3. Nitrogen Model Mid Wall Values

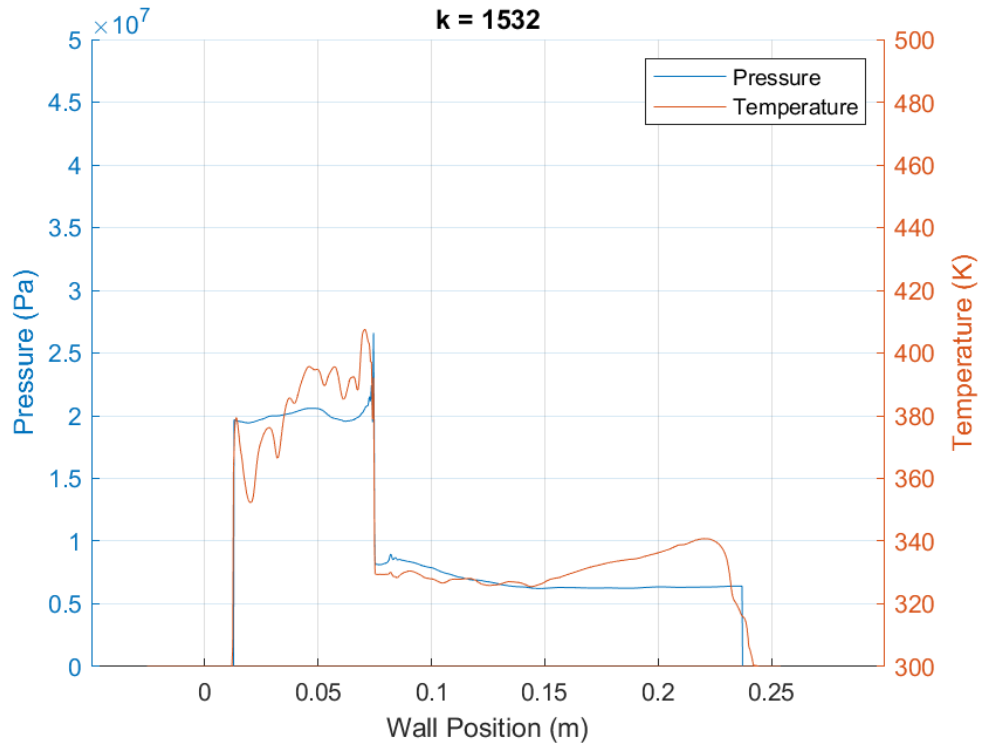


Figure A4. Nitrogen Model Wall Shock Combination

Combustion Model 5 Single Wall Values

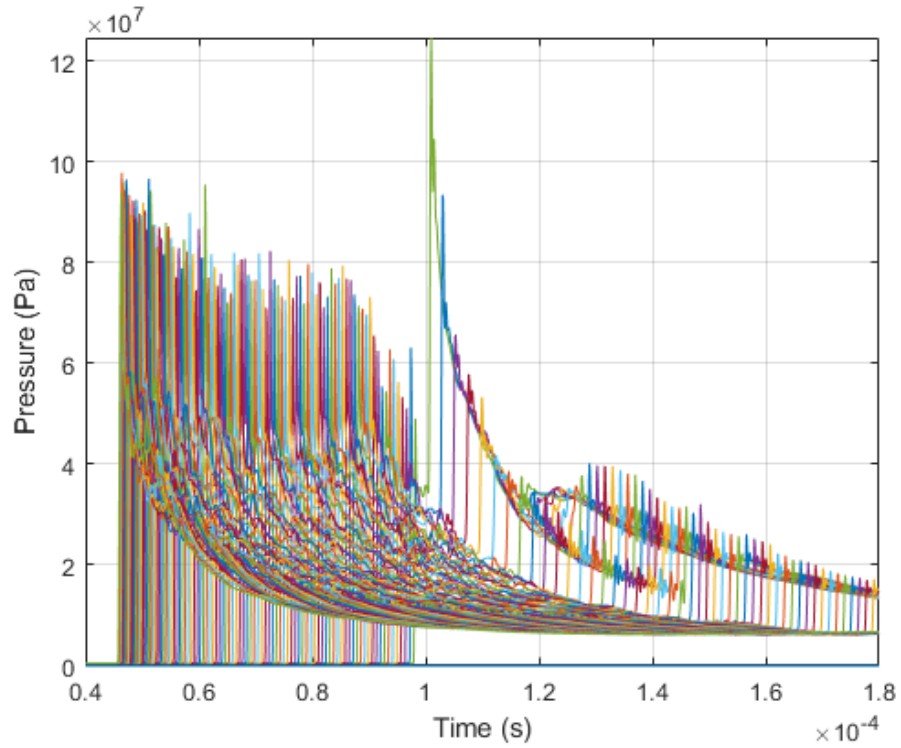


Figure A5. Nitrogen Model Pressure Values 1

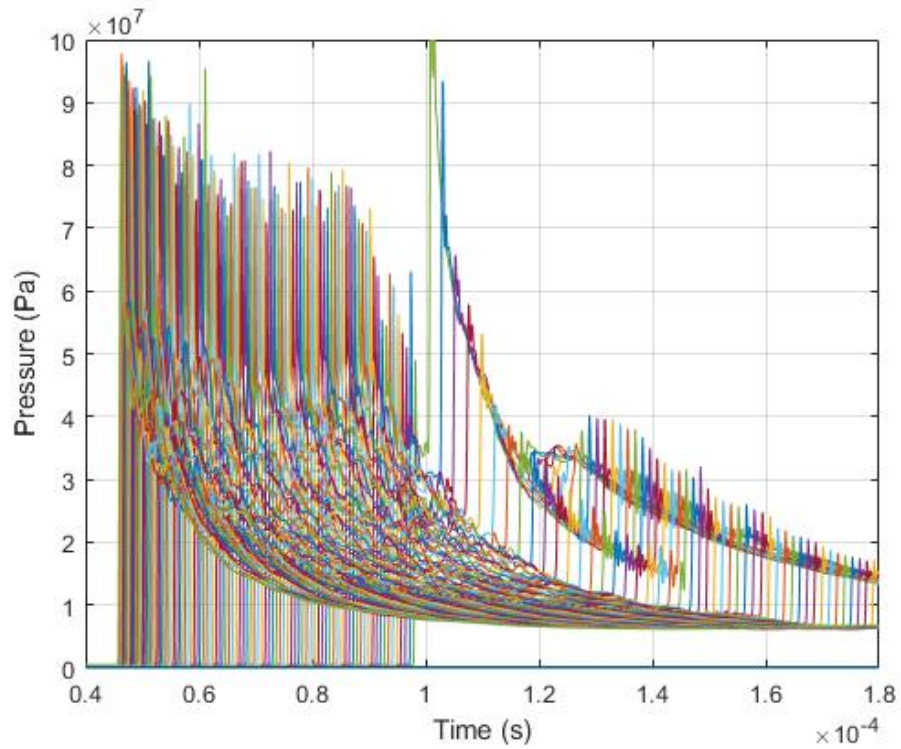


Figure A6. Nitrogen Model Pressure Values 2

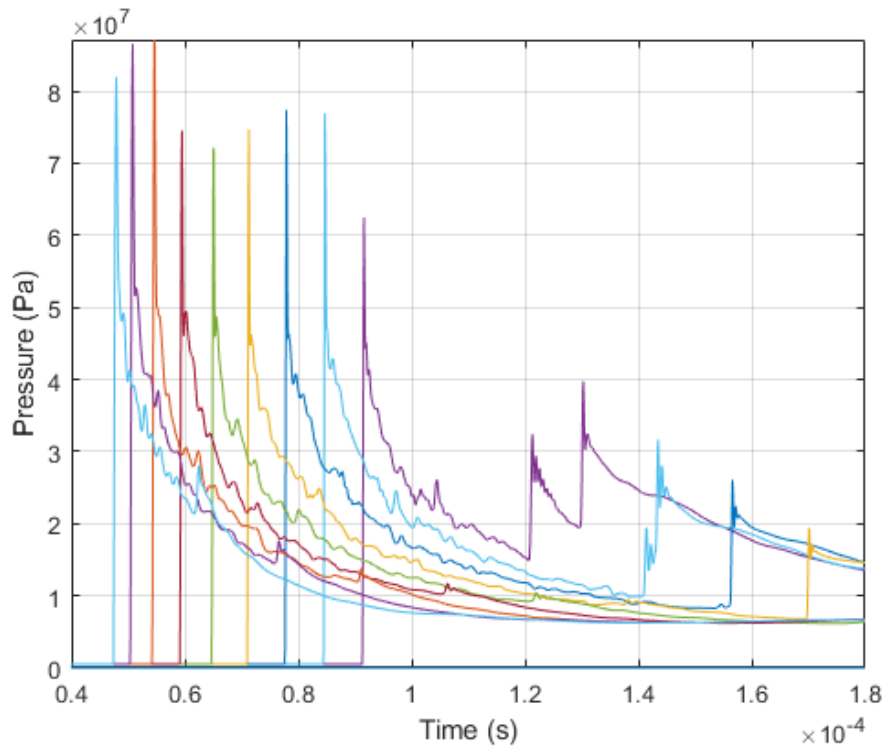


Figure A7. Nitrogen Model Pressure Values 3

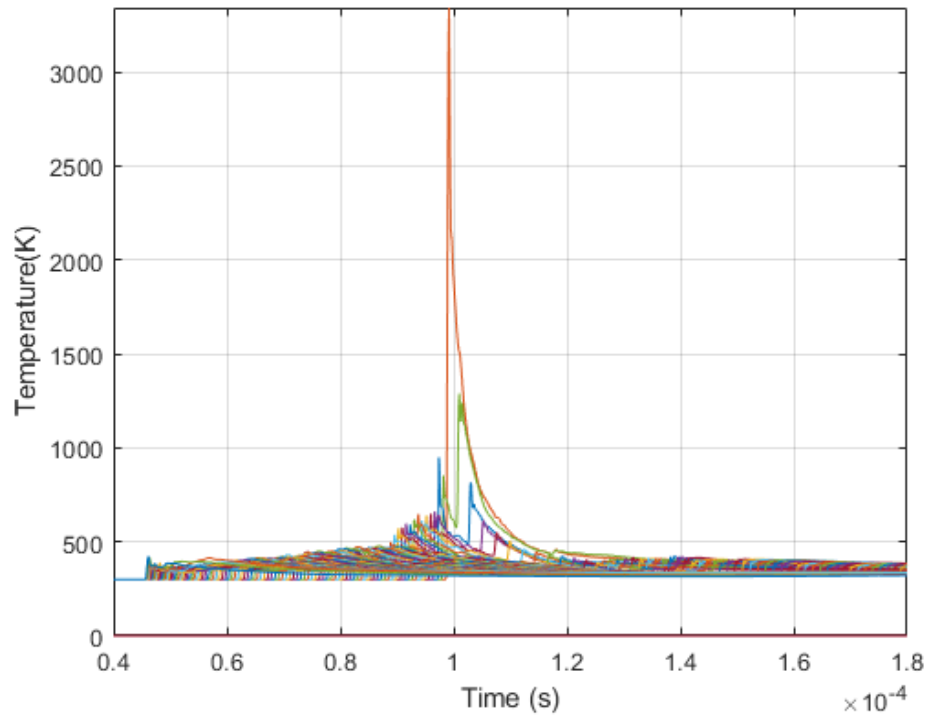


Figure A8. Nitrogen Model Temperature Values 1

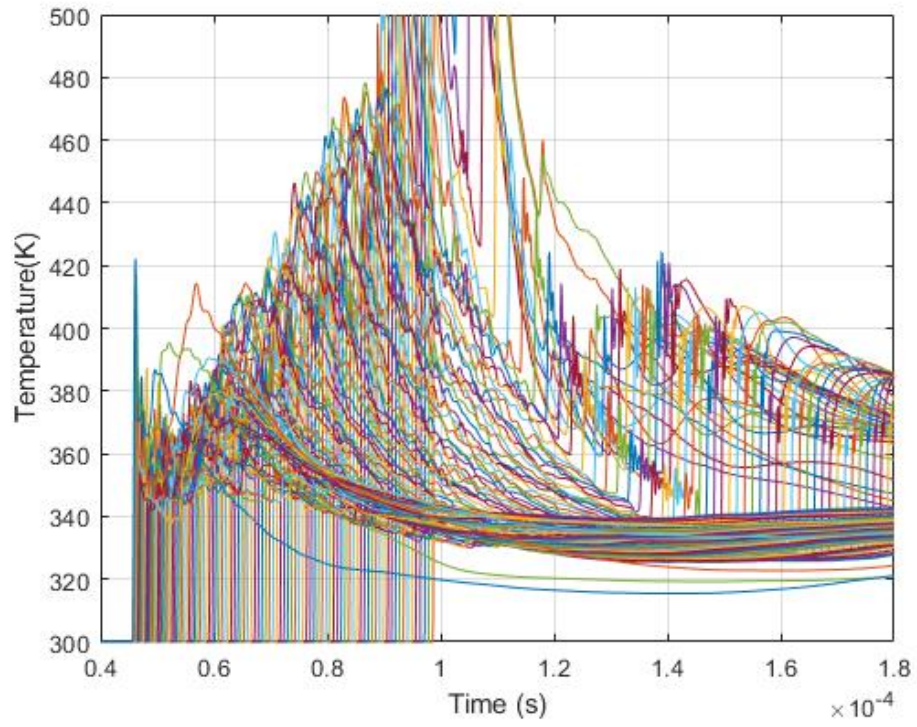


Figure A9. Nitrogen Model Temperature Values 2

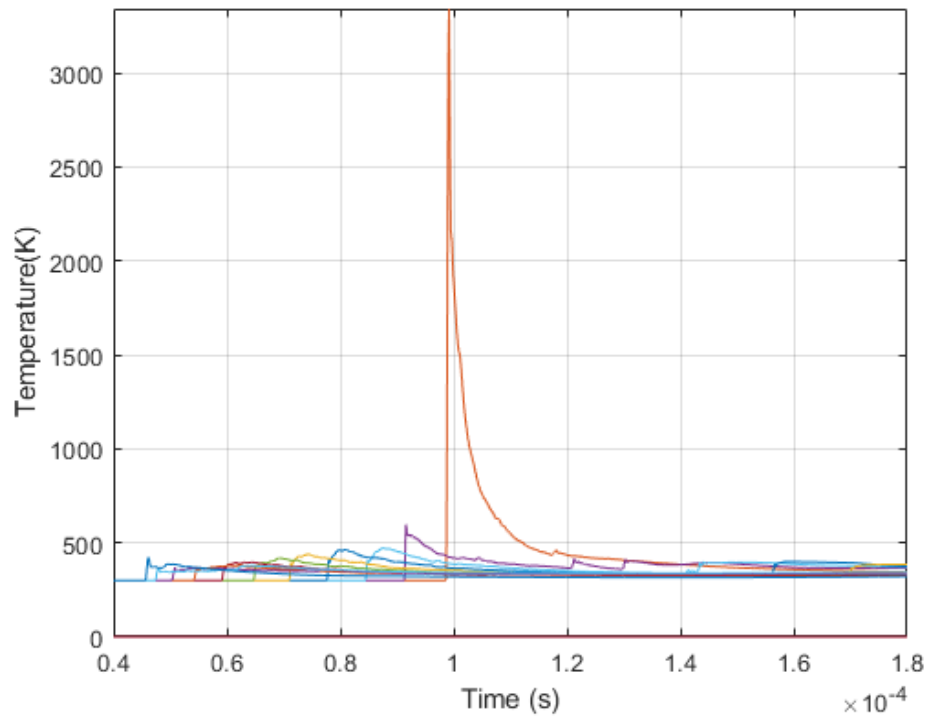


Figure A10. Nitrogen Model Temperature Values 3

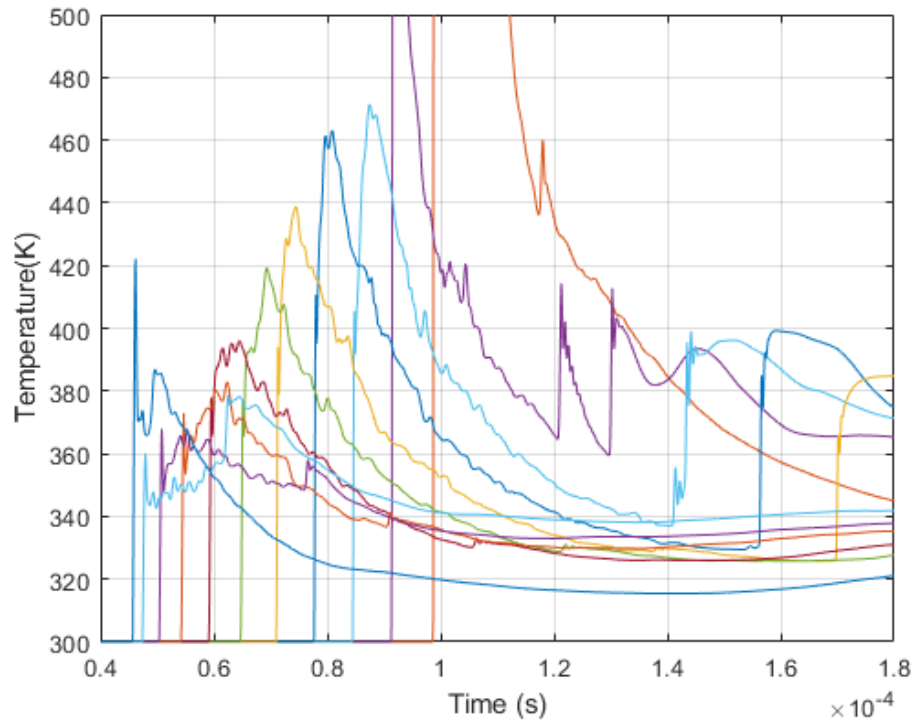


Figure A11. Nitrogen Model Temperature Values 4

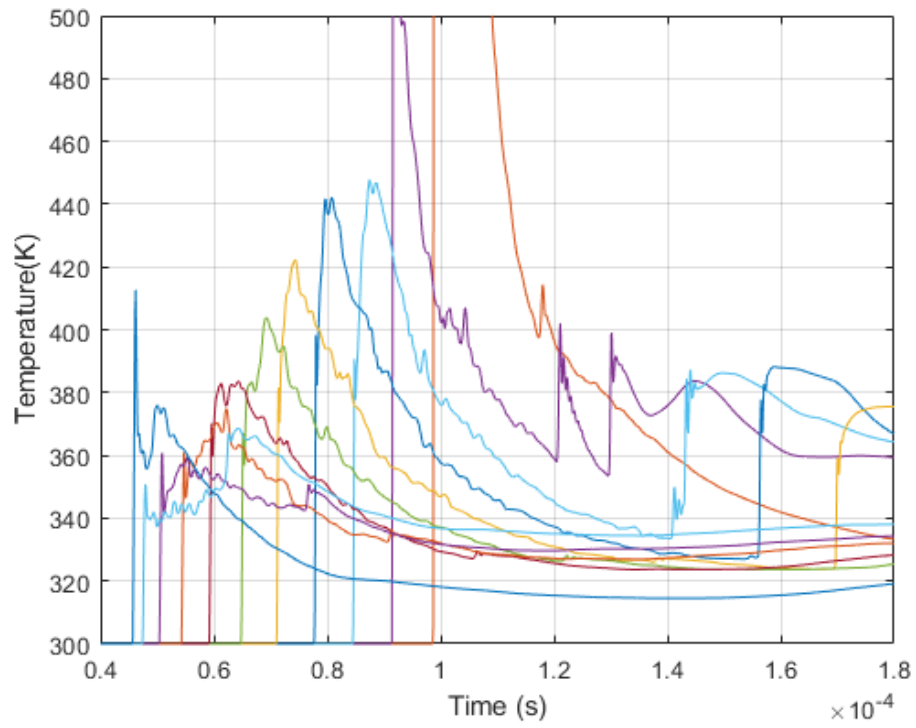


Figure A12. Nitrogen Model Temperature Values 5

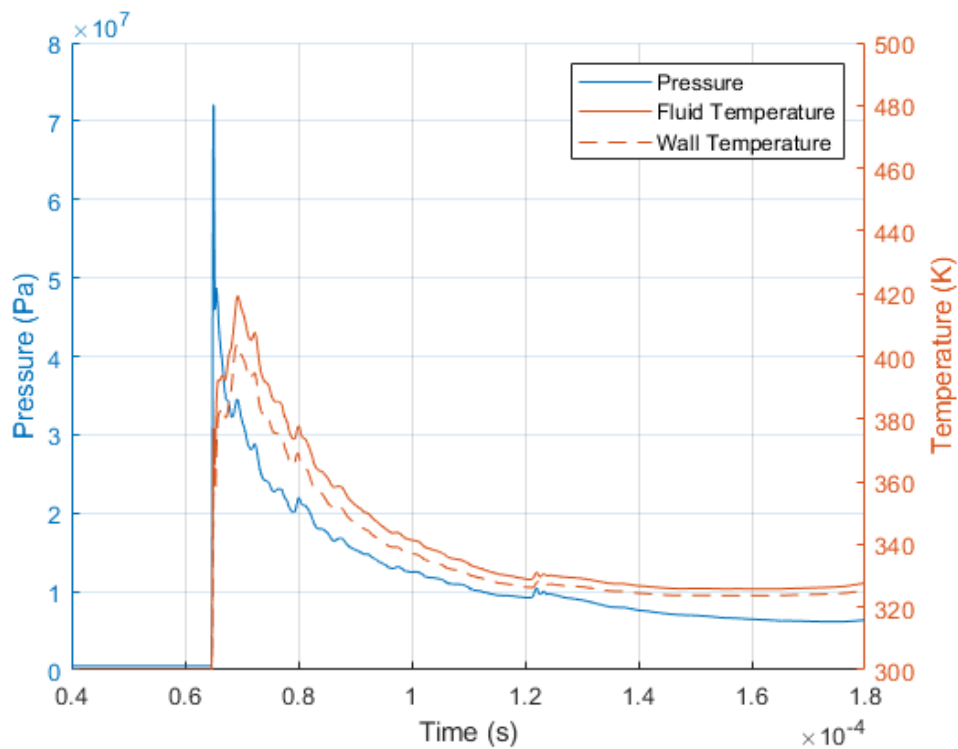


Figure A13. Nitrogen Model Pressure and Temperature at Position 1

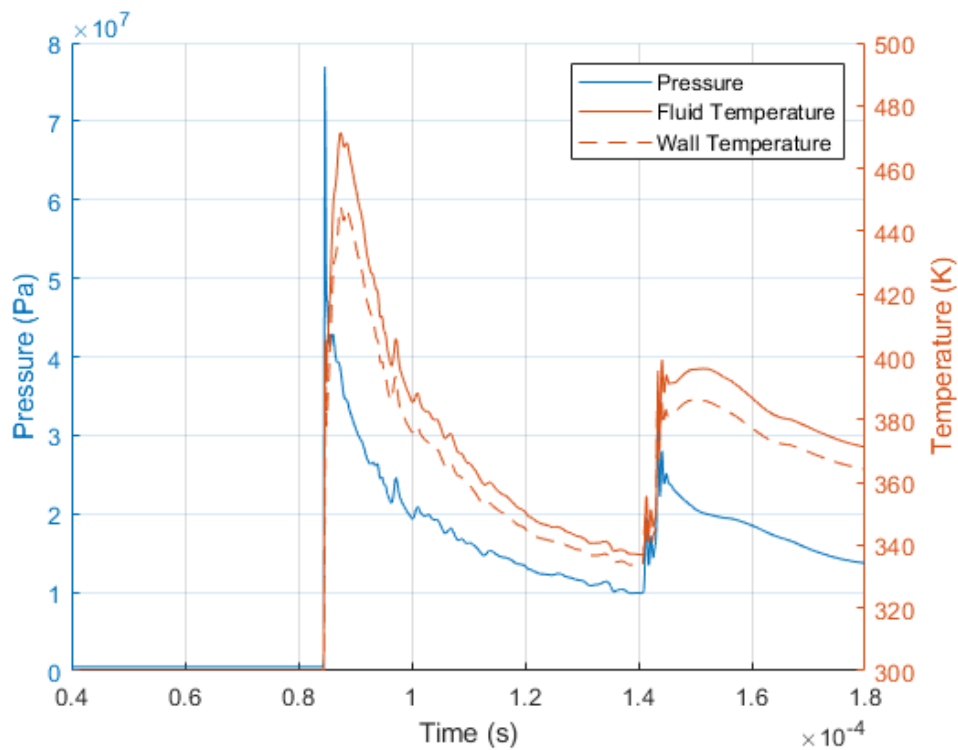


Figure A14. Nitrogen Model Pressure and Temperature at Position 2

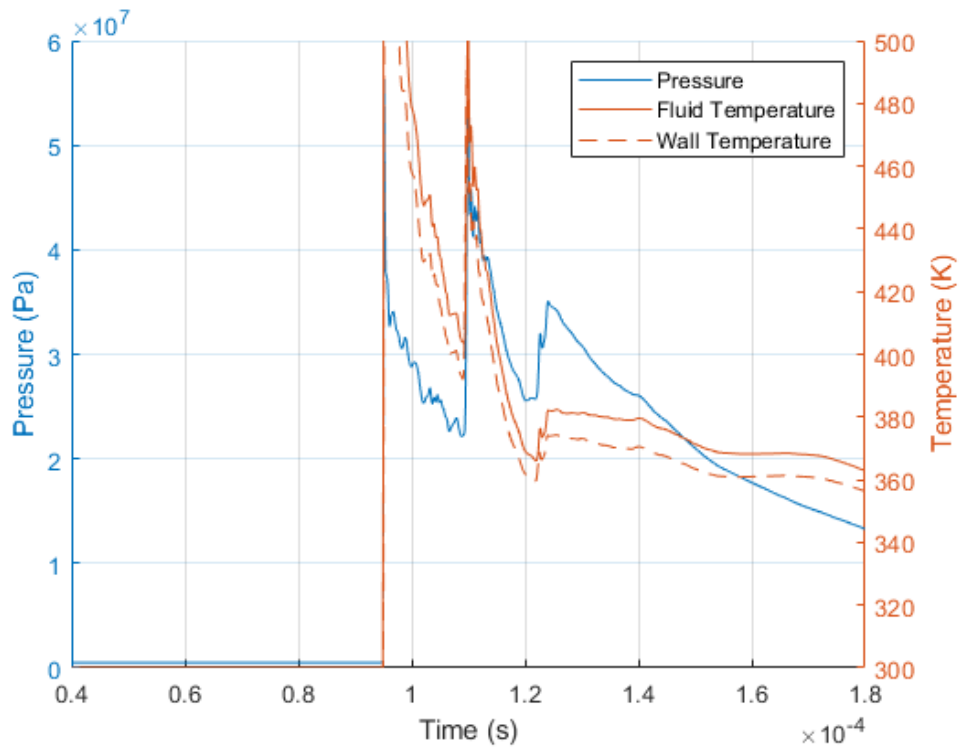


Figure A15. Nitrogen Model Pressure and Temperature at Position 3

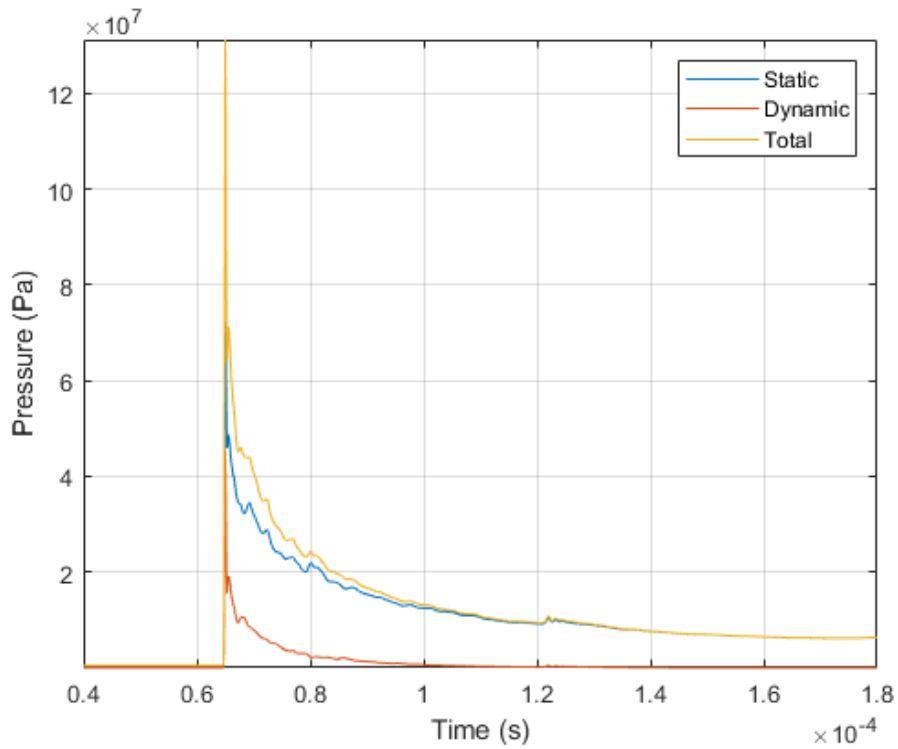


Figure A16. Nitrogen Model Pressures at Position 1

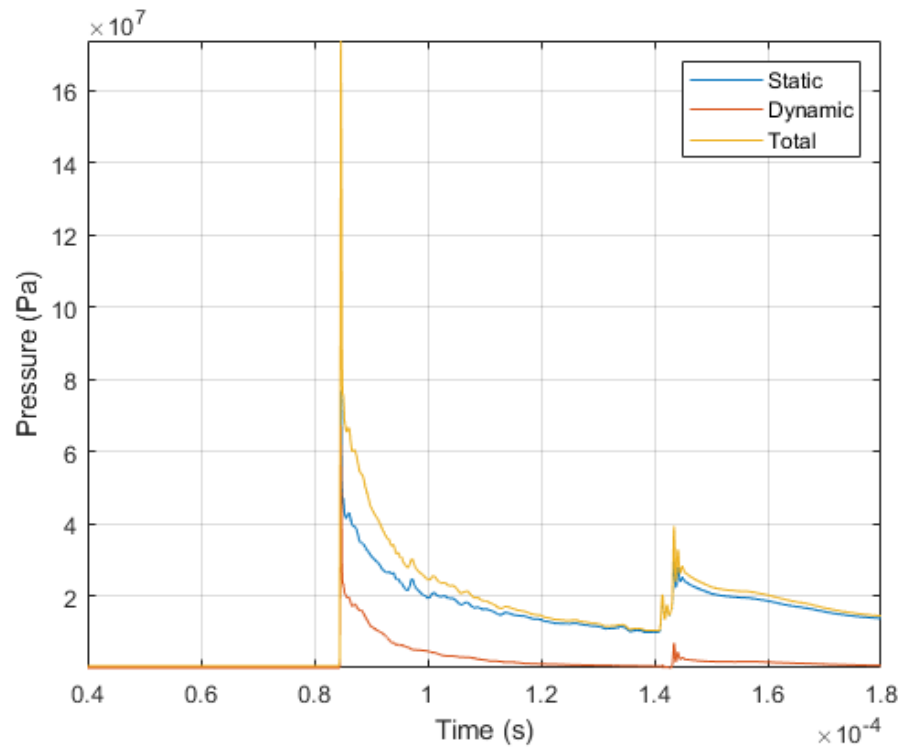


Figure A17. Nitrogen Model Pressures at Position 2

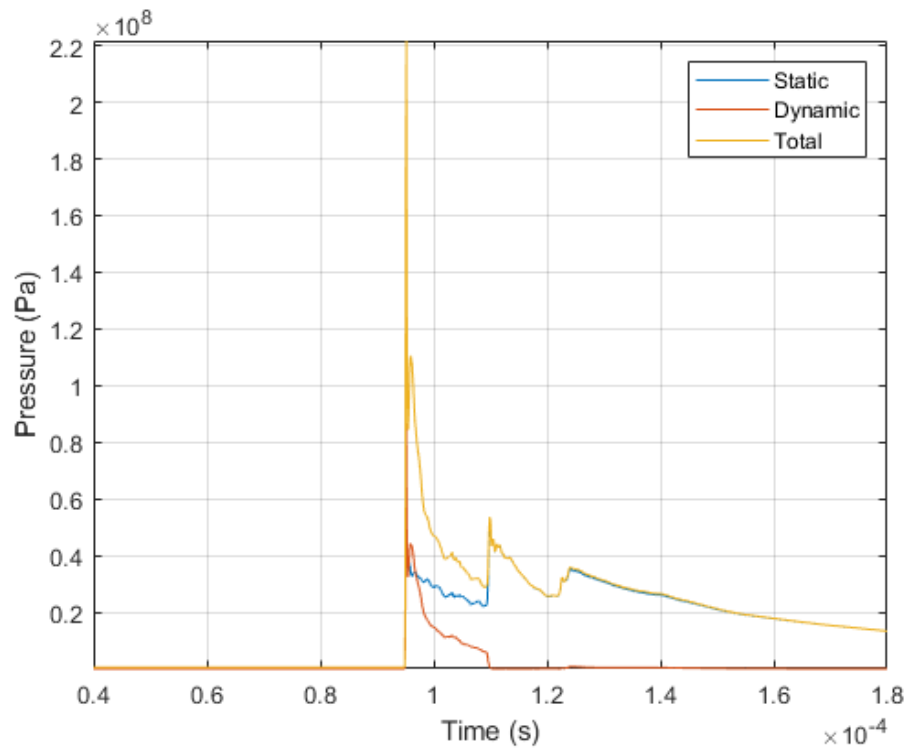
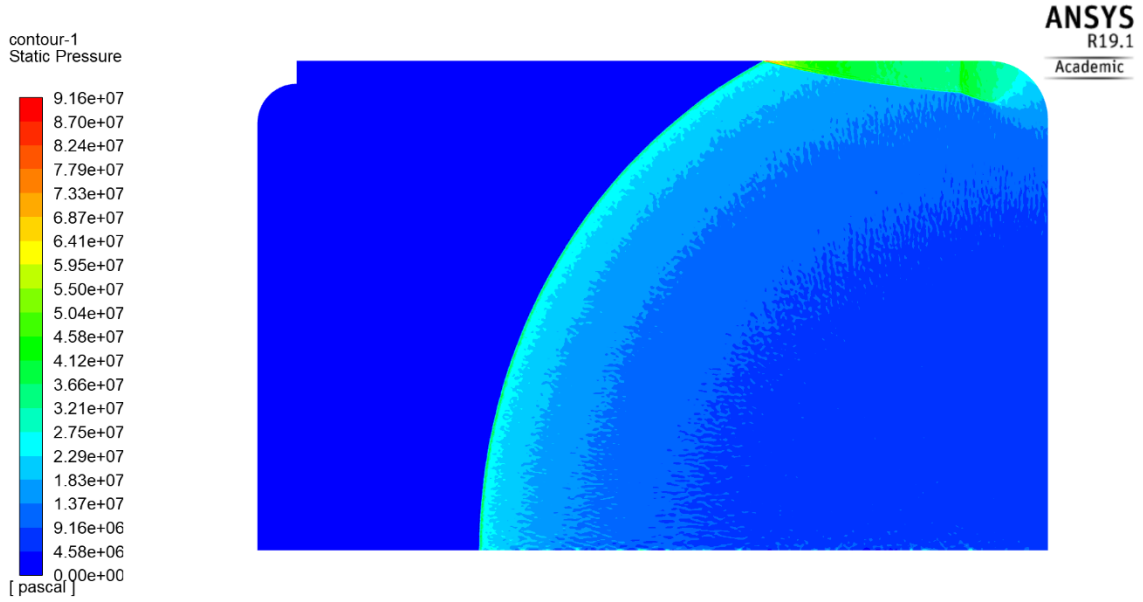


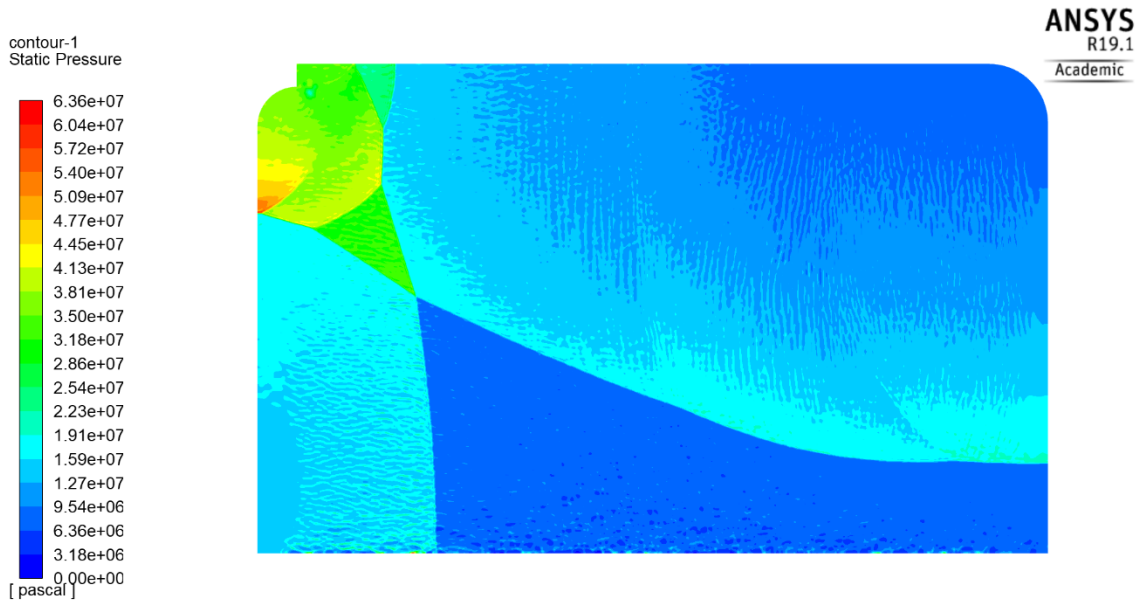
Figure A18. Nitrogen Model Pressures at Position 3

Combustion Model 6 (Stoichiometric Model)

Combustion Model 6 Contour Plots



(a)



(b)

Figure A19. Combustion Model 6 Pressure at timestep 5000 (a), 12500 (b),

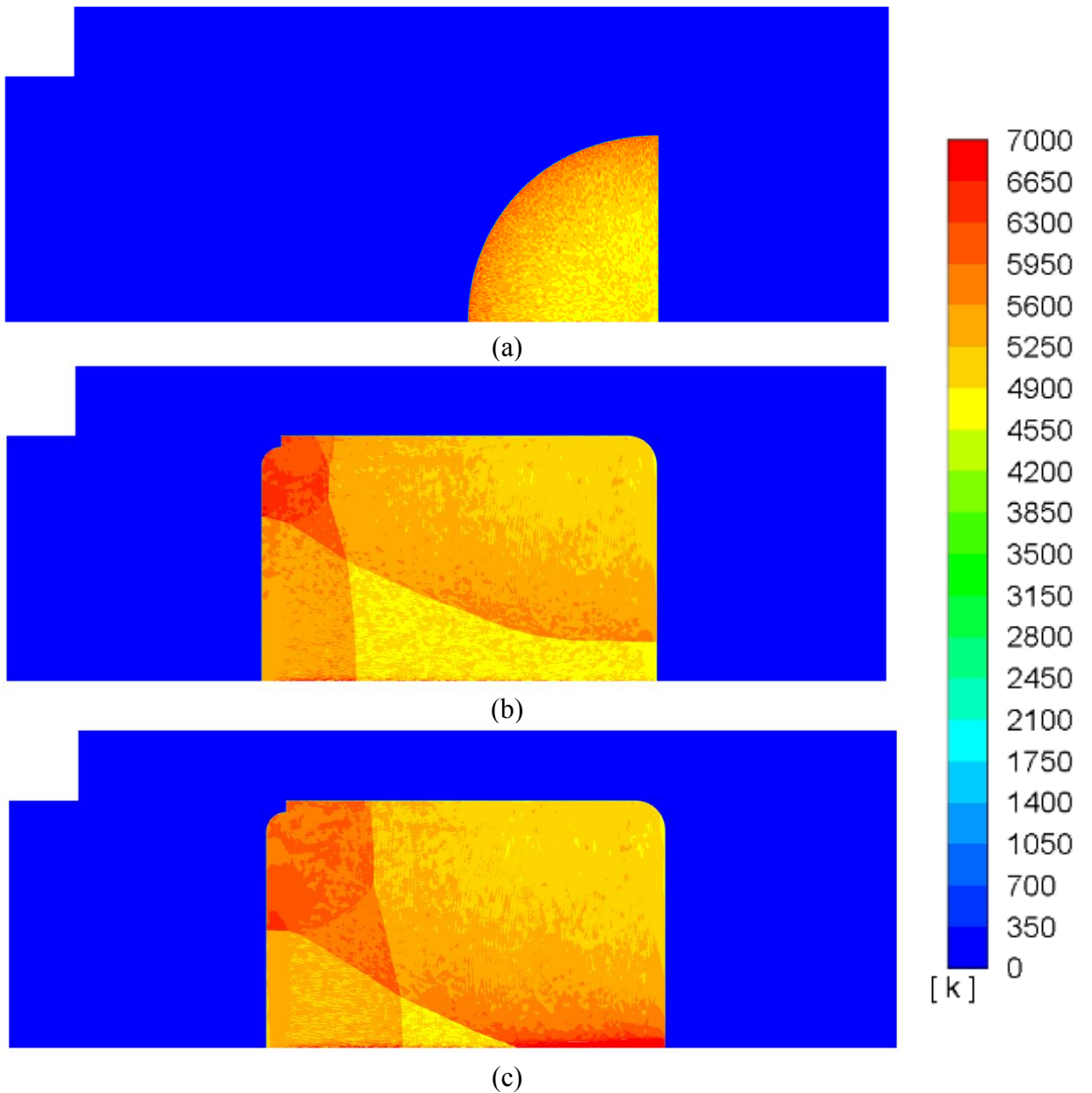


Figure A20. Combustion Model 6 Temperature at timestep 3000 (a), 12500 (b), 14500 (c)

Combustion Model 6 Full Wall Values

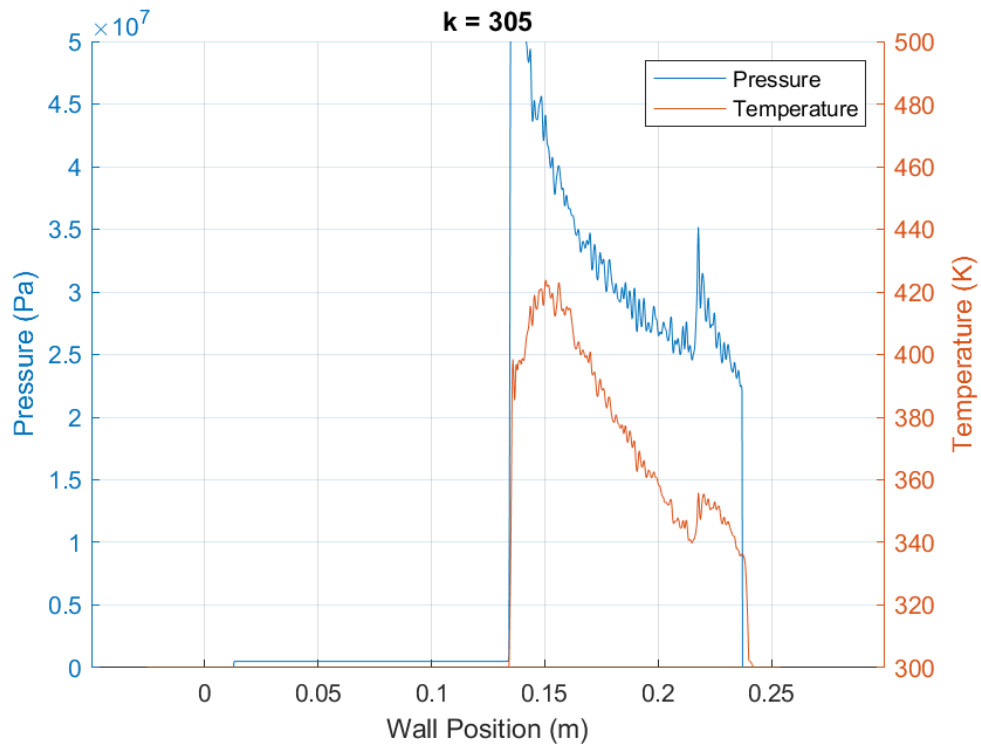


Figure A21. Stoichiometric Model Mid Wall Values

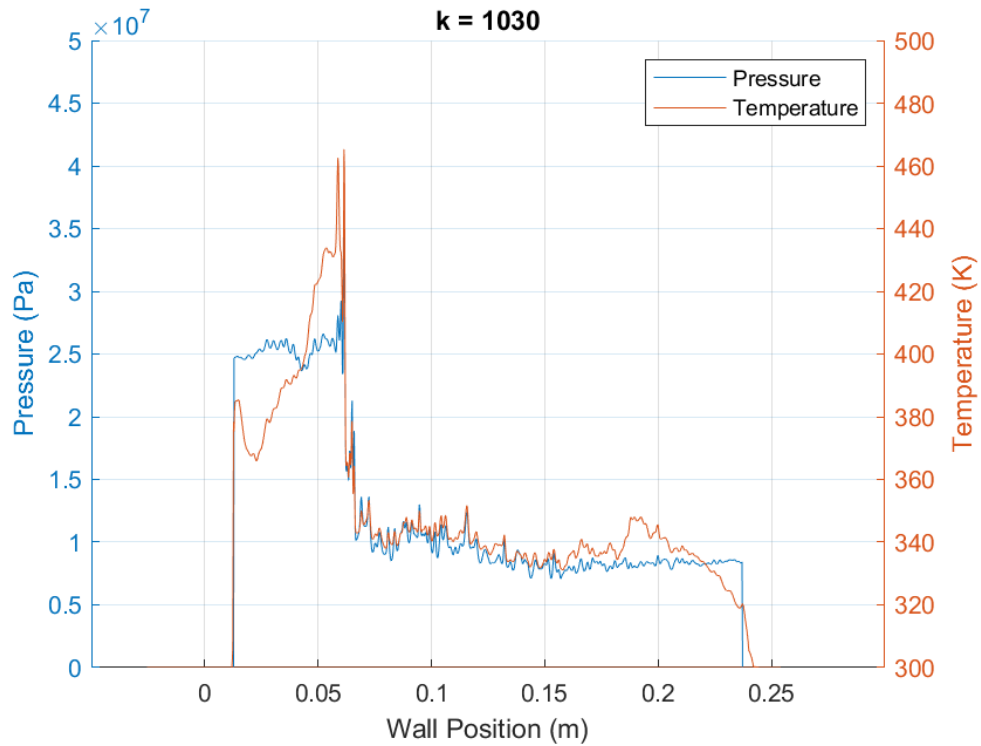


Figure A22. Stoichiometric Model Wall Shock Combination

Combustion Model 6 Single Wall Values

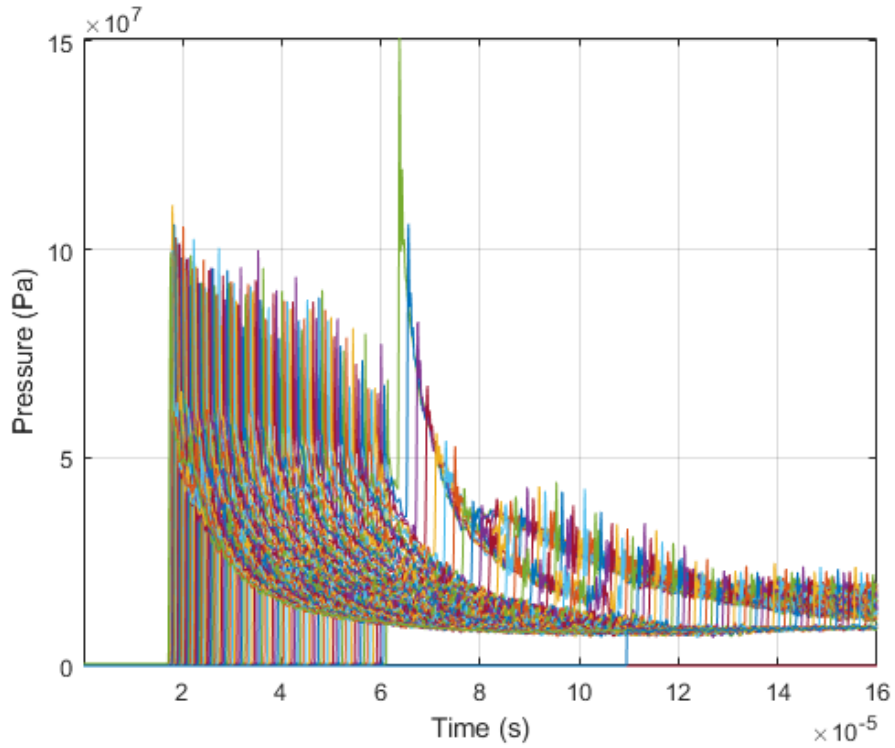


Figure A23. Stoichiometric Model Pressure Values 1

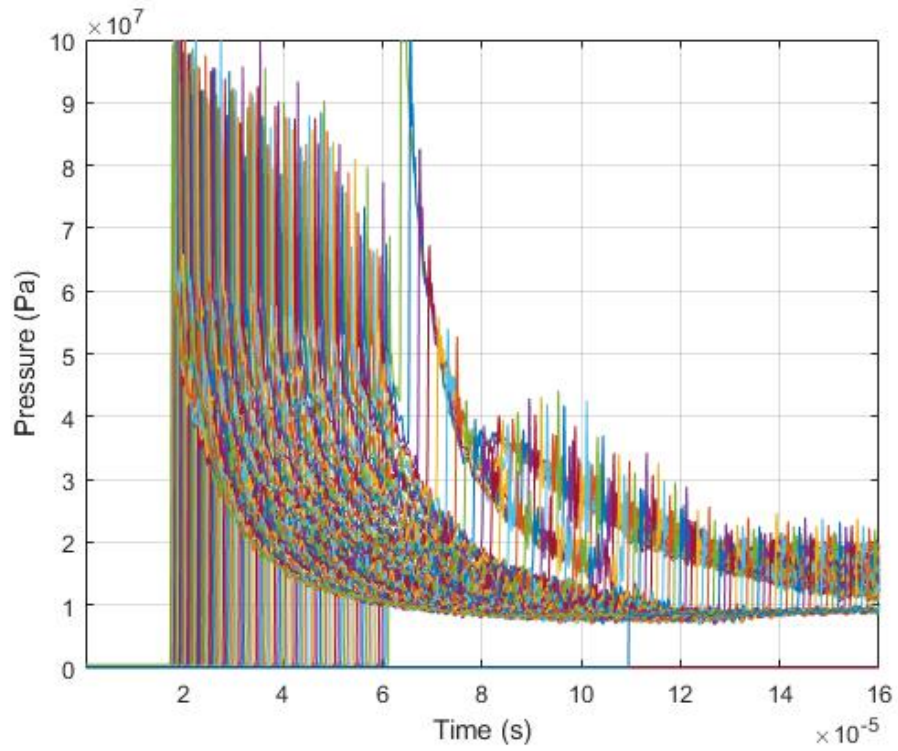


Figure A24. Stoichiometric Model Pressure Values 2

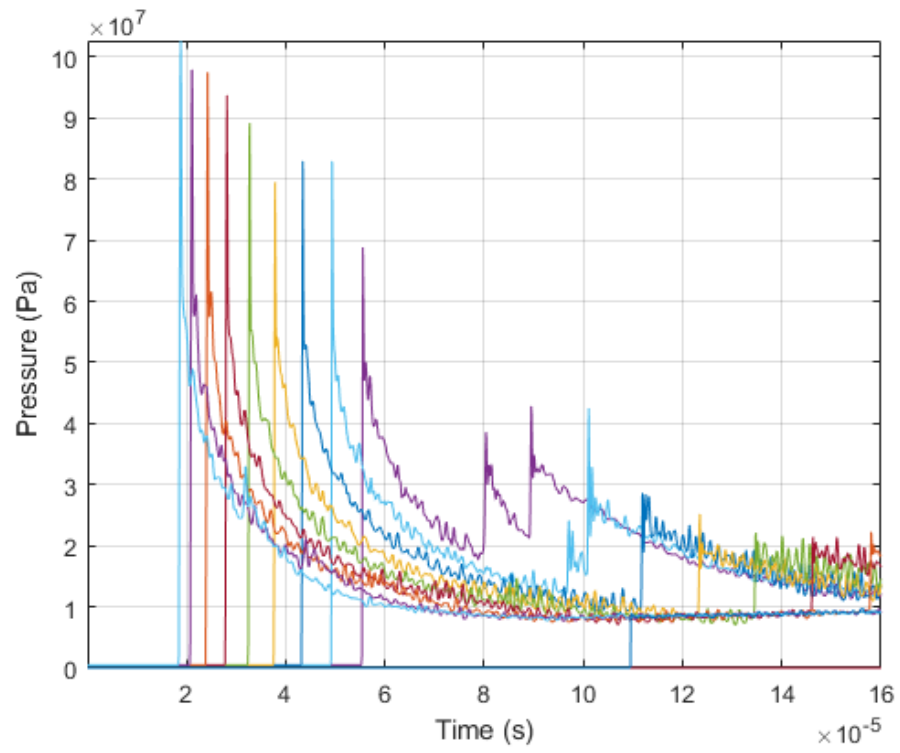


Figure A25. Stoichiometric Model Pressure Values 3

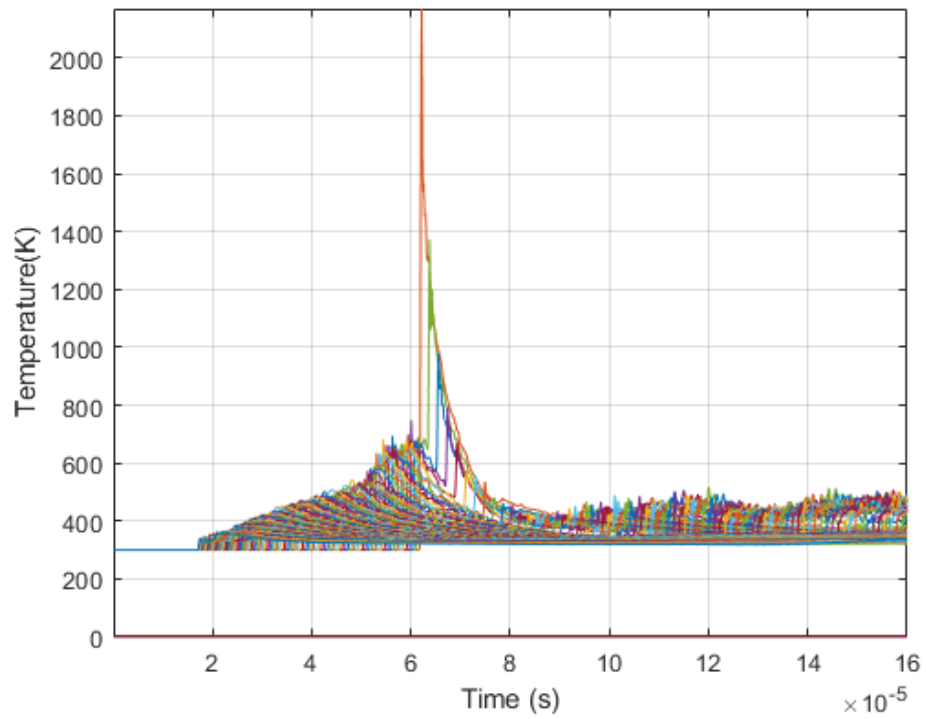


Figure A26. Stoichiometric Model Temperature Values 1

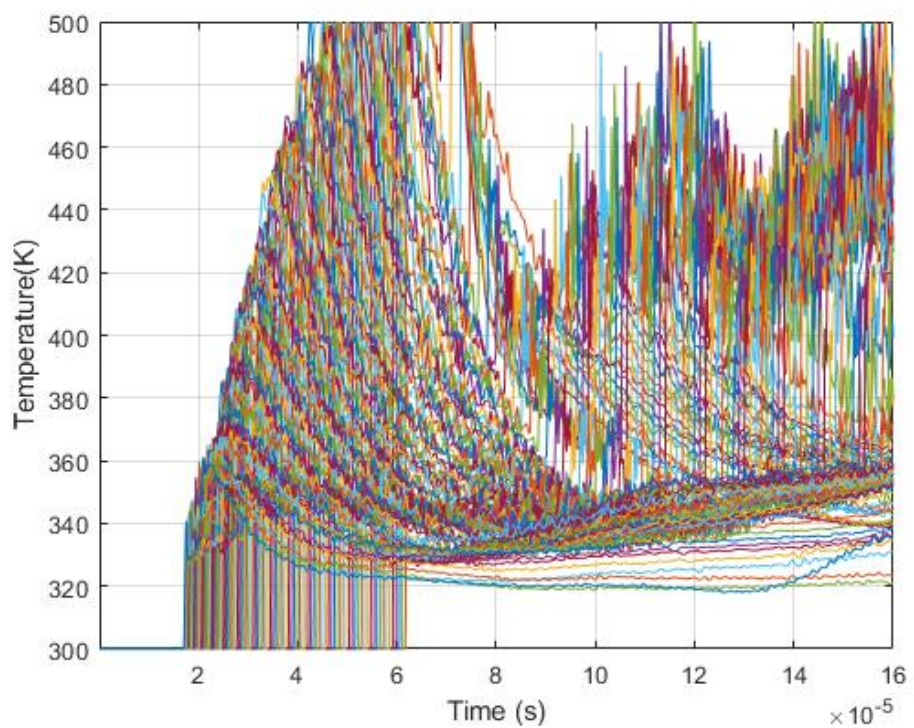


Figure A27. Stoichiometric Model Temperature Values 2

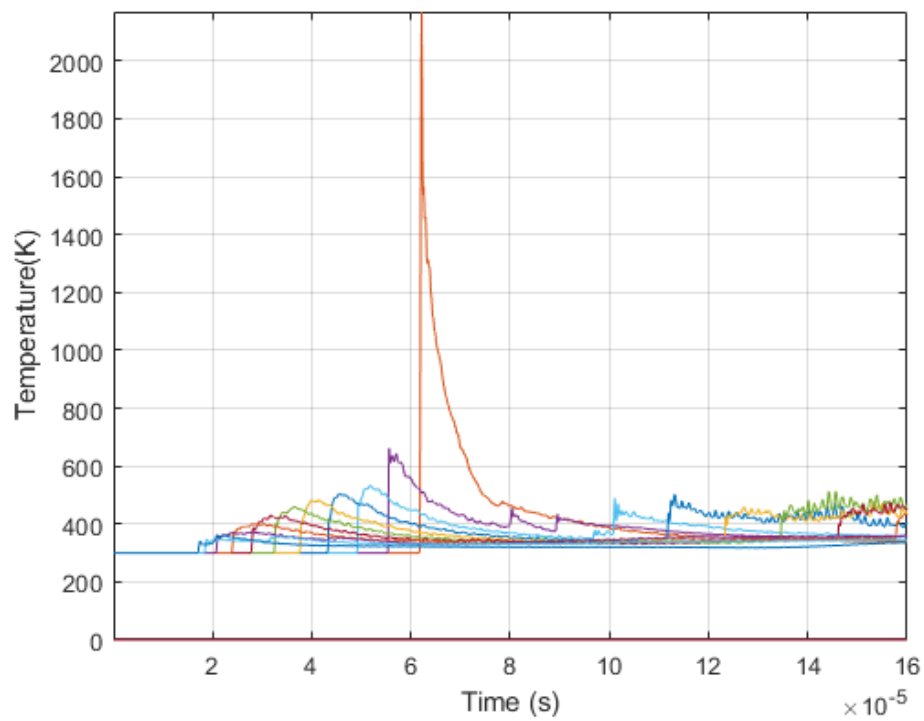


Figure A28. Stoichiometric Model Temperature Values 3

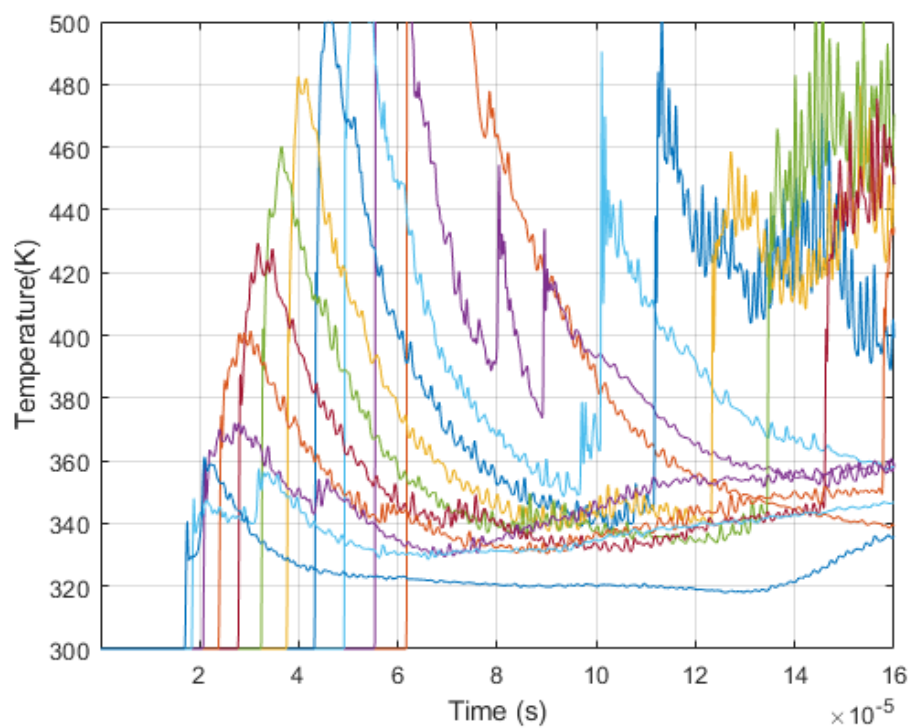


Figure A29. Stoichiometric Model Temperature Values 4

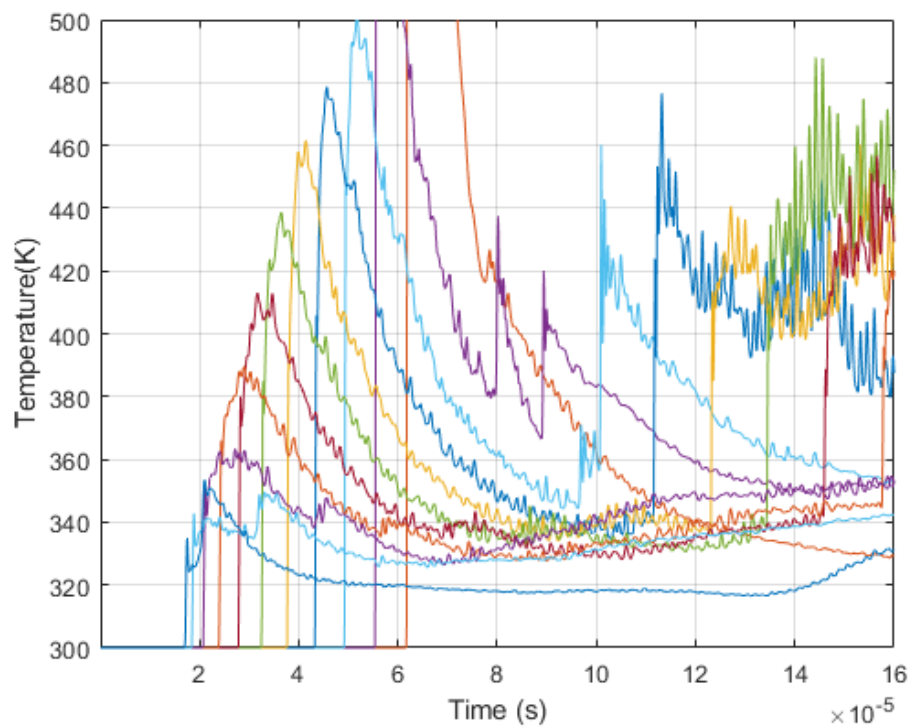


Figure A30. Stoichiometric Model Temperature Values 5

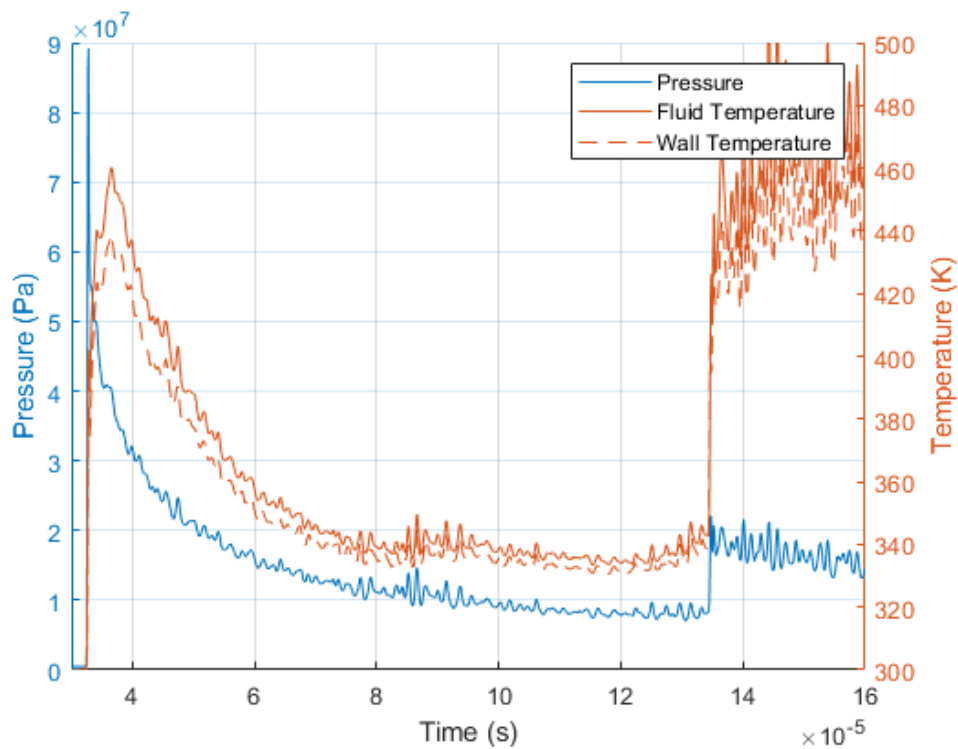


Figure A31. Stoichiometric Model Pressure and Temperature at Position 1

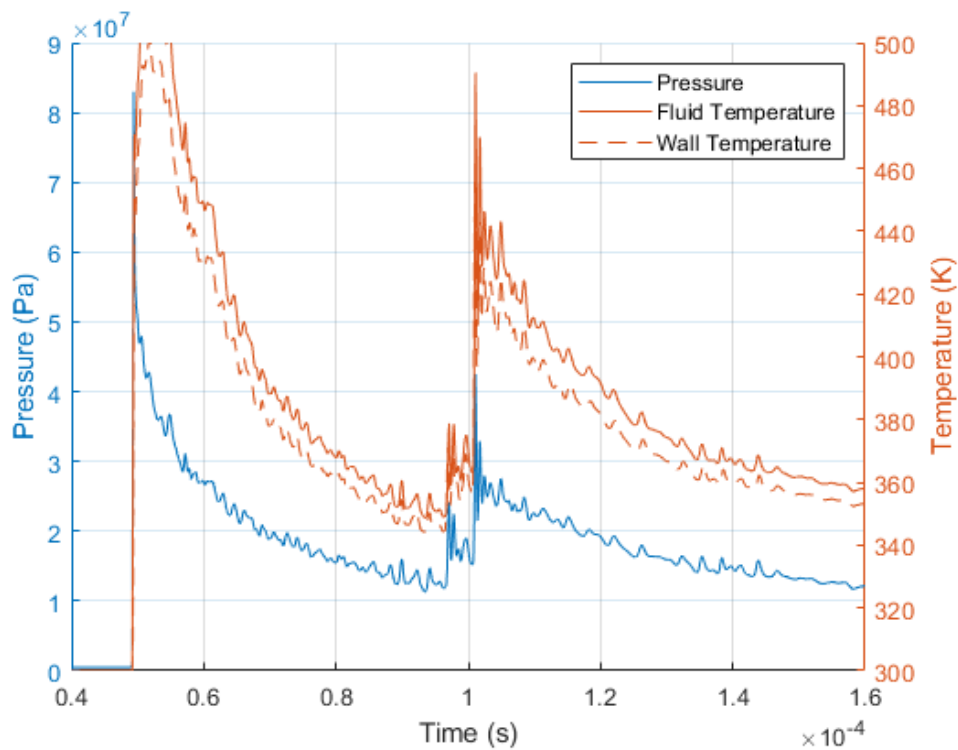


Figure A32. Stoichiometric Model Pressure and Temperature at Position 2

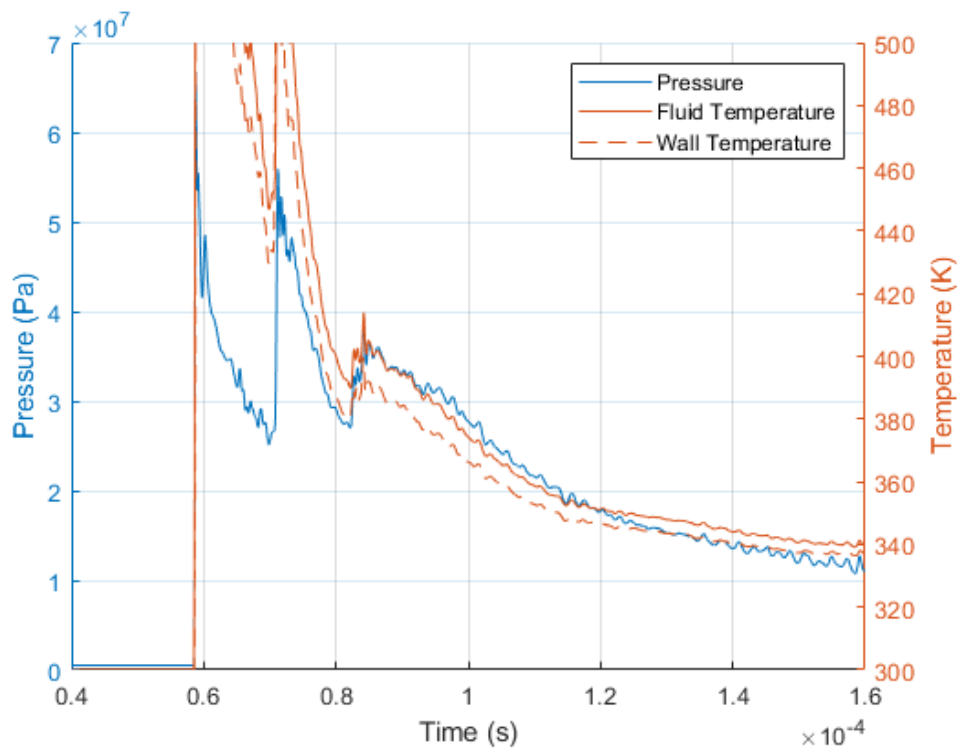


Figure A33. Stoichiometric Model Pressure and Temperature at Position 3

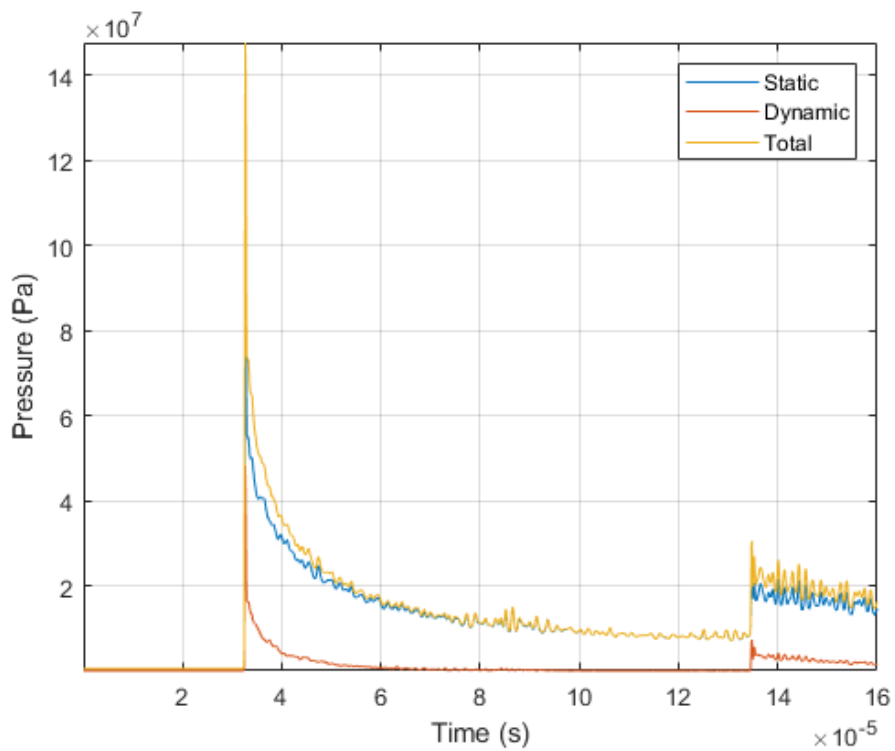


Figure A34. Stoichiometric Model Pressures at Position 1

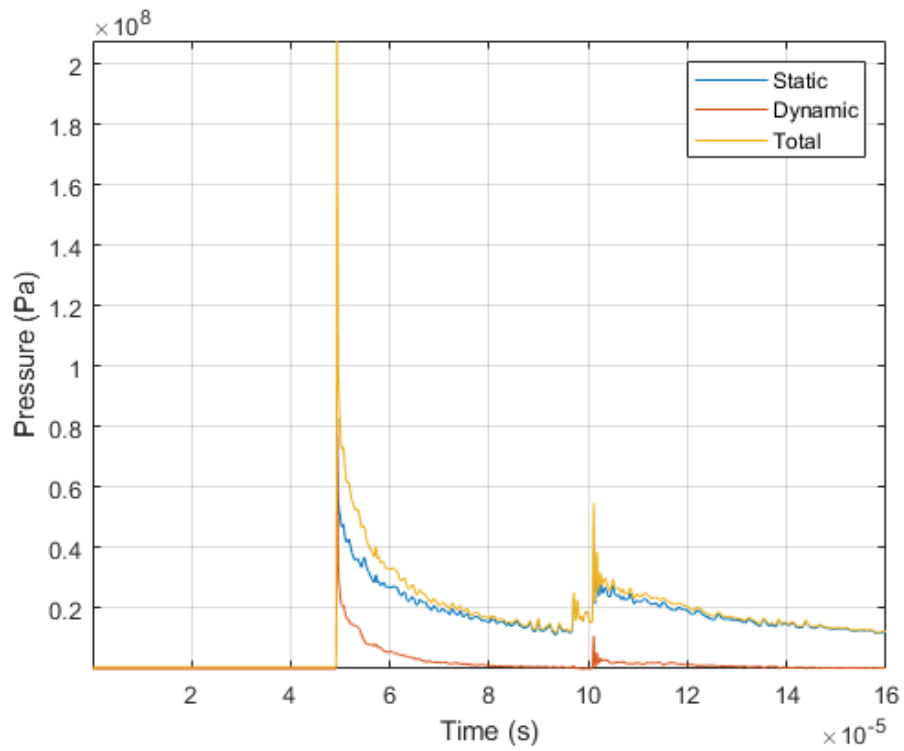


Figure A35. Stoichiometric Model Pressures at Position 2

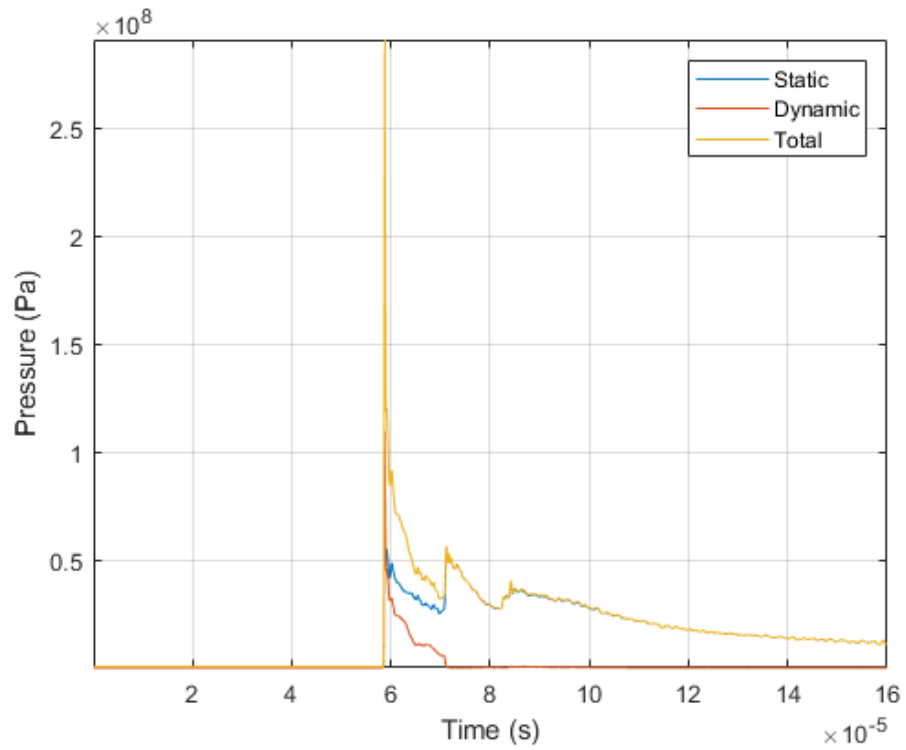


Figure A36. Stoichiometric Model Pressures at Position 3

Variable Properties

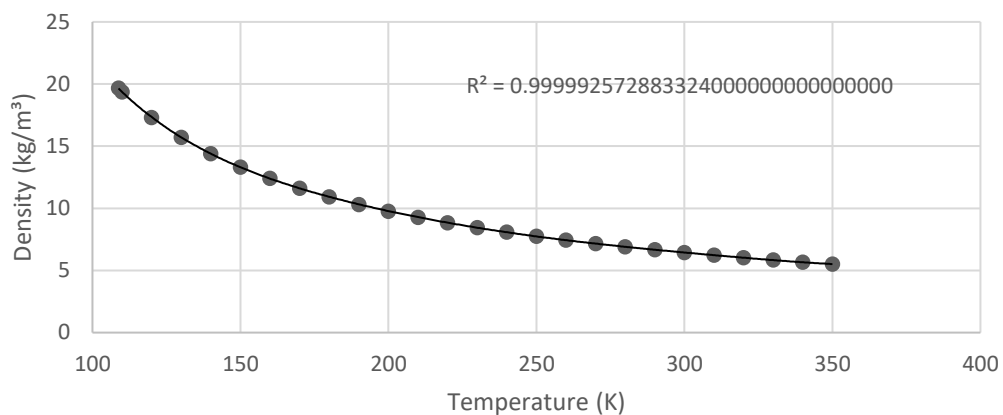
The values gathered to generate the equations used for the variable properties were obtained from NIST. These values were gathered for values up to 3000K. Due to the possibility of the combustion reaching values slightly higher than this limit, linear trendlines were done for the end of every property. This is due to the sudden extreme changes that can occur from the 6th order polynomials causing values that are physically not possible. These linear trendlines were created by selecting a cluster of data points at the end of the data and fitting a linear curve to the values. A linear curve is less accurate but will not generate extreme values. The equations are represented in the form of

$$y = AT^0 + BT^1 + CT^2 + DT^3 + ET^4 + FT^5 + GT^6$$

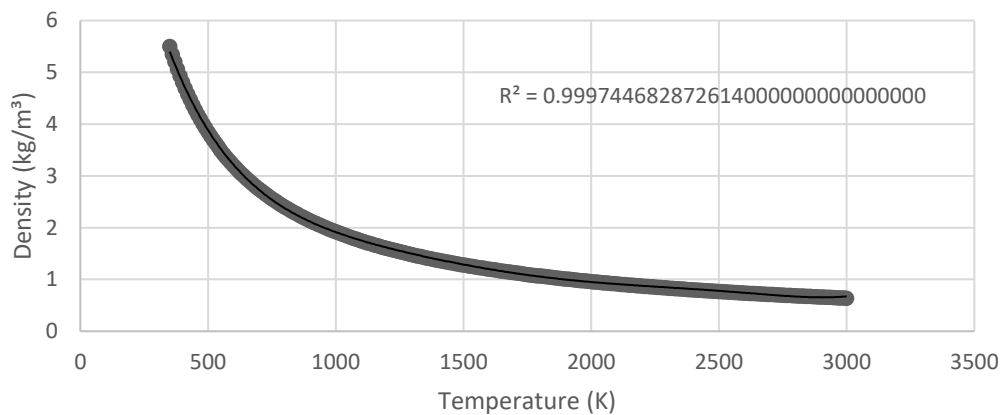
A	B	C	D	E	F	G	Equation
1.281E+02	-	2.346E-02	-1.225E-04	3.635E-07	-5.743E-10	3.754E-13	A1
1.322E+01	2.492E+00	4.735E-05	-3.515E-08	1.456E-11	-3.149E-15	2.765E-19	A2
1.404E+00	-3.519E-02	0	0	0	0	0	A3
1.087E-06	-2.555E-04	-5.466E-11	3.399E-14	-1.288E-17	2.661E-21	-2.280E-25	A4
2.883E-05	7.918E-08	0	0	0	0	0	A5
2.649E-04	2.426E-08	-5.088E-08	3.067E-11	-1.140E-14	2.323E-18	-1.971E-22	A6
2.978E-02	1.008E-04	0	0	0	0	0	A7
9.078E+02	4.693E-05	1.200E-03	-1.377E-06	7.216E-10	-1.807E-13	1.753E-17	A8
1.065E+03	-1.990E-01	0	0	0	0	0	A9
2.571E+01	5.978E-02	1.026E-03	-2.454E-06	3.256E-09	-2.250E-12	6.310E-16	A10
2.340E+00	-2.332E-01	0	0	0	0	0	A11
-1.518E-06	-1.413E-03	-1.008E-10	1.981E-13	-2.577E-16	1.804E-19	-5.147E-23	A12
7.764E-06	6.037E-08	0	0	0	0	0	A13
-1.954E-03	1.745E-04	-5.843E-07	2.077E-09	-2.948E-12	1.992E-15	-5.318E-19	A14
-4.475E-02	2.217E-04	0	0	0	0	0	A15
5.608E+03	-	2.061E-01	-4.805E-04	6.250E-07	-4.271E-10	1.190E-13	A16
1.357E+03	4.347E+01	0	0	0	0	0	A17
2.422E+01	3.239E+00	1.222E-04	-1.008E-07	4.521E-11	-1.040E-14	9.589E-19	A18
1.8276	-7.871E-02	0	0	0	0	0	A19
-1.606E-06	-0.0003	-2.818E-11	8.956E-15	-1.125E-18	-7.799E-23	2.515E-26	A20
2.678E-05	6.328E-08	0	0	0	0	0	A21
-6.517E-03	1.929E-08	3.686E-08	-5.232E-11	2.648E-14	-6.347E-18	5.950E-22	A22

5.657E-02	3.603E-05	0	0	0	0	0	A23
7.226E+02	4.184E-01	8.459E-04	-1.331E-06	7.595E-10	-1.981E-13	1.974E-17	A24
1335.378	0.024	0	0	0	0	0	A25
1.546E+01	-5.104E-02	8.050E-05	-6.729E-08	3.051E-11	-7.079E-15	6.574E-19	A26
1.159E+00	-1.995E-04	0	0	0	0	0	A27
1.250E-06	6.797E-08	-5.015E-11	3.289E-14	-1.291E-17	2.736E-21	-2.389E-25	A28
2.354E-05	2.107E-08	0	0	0	0	0	A29
8.284E-04	1.002E-04	-6.470E-08	4.253E-11	-1.663E-14	3.510E-18	-3.056E-22	A30
2.662E-02	4.139E-05	0	0	0	0	0	A31
1.165E+03	-8.425E-01	1.934E-03	-1.673E-06	7.298E-10	-1.600E-13	1.403E-17	A32
1243.024	0.026	0	0	0	0	0	A33
7.562E+00	-1.988E-02	2.623E-05	-1.910E-08	7.774E-12	-1.655E-15	1.434E-19	A34
7.474E-01	-1.289E-04	0	0	0	0	0	A35
3.531E-07	2.058E-08	4.956E-11	-5.346E-14	2.811E-17	-7.689E-21	8.693E-25	A36
1.271E-05	2.897E-08	0	0	0	0	0	A37
6.003E-02	-2.765E-04	7.354E-07	-7.228E-10	4.086E-13	-1.225E-16	1.508E-20	A38
-0.0655	0.0002	0	0	0	0	0	A39
4.945E+03	-	2.212E-02	-1.790E-05	7.736E-09	-1.715E-12	1.532E-16	A40
2557.865	1.305E+01 0.177	0	0	0	0	0	A41

Oxygen Density (A1)



Oxygen Density (A2)



Oxygen Density (A3)

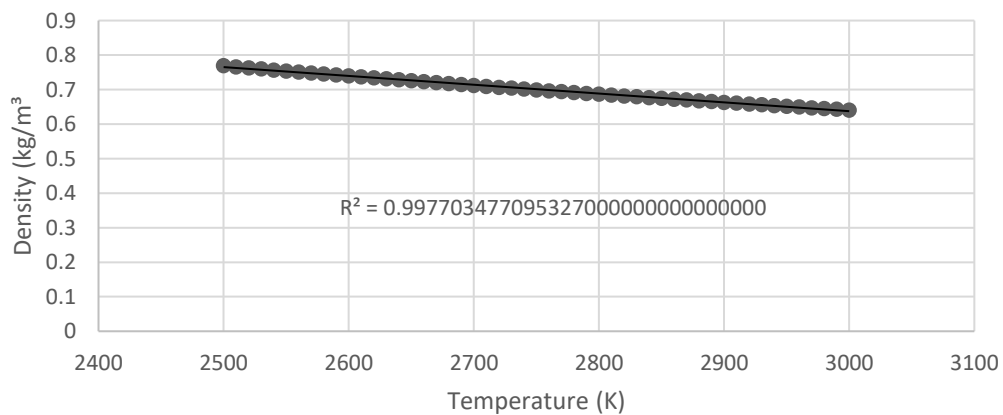


Figure A37. Variable Density of O₂

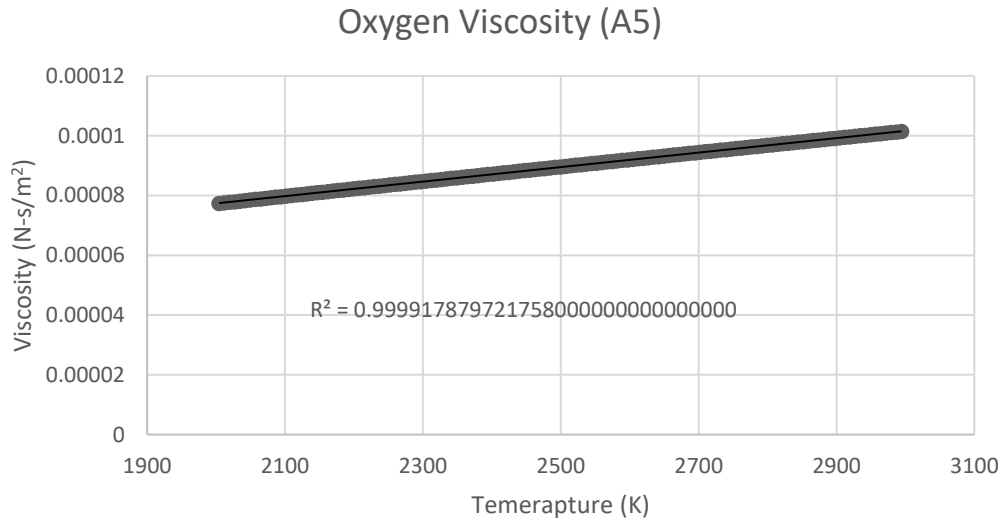
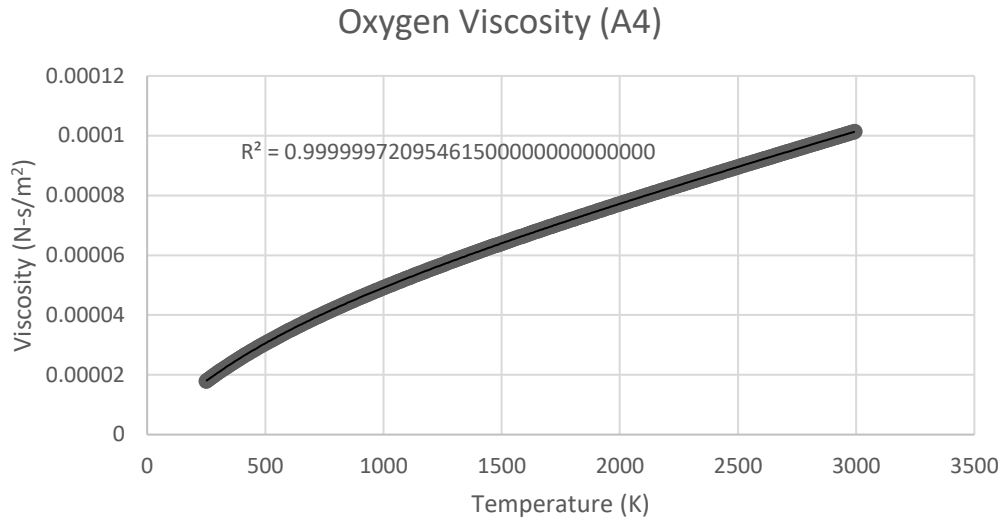


Figure A38. Variable Viscosity of O₂

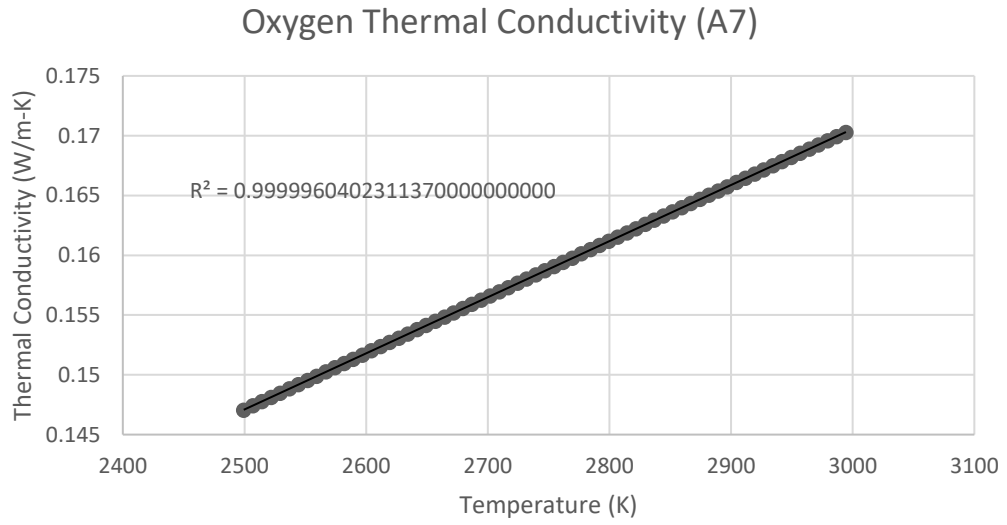
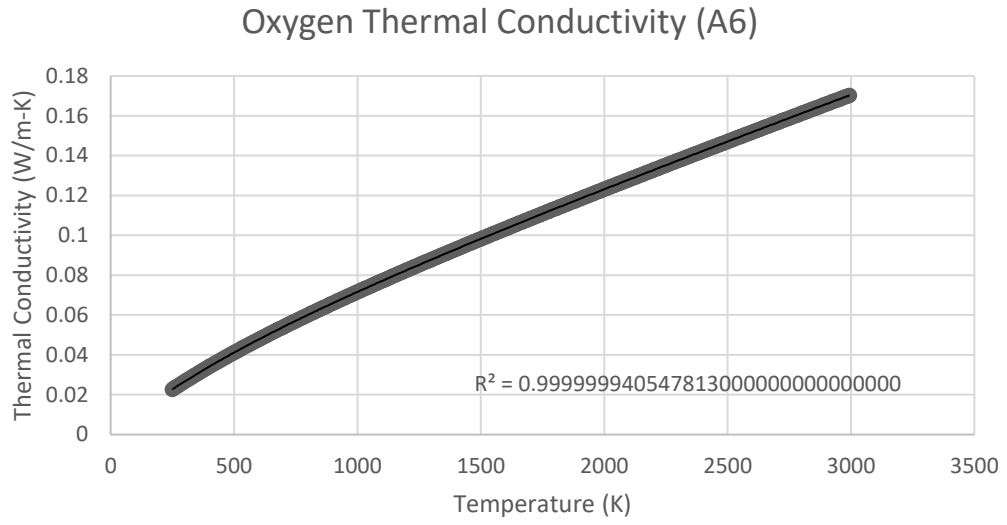


Figure A39. Variable Thermal Conductivity of O₂

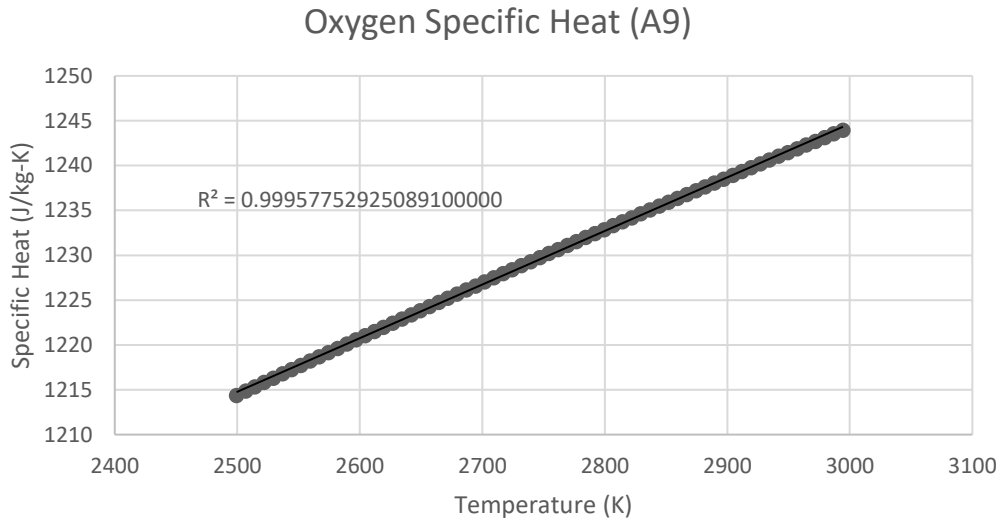
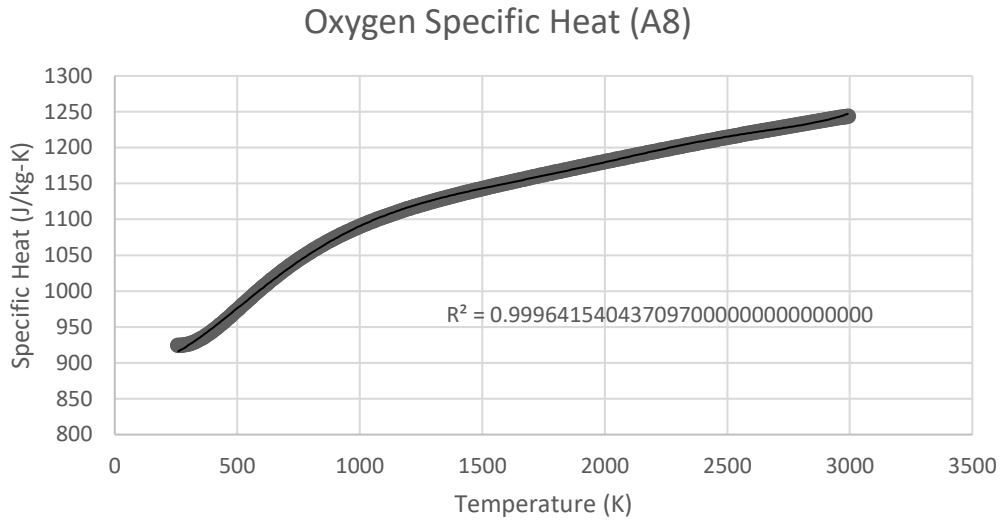
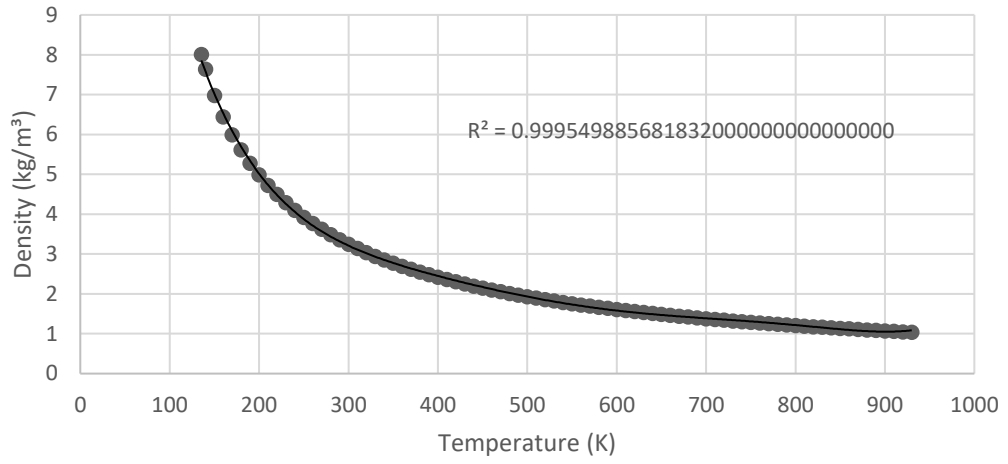


Figure A40. Variable Specific Heat of O₂

Methane Density (A10)



Methane Density (A11)

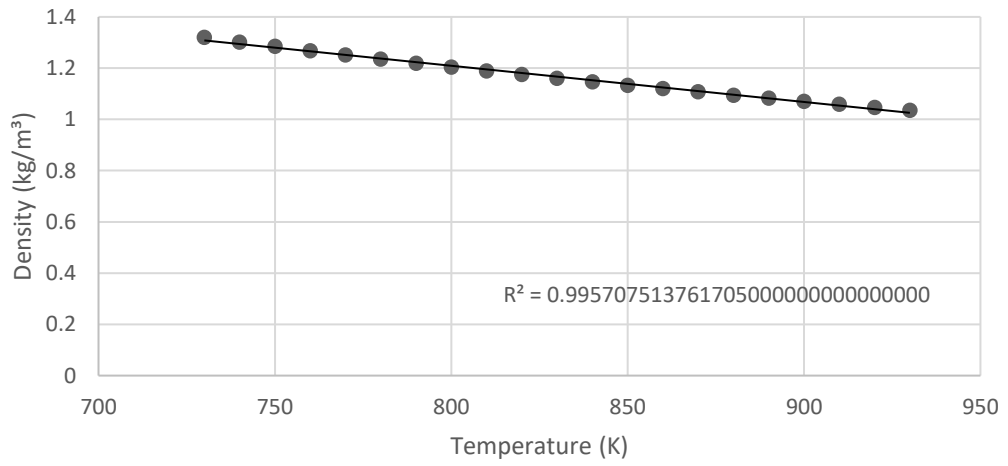
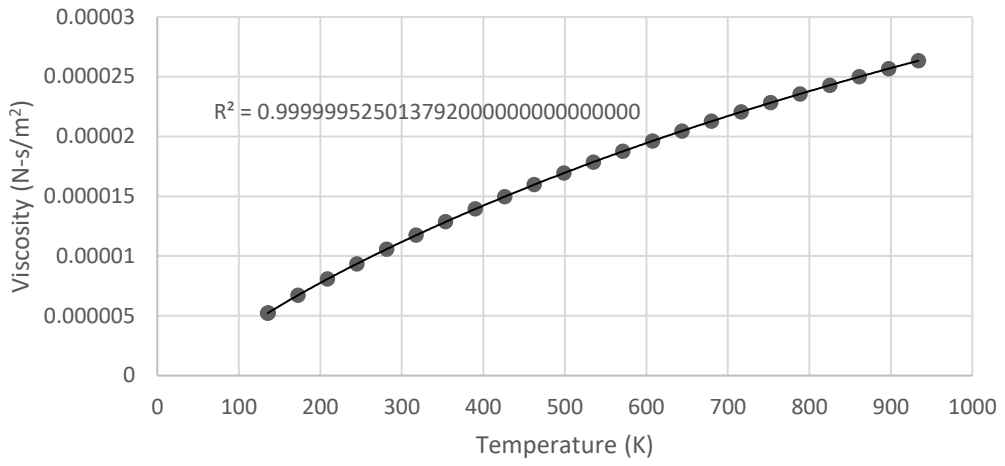


Figure A41. Variable Density of CH₄

Methane Viscosity (A12)



Methane Viscosity (A13)

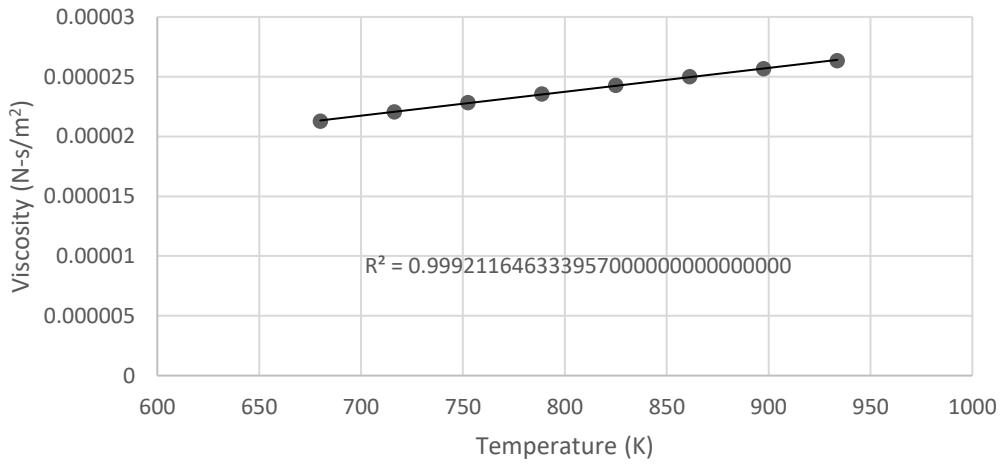
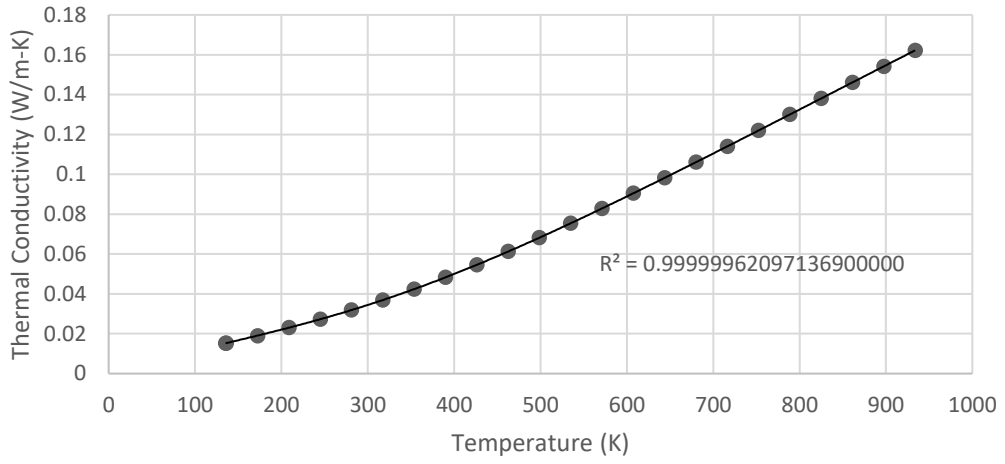


Figure A42. Variable Viscosity of CH₄

Methane Thermal Conductivity (A14)



Methane Thermal Conductivity (A15)

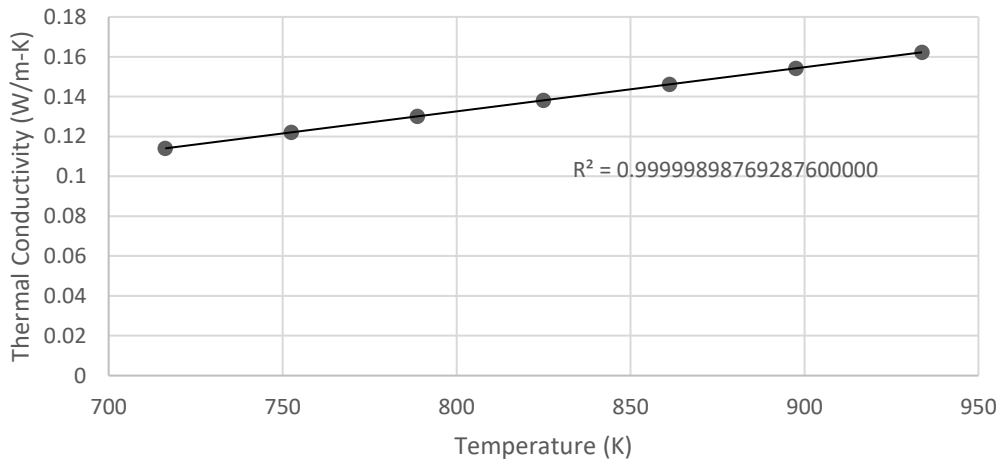
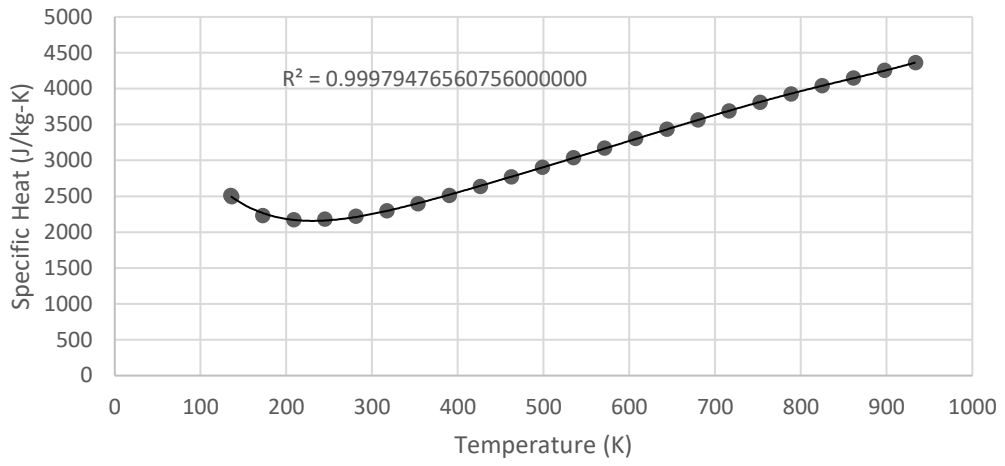


Figure A43. Variable Thermal Conductivity of CH₄

Methane Specific Heat (A16)



Methane Specific Heat (A17)

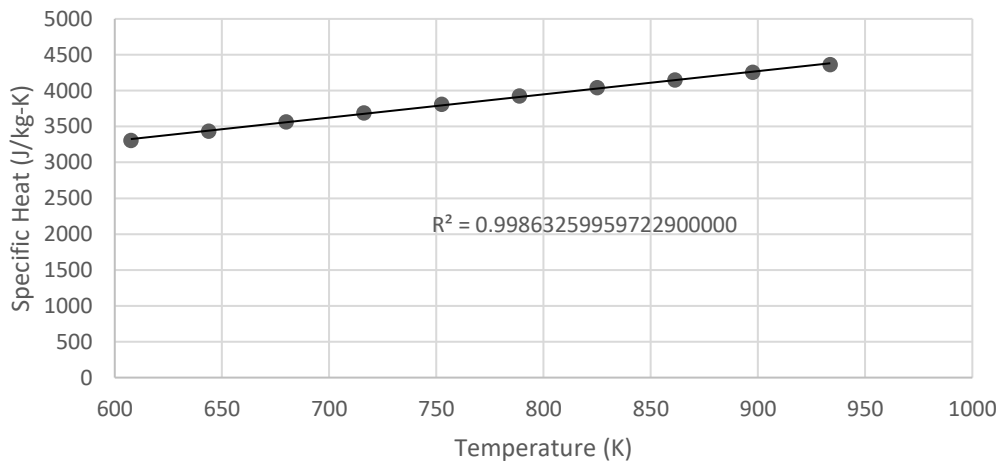
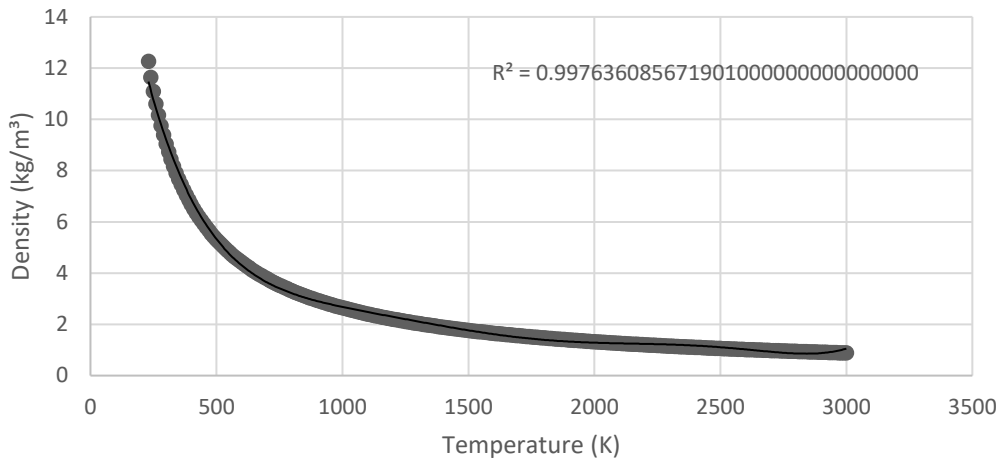


Figure A44. Variable Specific Heat of CH₄

Carbon Dioxide Density (A18)



Carbon Dioxide Density (A19)

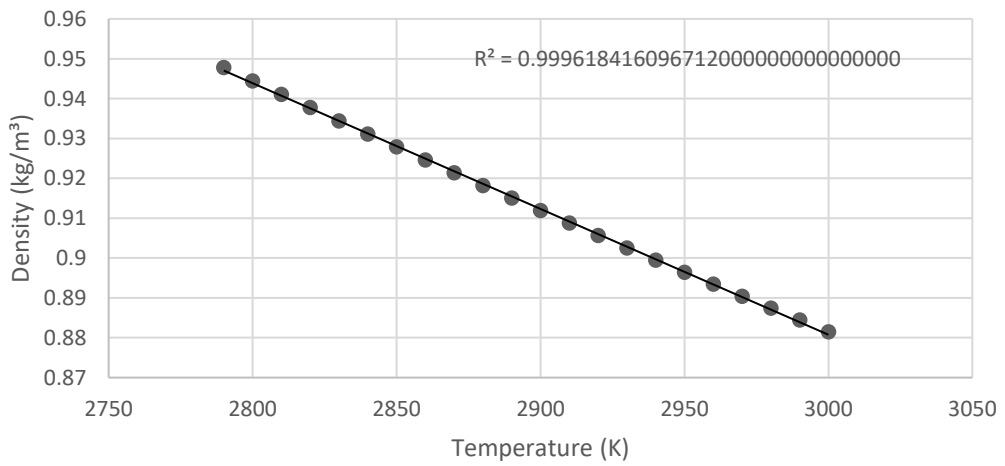
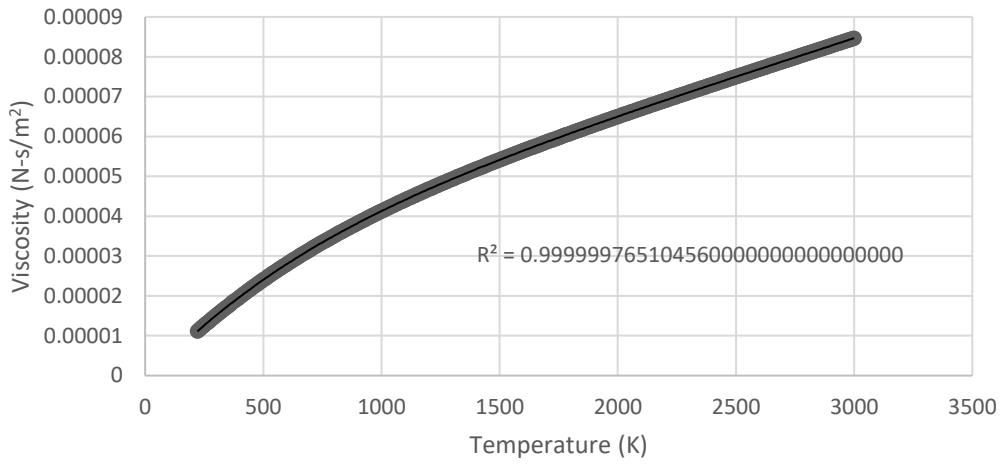


Figure A45. Variable Density of CO₂

Carbon Dioxide Viscosity (A20)



Carbon Dioxide Viscosity (A21)

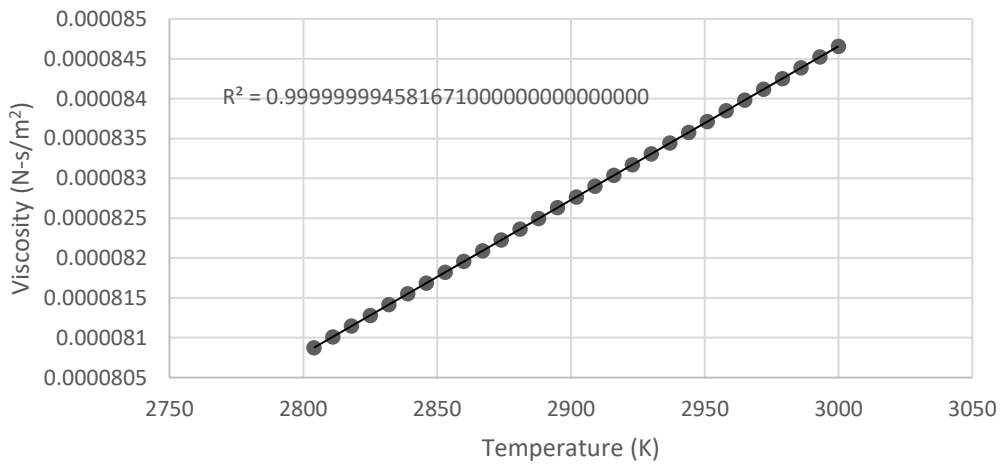
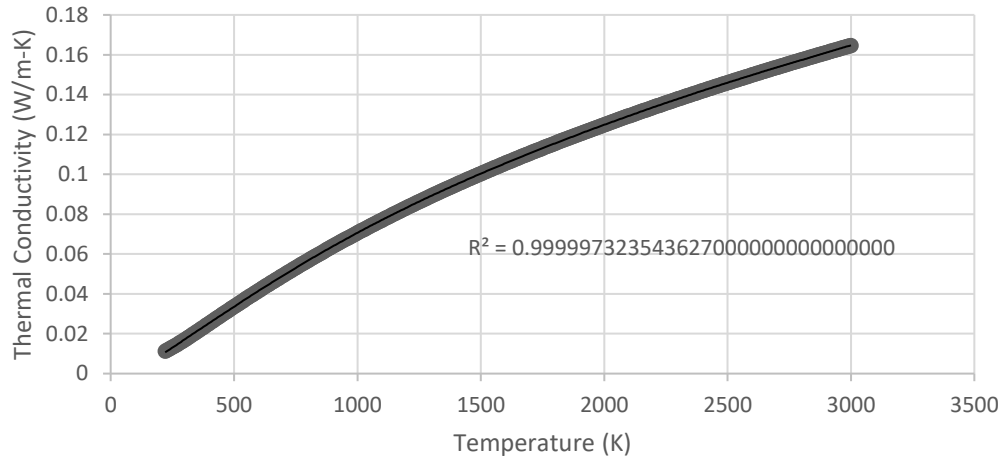


Figure A46. Variable Viscosity of CO₂

Carbon Dioxide Thermal Conductivity (A22)



Carbon Dioxide Thermal Conductivity (A23)

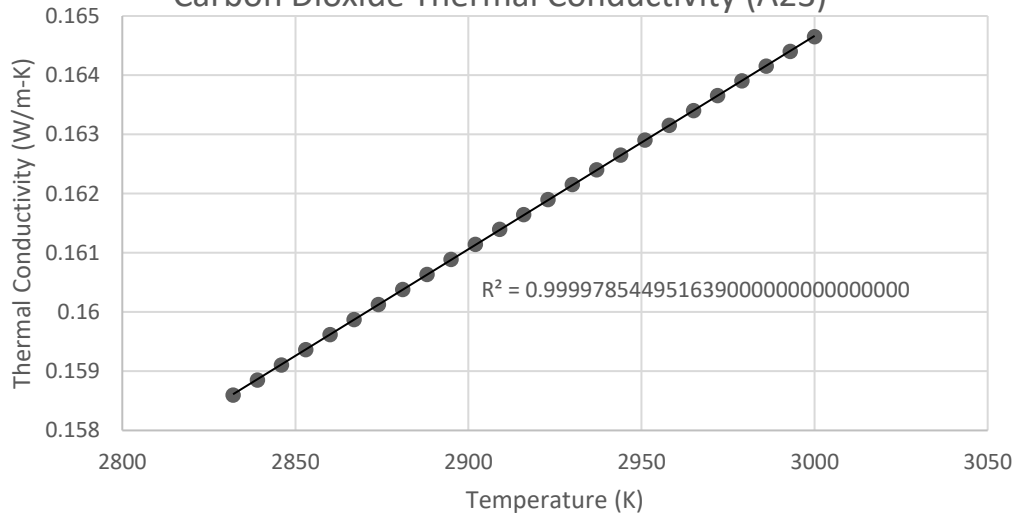
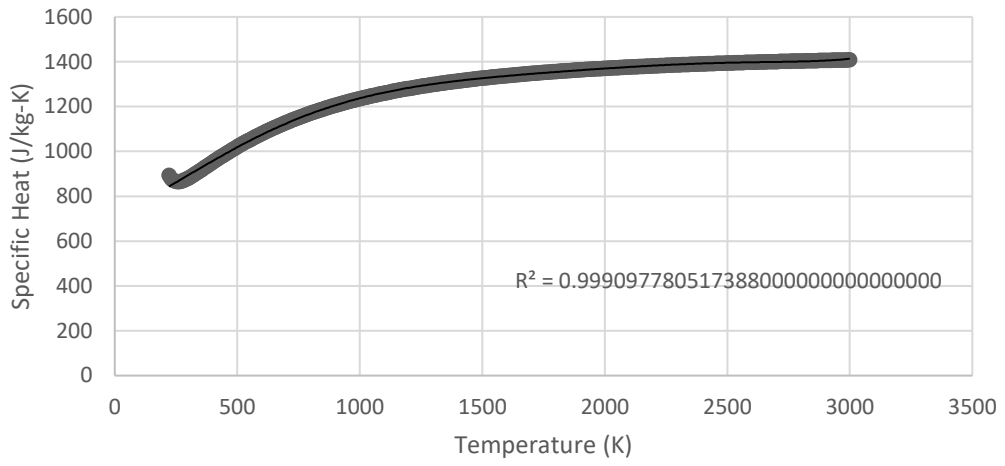


Figure A47. Variable Thermal Conductivity of CO₂

Carbon Dioxide Specific Heat (A24)



Carbon Dioxide Specific Heat (A25)

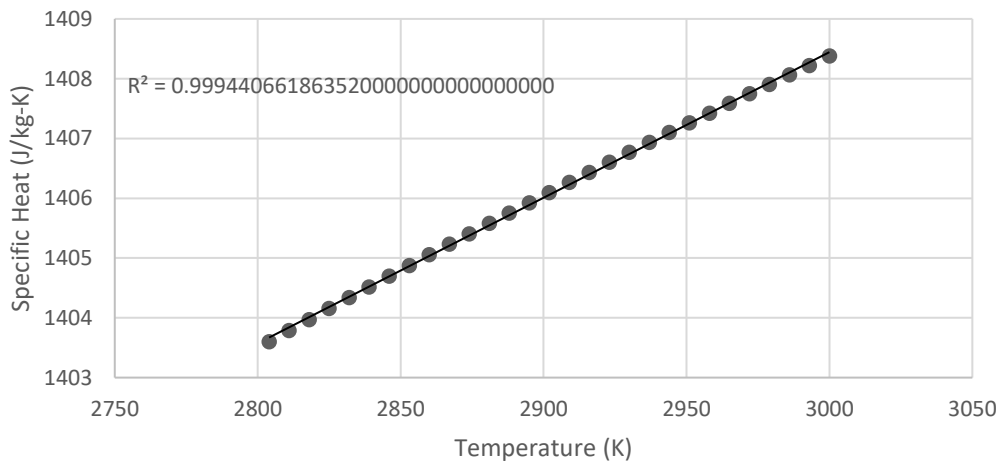
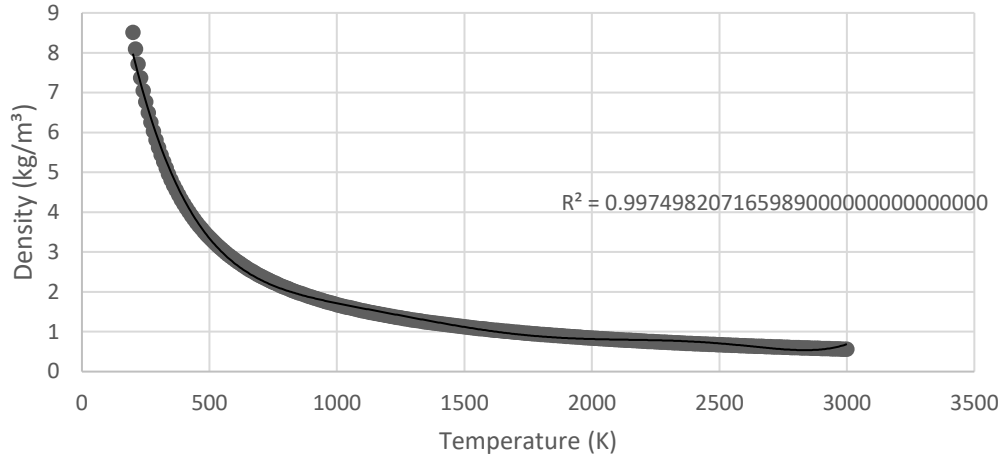


Figure A48. Variable Specific Heat of CO₂

Nitrogen Density (A26)



Nitrogen Density (A27)

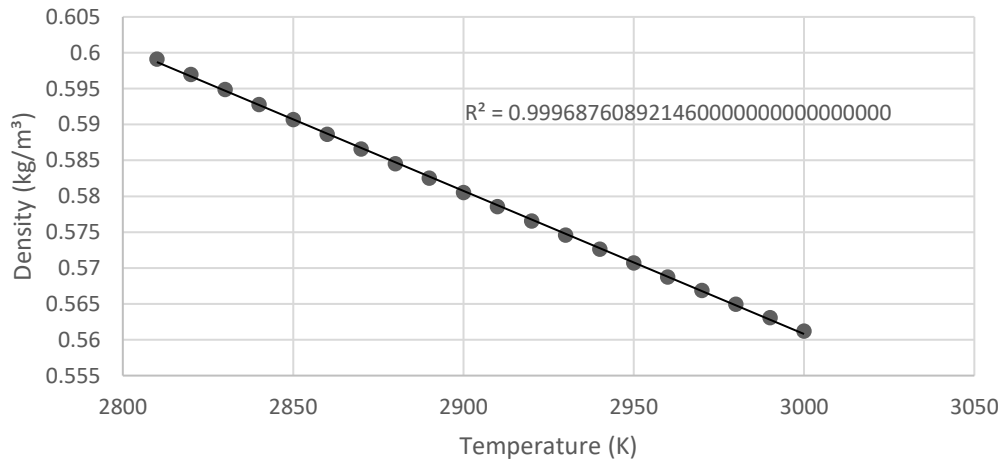


Figure A49. Variable Density of N₂

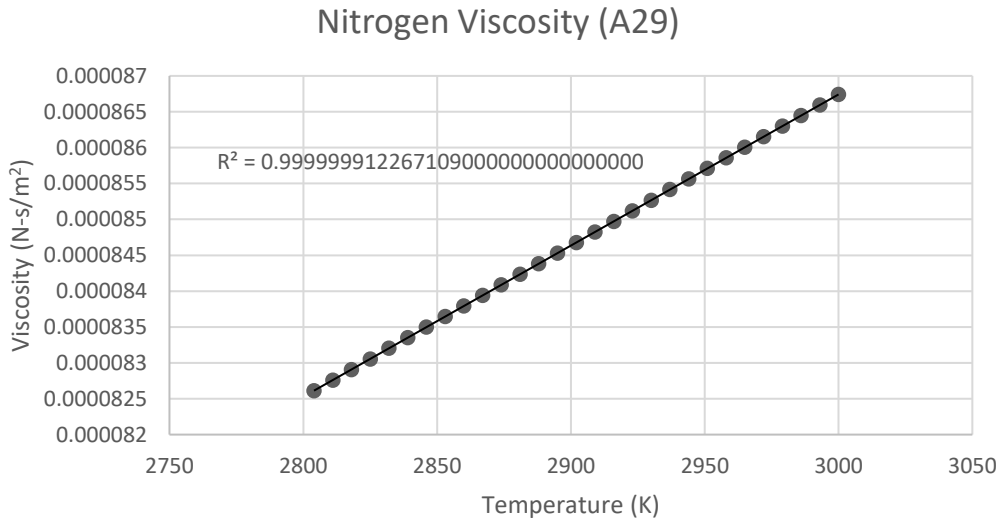
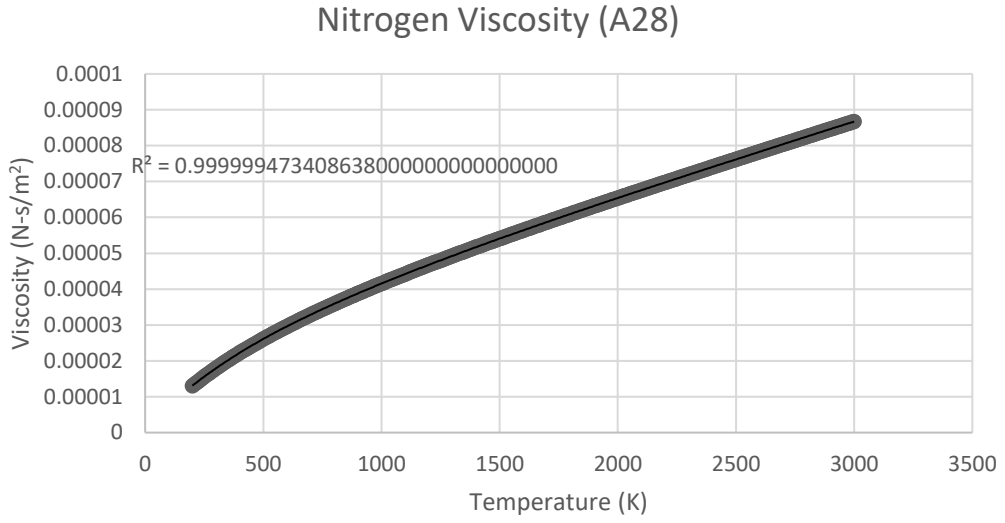


Figure A50. Variable Viscosity of N₂

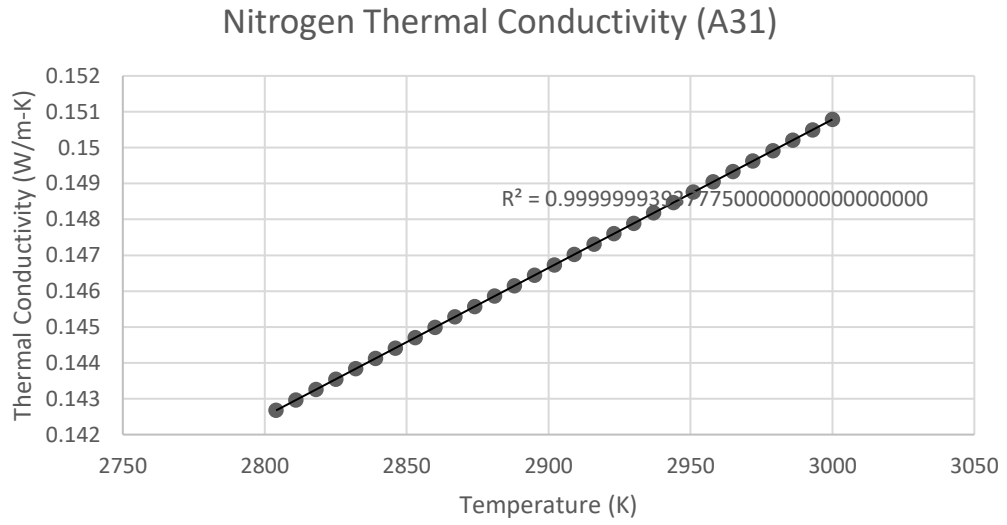
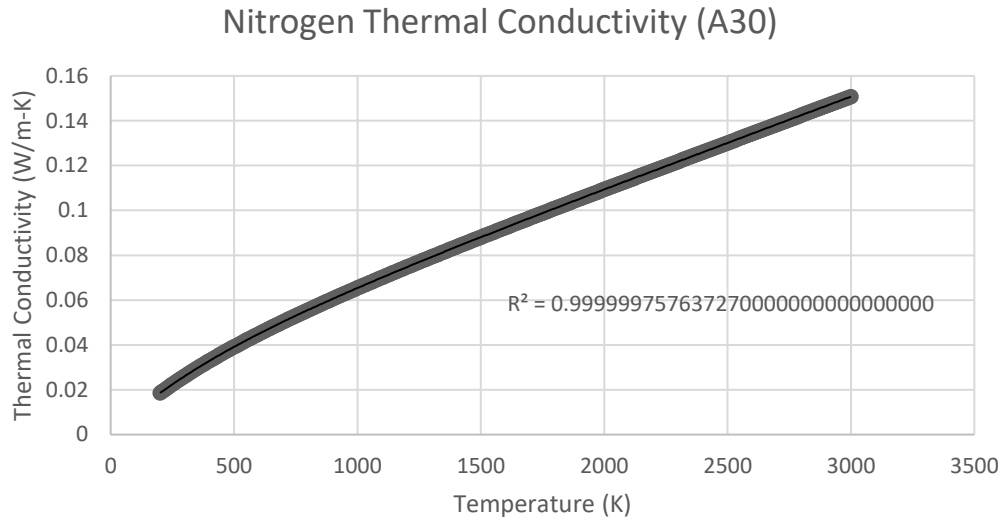


Figure A51. Variable Thermal Conductivity of N_2

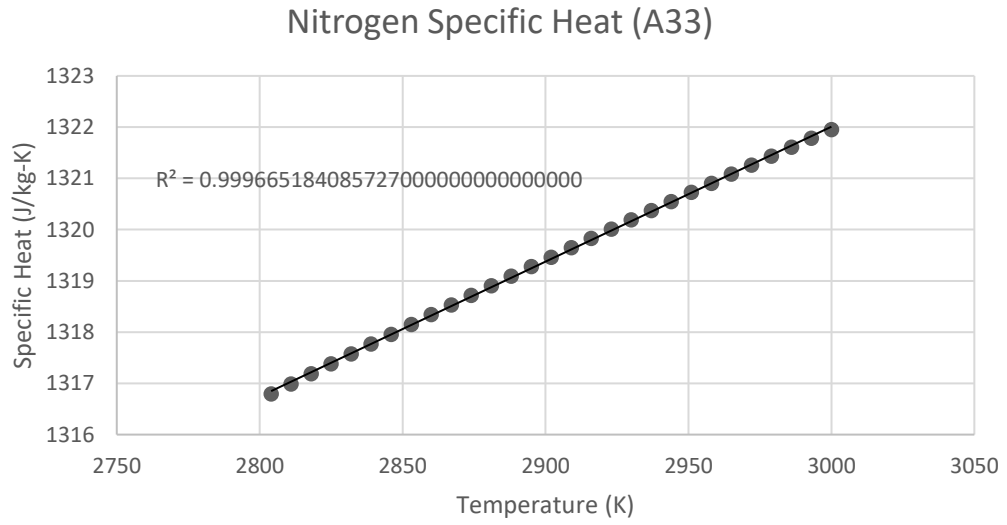
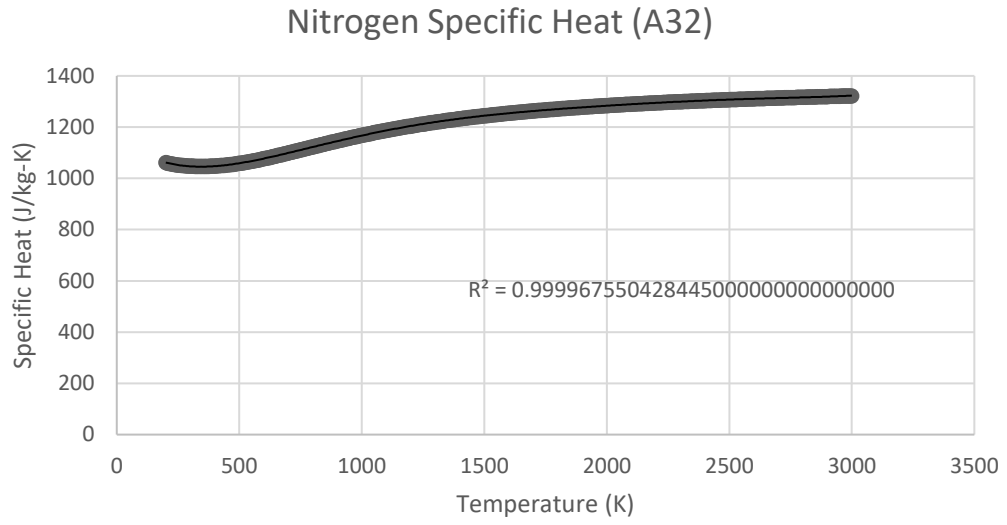


Figure A52. Variable Specific Heat of N₂

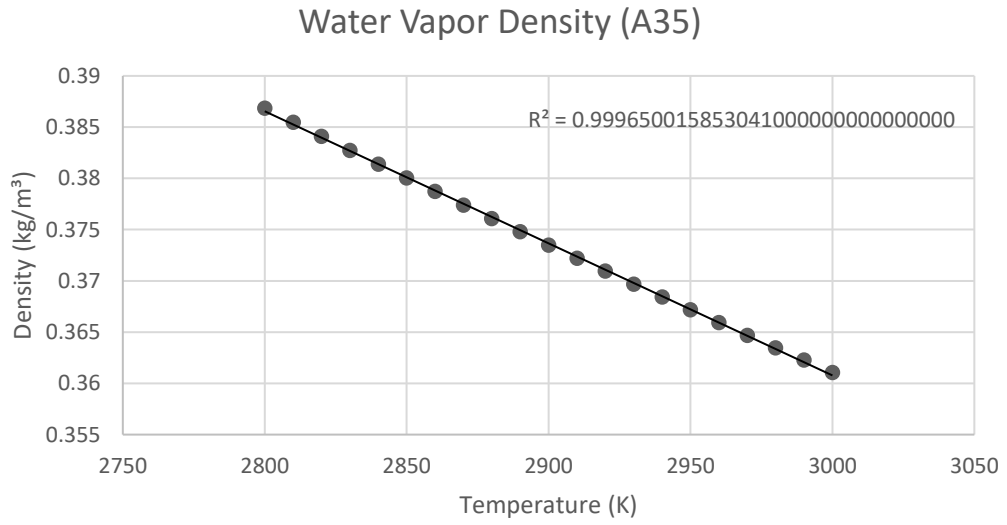
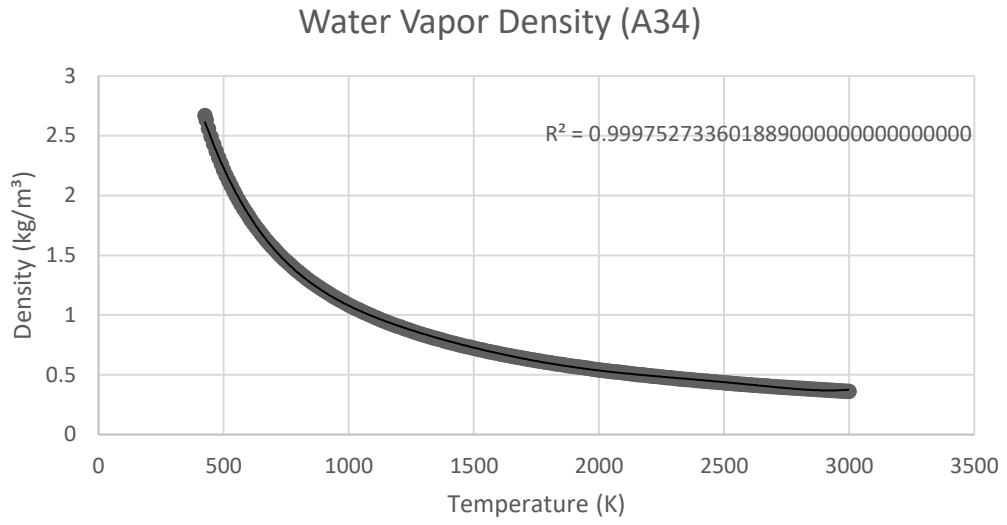


Figure A53. Variable Density of H₂O

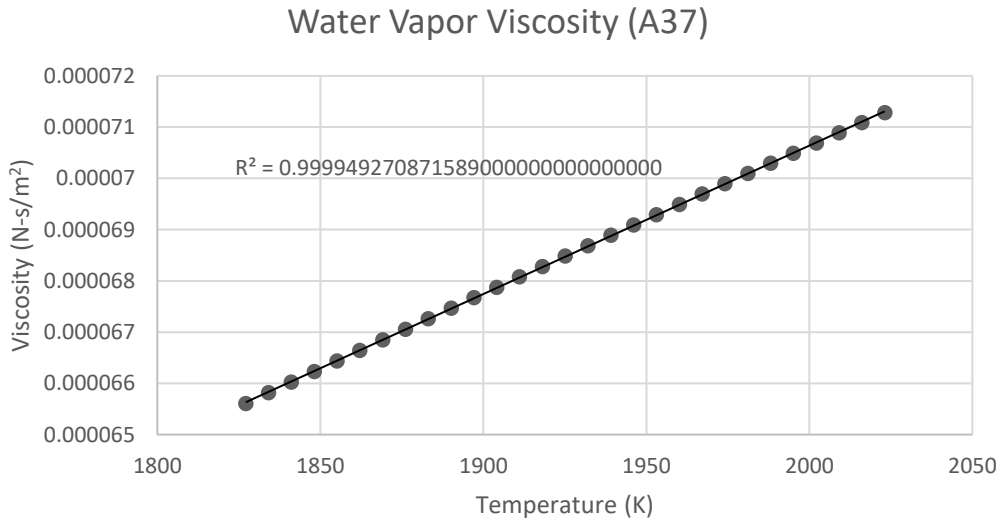
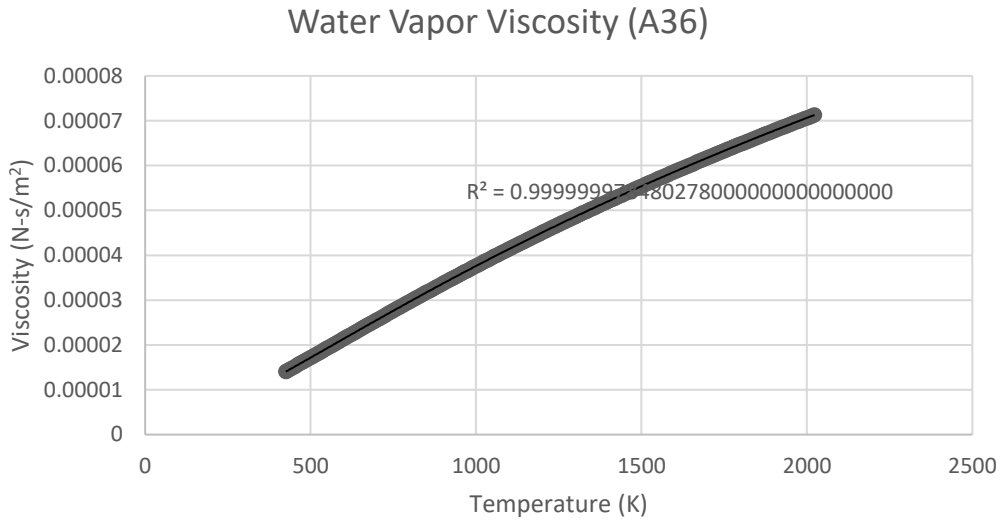
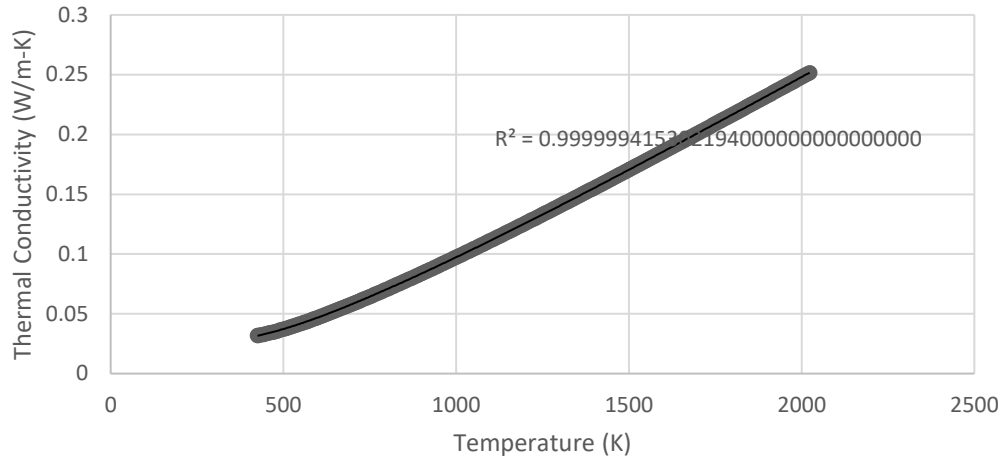


Figure A54. Variable Viscosity of H₂O

Water Vapor Thermal Conductivity (A38)



Water Vapor Thermal Conductivity (A39)

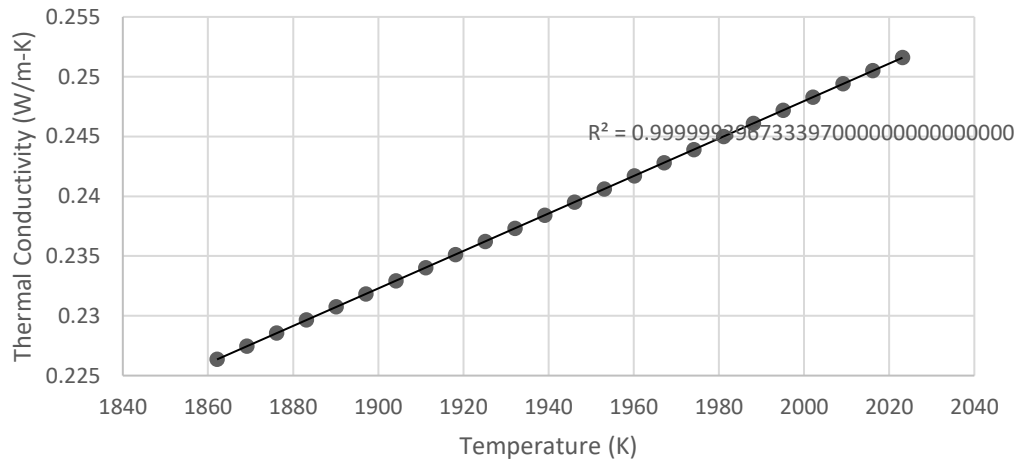
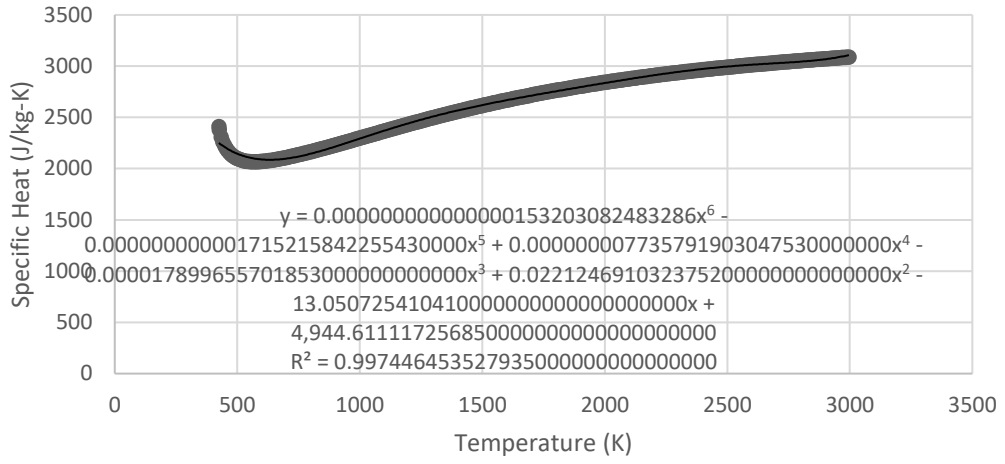


Figure A55. Variable Thermal Conductivity of H₂O

Water Vapor Specific Heat (A40)



Water Vapor Specific Heat (A41)

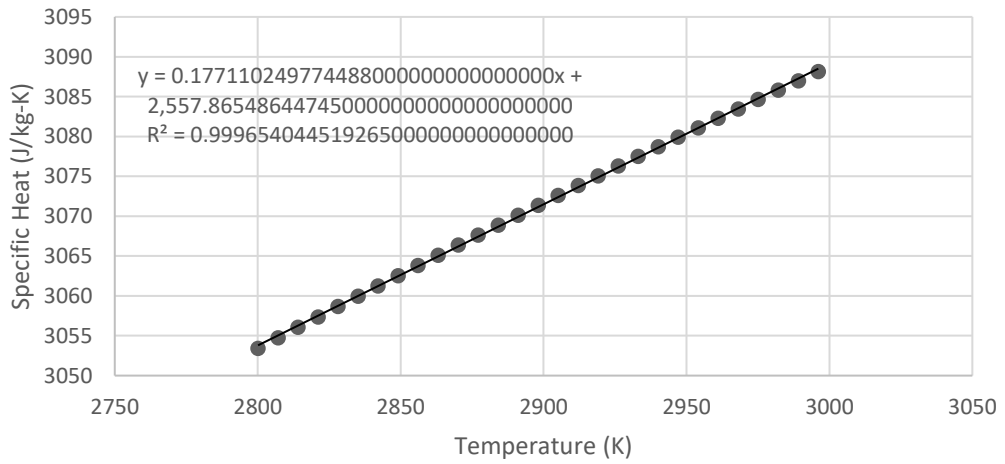


Figure A56. Variable Specific Heat of H₂O

Appendix B

Code

Low Pressure Model Code

```
clear all
clc
close all
z=0;
for n=4220:10:22220
    i=n-4219;
    numbercountstr=num2str(n);
    default="LowPressureV2--";
    load=default+numbercountstr;
    loadeddata=importdata(load, ' ');
    half=length(loadeddata.data(:,1))/2;
    for m=1:half*2
        if m<=half
            saveddatafluid(m,:,i)=loadeddata.data(m,:);
        else
            saveddatasolid(m-half,:,i)=loadeddata.data(m,:);
        end
    end
end
saveddatatitle=loadeddata.textdata;

for k = 1:10:i;
    z=z+1;
    if k == 1
        % Only create the plot for 1st iteration, update wave for
        % subsequent
        figure();
        hold('on'); grid('on');
        yyaxis left
        ylim([0 5e7]);
        set(gca, 'xtick', 0:0.05:0.25);
        h1 = plot(saveddatafluid(:,2,k),saveddatafluid(:,4,k));
        ylabel('Pressure (Bar)');
        yyaxis right
        ylim([300 500])
        h2 = plot(saveddatafluid(:,2,k),saveddatafluid(:,7,k));
        legend('Pressure','Temperature');
        ylabel('Temperature (K)');
        xlabel('Wall Position (m)');
    else
        % Update y data
        set(h1, 'ydata', saveddatafluid(:,4,k))
        set(h2, 'ydata', saveddatafluid(:,7,k))
    end
    title(['k = ' num2str(z)]);
    print(['Frame ' num2str(z)], '-dpng', '-r150');
end
GifName = 'TempAndPressure.gif';
delay = 0.001; % Delay between frames (s)
for ii = 1:z
    [A, ~] = imread(['Frame ' num2str(ii) '.png']);
end
```

```

[X, map] = rgb2ind(A, 256);
if ii == 1
    imwrite(X, map, GifName, 'gif', 'LoopCount', inf, 'DelayTime',
delay)
else
    imwrite(X, map, GifName, 'gif', 'WriteMode', 'append',
'DelayTime', delay)
end
end
end

```

Nitrogen Model Code

```

clear all
clc
close all
z=0;
for n=2010:10:20000
    i=n-2009;
    numbercountstr=num2str(n);
    default="NitrogenV2--";
    load=default+numbercountstr;
    loadeddata=importdata(load, ' ');
    half=length(loadeddata.data(:,1))/2;
    for m=1:half*2
        if m<=half
            saveddatafluid(m,:,i)=loadeddata.data(m,:);
        else
            saveddatasolid(m-half,:,i)=loadeddata.data(m,:);
        end
    end
end
saveddatatitle=loadeddata.textdata;

for k = 1:10:i;
    z=z+1;
    if k == 1
        % Only create the plot for 1st iteration, update wave for
        % subsequent
        figure();
        hold('on'); grid('on');
        yyaxis left
        ylim([0 5e7]);
        set(gca, 'xtick', 0:0.05:0.25);
        h1 = plot(saveddatafluid(:,2,k),saveddatafluid(:,4,k));
        ylabel('Pressure (Bar)');
        yyaxis right
        ylim([300 500])
        h2 = plot(saveddatafluid(:,2,k),saveddatafluid(:,7,k));
        legend('Pressure','Temperature');
        ylabel('Temperature (K)');
        xlabel('Wall Position (m)');
    else
        % Update y data
        set(h1, 'ydata', saveddatafluid(:,4,k))
        set(h2, 'ydata', saveddatafluid(:,7,k))
    end
end
title(['k = ' num2str(z)]);

```

```

    print(['Frame ' num2str(z)], '-dpng', '-r150');
end
GifName = 'TempAndPressure.gif';
delay = 0.001; % Delay between frames (s)
for ii = 1:z
    [A, ~] = imread(['Frame ' num2str(ii) '.png']);
    [X, map] = rgb2ind(A, 256);
    if ii == 1
        imwrite(X, map, GifName, 'gif', 'LoopCount', inf, 'DelayTime',
delay)
    else
        imwrite(X, map, GifName, 'gif', 'WriteMode', 'append',
'DelayTime', delay)
    end
end
end

```

Combination Plot Code

```

clc
clear all
close all

LocationSkip=100;

load('LPFluid.mat')
load('LPSolid.mat')
load('NFluid.mat')
load('NSolid.mat')

LPZoned=find(LPsaveddatafluid(:,4,1)>0);
LPmin=min(LPZoned);
LPmax=max(LPZoned);
LPTempStart=min(find(LPsaveddatafluid(LPmin,7,:)>300));

NZoned=find(Nsaveddatafluid(:,4,1)>0);
Nmin=min(NZoned);
Nmax=max(NZoned);
NTempStart=min(find(Nsaveddatafluid(Nmin,7,:)>300));

for Loc=LPmin:LocationSkip:LPmax
    z=0;
    zz=0;
    for i=LPTempStart:10:length(LPsaveddatafluid)
        z=z+1;
        LPFTime(z,Loc)=z*1*10^(-7);
        LPFT(z,Loc)=LPsaveddatafluid(Loc,7,i);
        LPFP(z,Loc)=LPsaveddatafluid(Loc,4,i);
        LPST(z,Loc)=LPsaveddatasolid(Loc,7,i);
    end
    for i=NTempStart:10:length(Nsaveddatafluid)
        zz=zz+1;
        NFTTime(zz,Loc)=zz*1*10^(-7);
        NFT(zz,Loc)=Nsaveddatafluid(Loc,7,i);
        NFP(zz,Loc)=Nsaveddatafluid(Loc,4,i);
        NST(zz,Loc)=Nsaveddatasolid(Loc,7,i);
    end
end

```



```
end

figure
hold on
yyaxis left
plot(LPFTTime(:,LPmin),LPFP(:,LPmin+50));
ylabel('Pressure (Pa)');
xlabel('Time (s)');
yyaxis right
plot(LPFTTime(:,LPmin),LPFT(:,LPmin+50));
ylabel('Temperature (K)');
ylim([300 500])
xlim([-inf inf])
grid on
plot(LPFTTime(:,LPmin),LPST(:,LPmin))
legend('Pressure','Fluid Temperature','Wall Temperature')
```